NASA CONTRACTOR REPORT

NASA CR-689

INVESTIGATION OF PLANETARY IONOSPHERES

by B. Mohr, Z. Poznanski, D. Luganski, G. Kraft, and S. H. Gross

Prepared by
CUTLER-HAMMER, INC.
Deer Park, N. Y.
for Goddard Space Flight Center

NATIONAL AERONAUTICS AND SPACE ADMINISTRATION • WASHINGTON, D. C. • MAY 1967

INVESTIGATION OF PLANETARY IONOSPHERES

By B. Mohr, Z. Poznanski, D. Luganski, G. Kraft, and S. H. Gross

Prepared under Contract No. NAS 5-9108 by
CUTLER-HAMMER, INC.
Deer Park, N.Y.

for Goddard Space Flight Center

NATIONAL AERONAUTICS AND SPACE ADMINISTRATION

For sale by the Clearinghouse for Federal Scientific and Technical Information
Springfield, Virginia 22151 – CFSTI price $3.00

ABSTRACT

The objective of Supplemental Agreement No. 2 to NASA Contract NAS 5-9108 with Airborne Instruments Laboratory, A Division of Cutler-Hammer, Inc., was to study the feasibility of experiments using radio-sounding techniques for the investigation of the ionospheric properties of the planets. The effort followed a previous study under the same contract and reported in the NASA Contractor Report CR-493, dated June 1966. The study effort was divided into two parts: instrumentation techniques and theoretical analysis. The former received the bulk of the effort. In that area, principal concern was with overall systems evaluation, signal processing, and transmitter design, for an advanced long-range sounder system using techniques recommended from the previous study. Sounding ranges of interest were from nearby to 40,000 km. Application of the new sounder system was made to typical planetary missions such as the Voyager-Mars Orbiter and the Mariner-Mars Fly-By spacecrafts. The theoretical analysis extended the previous effort in which virtual depth characteristics of ionospheric sounding echoes were investigated to include the effects of a planetary magnetic dipole field.

The signal-processing design study was based on the previous program, which concluded that digitized pulse-compression and integration techniques were the most desirable methods to be used in advancing the state of the art of ionospheric sounding. Investigations of these techniques and their applications to typical planetary sounding systems resulted in very detailed examinations of circuits, components, and characteristics. The nature of this design effort was directed toward providing a sounding capability from extremely long ranges, as well as from nearby, over a wide band of frequencies; 0.1 to 20.0 MHz.

The transmitter design consisted mainly of breadboarding efforts to realize a wide-band untuned system entirely of solid-state components. Desired power levels were based on the previous study and the design achieved the required goal in the main. The task also included a study of the design of matching networks for dipole antennas.

The report recommends continued efforts. A typical sounder consistent with the constraints (short dipole antenna, minimum weight, size, and power) of a planetary mission should be completely developed as a laboratory prototype of a flyable unit. In particular, the system devised to meet the Voyager application is recommended. In addition, the techniques should be demonstrated by construction of an experimental unit incorporating pulse compression and integration for bottomside sounding the ionosphere. Studies should be continued with respect to system and subsystem design and equipment specifications, data interpretations, and reduction methods, analyses of the significance of measurement and interpretation errors, and the physics of the ionospheres of the planets.

TABLE OF CONTENTS

LIST OF ILLUSTRATIONS

LIST OF TABLES

SECTION I
INTRODUCTION

This final report describes a feasibility study of experiments using radio-sounding techniques for the investigation of the ionospheric properties of the planets. The work was accomplished under NASA Supplemental Agreement No. 2, Contract NAS 5-9108 to Airborne Instruments Laboratory (AIL). The effort followed a previous feasibility study under the same contract which study was reported in the NASA Contractor Report CR-493 (reference 1).

During the previous study, various techniques were investigated to determine the relationship between their performance and such parametric quantities as range, power, weight, size, and complexity. The goal was to specify those experiments to be used for specific planetary missions. The study was principally parametric in nature, but also contained an application to the Voyager-Mars Orbiter. Of principal interest were those techniques most suitable for providing long-range capability with good resolution, while requiring relatively little weight, power, size, and data-output rates. In addition, the studies included theoretical propagation analyses to evaluate characteristics that were measurable from a distance. Of the various properties, it was concluded that the principal characteristic that provides the most information and, also, that is relatively easily measured is the propagation time delay. Most of the theoretical effort was devoted to an analysis of these phenomena.

This previous effort resulted in the conclusion that the received echoes should be processed on-board, particularly for long ranges, to minimize the data-output requirements. It was also concluded that the transmitted signal should consist of wide, coded pulses, and the digital techniques should be fully used (in contrast with analog techniques) to provide adequate precision not available in analog systems,

particularly for large-scale height regions and to permit dense packaging and minimize data-output requirements. Frequency-synthesis techniques were recommended, using small frequency increments. In addition, the synthesizer could be programmed to select specific frequencies or frequency ranges as desired for particular ionospheric investigations. The principal techniques recommended for long-range sounding were digitized pulse-compression and integration with control by digital programming. These techniques were used in a description of a system for a possible Voyager-Mars orbiter mission.

The work reported here is divided into two main tasks: studies of instrumentation techniques and theoretical analysis. The instrumentation techniques received the bulk of the effort, consisting of overall systems evaluation and specification, signal-processing techniques, and transmitter design studies. These techniques were applied to a Voyager-Mars orbiter and a Mariner-Mars fly-by as typical missions. The theoretical analysis consisted of ionospheric propagation studies beyond that of the previous effort in NASA CR-493 to include the effects of a planetary magnetic dipole field. Previous analysis had considered models of exponential electron density profiles with a constant superposed magnetic field. Of principal concern was the effect of the nonuniformity of a dipole field with respect to the results obtained with a constant magnetic induction.

The transmitter design consisted mainly of breadboarding efforts to realize a wide band (0.5 to 10 MHz) untuned system entirely of solid-state components capable of providing wide pulses with as high a peak power as feasible using presently available components. Desired power levels were based on the previous studies under the contract. The task also included the design of matching network systems for dipole antennas. The results of this work are described in Section IV.

The signal-processing design study was based on the previous program, which concluded that digitized pulse-compression and integration techniques were the most desirable methods to be used in advancing the state-of-the-art of ionospheric sounding. Investigation

of these techniques and their applications to typical planetary sounding systems resulted in detailed examinations of circuits, components, and characteristics. The nature of this design effort was directed toward providing a sounding capability from extremely long ranges, as well as from nearby, over a wide band of frequencies. A sounding period has to be a short enough time interval, so that the change in the spacecraft position relative to the planet corresponds to a small change in planetary latitude and longitude. The study also included digital programmer control. Details of these efforts are described in Section III.

The overall systems evaluation and specification task consisted of system requirement studies in terms of the basic experiment. Much of the more general aspects of this task had been accomplished under the previous program. Here, the principal emphasis was on the requirements for typical applications in order to provide guidelines for the signal processor and transmitter development tasks, as well as for the other system components. The specific missions were for the Voyager and the Mars-Mariner 1969 spacecrafts as typical applications. The details are contained in Section II.

Special terminology used here is that peculiar to ionospheric physics and radar technology. That part of radar terminology unfamiliar to ionospheric physicists may be found in reference 2. Particular pertinent terminology in this report is defined where used as much as possible. The word range is used here normally to mean virtual depth. In some cases a description is in terms of altitude or height above a planet; in others, in terms of range. The two descriptions are obviously not the same, but can be related. The virtual depth differs from the altitude by the virtual height of the reflecting layer (which can be negative as well as positive). In most cases, the virtual height of the reflecting layer is neglected, and the altitude of the spacecraft is taken as the range, since the latter is usually much greater than the former in this report. The approximation is reasonable except at low spacecraft altitudes, or for nearby reflecting levels in which case, where necessary, the quantities are treated in their complete sense.

SECTION II
GENERAL DISCUSSION

Planetary missions will eventually be made to the vicinity of all the terrestrial planets and Jupiter. Such missions may involve fly-bys or orbiters, and landers. These space missions will presumably carry ionospheric experiments. In the earlier missions, the degree of accuracy in placing the spacecraft near the planet is limited by technical problems, although in time these may be surmountable. Thus, these early missions could miss by a considerable distance. Even with proven ability to come close, there is always a possibility of an error or partial failure that will result in a trajectory much further from the planet than planned. Finally, the planetary ionosphere may extend to a considerable height, such as for the earth, and there is real scientific merit in sounding from great altitudes. For example, the presence of a magnetosphere and its relationship to the ionosphere is of interest. If the planet has no significant magnetosphere, the reaction of the ionosphere with the solar wind is also of interest. There are, in addition, special problems at high altitudes, such as the discrepancy between the high-altitude ionospheric knee detected by whistler measurements and the absence of this knee in direct measurements of the earth's ionosphere. The placement of satellites at a synchronous altitude can provide diurnal variation data (in particular, sunrise and sunset information). All of these considerations lead to the need for the development of a long-range sounder.

Although measurements can be made from great altitudes, these would be meaningless if there were not sufficient precision in detecting the details of interest. Precision, in this sense, refers to the inherent ability of equipment to measure the virtual depth to a particular layer. Multiple modes, nonuniformity, or irregularities introduce additional sounding echoes. Sufficient resolution is essential

to separate these echoes. A suitable scale of precision or resolving power is based on the density scale height of the ionospheric region producing echoes. The cell of resolution and precision should be at least several times smaller than the scale height so that good definition can result from the reduction of the measured data. Thus, the system must not only be capable of sounding from large distances, but must also provide sufficient resolution and precision.

The scale heights and radii of the planets vary from one planet to another and, in general, for each planet the scale height should vary with altitude.

With the exception of the earth, there is a scarcity of information on the ionospheres of the planets. Since the flight of Mariner IV some information for one occulting region of Mars was obtained. Although this is a definite measurement, even that measurement has caused considerable controversy as to its meaning and implications, as evidenced by the interpretations of Fjelbo (1966), Chamberlain and McElroy (1966), Smith and Beutler (1966), and Gross, McGovern, and Rasool (1966) (references 3, 4, 5, and 6). Nevertheless, there is a sufficient degree of plausibility in theoretical work to establish, within at least an order of magnitude, the ranges of the important parameters. For that purpose, the following was established as the parameters of interest for this program:

Range: Orbiters--low to synchronous, 1000 to 36,000 km (NOTE: Synchronous altitude sounding for Mars and earth only)

Fly-bys--near to far misses, 2000 to 50,000 km

Resolution: According to the planet--5 to 200 km

Precision: According to the planet--5 to 100 km

Angular resolution in latitude and longitude: 1 to 2 degrees

Sounding frequencies: 0.1 to 20.0 MHz in fine increments of 5 to 100 kHz according to frequency and scale height.

The sounding frequencies correspond to electron densities from about 10^2 cm^{-3} to above 10^6 cm^{-3} with the highest frequencies probably penetrating to the surface. Such penetration could permit the location of the surface relative to the ionosphere. Angular resolution in latitude and longitude is that sufficient to adequately describe the variation in ionization about the planet. This requirement principally constrains the time to complete a sounding cycle at any altitude.

For working purposes, the summary in Table I was used for the physical quantities that may possibly be characteristic of the upper ionospheric region of the terrestrial planets and Jupiter. With the exception of earth, the entries in this table are highly speculative and may be quite debatable, but serve the function of guiding the establishment of requirements. The scale height given in the table is that for very high altitudes and represents a mean value over the planet. It need not correspond to the scale height just above the peak density level, nor the range of values over the planet and during day or night. For example, in the case of Mars, the occultation measurement at 55 degrees south latitude in the Martian winter afternoon revealed a scale height of 20 to 25 km. This value was obtained for the region above the peak level, which had a density of about 10^5 electrons/cm^3 and a height of 125 km.

1. CONCEPT OF INSTRUMENTATION

An advanced ionospheric sounder must provide long-range capability with fine resolving power. It must be capable of precisely measuring the virtual distance of an echo for a wide band of frequencies while maintaining coherence during transmission. As such, the techniques required consists of digitizing, frequency synthesis, pulse compression, and coherent and noncoherent integration.

Standard sounders are analog in form and it is necessary to select points from an ionogram in interpreting and reducing the data. In regions of large-scale height, the rapid change of virtual depth with frequency has limited the accuracy of this procedure drastically, since for a given virtual depth the frequency is quite uncertain, or, for a

TABLE I

UPPER ATMOSPHERE AND IONOSPHERES OF THE TERRESTRIAL PLANETS AND JUPITER

	Mercury	Venus	Earth	Mars	Jupiter
Average exospheric temperature	800-1800(E)	800-1800(E)	1500	400-700 E (85° ?)	100-200
Likely principal neutral	0_2, 0, CO rare gases N_2	0_2, 0, CO rare gases N_2	0_2, 0, He, H, N_2	0_2, 0, C0 rare gases N_2	H_2, H, He -
Likely principal ion	0^+, rare gases$^+$	0^+, rare gases$^+$ (H^+ ?)	0^+, He^+, H	0^+, rare gases$^+$	H^+
$N_{e\ max}$	10^5-10^7	10^5-10^7	10^6+	10^5-10^6	10^6
h_{max} APPROX	~400 km	200-400 km above clouds	250-400	125 ?, 300-400 km	100-200 km above clouds
B	> 200 γ	< 500 γ	0.3 to 0.6 gauss	< 500 γ	10-20 gauss
h_{exos}	~1200 km	~ 600 km above clouds	~ 600 km	~ 900 km	400-500 km
magnetosphere (out to)	?	?	~ $10R_0$	?	many (?) R_J
High altitude electron density scale height	200-300 km	100-200 km	3000-5000 km	~100 km	~ 100 km

given frequency, the virtual depth is inaccurately determined. This situation is now well known as a result of Alouette measurements. Digitizing the measurement, therefore, avoids this difficulty since precise measurements are made at a precisely known frequency. Digital techniques may also be used to advantage, since much progress has been made in packaging such circuits in highly condensed geometries and for reducing data rate requirements significantly.

Standard sounders also use swept frequency generators in which the frequency is continually changing with time. The energy radiated during a pulse is actually spread over a small band of frequencies. Dispersion introduces errors in propagation time delay. Since the ionosphere is dispersive, the spread of the radiated pulse will add to the dispersion of the medium increasing the error. It would be preferable to maintain the frequency constant during a pulse to preserve coherence and improve system accuracy. In that event, the energy is spread over a much smaller bandwidth as determined by the stability of the source. For longer range systems where pulses are wider, the need for a constant frequency during radiation is even more imperative. Furthermore, processing by techniques such as digital pulse compression and coherent integration require a high degree of coherence and this is most easily accomplished by maintaining the frequency during radiation. Therefore, frequency-synthesis techniques must be used to permit the simultaneous achievement of wide-band coverage while maintaining coherence during a pulse.

Pulse-compression and integration techniques are necessary to provide the desired resolution and sounding range capability, while keeping the transmitter design within the state of the art.

These techniques are new to ionospheric sounders, but they are well developed in the radar technology. The full concept of the instrumentation described here, therefore, makes full use of these techniques.

A simplified block diagram of the instrument is shown in Figure 1 and a more elaborate diagram is shown in Figure 2. The

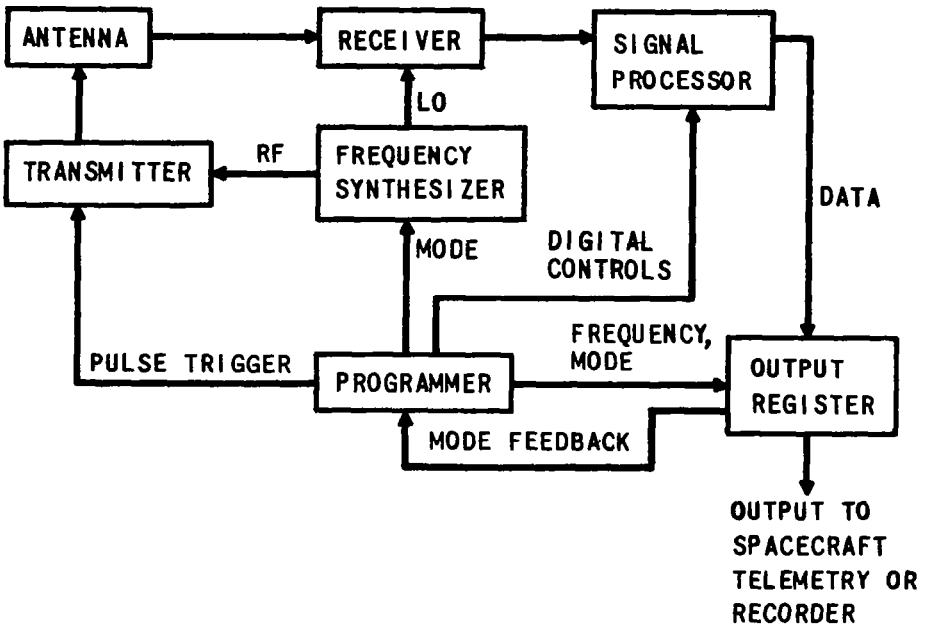

FIGURE 1. SIMPLIFIED BLOCK DIAGRAM OF ADVANCED PLANETARY SOUNDER

sounder, as presently conceived in its fullest form, transmits pulses which may be digitally coded for pulse compression according to the sounding range at frequencies from 0.1 to 20.0 MHz. The frequency range is covered in fine increments as controlled by a frequency synthesizer. The received echoes are processed in a Signal Processor using pulse-compression and integration techniques according to the range and under the control of a digital programmer. The processor compiles the digital-output signal and delivers it through an output register to the spacecraft telemetry system. This output signal consists of a digital word containing frequency, virtual depth (range) data, and mode type information. The echoes are detected and collected in small resolution cells in the processor--each cell corresponding to a different virtual depth. Cells that contain a signal above some suitably established

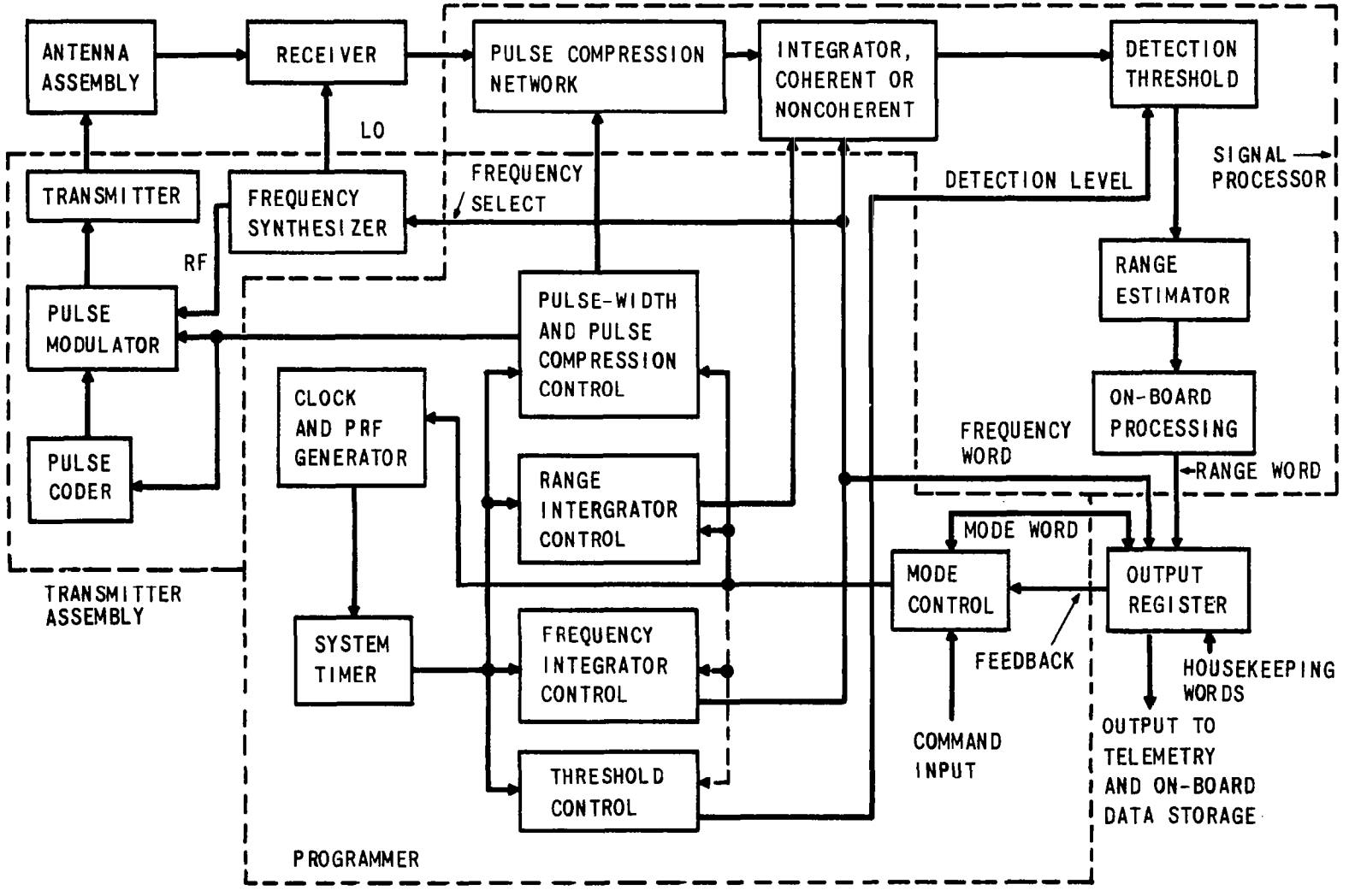

FIGURE 2. BLOCK DIAGRAM OF ADVANCED PLANETARY SOUNDER

threshold provide acceptable echoes corresponding to the ranges represented by each of such cells. In the fullest form of the system, all such cells are read out and provided to the telemetry system.

Various modes are necessary to accommodate signal processing as a function of range. The degree of pulse compression and integration increases as the range increases beyond some maximum range. Below this range, the system is simplest in form, consisting of simple uncoded pulses and integration is not usually required to bring the signal level above the threshold.

Since a group of cells are used which correspond to small increments in range, with the increments corresponding to the resolution capability of the system, the total number of cells required to cover the maximum range of the system would be very large. To avoid this large number of cells, a coarse ranging acquisition mode is included in the system to roughly measure the range of the echoes. This coarse measurement permits the placement of a range window containing a limited number of fine resolution cells. The window is placed about the rough range value and is used for finer location of the echoes. In the fine ranging mode, the window is located in this fashion by the action within the acquisition mode, and the range of the echoes is precisely determined by combining a sliding range scale readout of the acquisition mode with the fine cell location of the threshold detected signals. The same cell arrangement can also be used in the acquisition mode with each cell covering a coarse range interval. This interval can be sufficiently wide to include all echoes at some relatively high frequency at which the acquisition measurement can be made. In the fine ranging mode there may be several submodes according to the rough range and frequency band. The selection of the submode for a range interval can be automatically accomplished by the acquisition mode measurement. Selection of a submode for a frequency band can be accomplished by the programmer or by ground control, if so desired. Differences in range submodes are due to the extent of pulse compression and integration required for the associated range interval. Coarse ranging can be repeated as often as necessary.

The use of frequency synthesis to provide the RF signals to the transmitter and the local oscillator signals to the receiver permits a high degree of flexibility and relative ease in choosing the sounding frequencies. The frequency increments can be made very small with provisions for increasing the steps to reduce sounding time. It is also possible to select a limited frequency range in the total sounding band, as desired, to concentrate on sounding from a particular region of an ionosphere. In addition, the frequency is constant during a pulse, within the stability of the oscillators, reducing the degree of dispersion that necessarily occurs with swept frequency systems. This latter feature is also important where coherent integration is used in which the doppler effect is unknown and must be introduced.

The use of threshold detection in the processor also provides an additional degree of flexibility since the threshold can be readily changed by programming or ground control for specific experimental purposes. It is normally set to avoid false alarms but may be reduced or increased if a decision by ground personnel is desired as to the falseness of a particular echo.

Future missions that are not entirely devoted to ionospheric sounding will introduce sufficient constraints to force the sounder antenna to be as simple as possible. The transmitter will use simple dipoles and echo reception will generally be from the same antenna, or at most, from separate loops. These dipoles will tend to be shorter than desirable for maximum efficiency, since wide-band matching networks provided between the transmitter and the antenna system will introduce more losses than for an optimum antenna configuration. If greater weight and space are available to the experiment, larger antennas can be used and more than one antenna system can be provided. There are also special missions in which large poles are used for gravity-gradient stabilization, and a more efficient antenna system is possible, particularly at the lower frequencies. In general, the losses will be greater at lower frequencies, and although echoes will arrive from higher regions of the ionosphere, the smaller virtual depth will not

entirely compensate for the increased losses in the antenna system. Antenna systems may also be arranged to selectively receiver orthogonal polarizations with separate reception and time-shared processing, or separate processing, to extract mode information. More than one antenna system can be used, as well, to cover the frequency range more efficiently.

Since performance can be expected to be better at the higher frequencies, the acquisition mode need only operate at one such higher frequency. In that event, the fine-range window must be sufficiently wide to cover a range of echoes for sounding frequencies above and below the acquisition mode sounding frequency. For extremely low frequencies, it is conceivable that the virtual depth could lie outside the range window. However, it still is possible to program the window, shifting it to cover this part of the frequency band. The changes can be accommodated in a rather coarse fashion to cover a wide set of conditions.

The whole concept of the sounder described lends itself to the minimization of telemetry data requirements in contrast with conventional analog, swept frequency sounders. Digitizing the information, selecting only those returns above a threshold, and providing only the fine range measurements at the maximum rate and the coarse information at a reduced rate considerably reduces the data rate and capacity requirements--a significant advantage for the remote planetary missions. Furthermore, the major use of digital techniques and the restriction to solid-state devices tends to reduce considerably the size, weight, and power requirements for the experiment, compared with conventional sounders.

With respect to the early planetary missions, the constraints on weight, size, and power may preclude the use of the full concept as described. Thus, the antennas may be too short to efficiently cover the entire frequency range of interest, except from near ranges. For far ranges it may be necessary to use more efficient matching than provided by a wide-band matching network. In that event, fixed-frequency sounding

may be a suitable compromise with each frequency separately matched, provided that enough frequencies are used. In addition, the constraints of the mission may be severe enough to make it necessary to eliminate some of the signal-processing techniques. Thus, the concept of the processor for a Mariner mission, as described in Section III, only uses the noncoherent integration technique. As a result, the total sounding period may become excessive at very large ranges, and an optimum compromise restricts the maximum range and further forces the use of fixed frequencies. The total weight and power estimated for that hypothetical Mariner system was 13 pounds, including the weight of a dipole that is 60 feet long from tip-to-tip and 8 watts, respectively. With some additional weight and power, pulse compression could be added, significantly reducing the sounding time period and permitting many more sounding frequencies. With sufficient gain from this technique, the full frequency synthesis range with the finest frequency increments could be incorporated. In general, for a specific mission, the system adopted is a compromise between all of these factors and the scientific merit of the experiment.

2. ENERGY AND RESOLUTION

The relationships between the required transmitter energy, range, and frequency for a given signal-to-noise ratio were derived in CR-493. These are repeated here. The required radiated energy, E_R, is given by:

$$E_R = \left(\frac{8\pi H}{\lambda}\right)^2 \left(\frac{R_p + H}{R_p}\right)^2 \frac{kTc.n.}{L} \left(\frac{S}{N}\right) \qquad (1)$$

where

H = altitude,

R_p = radius of planet,

λ = wavelength,

$kTc.n.$ = cosmic noise power per cycle of bandwidth

$= \frac{\lambda^2}{2} b$,

b = cosmic noise brightness (watts/m^2/ster/Hz)

$\frac{S}{N}$ = desired signal-to-noise ratio for a given probability of detection and false alarm probability.

L = fixed losses due to mode splitting, orientation and polarization.

This radiated energy is fundamental and independent of the modulation. The required energy, E_T, from the transmitter is of interest, since this is a practical quantity of vital importance in the design of the transmitter. It is the energy supplied to the matching network preceding the antenna, and it is given by:

$$E_T = \frac{E_R}{G^2(f)\, L_m(f)} \qquad (2)$$

where

$L_m(f)$ = matching network loss,

$G(f)$ = antenna gain.

Certain assumptions were made in deriving equations 1 and 2. In equation 1, it was assumed that the receiver bandwidth is based on a matched filter design. For that case, bandwidth $B = 1\ \tau$, where τ is the pulse width. Also, in equation 2 it was assumed that the same antenna is used for transmission and reception. With a relatively high impedance receiver, the matching network loss only enters once, and that is for transmission.

The cosmic noise brightness is incompletely known. There have only been a few measurements below 5 MHz and extremely few below 1 MHz. More precise and certain information is of great importance to the design of a sounder, particularly for frequencies below 1 MHz, since cosmic noise is the principal source of noise in this frequency range. The cosmic noise data provided in CR-493 were based on the measurements of Alexander and Stone, Walsh et al., Huguenin et al., Ellis and Hartz (references 7, 8, 9, 10, and 11). Present data is essentially the same as was used in the previous report. To carry out calculations below 1 MHz, it was necessary to extrapolate the

decrease in the cosmic noise level from the peak level in the 2 to 4 MHz range. This procedure had been followed in the previous work and is used here.

Figure 3 has been prepared to exhibit the energies required. This is a plot of range versus frequency for various energy levels delivered by the transmitter. The assumed parameters are also shown. The calculation was made for earth. For comparison, the figure exhibits the performance capability of Alouette II. Similarly, calculations can be readily made for any of the planets. It should be noted that the assumed matching network loss is less than that for Alouette. Consequently, the Alouette point shown on the graph is probably more optimistic than the satellite's actual capability, though the additional integration of the ionogram partially compensates for this difference. The S/N ratio of 13.5 db is based on a probability of detection $P_d = 0.9$ and a probability of false alarm $P_{fa} = 10^{-6}$. The curves exhibit a somewhat smaller energy requirement to achieve the same range at frequencies below 0.5 MHz. This is due to the fall-off in the cosmic noise and the assumption of a fixed matching network loss. Actual network losses will increase as the wavelength increases, for a given antenna, and the curves will look more like that shown as a dashed line for the 20 Joules curve. From the curves, it can be seen that about 12 to 20 Joules are required to sound from synchronous altitudes.

Present systems are limited with respect to their ability to supply the required energy for the longer ranges due to peak-power limitations and the average power available from the spacecraft. Although vacuum-tube transmitters can be used to achieve high peak powers, their use is limited by the filament power and plate dissipation. In addition, high power necessitates large bulky tubes with attendant problems in reliability and the ability to withstand acceleration and vibration. Ceramic tubes are more limited in power, but are more suitable for the applications. However, transistors appear to be ideal in all respects, except in their ability to deliver very high power. Although the average power taken from the spacecraft may be satisfactory,

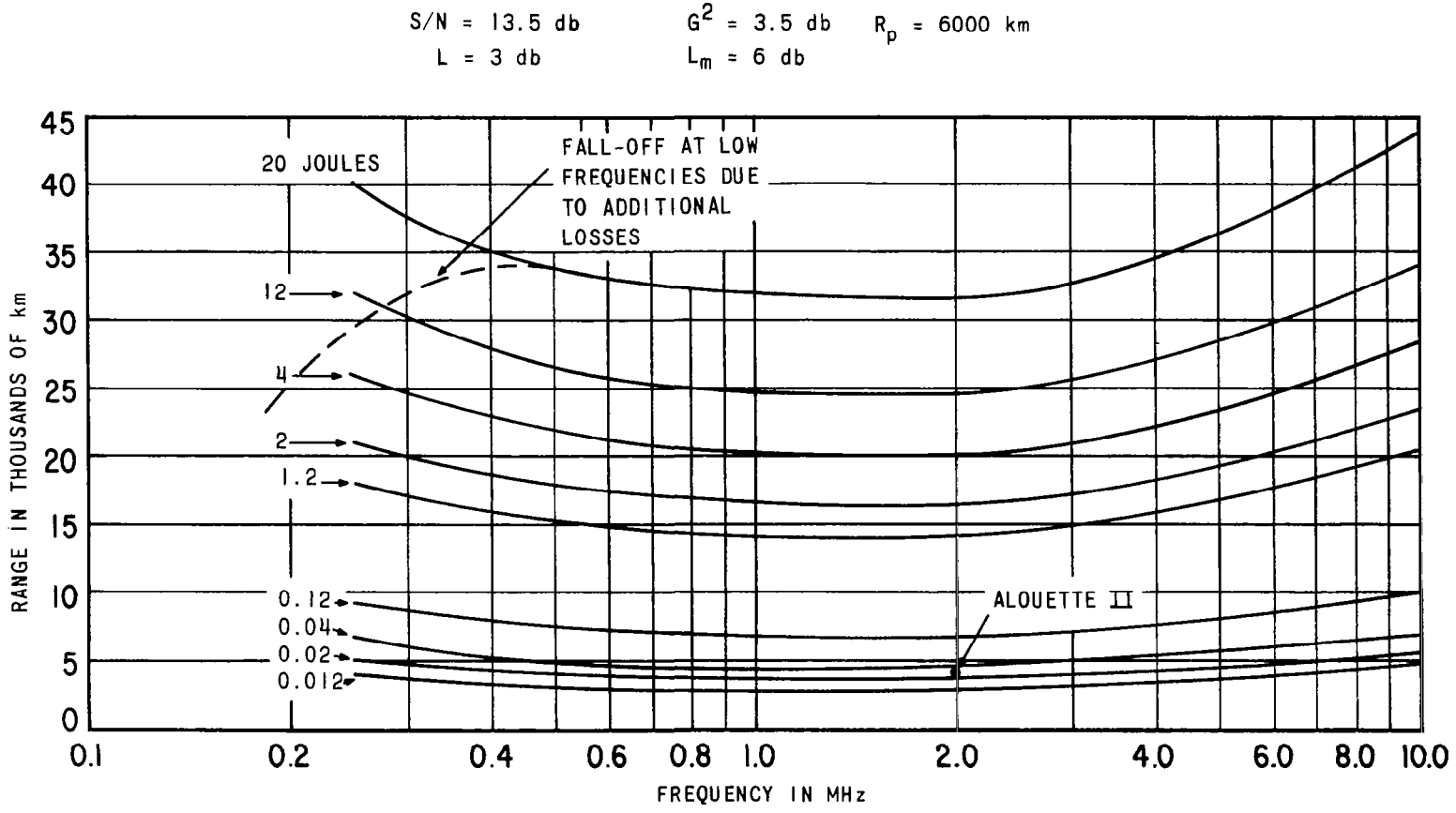

FIGURE 3. RANGE VS FREQUENCY FOR SINGLE PULSE ENERGY LEVELS

the high peak pulse power implies high peak current drainage. The power supply also must be capable of supplying this current pulse and, consequently, higher pulse power requires a more complex and bulky power supply. It would appear preferable to widen the pulse and to keep the peak power within bounds in providing the needed energy, while adjusting the prf to maintain the average power level. However, the wider the pulse, the poorer the resolution for an unmodulated pulse. The relationships and pulse shapes are shown in Figure 4.

For a simple unmodulated pulse sounder, one can relate range and peak pulse power for a given resolution capability. For the same parameters as in Figure 3, the relationships are shown in Figure 5. A somewhat optimized capability for Alouette II is also shown for comparison. It can be seen that at a range of 35,000 kilometers peak pulse powers from about 20,000 watts to 280,000 watts are required at 2 MHz as the resolution improves from 200 to 15 km.

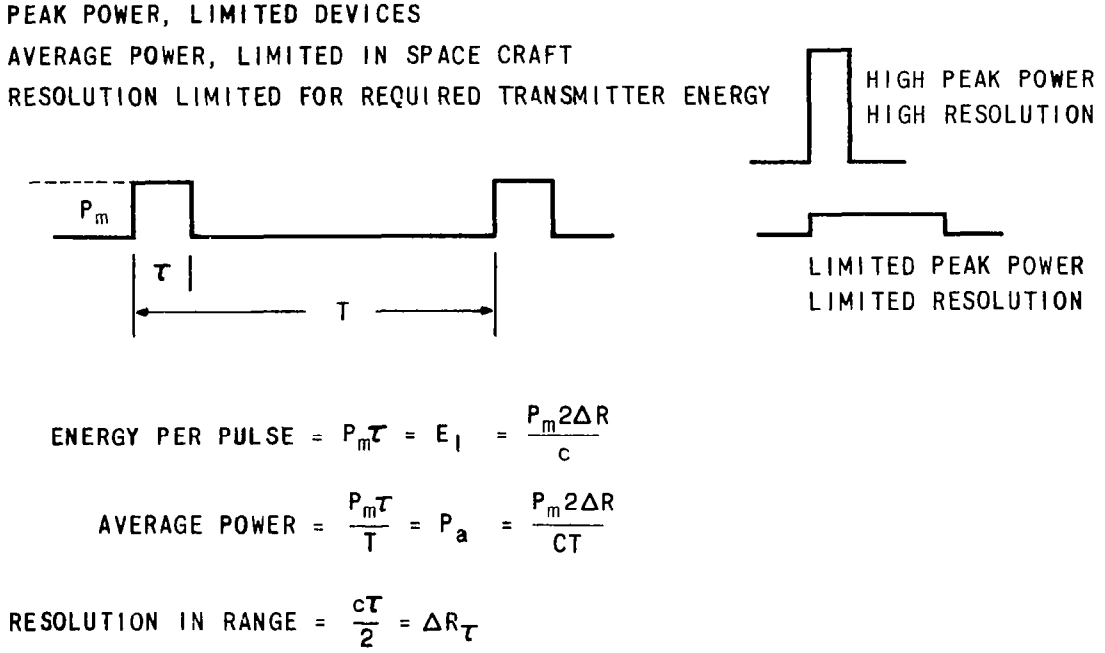

FIGURE 4. LIMITATION OF PRESENT SYSTEMS

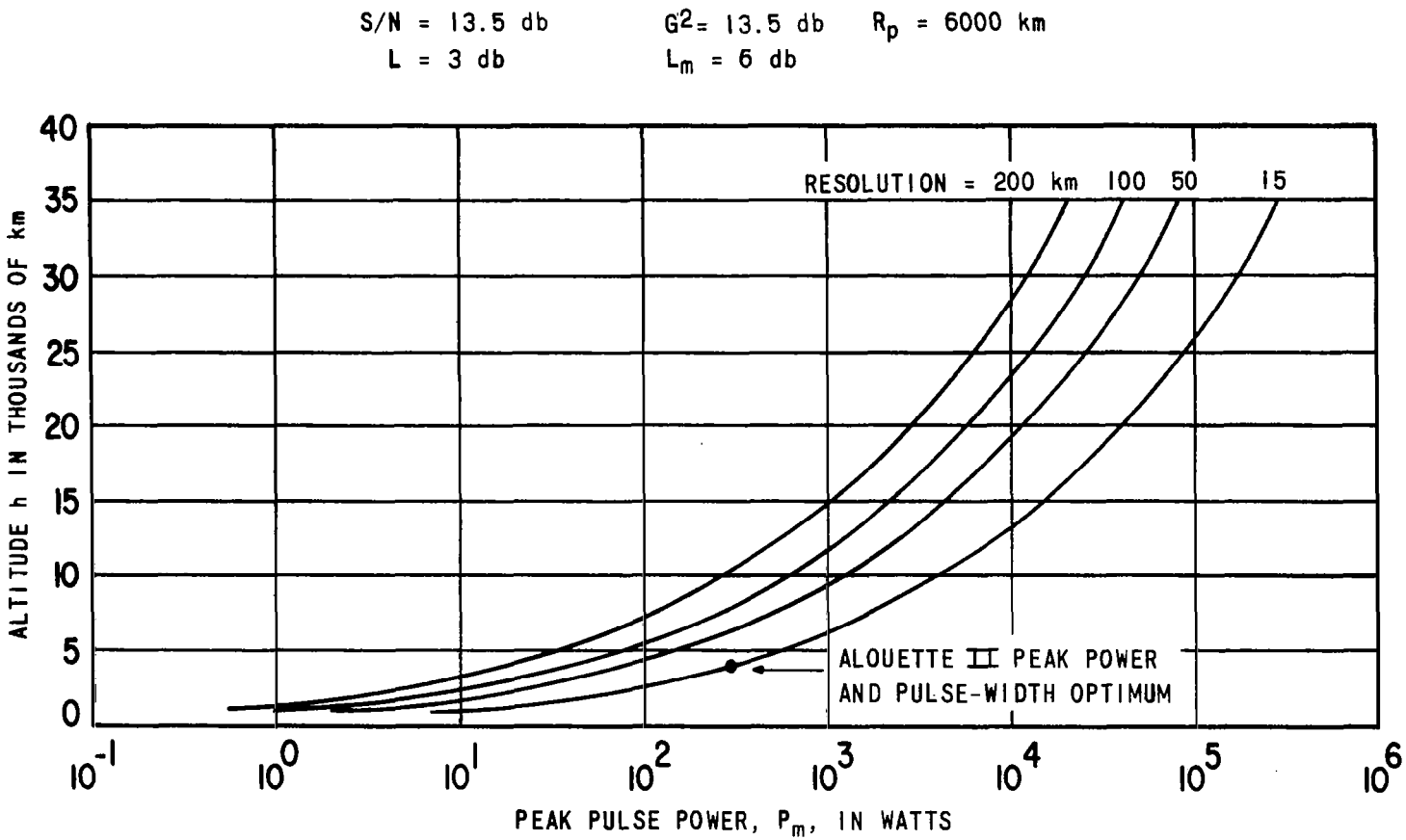

FIGURE 5. ALTITUDE VS PEAK PULSE POWER AT 2 MHz FOR DIFFERENT RANGE RESOLUTIONS

One can proceed in several ways to achieve the energy level required for the larger ranges without deteriorating the resolution. One way is to increase the peak pulse power output keeping the pulse width as narrow as required by resolution. For transistors, a state-of-the-art advancement is necessary to achieve greater power for the frequency range of interest. In addition, this method suffers from other complications. The antenna matching network becomes more difficult due to the exceedingly high voltages across some of the elements. The whole output circuitry must be insulated for higher voltages and the transmitter and its power supply must be capable of delivering very large currents. If the receiver works off the same antenna, it must be protected by T/R type devices with much higher RF voltage ratings. Also, it can be expected that the generation of such large pulses will complicate the RFI problem. These complications arise with any of the various power delivering components.

Another way is to increase the energy by integrating pulses, either coherently or noncoherently, or by introducing pulse compression. Integration uses less energy per pulse and achieves the desired energies by accumulation. In this way, the pulse width can be as narrow as required by resolution. Noncoherent integration suffers by requiring more samples to be integrated than coherent, producing, in radar terminology, the equivalent of a loss. It also takes longer to accumulate, since more samples are required. However, noncoherent integration is easier to accomplish. Table II shows typical integration times for coherent and noncoherent integration as a function of range and frequency.

In pulse compression, one takes advantage of the fact that resolution is determined by the receiver bandwidth and not by the pulse width. It is only necessary to code a wider pulse, such as by frequency or phase modulation or phase coding, so that the bandwidth of the coded pulse corresponds to the desired resolution. In phase coding, the pulse is actually broken into smaller time intervals. Thus, if the code contains N bit positions over a pulse of width τ, each position being of

TABLE II

INTEGRATION TIMES VERSUS RANGE AND FREQUENCY

Range / f 10^{-3} km	Coherent Integration Time (min prf) sec				Coherent Integration Time, prf 3.5 sec				Noncoherent Integration Time prf, 3.5 sec			
	0.25 MHz	0.5	2.0	5.0	0.25 MHz	0.5	2.0	5.0	0.25 MHz	0.5	2.0	5.0
35	7.0	9.7	14.0	8.4	8.6	12.0	17.0	10.3	25.7	44.3	77.0	34.4
30	4.0	4.8	6.4	5.6	5.7	6.9	9.1	8.0	13.7	18.3	28.6	22.8
25	1.3	2.3	2.7	2.0	2.3	4.0	4.6	3.4	3.7	7.7	9.4	6.0
20	0.5	0.8	1.1	0.7	1.2	1.7	2.3	1.4	1.7	2.6	3.7	2.0
15	0.2	0.2	0.3	0.1	0.6	0.6	0.9	0.3	0.9	0.9	1.1	0.6
10	0.1	0.1	0.1	0.1	0.3	0.3	0.3	0.3	0.6	0.6	0.6	0.6

τ/N seconds wide, the filter in the receiver is matched to a time interval τ/N. That is, its bandwidth is N/τ. The factor N is called the pulse-compression factor and represents the improvement over an unmodulated pulse

There are some basic relationships that link the measurement time, required energy, average delivered power P_a, range, pulse-repetition frequency, energy per pulse, and resolution. The measurement time per frequency ΔT_f is given in terms of the required energy and average power by:

$$\Delta T_f = \frac{E_T}{P_a} \tag{3}$$

This result is independent of modulation, compression schemes or integration and, therefore, since the desired range establishes the required power, the measurement time can be related to the average delivered power and the range. (Note that the power used by the transmitter is simply related to the delivered power by the overall transmitter efficiency--a practical quantity expected to be between 20 and 35 percent. Also, the total power taken by the equipment includes other components. For optimum design, the transmitter must take a major portion of the power.) The relationship is shown in Figure 6 for the same conditions as in Figures 3, 4, and 5. The greater the range for a given power, the longer the measurement time. Only by increasing the average power can the time be reduced. The upper scale in the figure also shows the total sounding time for 100 frequencies. It can be seen that for an average power of 5 watts, 100 frequencies are sounded in about 2 seconds at a range of 35,000 km.

Another fundamental, but simple, relationship is the average delivered power, P_a, in terms of the energy per pulse and the prf. P_a is given by:

$$P_a = E_p \times \text{prf}, \tag{4}$$

where E_p is the energy per pulse. Since the range determines the maximum prf, if ambiguity is to be avoided, there is a minimum energy per

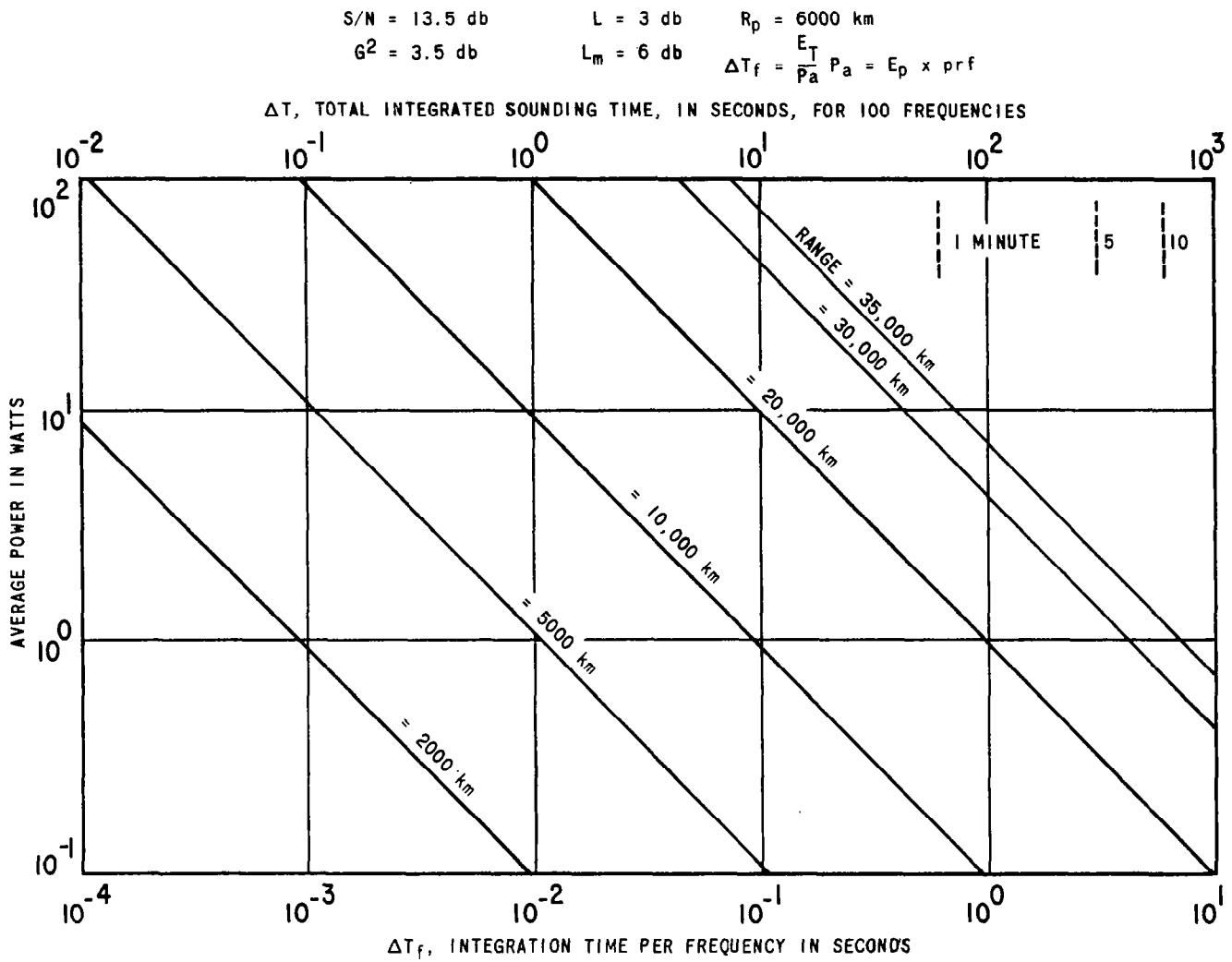

FIGURE 6. AVERAGE SOUNDING TIME PER FREQUENCY AND TOTAL INTEGRATION TIME FOR 100 FREQUENCIES VS AVERAGE POWER FOR VARIOUS RANGES

pulse for any range with a given average power. If a lower prf is used, the energy per pulse may be greater. Since the number of coherent integrations, n, required to achieve the required energy E_T is E_T/E_p, it is preferable to increase the energy per pulse by decreasing the prf, for a given P_a. Although the measurement time, ΔT_f, remains the same, the number of required integrations is minimized. The increase of E_p is achieved by widening the pulse, P_m being limited. The wider pulse results in poorer resolution, unless pulse compression is used. Without pulse compression, the pulse width must correspond to that for the required resolution. As a result, the energy per pulse is the minimum for a fixed peak power, and the prf is maximized. The number of integrations is consequently maximum to achieve the required transmitter energy E_T. Thus, pulse compression reduces the amount of integration required while retaining the desired resolution.

If the average delivered power is increased for a given prf, the energy per pulse must increase. With a fixed peak power, more energy is obtained by widening the pulse and a greater pulse-compression factor is required to attain the same resolution. The tendency will be to increase the power taken by the signal processor, resulting in an increase of the total power drain. Thus, there is some optimum level for the transmitter, which will maintain the total power drainage below some level for a desired resolution. Maintenance of resolution and range for a minimum power drainage is only possible by increasing the peak pulse power or reducing the prf. Since the former is a state-of-the-art problem, the latter course has been followed. The tradeoff is between measurement time, total average power drainage, peak pulse power, and the pulse compression factor.

If a complete sounding cycle involves sounding at n_f frequencies, the angular motion in latitude and longitude of a spacecraft in orbit about a planet may be found once the altitude and average power are specified. The total time for a complete sounding may be deter-

mined as in Figure 6 and from this the $\Delta\theta$ representing the angular motion. The relationship is given by:

$$\Delta\theta = 8.56 \times 10^{-6} \left(1 + \frac{H}{R_p}\right)^2 H^2 \frac{n_f}{P_a} \qquad (5)$$

where $\Delta\theta$ is in degrees and H, the altitude, is in thousands of kilometers. For the same parameters as in the previous figures, Figure 7 exhibits the relationship for earth with $n_f = 100$. Altitude is plotted versus $\Delta\theta$ for various values of the average power P_a. For $P_a = 1$ watt, and $H = 35,000$ km, $\theta = 1.7$ degrees. If $P_a = 1/2$ watt at the same altitude, $\Delta\theta = 5.3$ degrees. Again, this relationship is independent of modulation methods or processing and is fundamental for any system. To achieve a value of $\Delta\theta$ between 1 and 2 degrees for altitudes between 20,000 and 35,000 km, P_a must be between 1/2 and 3 watts for $n_f = 100$ in this particular calculation for the Earth. As n_f increases beyond 100, $\Delta\theta$ increases proportionately. Either P_a must be correspondingly increased or the maximum altitude must be reduced to maintain $\Delta\theta$. The reduction in H goes roughly as the 4th root of the change in n_f for altitudes large compared with the planetary radius, as would be the case for Mars and Mercury. For a large planet, such as Jupiter, the change in H would be closer to the square root of the change in n_f. For Earth and Venus, the root would be intermediate. Thus, H (actually the sounding range) does not change as rapidly as the change in n_f for a given $\Delta\theta$.

For a simple pulse of width τ, the resolution is $\Delta R_\tau = c\tau/2$. The minimum period between pulses for a range H is $T = 2H/c$. Therefore, the average delivered power $P_a = P_m c\tau/2H$, where P_m is the peak pulse power. If both P_a and P_m are fixed, then $\Delta R_\tau = P_a H/P_m$, and it is seen that ΔR_τ must increase with H. Figure 8 shows this relationship. The variation of P_a with H for a constant τ and P_m is also shown. Thus, the simple pulse system either does not fully use the average delivered power (actually the power taken by the transmitter) by maintaining its resolution capability or its resolving power is degraded if P_a is to remain

$S/N = 13.5$ db $\quad G^2 = 3.5 \quad R_p = 6000$ km

$L = 3$ db $\quad L_m = 6$ db

n_f = NUMBER OF FREQUENCIES = 100

$$\Delta\Theta = 8.56 \times 10^{-6} \left(1 + \frac{H}{R_p}\right)^2 H^2 \frac{n_f}{P_a}$$

H = ALTITUDE IN THOUSANDS OF km

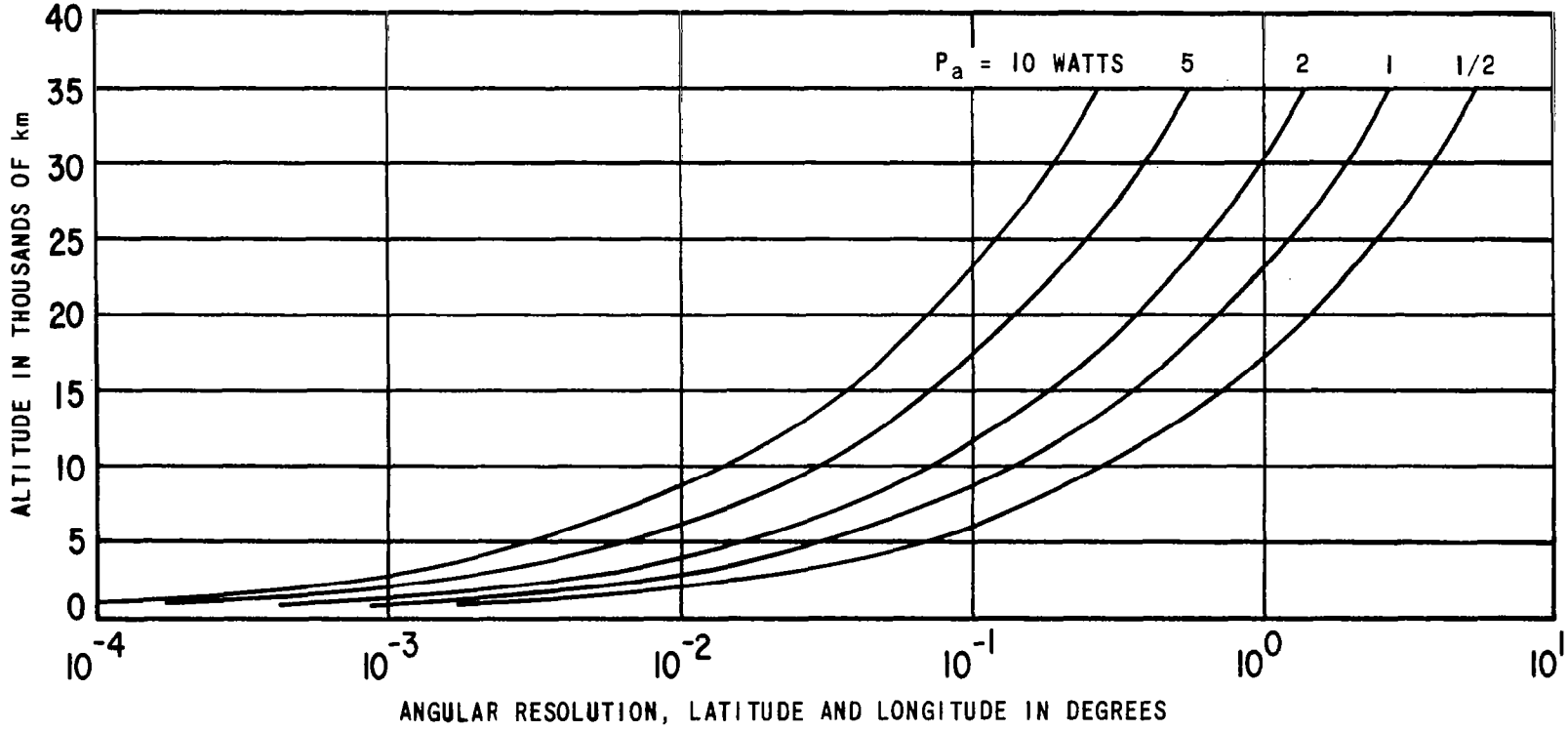

FIGURE 7. MEAN ANGULAR RESOLUTION IN LATITUDE AND LONGITUDE VS ALTITUDE FOR VARIOUS AVERAGE RANGES

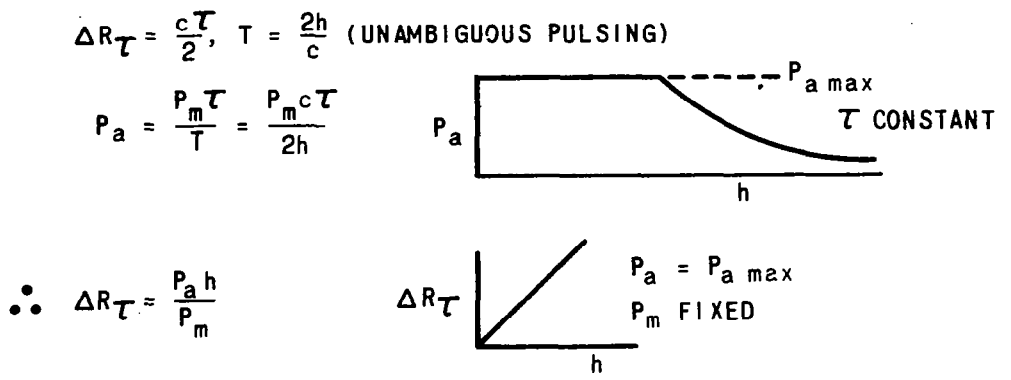

FIGURE 8. RESOLUTION

at its maximum value. In using pulse compression, the resolution is improved by the pulse-compression factor N. However, the same basic variation shown in Figure 8 is retained unless N varies with H. N is actually varied; however, it is simplest to change the compression factor in steps so that one actually has a set of submodes in the operation of the system. The simplest form would be to add pulse compression at the greatest ranges. Nevertheless, a fixed pulse width and fixed N factor will result in incomplete use of the available power at the greatest ranges.

3. APPLICATIONS TO MARS

Two typical missions were considered. One for the Mars-Voyager orbiter, the other for the Mars-Mariner fly-by mission.

In view of the fact that these missions were to contain a number of other experiments and that the total available space, power, and weight for all experiments are limited, constraints were arbitrarily placed on weight, power, and size. In addition, the interface of the spacecraft with the antenna was considered a particularly severe problem. As hypothesized, the missions would be the first to contain complete sounding equipment for planets other than earth. In addition, the long flight to the planet necessitated very high reliability. Therefore, it was decided to simplify the system by: (1) using a smaller number of frequencies in a fixed frequency version, (2) restricting the frequency range, (3) limiting the maximum range of the sounder to no more than 20, 000 km, and (4) requiring the smallest antenna reasonable for the frequency band and maximum range.

This investigation was an extension of work performed during the previous effort reported in CR-493. In that work, a system was described for sounding out to 40, 000 km with a 120-foot and 40-foot dipoles (tip-to-tip length) with a transmitter delivering a peak pulse of 500 watts and any number of frequencies. The systems are here investigated to a much greater extent in comparison with the previous study. The details are described in Sections III and IV. A smaller transmitter and simpler signal-processing system were included.

Section III describes various applications. For Voyager there are two:

1. An updated 40, 000 km system with improved resolution,
2. A more limited maximum range system ($\geq$15, 000 km).

For Mariner there is a single application. In this section, the requirements for these applications will be described as well as some of the underlying thinking and the overall system description.

3.1 MARS-VOYAGER ORBITER

For the Voyager orbiter, the 120- and 40-foot dipoles were assumed so that the energy requirements established in the previous program were the same. Thirty sounding frequencies were assumed in the band 0.5 to 12 MHz with 0.25 and 0.5 MHz spacings. Resolution requirements were based on the Mariner IV discovery that the scale height above the peak density is 20 to 25 km. Soundings were required for ranges less than 15,000 km and acquisition for ranges equal to or greater than 15,000 km (except in the case of the updated 40,000 system). Therefore, the resolution requirement for ranges less than 7000 km was set at 7.5 km and, for greater ranges, 30 km. The first resolution figure is $\approx 1/3$ of the Mariner IV measured scale height. The second figure is greater than the measured value. It is based on a compromise between the performance desired at long ranges and the speculation that much of the electron density scale heights of Mars could be as great as 100 km or greater. To provide the smaller resolution at long ranges would increase the system weight, power, and size. In any event, much useful data permitting interpretation could be obtained with a 30-km resolution, even if the Martian ionosphere possessed scale heights of about 25 km. In view of the precision being about half the resolution, these resolution requirements also implied an ability to measure to an accuracy of 3.75 and 15 km, respectively. The 15-km figure is smaller than the measured scale height and further justifies the 30-km resolution figure. The transmitter peak pulse power was reduced to 250 watts (500 watts in the updated system) consistent with available transistors and constraints in weight and power. The maximum weight, size, and power permitted was 20 pounds (including the antenna weight), 0.5 cubic feet, and 15 watts, respectively. These numbers were considered suitable for a mission such as Voyager and a compromise between the total weight, size, and power requirements specified for all the experiments of the mission--namely, 150 pounds, 7.5 cubic feet, and 50 watts, respectively.

The orbit was taken as elliptical about Mars and for guidance purposes a set of orbits with a periapsis altitude of 2000 km and various apoapsis altitudes out to 46, 600 km were used. Figures 9 and 10 are graphs of time from periapsis versus altitude and doppler shift versus altitude, respectively. The parameter is the apoapsis altitude. It can be seen from these curves that the maximum doppler shift increases as the eccentricity increases, reaching 11.3 Hz per MHz at an altitude of about 6000 km for the 46, 000-km apoapsis curve. The doppler shift curves provided needed input information for the coherent integration technique. From the time versus altitude curve, the number of soundings per orbit and per 1000 km of altitude can be computed as a check on the suitability of a system.

Figure 11 is a plot of time, angular rate, and time available for a complete sounding cycle for an elliptical orbit with an apoapsis altitude of 40, 000 km and a periapsis altitude of 1000 km. The time for a number of values of increments in latitude or longitude per sounding cycle is also shown. The values in the graph are for horizontal surface distances of 50, 100, and 150 km, which correspond to $\Delta\theta = 0.84$, 1.7, and 2.5 degrees, respectively.

Figures 12 and 13 are the same as Figures 9 and 10 except for a periapsis altitude of 500 km.

From Figure 11 it can be seen that the available time fortunately increases with altitude, since the range to the reflecting level is increasing. For the less eccentric orbits reaching lower maximum altitudes, less time would be available. One could equate ΔT_f, which is range dependent, to the available time derived from the orbit calculations and establish limits for P_a based on a given angular increment $\Delta\theta$. Since the nominal orbit was not specified, this calculation was not performed.

To use only a small part of the data rate capability of the telemetry system, the threshold detection scheme was required to transfer only a very few returns per sounding frequency. Detection of only

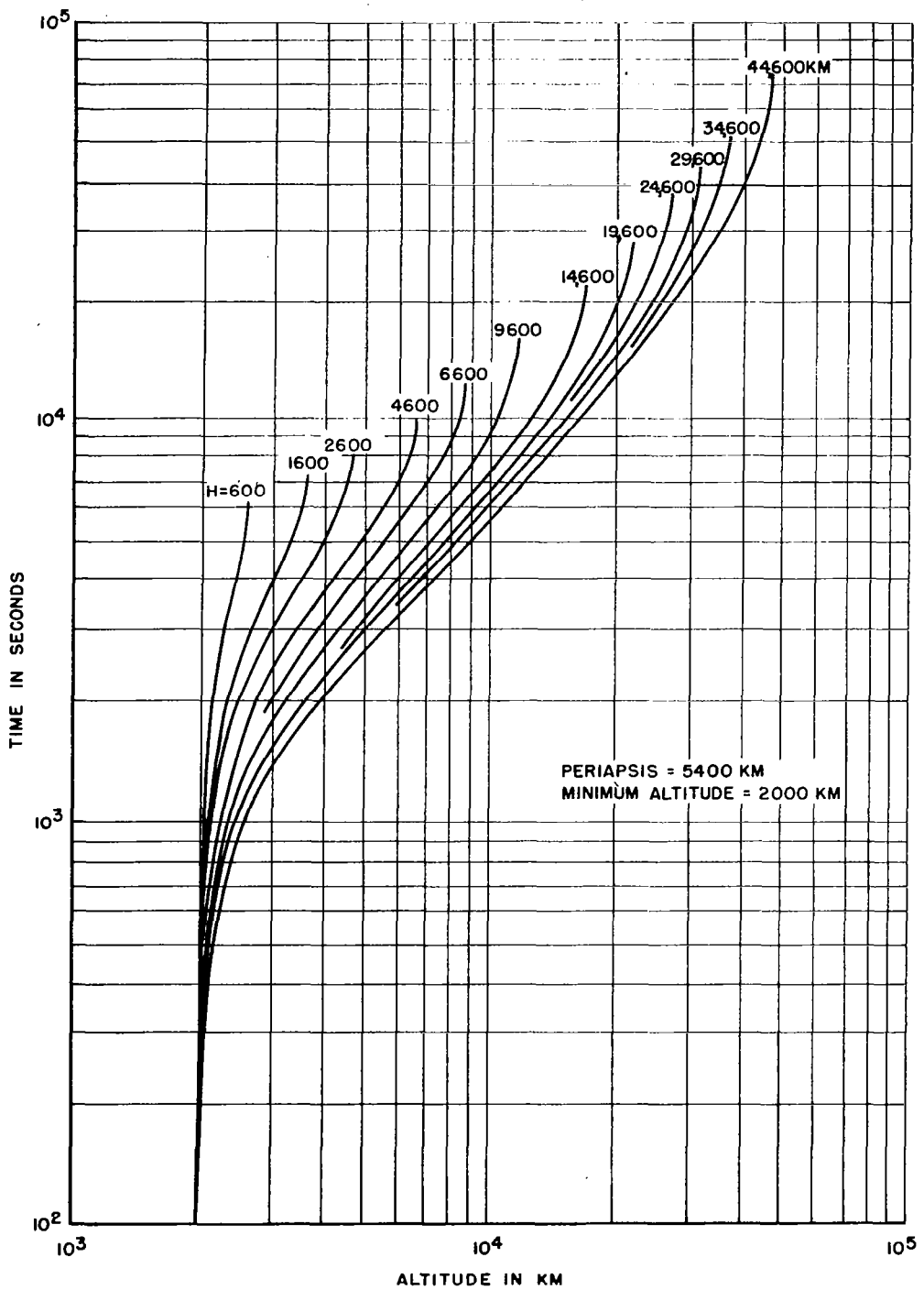

FIGURE 9. TIME VS ALTITUDE IN ELLIPTICAL ORBIT ABOUT MARS - 2000 km MISS DISTANCE

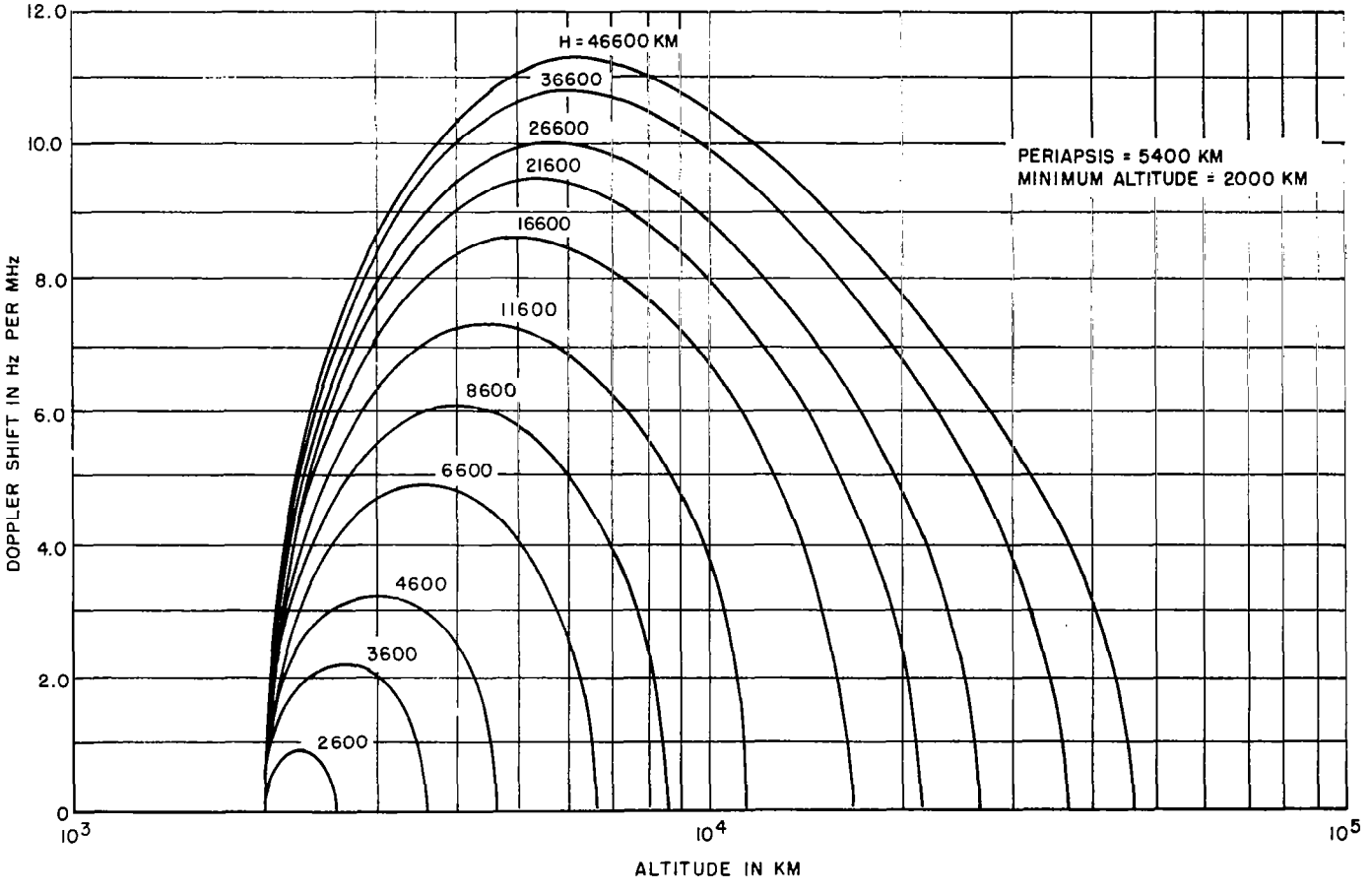

FIGURE 10. MARTIAN ELLIPTICAL ORBIT DOPPLER SHIFT VS ALTITUDE - 2000 km MISS DISTANCE

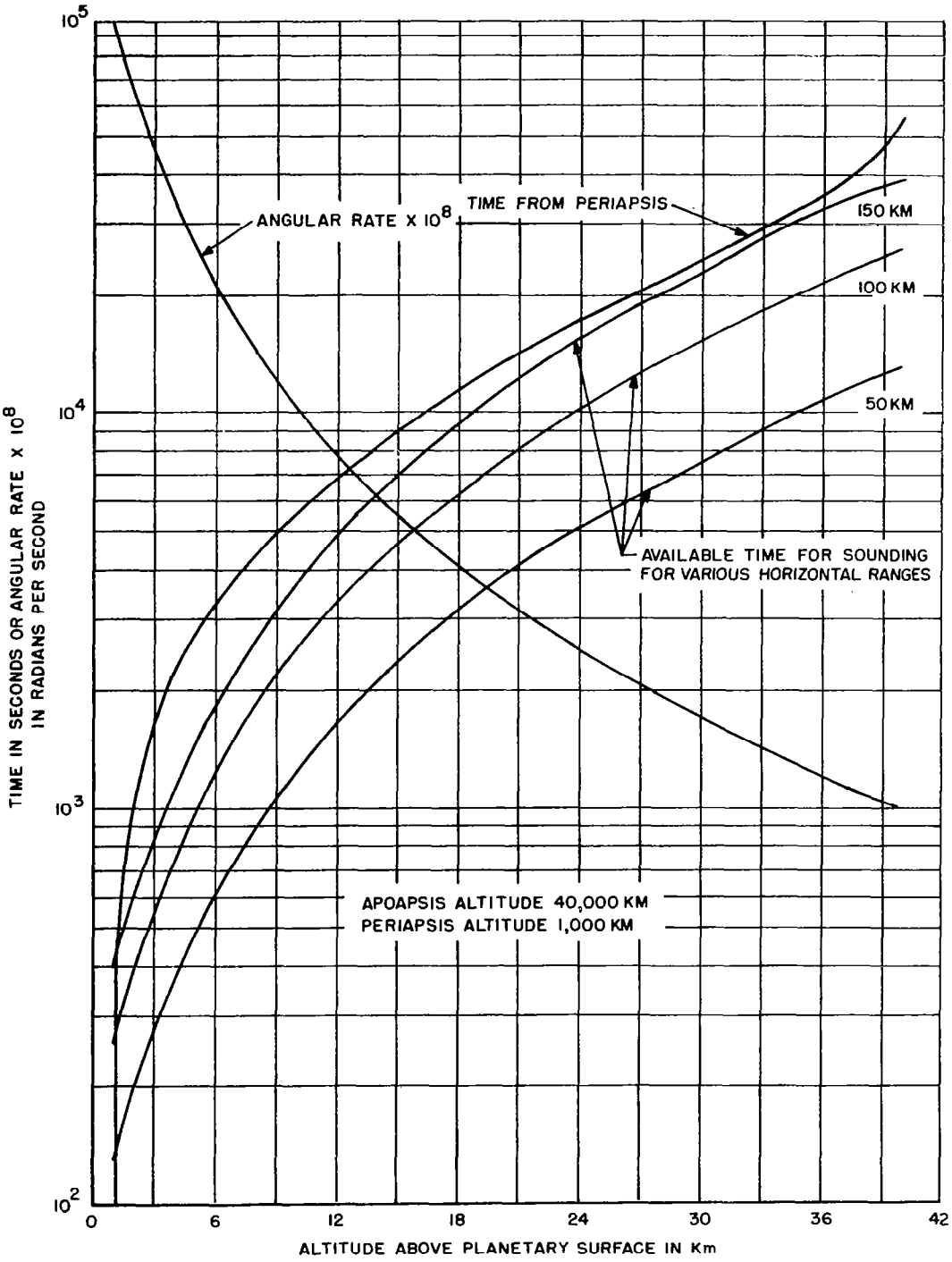

FIGURE 11. TIME, ORBITAL RATE, AND AVAILABLE TIME FOR SOUNDINGS VS ALTITUDE - MARTIAL ELLIPTICAL ORBIT

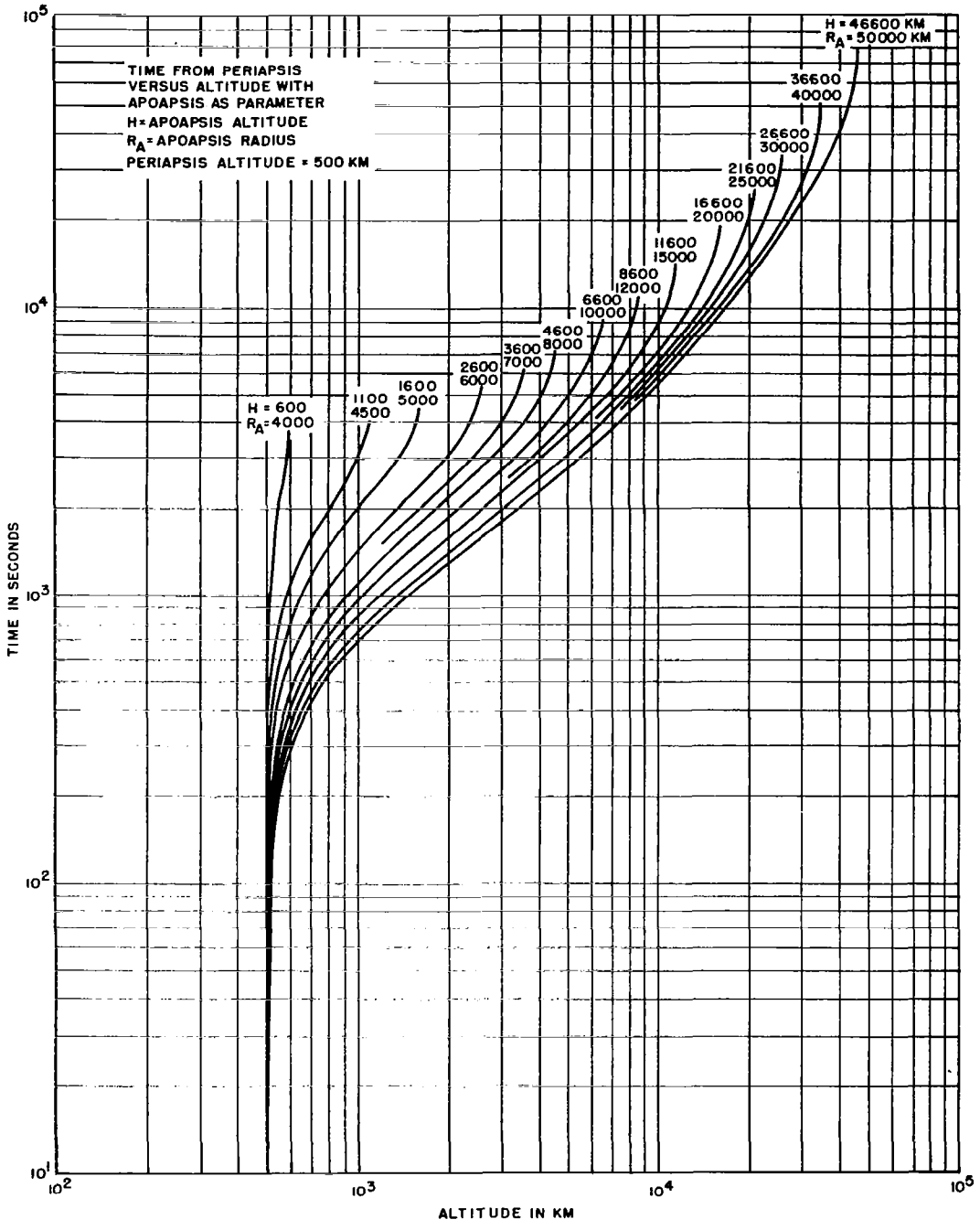

FIGURE 12. TIME VS ALTITUDE IN ELLIPTICAL ORBIT ABOUT MARS - 500 km MISS DISTANCE

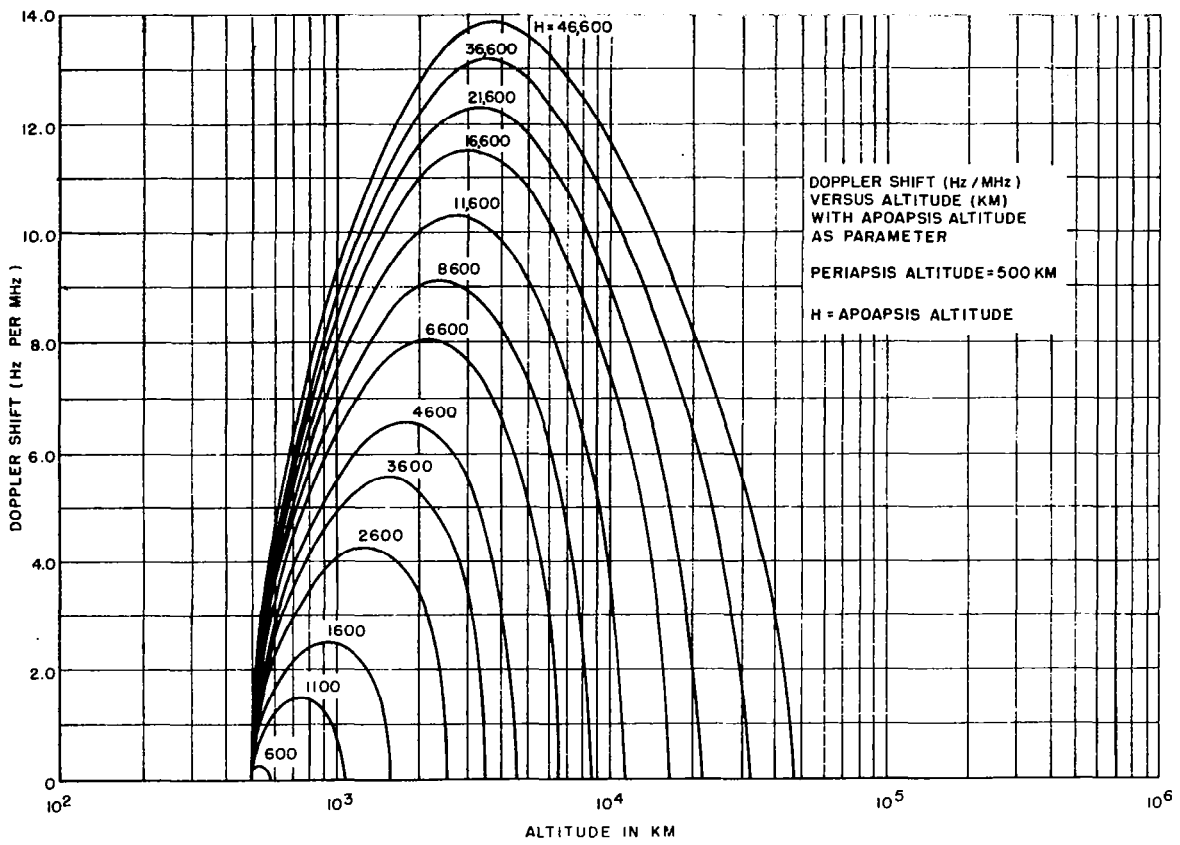

FIGURE 13. MARTIAN ELLIPTICAL ORBIT DOPPLER SHIFT VS ALTITUDE - 500 km MISS DISTANCE

a very limited number of echoes per sounding was further justified, since mode splitting was not expected as a result of the absence of a significant magnetic field about Mars. However, with higher data rates, all detected echoes could be readily provided.

Figure 14 is an overall block diagram of the reduced range (15,000 km) Voyager system. This system also contains provision for measuring radio noise. The transmitter consists of power output and lower level stages driven by a modulator and code generator to provide the pulse-compression signal. The source is a frequency synthesizer that also provides local-oscillator signals to the receiver. The receiver consists of T/R devices to protect the receiver during transmission, an RF amplifier, mixer, IF amplifier, and a filter limiter combination (Dicke-Fix) for each mode of operation. The signal processor provides pulse compression and noncoherent integration (Section III). A programmer controls the entire experiment and provides the digitized output data. Table III shows the estimated weight, size, and power for the entire system with antennas. The data-rate requirement is 30 bits/sec for soundings in the near and intermediate ranges. In the far range, the bit rate can be as low as 5 bits/sec. Out to a range of 7000 km a complete sounding can be performed every 20 seconds. Beyond 7000 km, complete soundings are made every 120 seconds. Under these conditions, between 400 and 1000 ionograms will be obtained per orbit, the number depending on the orbit, semimajor axis.

TABLE III

ESTIMATED WEIGHT, VOLUME, AND POWER FOR MARS-VOYAGER ORBITER

	Weight (pounds)	Volume (in^3)	Power (watts)
Signal Processor	3.0	350	3.0
Programmer	1.0	50	1.0
Power Converter	1.5	50	3.5
Transmitter	3.0	200	5.0
Receiver	3.0	200	2.5
Antennas (120-foot, 40-foot dipoles)	6.5	-	-
Total	18.0	850	15.0

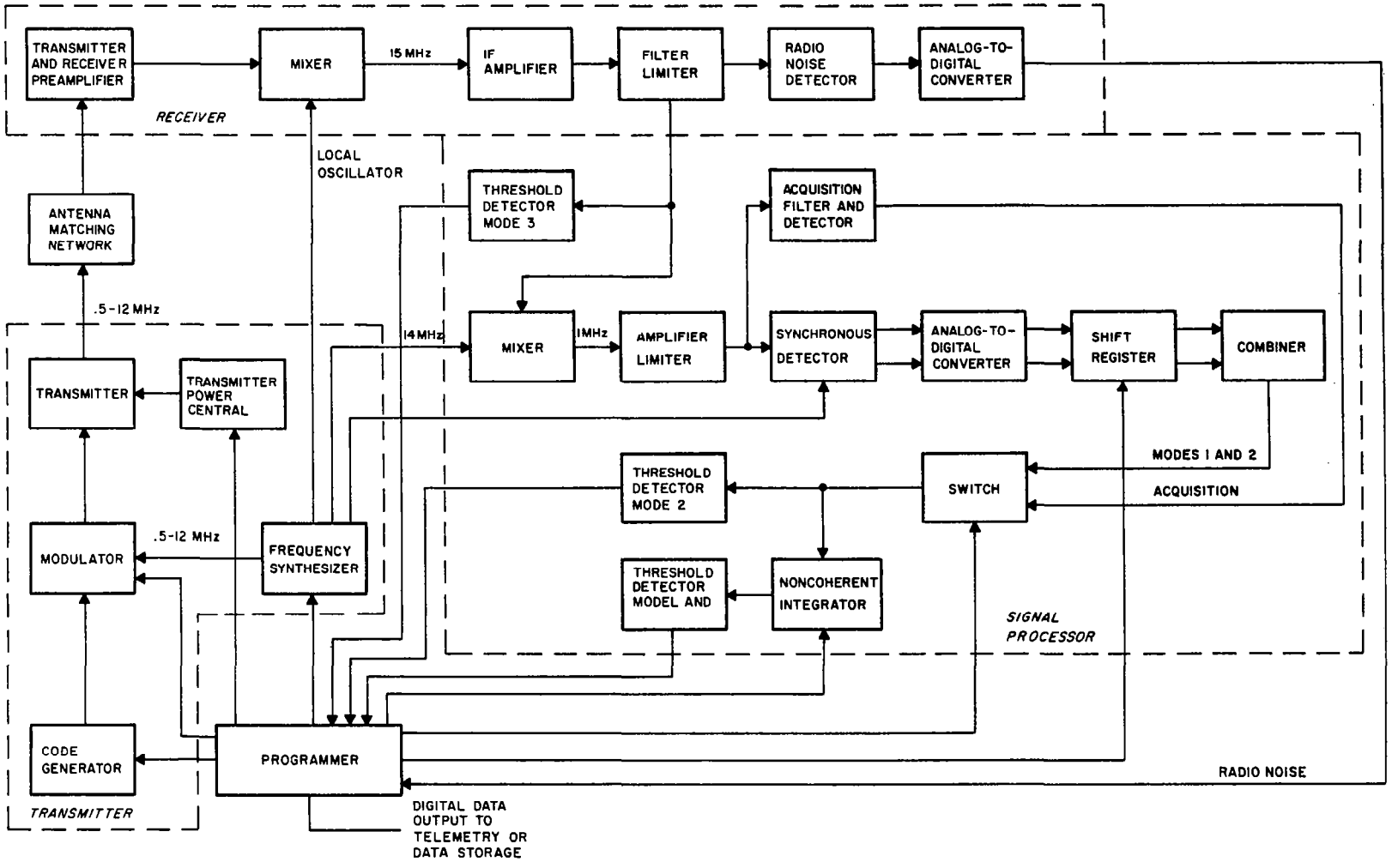

FIGURE 14. BLOCK DIAGRAM OF MARTIAN IONOSPHERIC SOUNDER

3.2 MARS-MARINER FLY-BY

It was assumed that the orbit would be parabolic, in which case Figures 15 and 16 illustrate the time-altitude and doppler shift-altitude relations. These curves were drawn for various values of the periapsis altitude (miss distance). 15,000 km was taken as the maximum periapsis altitude. (A large miss distance would, presumably, only result from a malfunction in the guidance system.) A 2000-km periapsis was considered nominal and the maximum range capability was set at 20,000 km. It can be seen from Figure 16 that the doppler shift is greater, the smaller the periapsis altitude, reaching 14.75 Hz per MHz at an altitude between 5000 and 6000 km for a periapsis altitude trajectory of 1000 km. 13.5 Hz per MHz is reached at 7000 km for a periapsis altitude of 2000 km. Figure 15 permits a determination of latitude and longitude increments per sounding once a system is designed and a relationship can be established involving P_a and the desired increment $\Delta\theta$ as stated before for the Voyager mission.

Since the payload capability of this mission is smaller than that of the Voyager, it was decided to simplify further the system while retaining the long-range features. For that purpose, the number of sounding frequencies was reduced to 12, and noncoherent integration was chosen as the technique to provide the range capability. In this system, resolution was determined by the pulse width, thereby necessitating a longer total measurement time. The resolution requirements were degraded somewhat, according to range, to 30 km, 60 km, and 120 km; that is, near, intermediate, and far, respectively. Based on accuracy, these figures appeared to be good for near ranges, but sacrificed some definition at the longer ranges. The near range was to extend to about the midpoint--namely, 7500 km. The intermediate range was to extend from 7500 to about 10,000 km and the far range was for distances exceeding 10,000 km. This division of range was somewhat arbitrary but considered good practice for a first mission. Fine ranging was desired to 15,000 km with acquisition to 20,000 km.

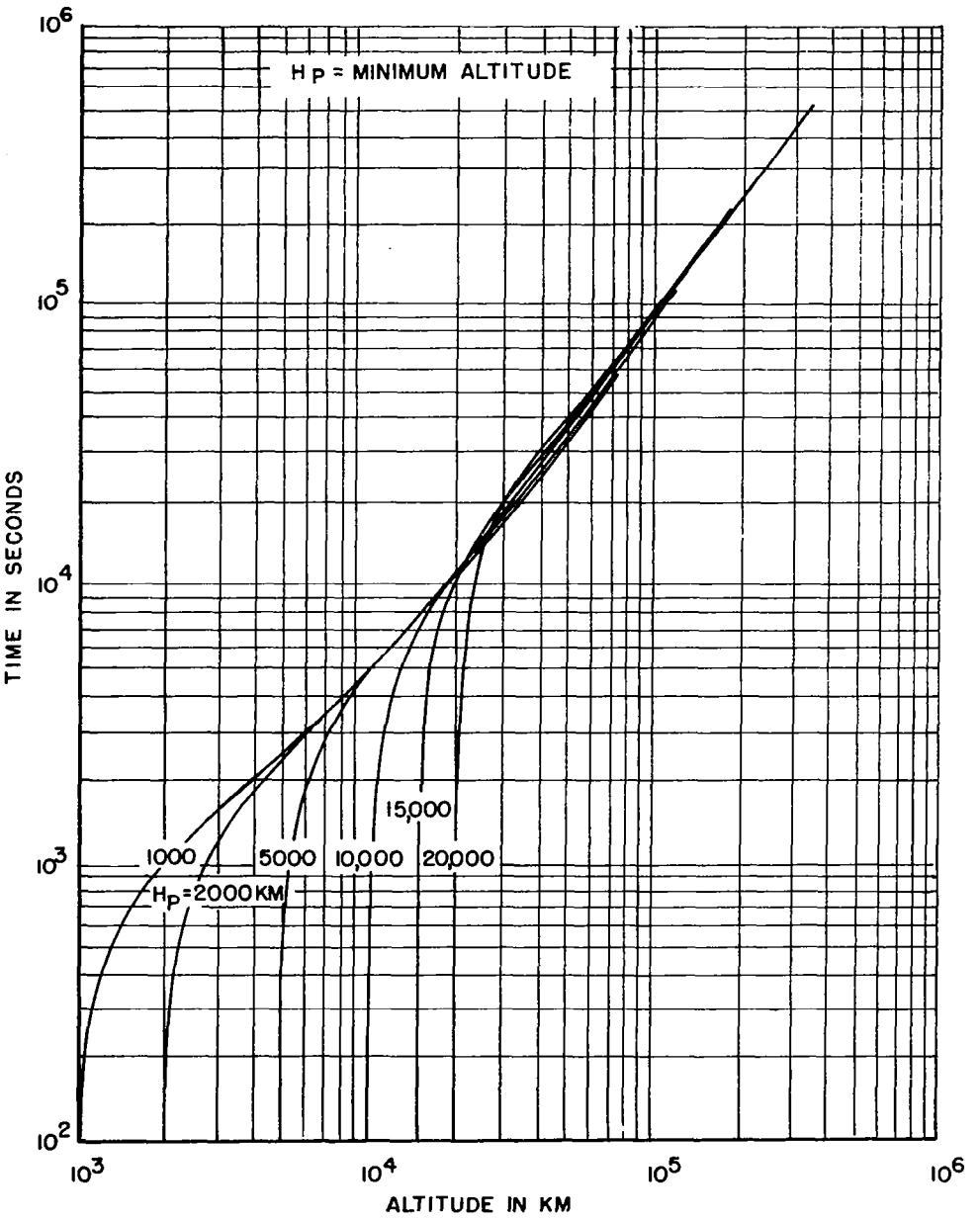

FIGURE 15. TIME VS ALTITUDE IN PARABOLIC ORBIT ABOUT MARS

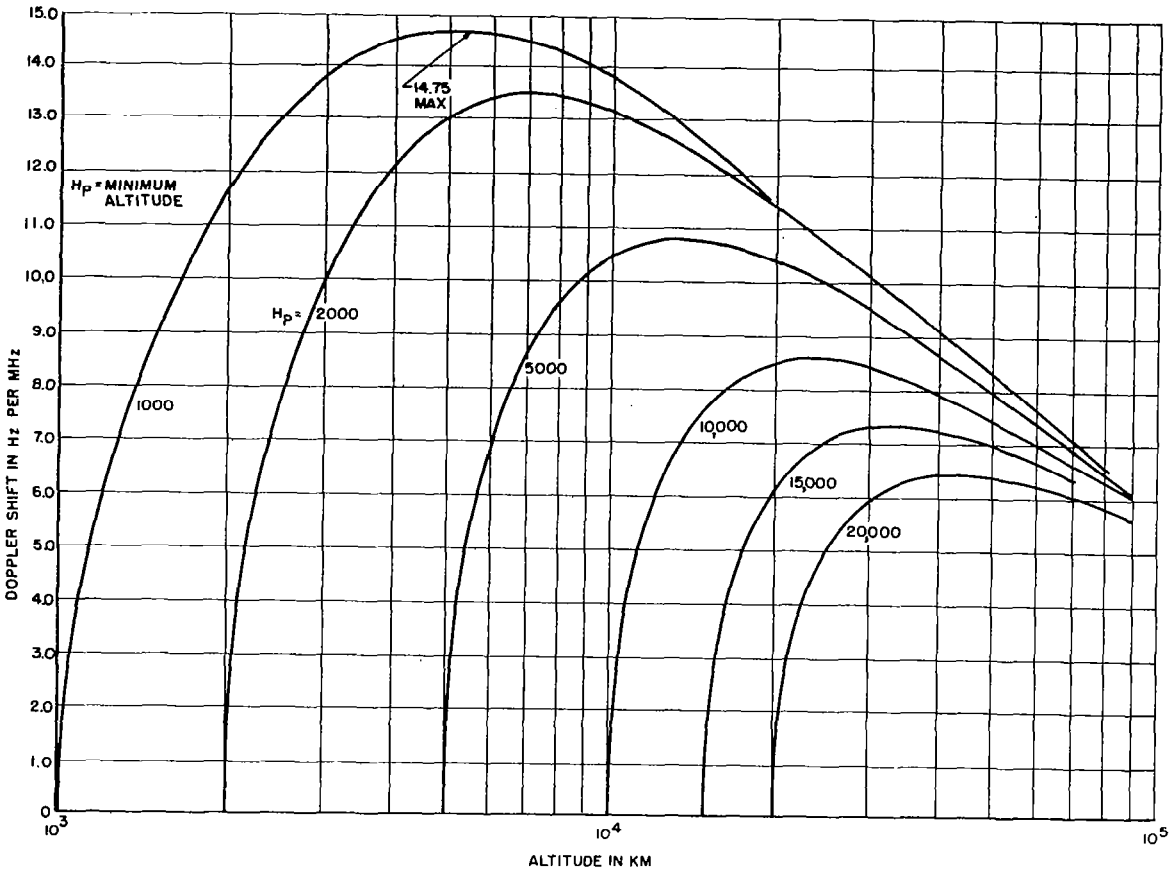

FIGURE 16. MARTIAN PARABOLIC ORBIT DOPPLER SHIFT VS ALTITUDE

The frequency range was 0.5 to 10 MHz spaced logarithmically. Figure 17 shows a model of the Martian ionosphere electron density profile above the peak based on an extrapolation of the Mariner IV results. Indicated on the profile are the reflection points for 12 typical frequencies. The two higher frequencies would be reflected from the surface of the planet. To save weight, the antenna consisted of a single 60-foot dipole (tip-to-tip). Its impedance is shown in Figures 57 and 58.

Using equations 1 and 2, the transmitter energy was calculated assuming a matching coil for each frequency, a signal-to-noise ratio of 12.5 db ($P_d = 0.9$ and a $P_{fa} = 10^{-5}$), and zero fixed losses (the medium is assumed isotropic and the antenna is properly oriented). The results are shown plotted versus frequency in Figure 18 for various values of matching coil Q's and ranges. It can be seen from these curves that the required transmitter energy increases significantly at the lower frequencies, but tends to level off below 1 MHz due to the decrease in cosmic noise. Above 8 MHz, the 60-foot antenna becomes inductive, but the pattern does not break up significantly until the frequency is closer to the full wavelength frequency of 16 MHz. At the lower frequencies, below about 2 MHz, the higher values of Q can be used to reduce the energy requirements. This procedure is also to be followed if the matching networks are not simple matching coils but, rather, match for more than one frequency. Then, the higher Q values can be used to compensate for the additional losses. Nevertheless, Figure 18 was used to guide the design of the system.

The required transmitter output was based on state of the art transistors. The desired characteristic is shown in Figure 19. The information of Figures 18 and 19 provided the design requirements for the signal processor and the transmitter. From these data, it was possible to devise a multimode processing system (Section III).

To reduce the sounding time for ranges greater than 12,000 km, the system was compromised by eliminating two of the lower frequencies; 0.5 and 0.85 MHz (Figure 17). Beyond 15,000 km, the system had to sound only from 1.9 MHz and up. These compromises permitted soundings to be completed in sufficient time to avoid repositioning the fine range window (Section III).

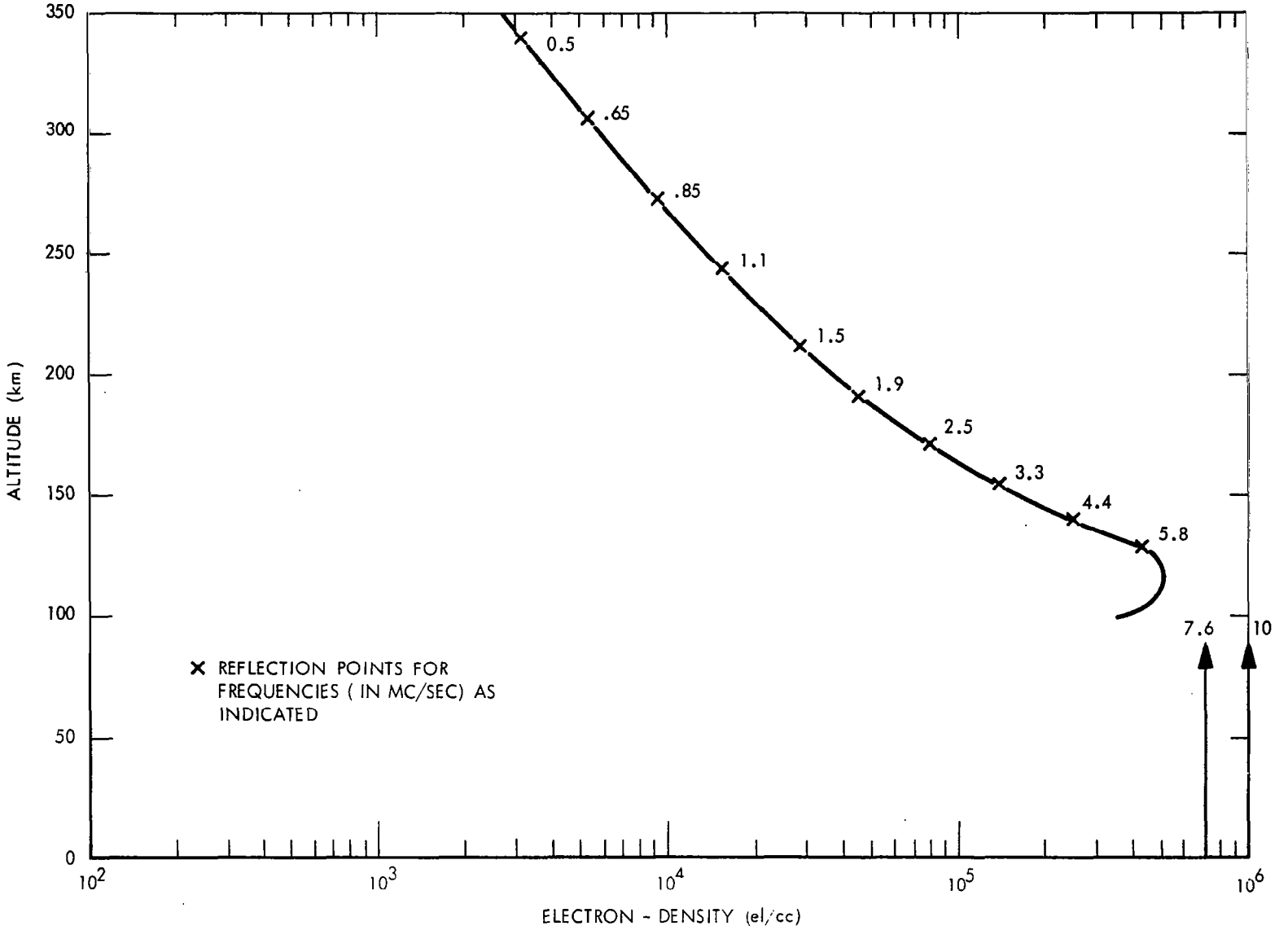

FIGURE 17. ELECTRON DENSITY MODEL

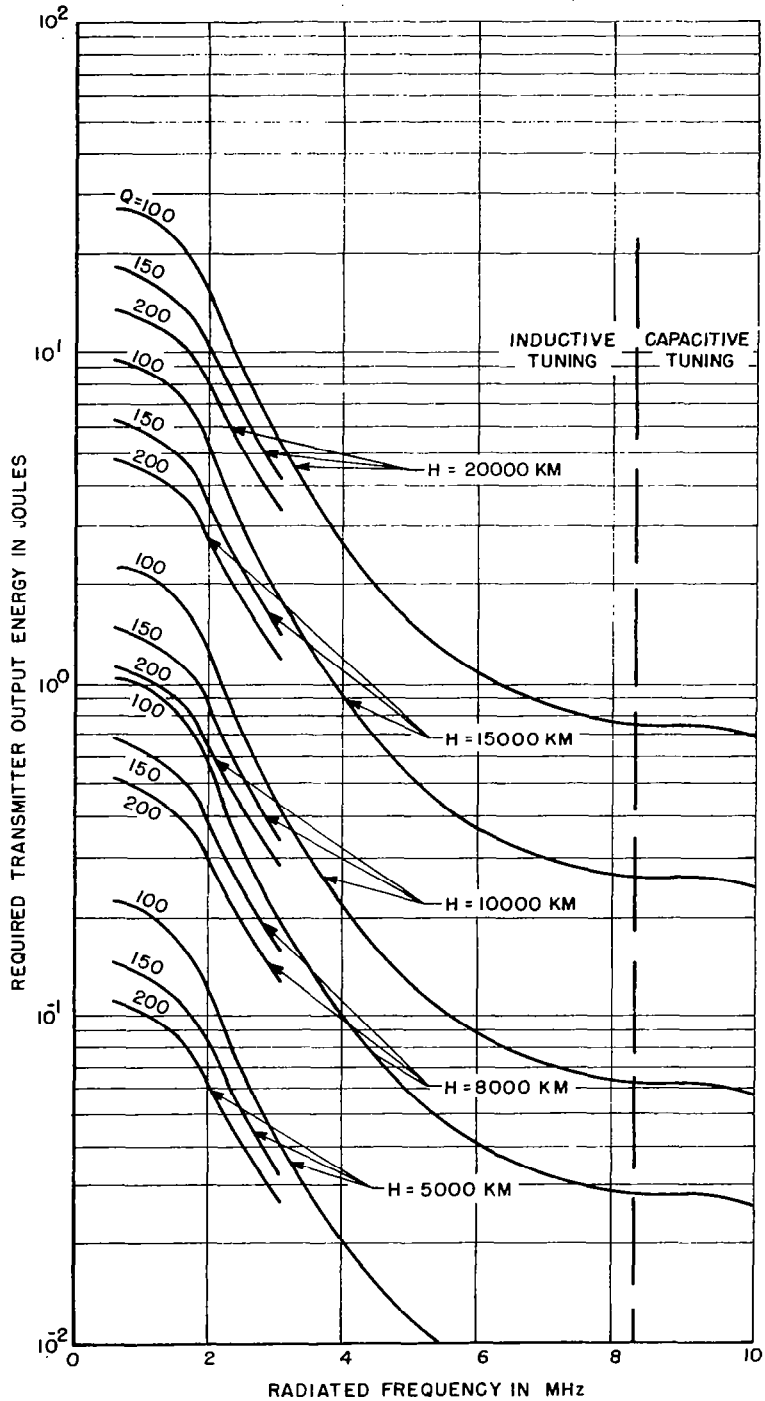

FIGURE 18. REQUIRED TRANSMITTER OUTPUT ENERGY VS FREQUENCY FOR 60-FOOT DIPOLE, PLANET MARS

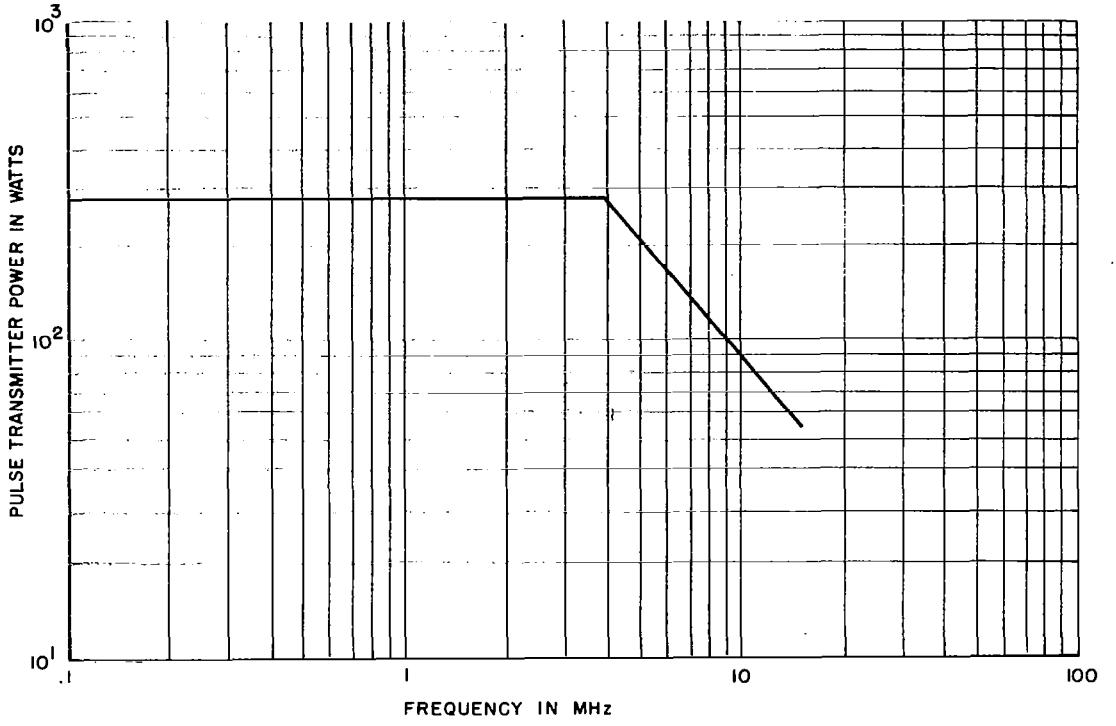

FIGURE 19. PEAK PULSE TRANSMITTER POWER VS FREQUENCY

The maximum weight (less antenna), volume, and power were specified to be 10 pounds, 0.33 cubic foot, and 8 watts. These figures were a compromise between system performance and the total weight and power available to all mission experiments; namely, 60 to 70 pounds and 30 to 40 watts. The maximum output data rate requirement was set higher than that for the Voyager-Mars orbiter, since fly-by missions have only one opportunity in flight. For that purpose, 60 bits/sec was arbitrarily chosen. The 60-foot dipole weight was essentially fixed and amounted to about 2.8 pounds, so that the total experiment weight was to be under 13 pounds.

The overall system block diagram is shown in Figure 20. The various units are shown in greater detail than in Figure 14 for the

Voyager mission. The major subsystems are the same in nomenclature, but the signal processor simply stores digital bits noncoherently until detection by a threshold device. The transmitter delivers pulses of three widths according to range. Operation of the system for ranges below 3000 km is as a simple pulse sounder, since integration is not required for these distances. The programmer and frequency synthesizer are also simpler; however, integration is still controlled according to range and frequency. The receiver is essentially the same as for Voyager and provides an output for cosmic noise measurement.

The estimated weight, size, and power fall within the requirements given. The time for a complete sounding varies from a minimum of 2.4 seconds for ranges less than 3000 km to 250 seconds at about 10,000 km and 750 seconds at 15,000 km. The minimum number of electron density profiles would be 25 if the guidance system erred and caused a miss distance of 15,000 km. The number of soundings increases with closer distances to the planet reaching 1500 soundings when the spacecraft trajectory comes within 2000 km of the planet. For the closer approaches, the increment in latitude and longitude per sounding is less than or equal to 2 degrees for most of the soundings. The data rate is satisfied, being no more than 55 bits/sec when the trajectory comes within less than 3000 km of the planet and reaching a minimum of 0.36 bits/sec at maximum range. The maximum number of bits accumulated is about 10^5.

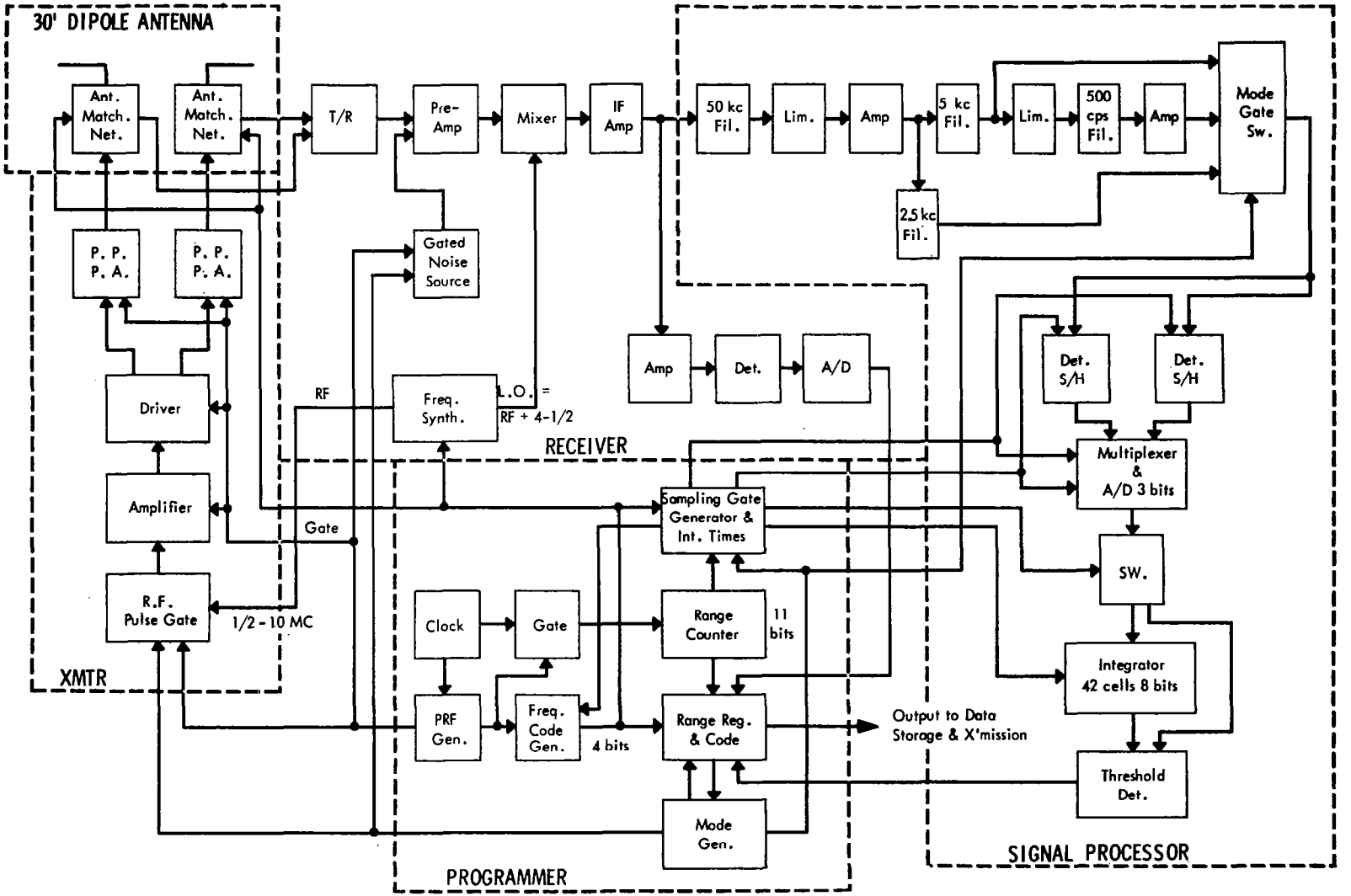

FIGURE 20. BLOCK DIAGRAM OF MARS-MARINER TOPSIDE SOUNDER EXPERIMENT

SECTION III
SIGNAL PROCESSOR

1. INTRODUCTION

There were two phases to this part of the study. One was concerned with a signal processor for the Voyager-Mars orbiter mission, the second for the Mariner-Mars fly-by.

The Voyager application consisted of two parts. One updated the 40,000-km system in CR-493 to resolution requirements resulting from the Mariner IV mission. The other was for a reduced range system with a maximum range requirement of some distance greater than or equal to 15,000 km. The latter was simplified compared with that of the first part by eliminating the coherent integration system. Pulse compression and noncoherent integration were provided. Most of the effort for this application was theoretical, consisting of studies of digital compression schemes, coding and losses due to quantization and limiting. The results of these analyses are essential to the design of the required system.

For the Mariner mission, the system was further simplified by using only noncoherent integration. The application received considerable design effort. The various blocks of the system were examined in detail and block diagrams of each were worked out. Important components were reviewed and preliminary selections were made.

In this section, the signal processor for each of these applications will be described.

2. VOYAGER APPLICATION

2.1 40,000-km SYSTEM

In the previous study, a system was outlined with this maximum range capability based on a 75-km resolution requirement.

Since the Mariner IV mission measured a scale height of 20 to 25 km at the Martian latitude 55 degrees South in the late afternoon, it is apparent that any sounding system must have far better resolution capability. The first requirements were for a 7.5-km resolution to at least 7,000 to 8,000 km with degraded resolution beyond. A figure of 45 km was adopted for the latter, since the expected precision of half the 45 km (22-1/2 km) is comparable with the measured scale height.

In this part of the report, the entire processor system will be reviewed and a system described which attains the much greater resolving ability. As in the previous study, the peak transmitter pulse will be taken as 500 watts, and the 120-foot and 40-foot dipoles are assumed. The energy requirements are then the same as in CR-493. Here again, the most efficient approach is to provide a low-resolution acquisition mode to reduce the number of high-resolution cells for which integration storage is necessary. Sounding is then continued in the range window that is established, using pulse compression to increase the energy per pulse, without loss of resolution, and coherent integration over a number of transmissions.

2.1.1 DESIRED PARAMETERS

The previous work used a 10-msec pulse at long ranges. The choice of this pulse width is somewhat arbitrary. It depends, to some degree, on the desired number of coarse range elements or range storage cells, the subsequent use of these cells in the range window for fine range sounding, limitations on coherent integration, prf, and average power. The number of cells depends on the availability of storage units, since for economy one wants to design a system in which a standard unit will be utilized. Several versions of a system may be realized with differing pulse widths, prf's and range cells, since selection between them may be arbitrary. Therefore, for the purposes here, the 10-msec pulse is retained, and the energy per pulse is 5 Joules. The acquisition range cell for this pulse width is 1500 km.

At the longest range, 40,000 km, the previous report indicates that about 100 Joules are required at the higher frequencies for acquisition. Coherent integration of 20 pulses would provide this energy. However, quantization and Dicke-Fix losses, as described in the appendices, require somewhat greater energy, and an additional 3 db of energy will be used by integrating 40 pulses. The maximum prf for 40,000 km is somewhat less than 4. For this prf, the average delivered power is 20 watts, which is excessive. Therefore, the prf was set equal to 2, halving the delivered power. With a prf of 2, 40 pulses are provided within 20 seconds.

For fine ranging beyond 20,000 km, the same pulse width (10 msec) is used. However, to obtain a resolution of 45 km, it is necessary to use pulse compression with a factor N = 33-1/3. The same prf then provides the required energy at 40,000 km after 20 seconds of coherent integration. For ranges between 20,000 km and 40,000 km, less energy is required, falling off inversely with the distance at a power between 3 and 4. At 20,000 km, the energy is 14 Joules, so that far less integration is needed. However, these energy figures apply to the higher frequencies only. At low frequencies, the additional losses due to the matching network require about 10 db of gain which would be available from the excess coherent integration at 20,000 km, but requires additional integration at 40,000 km. This additional integration may be obtained by coherently or noncoherently integrating for a longer period.

The total integration time is limited by the resolution desired and radial motion of the spacecraft. During the integration time, the change in the range due to spacecraft motion cannot exceed the resolution cell without degradation of resolution, unless the integration is fully compensated for relative range velocity. Coherent integration requires doppler compensation, and it has been used in the previous system. However, over the time interval, the radial motion remains within a range cell. Here we refer to additional corrections pertaining to motion out of a range cell. If this extent of

motion is to be avoided during a measurement, then the following relationship, which is stated in terms of the doppler shift, must hold:

$$t = \frac{f_m \Delta t_\mu}{\Delta f} \tag{6}$$

where

t = integration time,

f_m = RF in MHz,

Δt_μ = two-way propagation time in microseconds corresponding to the range cell,

Δf = doppler shift in MHz.

For a cell of 45 km, $\Delta t_\mu = 300$ and $\Delta f/f_m$ is the relative doppler shift, which is given in Figure 13 for various orbits. It can be seen that for orbits that reach 40,000 km, the doppler shift varies between 0 and 8 Hz per MHz, the larger figure being at 20,000 km. The doppler shift at 40,000 km could be as high as 3 Hz/MHz for the 46,600-km curve. For these figures, we see that the integration time may be 100 seconds at 40,000 km and 37.5 seconds at 20,000 km without degradation of resolution. These figures appear quite adequate in view of the preceding discussion. Furthermore, they are somewhat conservative, since the achieved orbit is apt to be better with lower doppler shift, and more time will be available, if needed. For acquisition, the range cell is so large (1500 km) that much greater time intervals can be used to ensure detection. Thus, noncoherent integration can be added for that purpose. Some integration can be added in fine ranging according to the orbit. More extensive use of it, however, would require cell-to-cell compensation by means of the measured doppler shift.

In this system being described, 20 seconds of coherent integration is incorporated for ranges beyond 20,000 km as well as

some noncoherent integration. However, the improvement in S/N ratio by coherent integration will minimize losses due to the additional noncoherent integration.

The system has been dimensioned as shown in Table IV. It achieves a good compromise between the resolution available at various ranges and the storage requirements of the coherent and noncoherent memory. It provides for 5 modes, with Mode 1 being the acquisition mode. This mode uses a simple pulse with coherent and noncoherent integration.

The long-range sounding mode for ranges beyond 20,000 km will provide a 45-km resolution using coherent and noncoherent integration, whereas at shorter ranges, Mode 3 (8000 km to 20,000 km), the noncoherent integration will be dropped and the data rate increased. In the short-range sounding Mode 4 (4000 km to 8000 km), a resolution of 7.5 km will be provided. This mode uses noncoherent integration and pulse compression with a factor N = 7. The coherent integration is dropped with a further increase in data rate. Mode 5, for ranges below 4000 km, provides a resolution of 7.5 km and requires no integration. Only pulse compression is incorporated. Although this mode could consist of a narrower pulse without compression, the 350-μsec system with pulse compression is available from Mode 4. To incorporate another pulse-width system would entail unnecessary additional hardware.

The prf's for the first three modes are the same and equal 2. A higher prf could be used in Mode 3; however, the average delivered power would be higher. Modes 4 and 5 use convenient values of prf's closer to the maximum value for the maximum range of each mode. About 2.6 watts is the average delivered power for Mode 4 and 4.4 watts for Mode 5. The pulse-compression ratio of 7 is a convenient value, since there is a Barker code of this length and it may be contained within the 31 bit code required for the longer range compression (thereby saving equipment). Suitable codes are described in Appendix I.

TABLE IV
40,000-km VOYAGER (UPDATED) SYSTEM

Mode	Pulse Width	Resolution (km)	Pulse Compromise Factor	PRF	Coherent Integration	No. Range Cells	No. Doppler Cells	Noncoherent Integration	No. Cells for Noncoherent Integration	Operating Range (km)
1	10 msec	1,500	1	2	yes	27	40	yes	40 x 27	40,000
2	10 msec	45	33-1/3	2	yes	27	40	yes	40 x 27	40,000 20,000
3	10 msec	45	33-1/3	2	yes	27	40	no		20,000 8,000
4	350 μsec	7.5	7	15	no			yes	320	8,000 4,000
5	350 μsec	7.5	7	25	no			no		<4,000

The implementation of the system hardware is shown in Figure 21 and the operation of the processor described in the following sections.

2.1.2 BLOCK DIAGRAM DESCRIPTION

MODE 1 - ACQ. Due to the limited average power and, hence, the requirement for 20 seconds of coherent integration to extract the return signal from the cosmic noise at maximum range, it is necessary to perform a coarse measurement of the ionosphere before each sounding mode. An optimum acquisition at a single higher frequency, 7 Mc or above, will be used to sound the ionosphere coarse range. The received signal will also undergo a doppler frequency shift due to spacecraft movement. The maximum range is divided into thirty 1500-km range elements. A 10-msec (1500 km) pulse is transmitted and each of the 27 longest range elements are coherently detected (preserving amplitude and sine-cosine phase information), converted to a digital form and stored. This process is repeated for 40 range periods to provide a storage matrix of 27 by 40 which is shown in Figure 21. When the matrix is filled, a nondestructive readout occurs. This is performed serially, in quadrature from the read-in--that is, the first range element in each range period is read out in sequence. The sine and cosine portions of each range element are combined in a digital-to-analog processor in the form of a balanced modulator, and the signal converted back to an IF. This signal is then mixed with a fine doppler scan oscillator and converted to video in a detector. The scan oscillator frequency is held constant while the matrix is read out; this results in an output matched to the doppler frequency determined by the doppler scan oscillator. The oscillator frequency is then shifted slightly and the matrix readout repeated. Thus, the scan oscillator will be stepped through the range of expected doppler frequency shift. At some doppler frequency, the range elements in a given column of the matrix will provide a maximum response at the detector and an indication of the range. This information will be

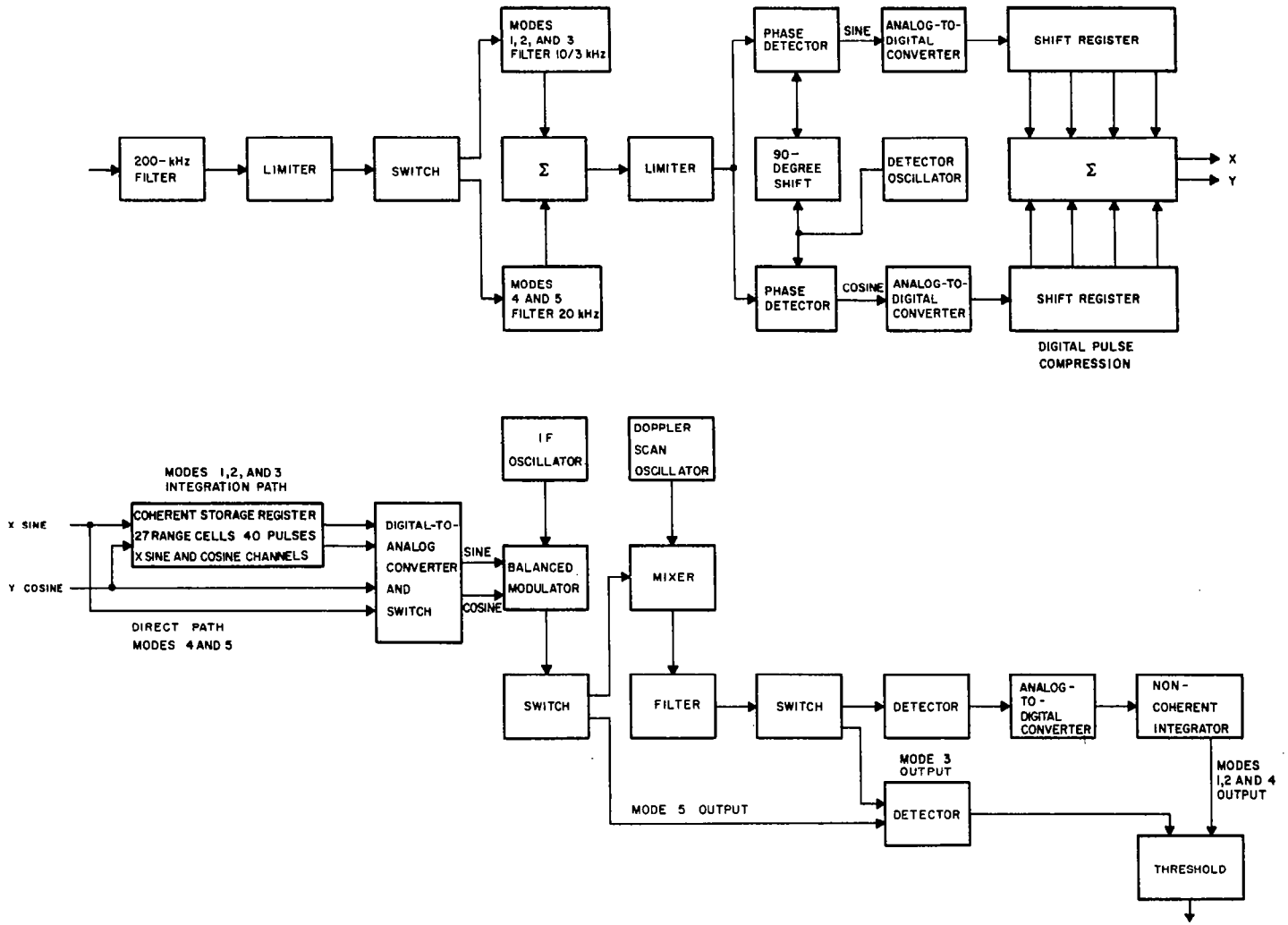

FIGURE 21. VOYAGER PROCESSOR BLOCK DIAGRAM

stored in the noncoherent integrate memory where a space for each of the range cells and each of 40 doppler frequencies will be provided, resulting in a storage of 27 by 40 cells. At the end of the noncoherent integration period the signal will be read out sequentially from the memory and compared to a threshold.

MODE 2 - FAR RANGE. If the acquisition mode determines that the ionospheric range is between 20,000 and 40,000 km, Mode 2 operation commences. As shown in Figure 21, Mode 2 is similar to the operation in Mode 1. The approximate range is now selected by the acquisition gate (range window) and examined in greater detail. To obtain a resolution of 300 μsec (45 km) a 3.33-kc bandwidth is required. The 10-msec transmitter pulse is phase coded in 300-μsec (3.33 kc) sections to achieve this resolving power. Upon reception, the coded signal is compressed by a matched phase-coded network. It is compressed from the original 10-msec duration to a 300-μsec duration, a ratio of 33-1/3 to 1. The signal entering the coherent detector is now at the same level as it was during acquisition, but the resolution has been improved by a factor of 33-1/3. Detection of the doppler shifted return is accomplished in the same manner as during acquisition, except that the target range is known to exist within the acquisition gate. This gate is 8.1 msec wide (1215 km) and is divided into twenty-seven 300-μsec (45 km) elements and stored for 40-gate periods. The doppler ambiguity is resolved in the same manner as during acquisition, For very far ranges, the additional losses in the antenna matching network are compensated by additional noncoherent integration. For an average gain of 10 db, 340 seconds of total integration is required to extract the signal. The gated information is envelope-detected and stored in a register matrix. The output of this matrix is then threshold detected.

MODE 3 - INTERMEDIATE RANGE. If the acquistion mode determines that the ionospheric range is between 8000 and 20,000 km, Mode 3 operation commences. This mode is identical with Mode 2 operation except that the noncoherent integration is no longer needed because of decreased path and defocusing loss.

MODES 4 AND 5 - NEAR RANGE. If the spacecraft is between 1000 and 8000 km from the ionosphere, the received signal level will be sufficient for noncoherent integrated pulse detection. The acquisition mode will indicate a short range and place the system in this mode. The transmitter will radiate 350-μsec pulses.

Since at these short ranges a resolution of 7.5 km is desired, the pulse will be phase coded with a compression ratio of 7. The operation will use incoherent integration to 4000 km, the single-pulse S/N ratio at these ranges being sufficient for a low-loss operation. A range window of 1200 km is used with storage in 320 overlapped cells. At ranges shorter than 4000 km (Mode 5), the system provides single-pulse detection. Pulse compression with a factor N = 7 is still used.

2.1.3 SPECIAL PROBLEM AREAS

Referring to the implementation shown on the block diagram, a number of areas were studied that needed specific attention before decisions on the complexity of the required hardware and the exact ranges to be associated with each mode could be made. The results of these studies were only partially applied to the above described system. (It should be noted that these results were fully applied to the Mariner application, where pertinent.)

The first area that required investigation was that of the loss to be associated with the constant false alarm rate (CFAR) operation. This results from the change in noise (and signal) probability distribution introduced by the limiters used ahead of each matched filter, which provide the CFAR operation. This loss is not only the function of the pre- and postfiltering bandwidth but also of the degree of postfiltering integration, which further transforms the probability distribution. The results of the study are given in Appendix III.

The next area of interest is that of pulse compression and coherent integration. Since analog pulse compression results in bulky hardware, it was decided to use a digital pulse-compression approach.

The most suitable type of code for a digital approach is a phase code where succeeding sections of the transmitted pulse are coded by 180-degree phase shifts. Since two such codes are necessary (33 to 1 and 7 to 1), it is necessary to identify the higher order code that will permit the use of the same hardware for decoding the lower order code. The criteria used for selection are that the code should result in low level "range side lobes" and that it should be "doppler resistant"; that is--it should not have "high range side lobes" in the presence of a doppler shift. Appendix I contains details on the codes. 31- and 28-bit codes described there contain a Barker 7-bit code. Either code may be used with appropriate modifications on the parameters for the long range system. Modification is slight in changing from a 33-1/3 to a 31 to 1 compression ratio.

Since the pulse-compression process is to be followed by a coherent integration process, the pulse coherence must be preserved. In a digital system, this is maintained by processing separately two quadrature signals that are recombined only after pulse compression. In such a system, it is necessary to determine the losses that will be associated with the granularity of the phase detector output in each of the two channels, and the optimum method of combining the two channels. Analytical work and computer simulation to provide answers to these questions are reported on in Appendix II.

2.2 REDUCED RANGE VOYAGER SYSTEM

This system was designed to sound to ranges greater than or equal to 15,000 km. It differed from that of the longer range system by purposely eliminating the coherent integration system. It incorporates an acquisition mode, and the resolution requirements are 7.5 km for ranges to 7000 km and 30 km beyond. The near range resolution is the same as that for the longer range Voyager system; ever, the resolution for ranges greater than 7000 km was purposely improved because of the smaller total range capability. The transmitter pulse power was reduced to 250 watts and the maximum average

delivered power to 2-1/4 watts. Comparison of this system with that for the longer range Voyager (as well as the Mariner application to follow) exhibits the degree of variation that is possible with these systems.

Based on the energy requirements for ranges less than 20,000 km and the transmitter single pulse energy, a set of parameters was devised. These were determined by compromises between integration times, storage requirements and equipment complexity. A 4-mode system was established, one (Mode 1) being for acquisition. The parameters of the system are shown in Table V and the signal processor system block diagram in Figure 22.

As may be seen from the table, noncoherent integration is only used in Modes 1 and 2. Pulse compression is used in Modes 2 and 3. The ratios are 30 and 7 to 1 and the codes of Appendix I are applicable. The acquisition cells are 225 km in width and 48 in number, which combine to give 10,800 km. Since the signal for ranges less than 7000 km (Modes 3 and 4 output in Figure 22) is strong enough to cause detection, acquisition is used to establish the coarse range. When acquiring, the location of the echo will establish whether the range is less than or greater than 7000 km. If less than 7000 km, the signal will be automatically present at the Modes 3 and 4 output. The acquisition output will also indicate this condition and the programmer control will be set accordingly. For ranges greater than 7000 km, the acquisition range input is necessary to control the range window in Mode 2. This window is set to 1550 km. Its trailing edge is set about 200 km below the center of the acquisition cell to provide about 1300 km above. This arrangement will cover most echoes over the frequency range for Mars. A maximum of 25 pulses are integrated at the furthest range. With a PRF of 6, the time per sounding per frequency and time for acquisition is about 4 seconds. Since this system is based on soundings at 30 frequencies, the time for sounding over the range is 120 seconds. For ranges below 7000 km, a complete sounding with a PRF of 1.5 is accomplished in 20 seconds.

TABLE V
15,000 km VOYAGER SYSTEM

Mode	Pulse Width	Bandwidth (kHz)	Resolution Cell (km)	Number Resolution Cell	Range Window (km)	Operating Range (km)	Energy Per Pulse (joules)	S/N Min (db)	Integration Period Per Frequency (seconds)	Number of Integrations	PRF	Average Power (watts)	P_{fa}	P_a
1	1.5 msec	0.670	225	48	-	0 to 15,000	0.375	15.5	4	25	6	2.25	5×10^{-5}	99.99
2	1.5 msec	4.7	32	48	1550	7000 to 15,000	0.375	15.5	4	25	6	2.25	10^{-1}	99.99
3	1.5 msec	20	7.5	0	-	2000 to 7000	0.375	15.5	0	0	1.5	0.56	10^{-4}	99.99
4	50 μsec	20	7.5	0	-	0 to 2000	0.0125	16.5	0	0	1.5	0.02	3×10^{-4}	99.99

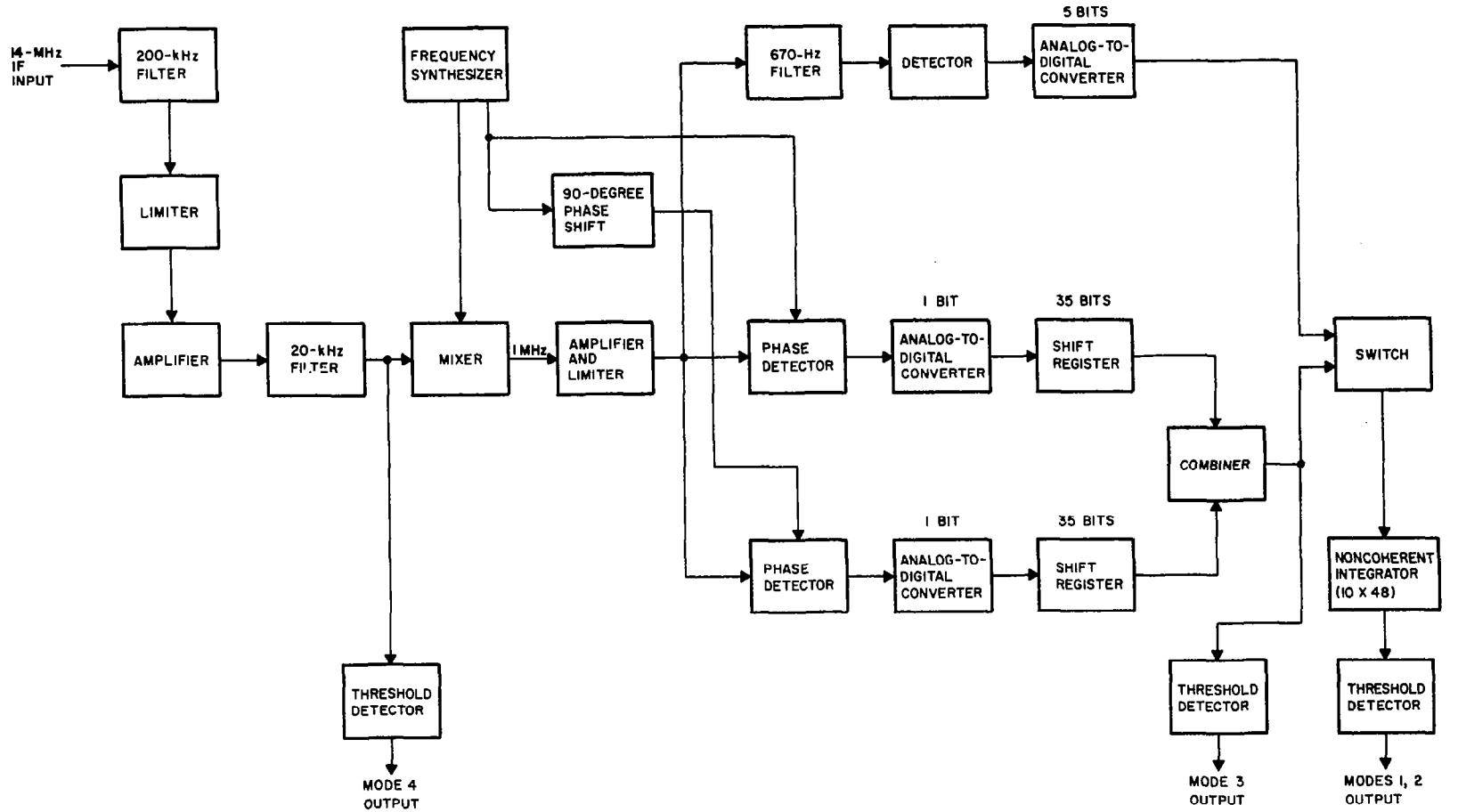

FIGURE 22. BLOCK DIAGRAM 15,000 km SIGNAL PROCESSOR

As seen in Figure 22, the noncoherent integration contains 48 cells with a 10-bit capacity per cell for accumulation. Pulse compression is accomplished digitally as before by phase coding. During acquisition, the compression network is bypassed and the signal is processed through the 670-Hz filter path. The 14-MHz signal is provided by the receiver IF output. The signal is processed through a Dicke-Fix with an output bandwidth of 20 kHz. This signal is mixed to reduce the frequency to 1 MHz, which is the reference frequency for for the phase detectors in the compression network. Prior to entering the compression network or 670-Hz acquisition filter, the signal is amplified and limited. The losses introduced by these limiter-filter circuits are analyzed in Appendix III.

It should be noted in Table V that high, minimum S/N ratios have been used in all modes. These values ensure a high probability of detection. A relatively high P_{fa} has been used in Mode 2 on the basis of a good likelihood of detecting false alarms after acquisition and in view of the relationship between the echoes at 30 frequencies. It is important, however, that P_{fa} be very small in acquisition.

3. MARINER APPLICATION

Because of constraints on the mission, a system using simple pulses and noncoherent integration was adopted. Soundings are made at a limited number of frequencies with sufficient resolution to provide the required data and with sufficiently high periodicity to yield the desired angular resolution as the sounder flies by the planet. The trajectory results in a variation of the range to the planet with the consequent variation of requirements on sounding energy. Since the total power to operate the sounder is limited, an adaptive approach is indicated in which a fixed amount of power is used and the number of soundings performed varies inversely as the distance to the planet.

The peak power available from the sounder transmitter is limited by various practical considerations and thus the energy per transmitted pulse is, in general, insufficient to provide adequate performance at the ranges of interest. The system must, consequently, integrate a number of pulses to achieve detection. While the most efficient implementation involves coherent integration, this imposes severe requirements on transmitter stability and results in much more complex hardware for the integrator. The simplest implementation involves a noncoherent digital integrator. If the system parameters can be chosen to provide the desired number of soundings (even though the integration time has to be increased to compensate for losses due to noncoherent integration) the simplest system will result.

Another constraint on the integration time must be considered: movement of the platform. Since signals will arrive with increasingly shorter delays as the sounder approaches the planet (or longer as it

recedes) they may not add in the same resolution cell. Here, either the integration time must be limited, or, if the platform velocity is known, an integration timing correction must be introduced.

The final system requirement that must be considered is the probability of detection of the echoes and the relation of the false alarm rate to storage and telemetering requirements. Since burdening of the telemetry system with false alarms is undesirable, the detection thresholds must be set suitably high. In the acquisition mode, it is especially important to position properly the range window, a process that takes a short time, to ensure detections in the sounding mode, a process that takes a longer time.

3.1 DESIRED PARAMETERS

The relationships of the basic requirements discussed were considered in arriving at a suitable signal processor configuration. The system approach adopted attempts to balance the resolution obtainable versus the range to the planet as a function of frequency and integration time. Table VI lists the parameters of the system. A long pulse of 2 msec with a PRF of 0.675 for acquisition (Mode 1) minimizes the number of integrations and, thus, the acquisition time. For sounding at ranges less than 6600 km (Mode 4), a 200-μsec pulse with a PRF of 5 is used, and the number of integrations performed varies as a function of frequency and range. For longer ranges between 6600 and 8600 km (Mode 3), a 400-μsec pulse with a 2.5 PRF is used, again with a variable integration period; for very long ranges beyond 8600 km (Mode 2), the system radiates 800-μsec pulses with a PRF of 1.25. Modes 2, 3, and 4 are the fine ranging modes.

The purpose of the Signal Processor is: (1) to extract range information from the received echoes, and (2) to program the trams-mitter and the signal-processing circuits.

Only one frequency, such as 6 MHz, is used in the acquisition mode, but 12 logarithmically spaced frequencies are used in sounding.

TABLE VI

PARAMETERS FOR MARINER - MARS FLY-BY SOUNDER

Mode	Pulse Width (μsec)	Band Width (kHz)	Resolution (km)	No. of Integration Cells *	Window (km)	Range Interval (km)	PRF	P_{AV} (watts)	S/N Min (db)
1	2000	0.5	300	80	∞	0 to 20,000	0.675	0.25	15.5
2	800	1.25	120	80	4800	8600 to 15,000	1.25	0.25	12.5
3	400	2.5	60	80	2400	6600 to 8600	2.5	0.25	12.5
4	200	5.0	30	80	1200	0 to 6600	5	0.25	12.5

* Cells are based on two overlapping groups of 40 cells.

The range storage is divided into range cells whose size is made to match the pulse width. In acquisition, range cells are 300 km long; in sounding, cells are 30, 60, or 120 km. To reduce the losses resulting from energy division between two adjacent cells, the cells are made to overlap each other by one-half of the pulse width. This arrangement results in average losses of about 1.25 db.

Since the peak power from the transmitter is limited to 280 watts maximum, operation beyond a certain range requires integration of a number of pulses if a desired signal-to-noise ratio is to be achieved. For the acquisition mode, a S/N ratio of 15.5 db is obtained without integration at ranges up to 10,800 km. Integration of 16 pulses suffices to extend this range to 20,000 km for the same signal-to-noise ratio. In the sounding mode, the number of required integrations depends not only on the pulse width and the distance to the target, but also on the operating frequency. At higher frequencies, the peak power from the transmitter decreases. The decrease in the cosmic noise level more than offsets the decrease in signal level with the net result that few integrations are required. Table VII shows the number of integrations necessary to achieve a 12.5 db S/N ratio for various ranges and frequencies. This S/N ratio corresponds to a 90-percent detection probability with a probability of false alarms of 10^{-5}. The table is in a matrix format with range intervals (in thousands of km) along a horizontal row at the top and the frequency (in MHz) along the vertical column to the left. With the exception of the first range interval, all others are labeled with the maximum of the interval, the minimum being the quantity in the box to the left. The number of integrations are arranged in vertical columns corresponding to each range interval. Each listed number corresponds to the frequency on the left in the row of the number. Thus, the number of integrations required at a given frequency and range interval is found from the intersection of the corresponding frequency row and the range interval column. Two sets of numbers are shown, one being in parenthesis. The other set is the nearest whole number of integrations required. The number in parenthesis is a nearby binary or easily generated number. In implementing

TABLE VII

NUMBER OF NONCOHERENT INTEGRATIONS VERSUS FREQUENCY AND RANGE TO ACHIEVE 12.5-db S/N RATIO

	PW = 200 μsec at 5 Hz				PW = 400 μsec at 2.5 Hz		PW = 800 μsec at 1.25 Hz					
Range (kkm) / Freq. (MHz)	1-3.2 R_1	4.8 R_2	5.6 R_3	6.6 R_4	7.6 R_5	8.6 R_6	10.5 R_7	12 R_8	13.5 R_9	15 R_{10}	17 R_{11}	17-20 R_{12}
0.5	1 (1)	4 (4)	7 (8)	16 (16)	Same as preceding column	20 (24)	Same as preceding column	40 (48)	80 (96)	150 *	300 *	700 *
0.65	1 (1)	4 (4)	7 (8)	16 (16)		20 (24)		40 (48)	80 (96)	150 *	300 *	700 *
0.86	1 (1)	4 (4)	7 (8)	16 (16)		20 (24)		40 (48)	80 (96)	150(160)	300 *	700 *
1.12	1 (1)	3 (4)	5 (8)	13 (16)		16 (16)		32 (32)	63 (64)	120(128)	240 *	550 *
1.47	1 (1)	3 (4)	5 (8)	10 (16)		16 (16)		32 (32)	56 (64)	100(128)	200 *	500 *
1.93	1 (1)	2 (4)	3 (4)	7 (8)		9 (8)		17 (16)	35 (32)	64(64)	130(128)	300 *
2.54	1 (1)	2 (4)	3 (4)	5 (8)		7 (8)		12 (16)	21 (32)	40(64)	85(128)	160(160)
3.34	1 (1)	1 (1)	1 (1)	2 (4)		3 (4)		5 (8)	8 (8)	16(16)	25(32)	62(64)
4.38	1 (1)	1 (1)	1 (1)	1 (1)		1 (1)		3 (4)	4 (4)	7(8)	13(16)	28(32)
5.75	1 (1)	1 (1)	1 (1)	1 (1)		1 (1)		2 (4)	3 (4)	5(8)	8(8)	16(16)
7.54	1 (1)	1 (1)	1 (1)	1 (1)		1 (1)		2 (4)	3 (4)	5(8)	8(8)	16(16)
10.00	1 (1)	1 (1)	1 (1)	1 (1)		1 (1)		3 (4)	4 (4)	7(8)	13(16)	28(32)
Total pulses	12	33	53	104	104	128	128	264	504	592	592	320

S/N = 12.5 db, P_D = 90 percent, $P_{FA} = 10^{-5}$

Notes: 1. Numbers in parenthesis represent the suggested number of integrations selected on the basis of convenient implementation.
2. (*) No integrations will be performed because the number is too large.
3. kkm means thousands of kilometers.

this bivariate function, it is simpler to use the binary numbers, rather than the other set, and the system is designed in this way. The table also has a set of totals at the bottom. These totals represent the number of pulses required for each sounding cycle. For a given PRF, the number of pulses is proportional to the complete sounding period, so that this set of totals, when multiplied by the period between pulses gives the distribution of sounding time versus range. The PRF's and pulse widths appropriate to the range intervals are shown above the table.

Having acquired the target, the signal processor no longer scans the entire range in search of an echo, but limits its operation to a small sector in the immediate vicinity of the target with limits defined by the range window. The size of the window varies with each mode but it must always be sufficiently wide to include the maximum probable height of the ionosphere to the lowest density regions of interest (based on Mariner IV results, about 400 km was used for Mars). For higher exospheric temperatures, 800 km is a more appropriate number. Other considerations are (1) the range uncertainty of the acquisition mode (300 km total), and (2) additional range to include ionospheric propagation delays. The window sizes for each mode are listed in Table VI. On the basis of a surface detection in acquisition at one of the higher frequencies, the relative position of the Martian surface within the range window is important. This position would be known accurately when sounding at higher frequencies in the fine ranging modes. It serves as a reference for the entire profile. If the profile reaches high enough density to prevent detection of the surface, the highest density detected becomes the eventual reference. However, the positioning of the window is done by digital biasing of a range counter with a fixed relation relative to the count obtained in acquisition. On interpreting the data, this range counter setting must be compared with the acquisition range to provide a fixed correction in the range readings which must be subtracted from the recorded data to properly interpret the virtual depths.

There are two corrections that are necessary in interpreting the data properly. They arise from errors due to delays in the signal processor. The first correction is caused by the A/D converter and the other one by the digital addition. The duration of A/D conversion varies with the signal level and reaches a maximum of 28 μsec, which is equivalent to a range error of less than 5 km. Digital addition always requires 40 μsec and the resulting error can be corrected in the range measurement.

Acquisition of the target depends on two successive detections in the same range cell (or in one of the adjacent cells). This stringent requirement is deemed necessary because the range window has a limited coverage and improper positioning of it, as may be caused by a false alarm, could result in a loss of sounding cycle. With the integration of 16 pulses per acquisition cycle it takes 48 seconds to complete two successive detections. This interval of time would be required at 20,000 km. For ranges less than 10,800 km, integration is not required and two successive detections would take about 3.0 seconds.

The output word of the Signal Processor consists of a 10-bit range word, 4-bit frequency word, and 2-bit mode word. In addition, three bits are reserved for housekeeping and one bit for parity check, providing a total of 20 bits. Other formatting is certainly possible.

3.2 SYSTEM OPERATIONS

The system begins its operation on approaching the planet by initiating an acquisition mode designed to locate the surface of Mars with a 300-km resolution. Acquisition consists of two successive detections in the same range cell as in adjacent cells. This range information is used by the programmer to: (1) select one of the three sounding modes, (2) position the range windows, (3) determine the necessary number of integrations to be performed, and (4) select a proper threshold level.

Upon acquisition, the programmer controls the system operation and the soundings at 12 different frequencies are done sequen-

tially. It makes the necessary changes in the operating conditions as the requirements vary for each frequency. At the completion of the first frequency cycle, the programmer decides what the next step should be. If no detections were recorded within the entire frequency cycle, the system will be instructed to reacquire the target. If the range is greater than 12,000 km, the system always reacquires even without detections during a frequency cycle. If there is at least one detection and the target is within 12,000 km, the system will be permitted to continue soundings until four full frequency cycles have been completed. If, however, no detection occurs within any one of these four cycles, the system will be commanded to interrupt the sounding mode and to reacquire the target. The requirement for two successive detections applies to reacquisition.

After each detection at each frequency, the range information is temporarily stored in the range register for telemetry or for recording. Each successive detection replaces the preceding range information in the registers. The system continues to operate in the described manner until turned off.

3.3 CIRCUIT DESCRIPTION

Figure 23 shows the building blocks used in implementing the two major functions: signal processing and programming. The circuits associated with signal processing are the Dicke-Fix, detectors, A/D converter, Adder, Memory, Switch, Threshold, and Detection Analyzer. The remaining circuits constitute the Programmer. The functions of each box are explained, and detailed schematic diagrams of each box may be seen in Figures 24 to 49. The various modes are abbreviated on the schematics by utilizing the symbols M_A, M_8, M_4, and M_2 for the designations Modes 1, 2, 3, 4 of Table VI, respectively. The symbol M_S refers to any of the fine sounding modes M_2, M_4, or M_8 as distinguished from acquisition.

Dicke Fix (Figure 24) uses a limiter--band-pass filter technique to stabilize the noise level and to achieve a constant false alarm rate (CFAR). The circuit consists of a wide-band filter, a limiter, and

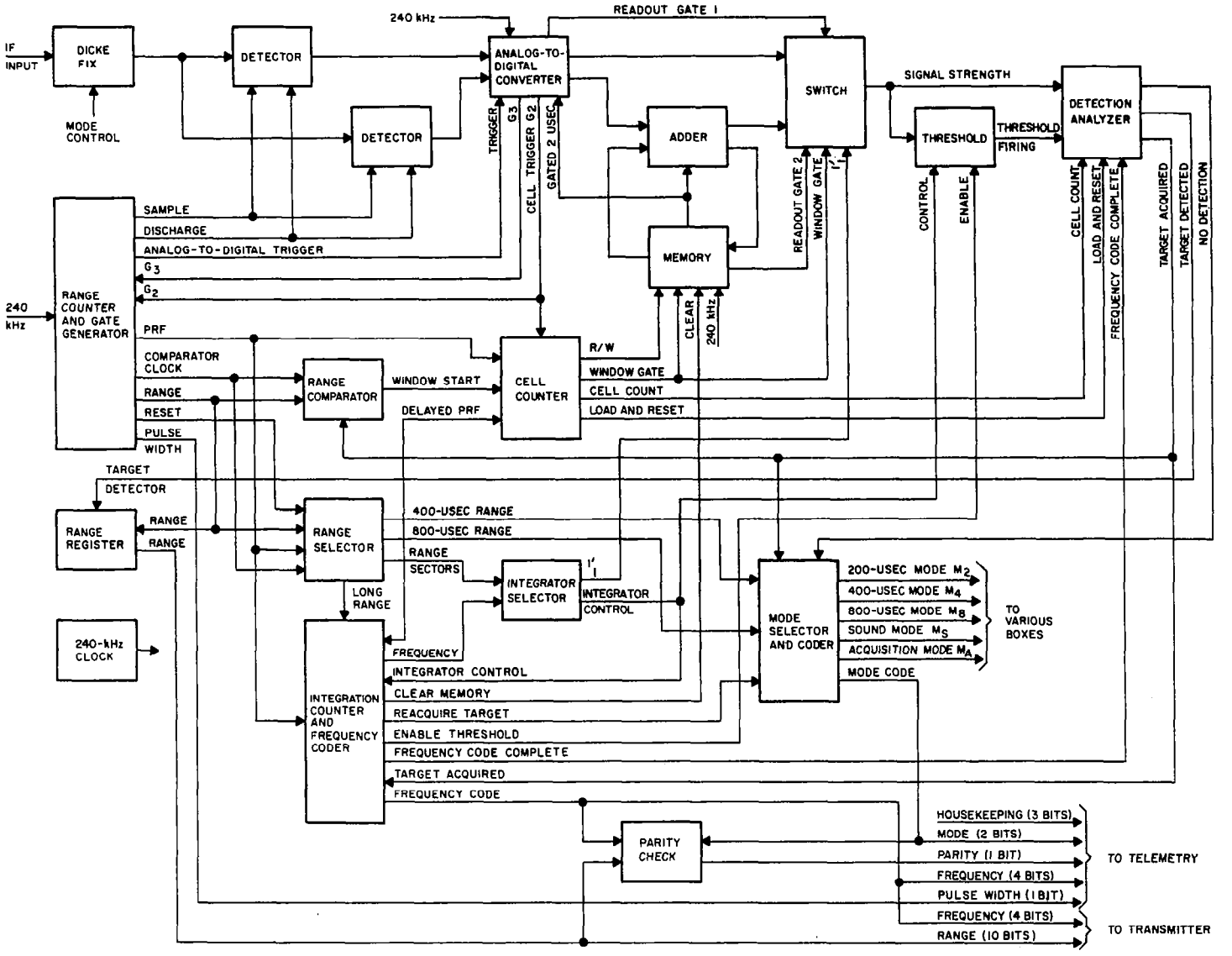

FIGURE 23. SIGNAL PROCESSOR BLOCK DIAGRAM

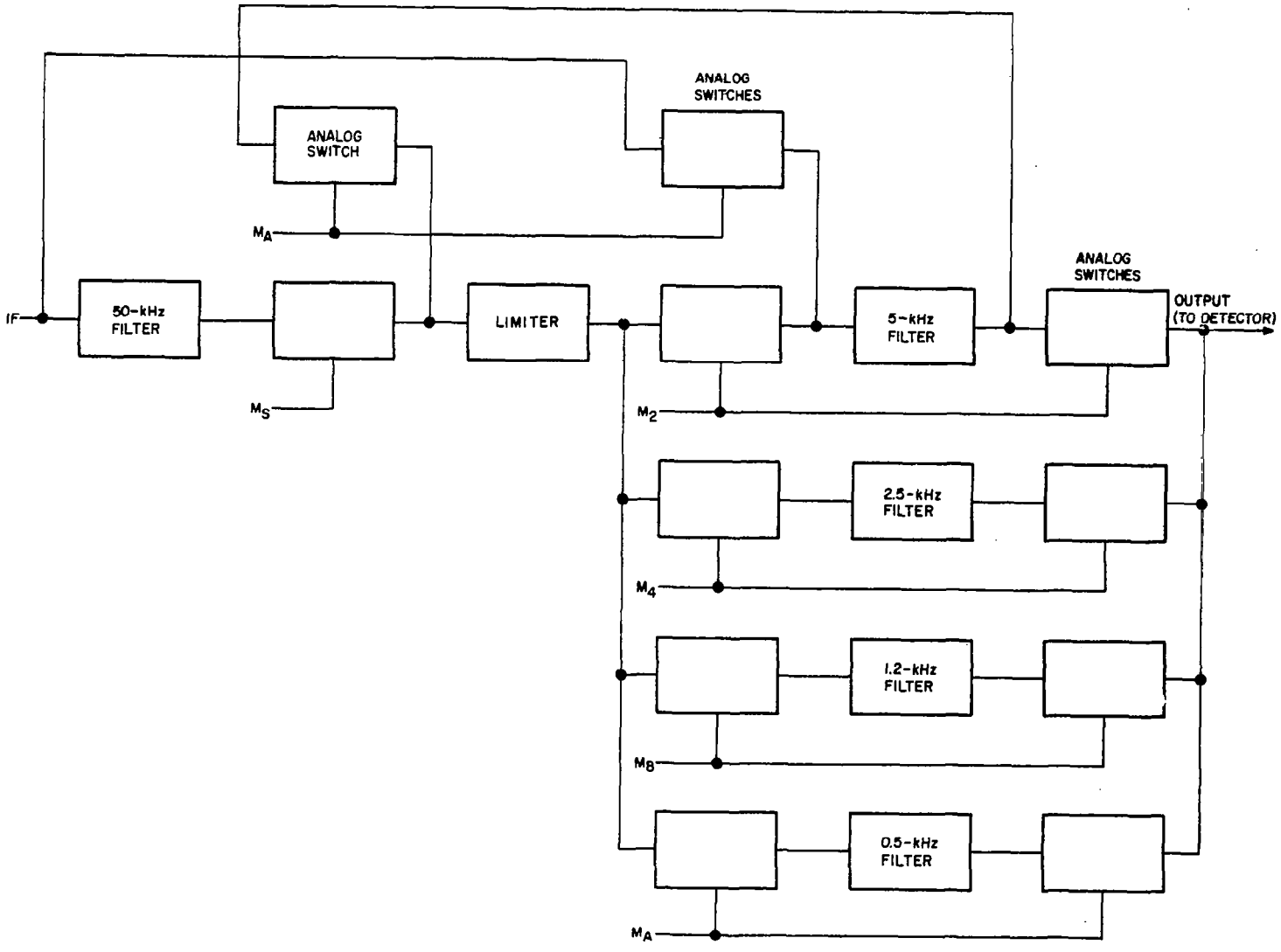

FIGURE 24. DICKE-FIX

a signal filter. Each mode requires a different signal filter: 200-μsec mode, 5-kc filter; 400-μsec mode, 2.5-kc filter; 800-μsec mode, 1.25-kc filter, and acquisition mode 0.5 kc. Mode control signals select the proper combination of filters for each mode with the aid of analog switches.

The Detector (Figure 25) is a peak detecting low-pass filter operating on the amplitude modulated envelope of the IF carrier frequency. Sampling and discharge gates are included in the detector. The spacing between the discharge pulses corresponds to the transmitter pulse width and the size of the range cell. There are two trains of discharge gates--one for each detector, staggered by one-half the pulse width with respect to each other. This arrangement results in overlapping range cells with the overlap of one-half the cell size. The sampling gates perform the function of multiplexing.

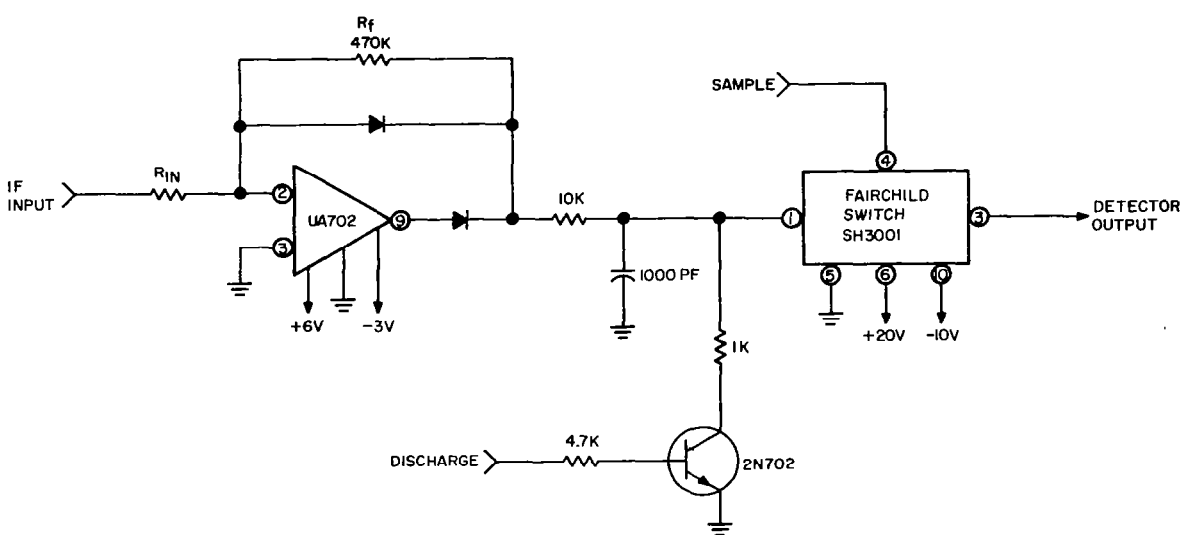

FIGURE 25. PEAK DETECTOR AND SAMPLE

The Analog-to-Digital Converter (Figures 26, 27, and 28) provides a three-bit word for every range cell output. The result of A/D conversion is stored in the three-bit register where it can be read out serially or in parallel. Parallel readout is required by the Threshold when no integration is necessary. Serial readout is used by the Adder. The two gates, G_2 and G_3, generated in the converter are used by the Gate Generator (Figure 38) to produce sampling and discharge pulses. The 240-kc clock (Figure 23) provides a timing signal used in conversion. The duration of conversion depends on the signal amplitude and a maximum count of seven requires 28 μsec. Should the detector reading exceed the equivalent of seven bits, the output of the A/D will still be registered as the count of seven.

The Digital Adder (Figure 29) adds the latest range cell reading serially to the sum of all the previous readings in the same range cell within one integration cycle. The result of addition is read out into the ten-bit register to be either stored in the Memory or to be examined by the Threshold. If the addition results in a reading which exceeds the maximum count of the range cell word, the overflow pulse is initiated to reset the register to the maximum reading. It takes 40 μsec to perform the addition of one range cell word.

The Memory (Figures 30 and 31) together with the Adder, acts as an integrator for the range cell readings. It is a small capacity storage device of 800 bits suitable to accommodate 80 range cell words each 10 bits long. Thin-film memory units manufactured by Interstate Electronics accept the data serially. The new micrologic version requires less than one watt standby power and is compatible with the TI digital logic. A four-bit counter and the 240-kc clock are used to generate 10-bit words. At the end of the range cell word a readout gate is generated for proper timing of Threshold operation.

The Threshold unit (Figure 32) compares the signal amplitude of each range cell with a preset level. The level of threshold firing is a function of frequency and range and is controlled by the integration selector circuit. When no integration is required, the signal from the

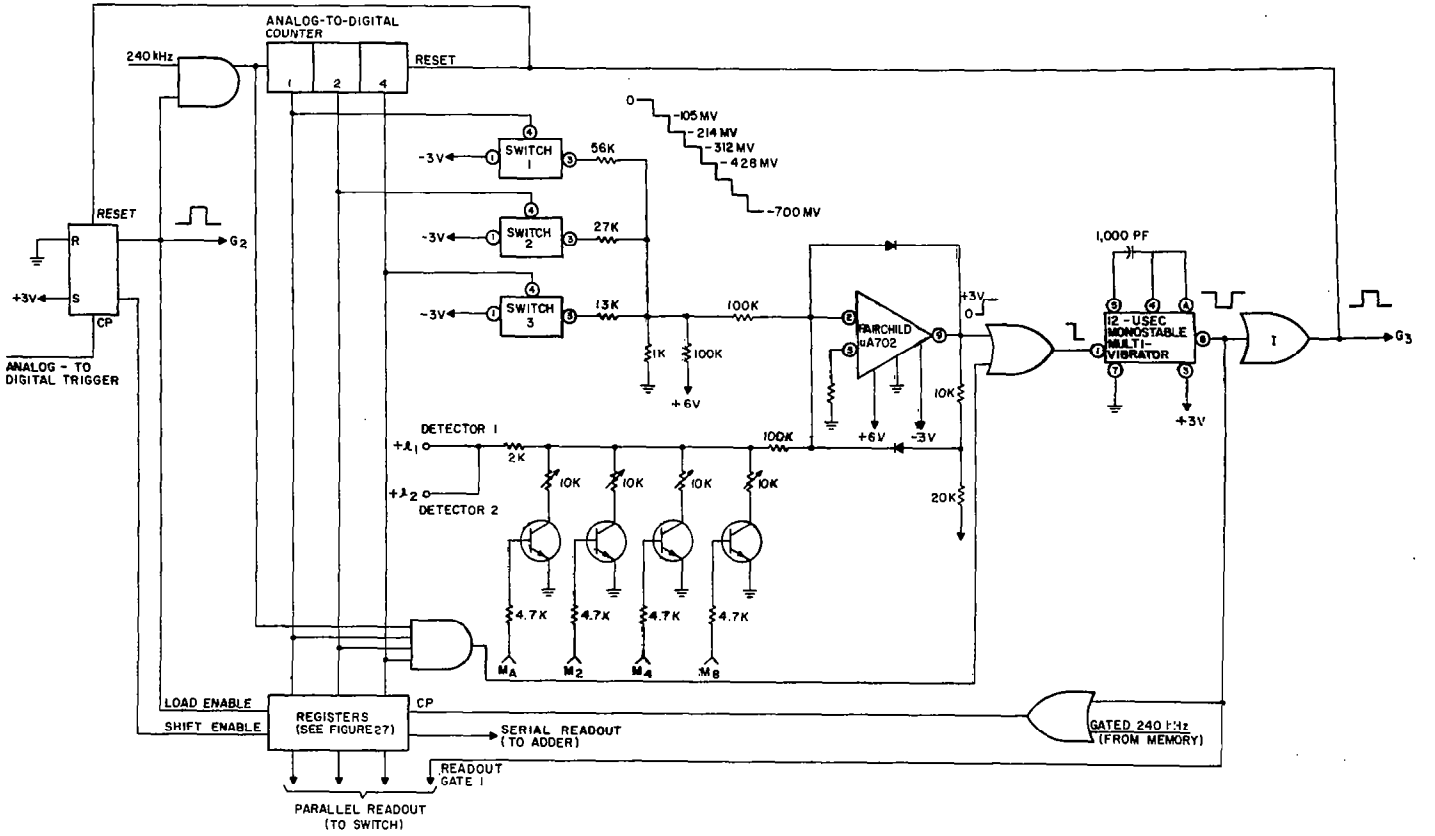

FIGURE 26. A/D CONVERTER

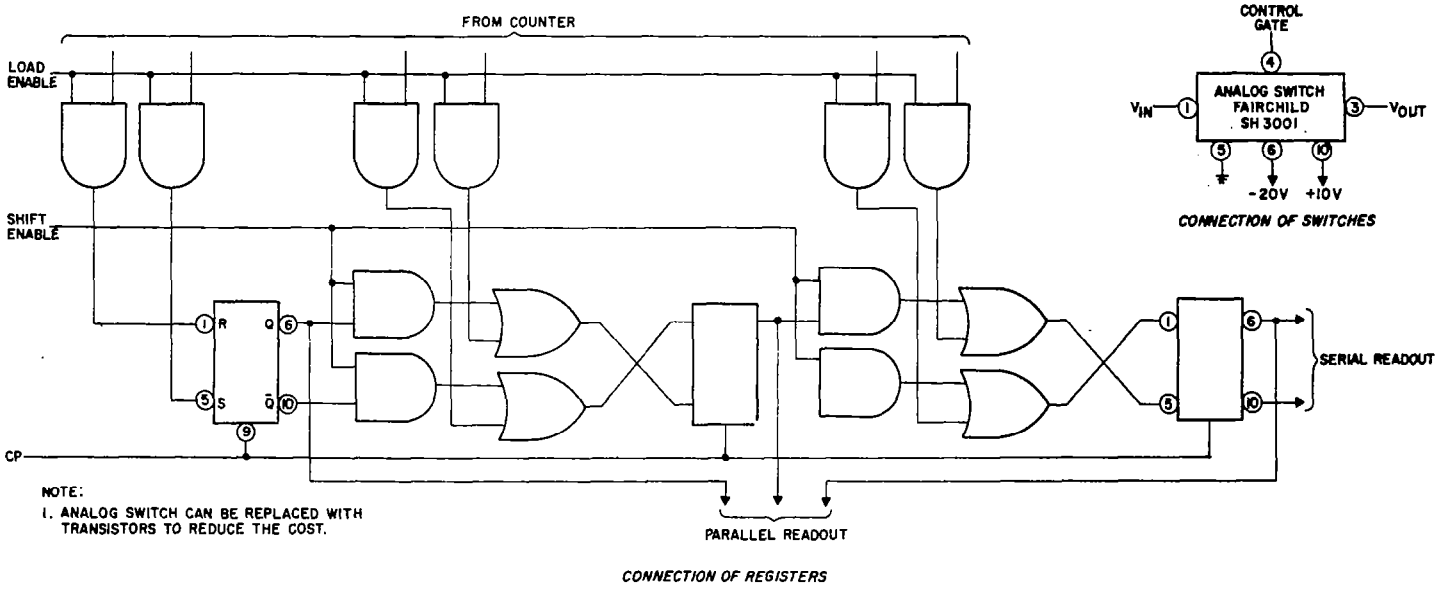

FIGURE 27. A/D CONVERTER, CONNECTION OF REGISTERS AND SWITCHES

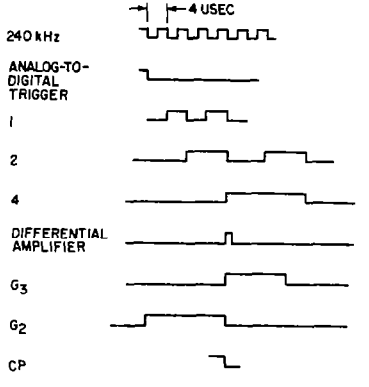

FIGURE 28. A/D CONVERTER, TIMING DIAGRAM

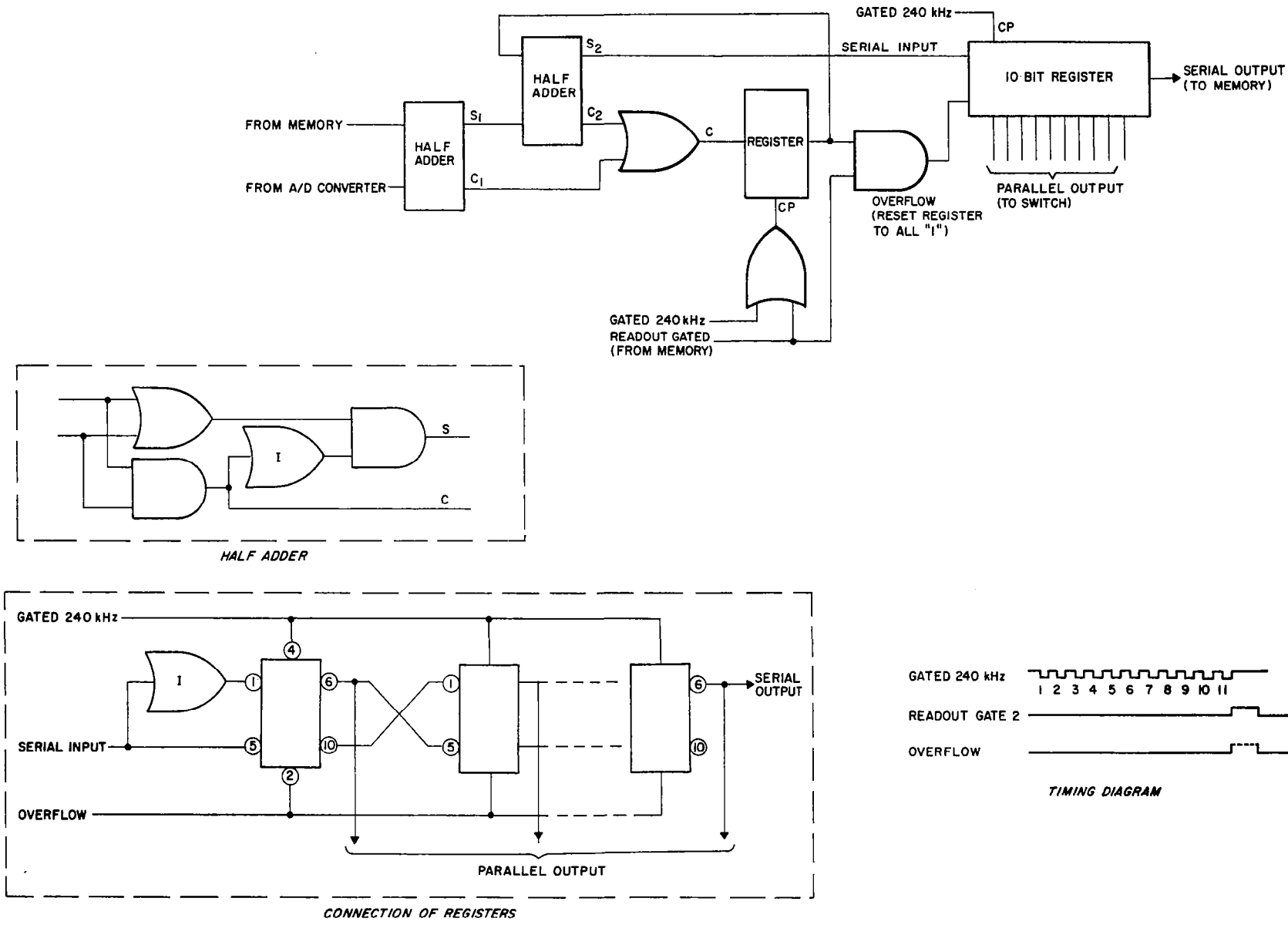

FIGURE 29. ADDER

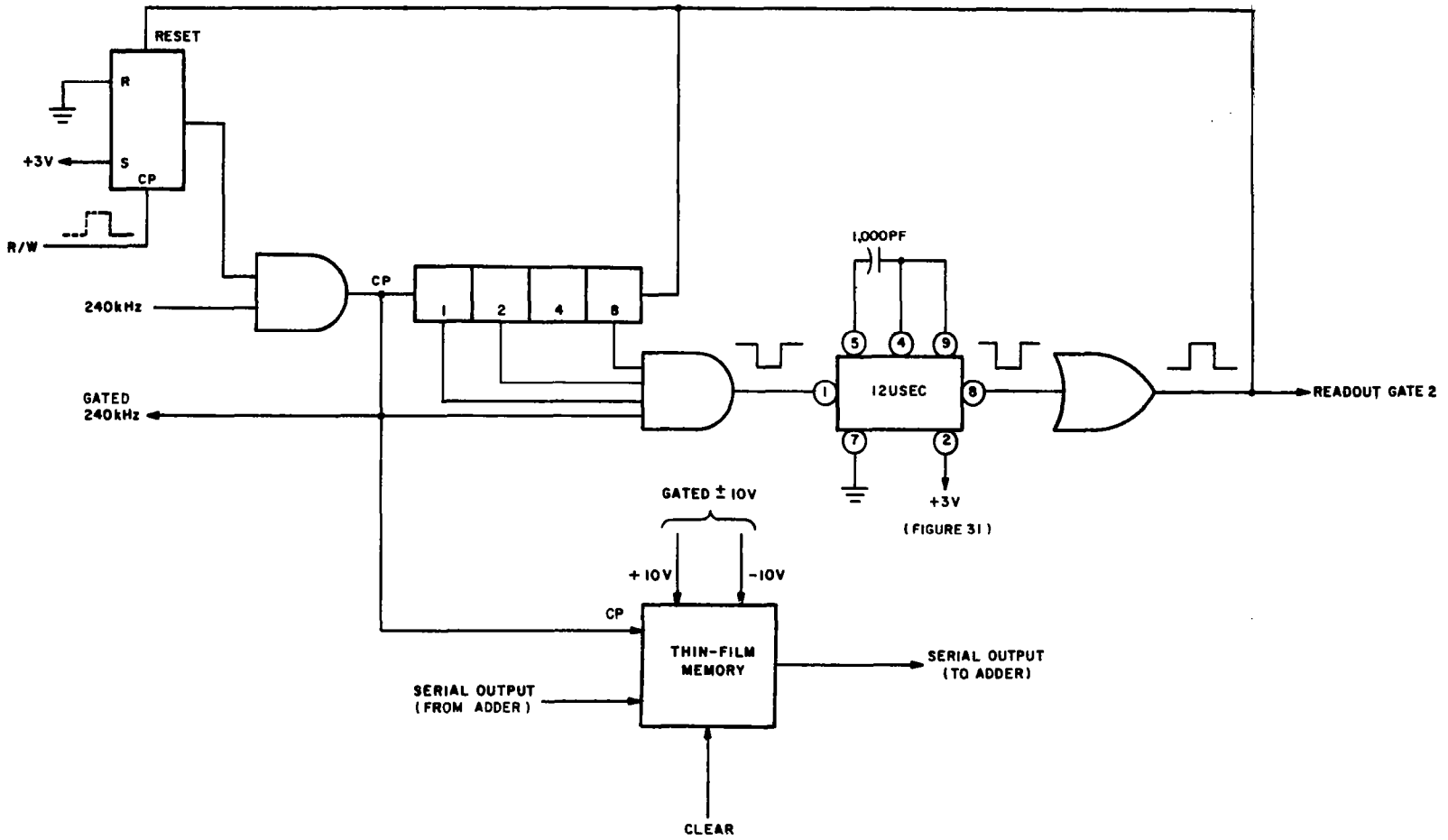

FIGURE 30. MEMORY

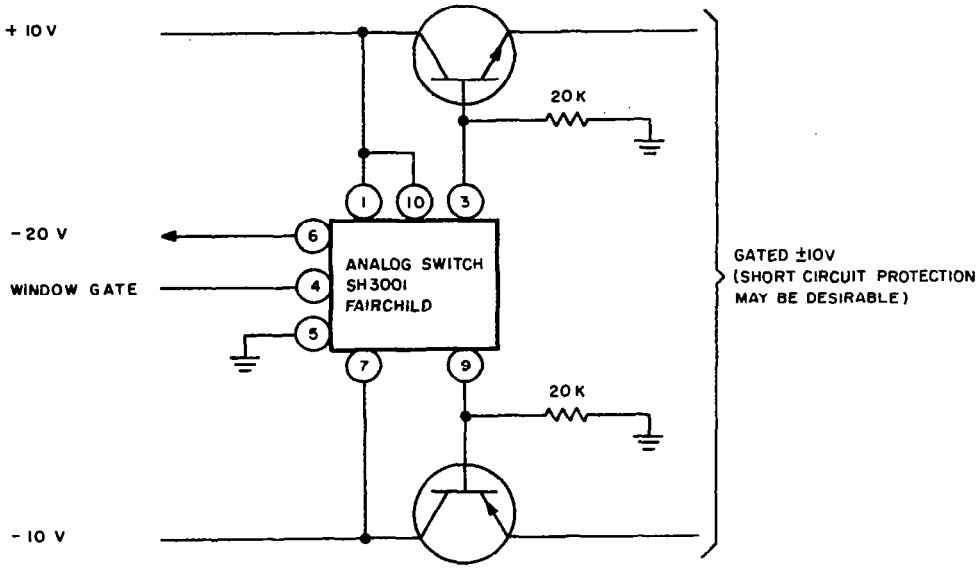

NOTE: GATING OF ±10V WILL NOT BE NECESSARY WITH THE NEW MICROLOGIC MEMORY

GATING OF ±10V

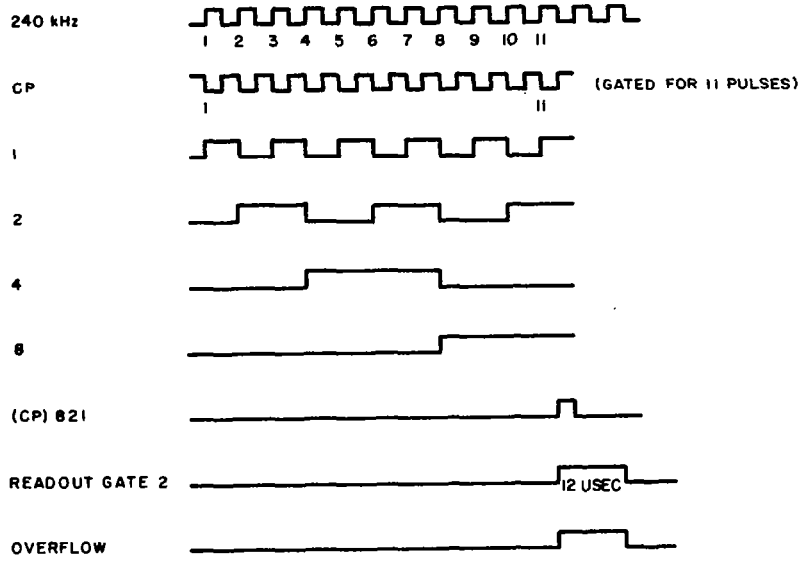

TIMING DIAGRAM

FIGURE 31. MEMORY GATING OF +10V AND TIMING DIAGRAM

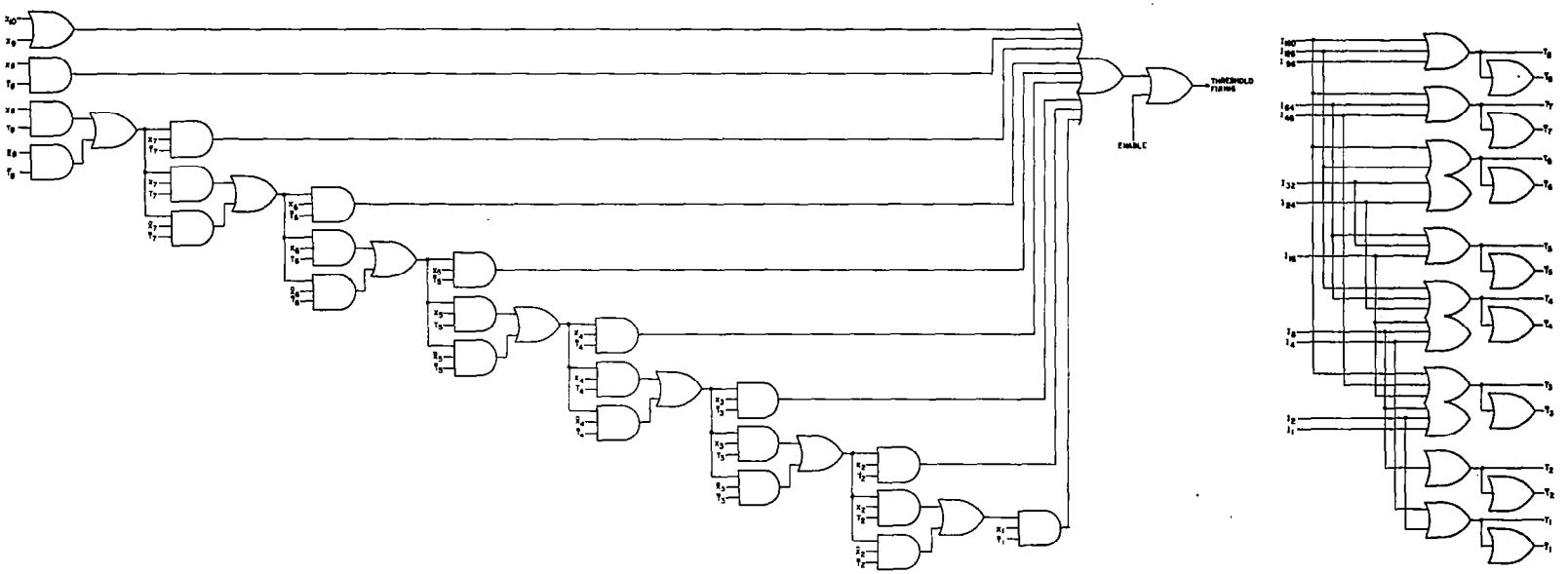

FIGURE 32. THRESHOLD

A/D converter bypasses the Adder and feeds directly to the Threshold through the Switch (Figure 33). In case of integration, the Threshold is permitted to examine the cumulative reading of each cell only upon the completion of the integration cycle. Every threshold firing goes to the Detection Analyzer for examination.

The Detection Analyzer (Figures 34, 35, 36, and 37) accepts the signal strength information, cell count data, and threshold firing pulses and examines the quality of the firings. Its decision making process in the sounding mode is appreciably simpler than that in the acquisition mode because of some additional requirements associated with the latter.

In the acquisition mode, whenever the threshold is exceeded, the analyzer records the signal amplitude and also the three readings of the cell counter which identify the cell with the signal and two adjacent cells. Should another cell exceed the threshold within the same PRF period, the Analyzer would then compare its signal amplitude with that of the previous cell that exceeded the threshold. If the signal is weaker, the second cell is ignored. If the signal is stronger, all the previous readings are replaced with the new data corresponding to the stronger cell. All cells with signals above the threshold within the same PRF period are examined in the same manner. As a result, the signal of greatest amplitude and the identifying cell count get recorded.

During the next PRF period the same process is continued with the following additional step. A comparison is made to determine whether the firing occurred in the same cell as in one of the three recorded during the preceding PRF period. If coincidence is detected, the analyzer concludes that the target was acquired and initiates the acknowledging pulse. If no coincidence is observed, the acquisition process continues until the coincidence takes place. At the end of each PRF period the Analyzer retains a complete set of data associated with the strongest signal of the last period.

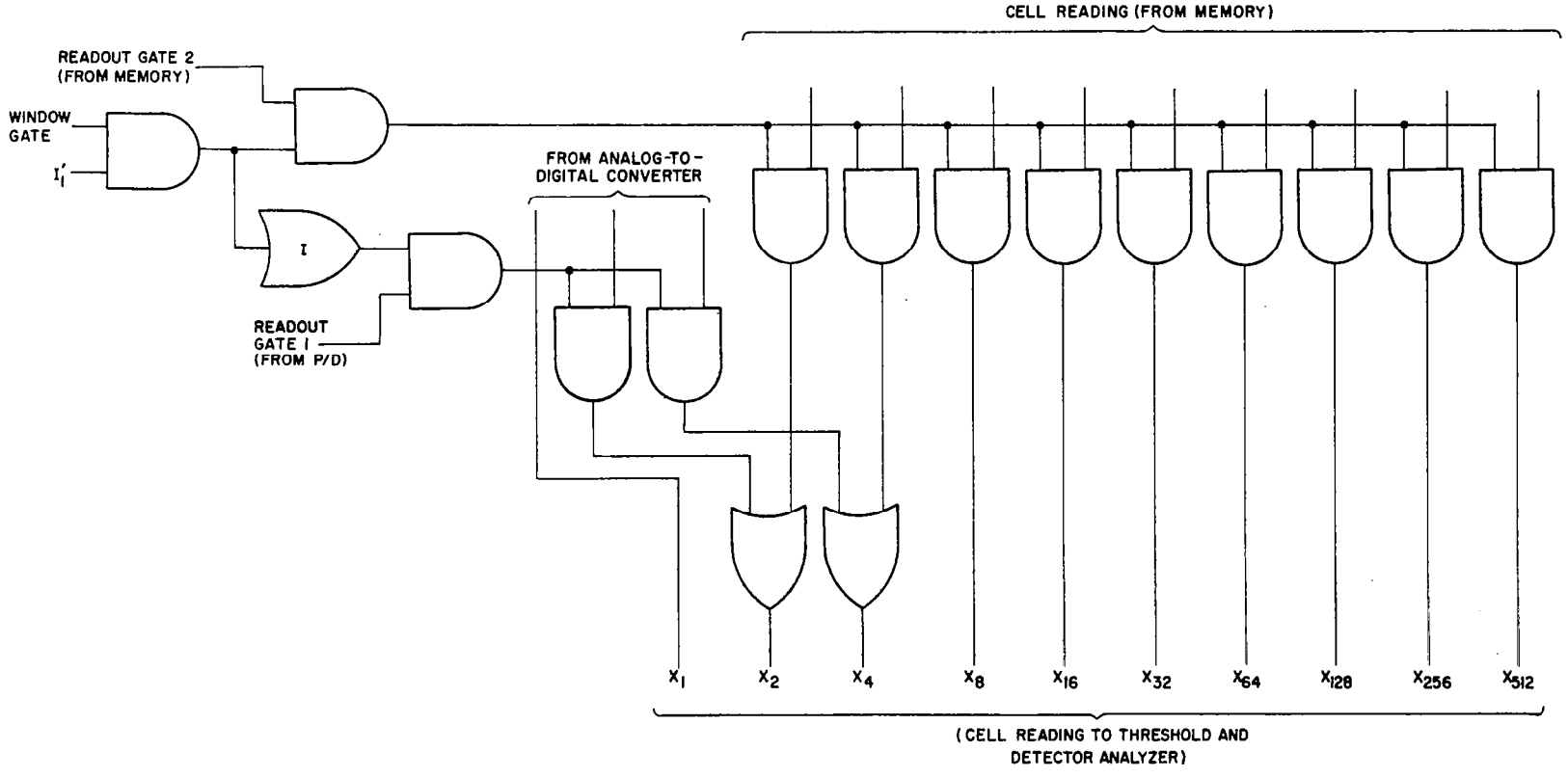

FIGURE 33. SWITCH

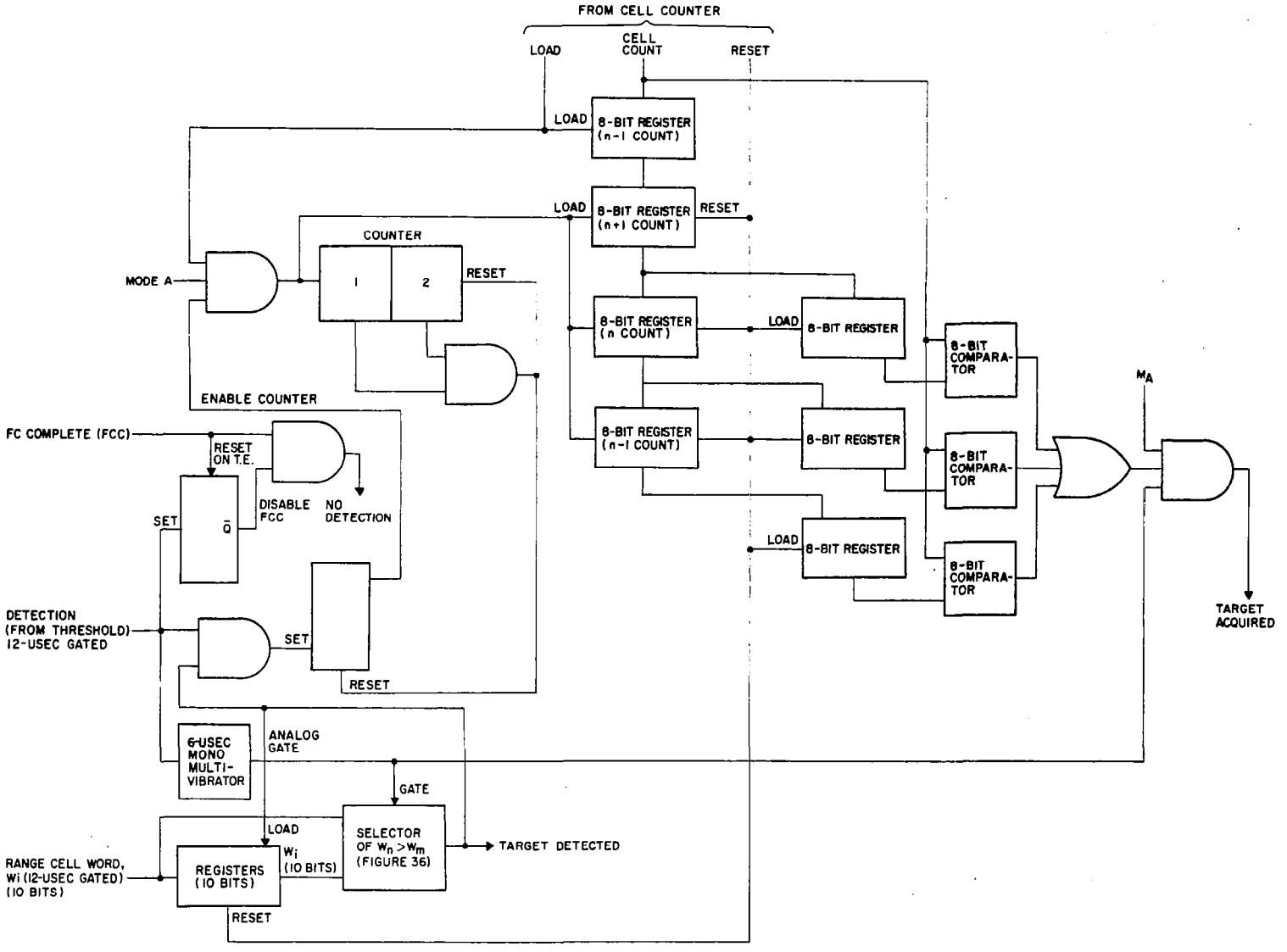

FIGURE 34. DETECTION ANALYZER

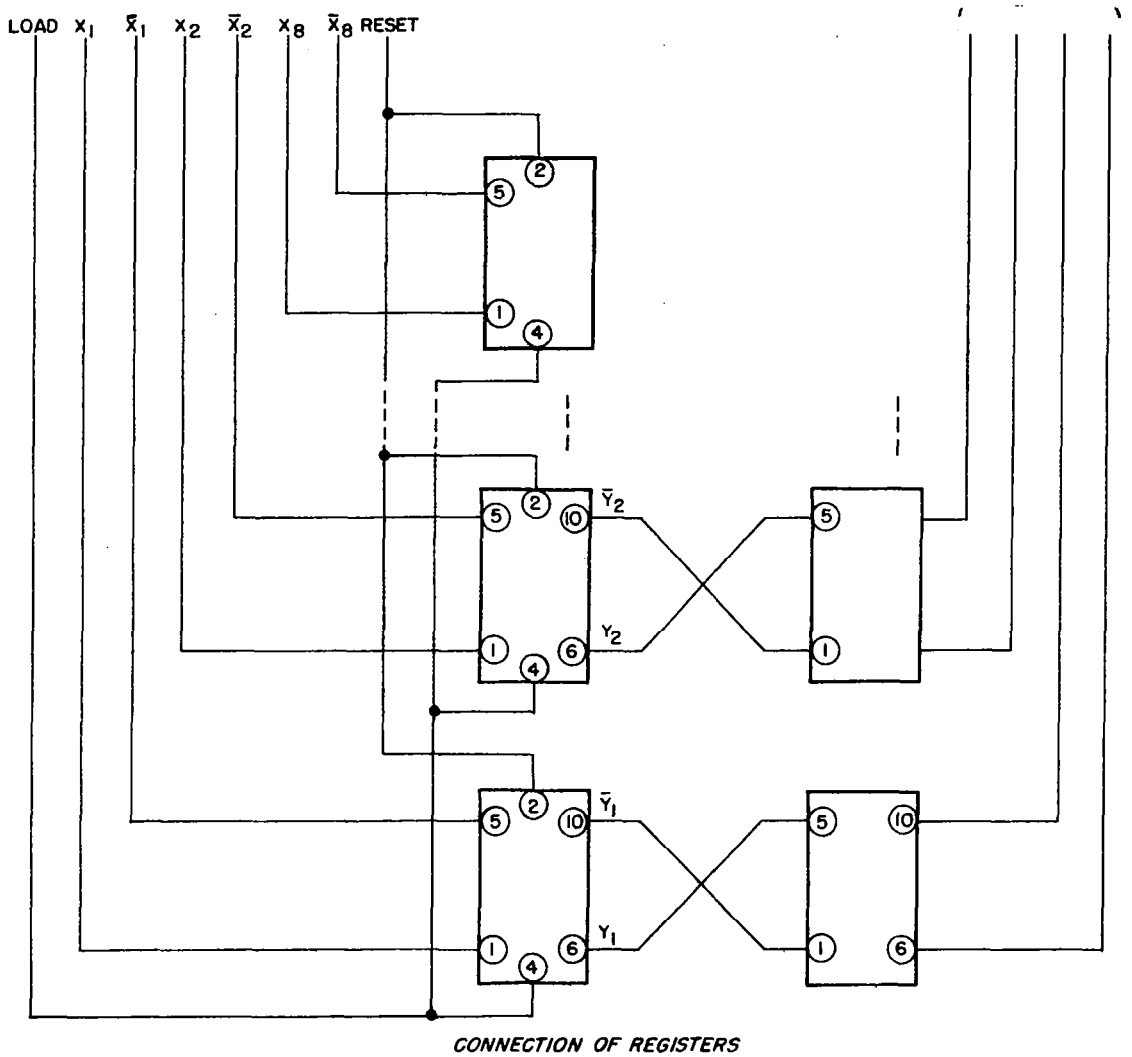

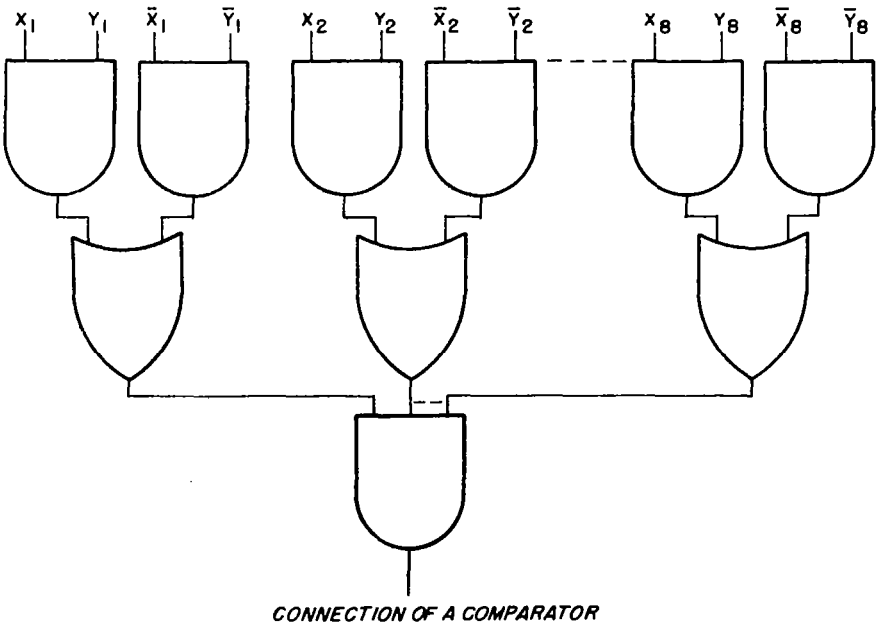

FIGURE 35. DETECTION ANALYZER, CONNECTION OF REGISTERS AND COMPARATOR

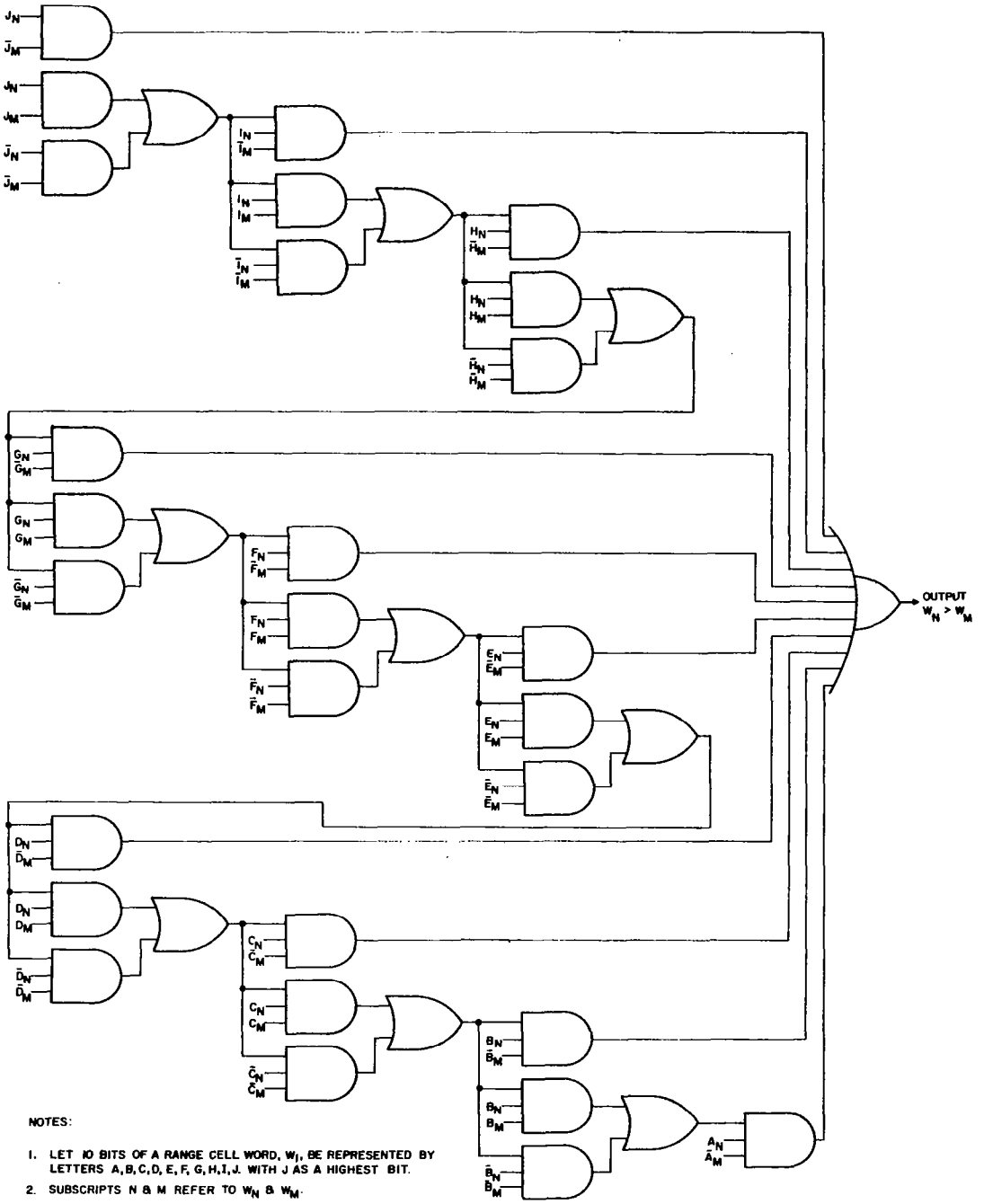

FIGURE 36. DETECTION ANALYZER, SELECTOR $W_n > W_m$

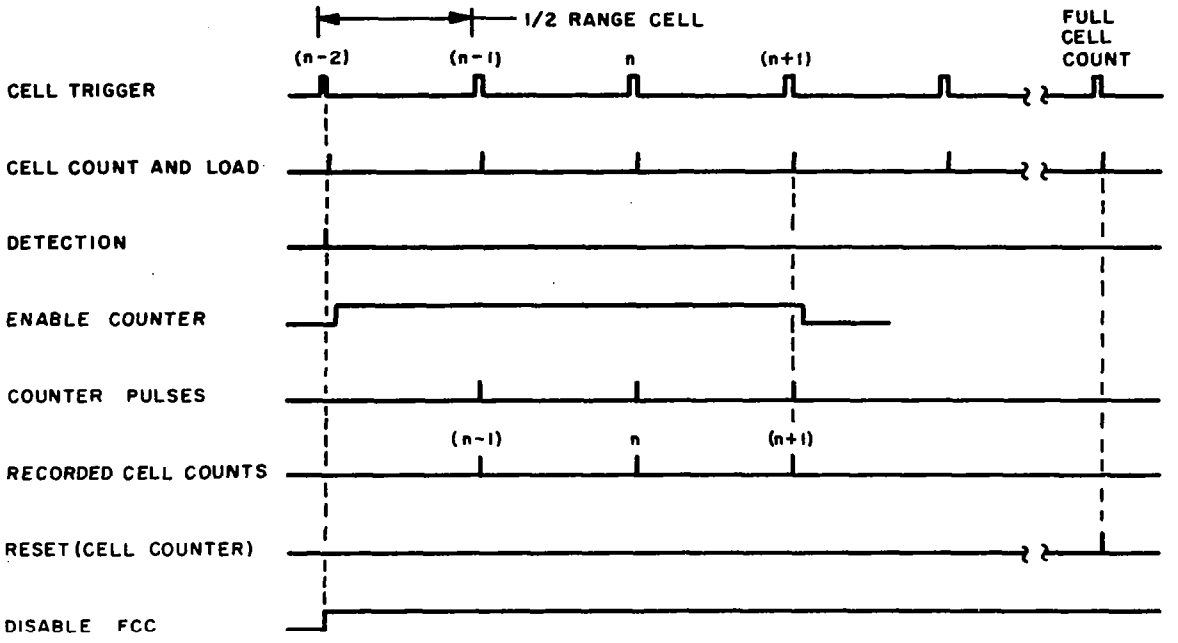

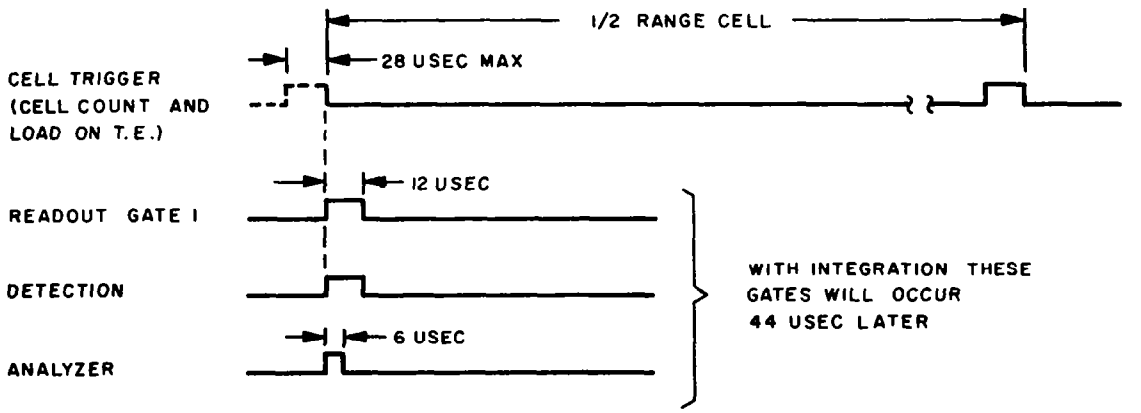

FIGURE 37. DETECTION ANALYZER, TIMING DIAGRAM

In the sounding mode, the comparison of signal amplitude is made after the signal exceeds the threshold in a cell. No action takes place if the signal is weaker. The stronger signal causes the analyzer to initiate a new "Target Detected" pulse which updates the range data recorded in the range registered by the previous detection. (Note that all cells exceeding the threshold can be provided to the telemetry if the data rate capabilities of the latter permit. For the earth, such data would permit the identification of Spread F and split modes, for example. For Mars, the probable isotropic ionosphere will produce a very limited number of echoes at each frequency.) At the completion of the sounding cycle a "No Detection" pulse is generated when there is no cell signal that exceeds the threshold.

The Range Counter and the Gate Generator (Figures 38, 39, 40, and 41) coordinate the proper timing of various gates. In addition to measuring the elapsed time between the transmitted pulse and the return echo, the circuit controls the PRF and pulse width, blanks the processor during the transmitter pulse, triggers the A/D converter, and controls the size and overlap of the range cells. All timing operations are synchronized with the 240-kc clock. In the acquisition mode, the range counter is reset to zero. In the sounding mode, the counter is reset to a positive count for the purpose of advancing the range window. This digital biasing of the range counter introduces a known fixed correction which must be subtracted from the range findings.

Whenever a detection or an acquisition signal is initiated by the Detection Analyzer, the content of the range counter is dumped into the Range Register (Figure 42) which acts as a temporary storage for telemetry or recording.

The Range Comparator (Figure 43) stores in the auxiliary registers the range information obtained in the acquisition mode. In the sounding mode this data is compared with the count of the range counter which has been offset to place the range window properly. When the same count is reached by the counter, the comparator generates a pulse which marks the beginning of the range windows. The three lowest bits are ignored as nonessential in the absolute position of the windows.

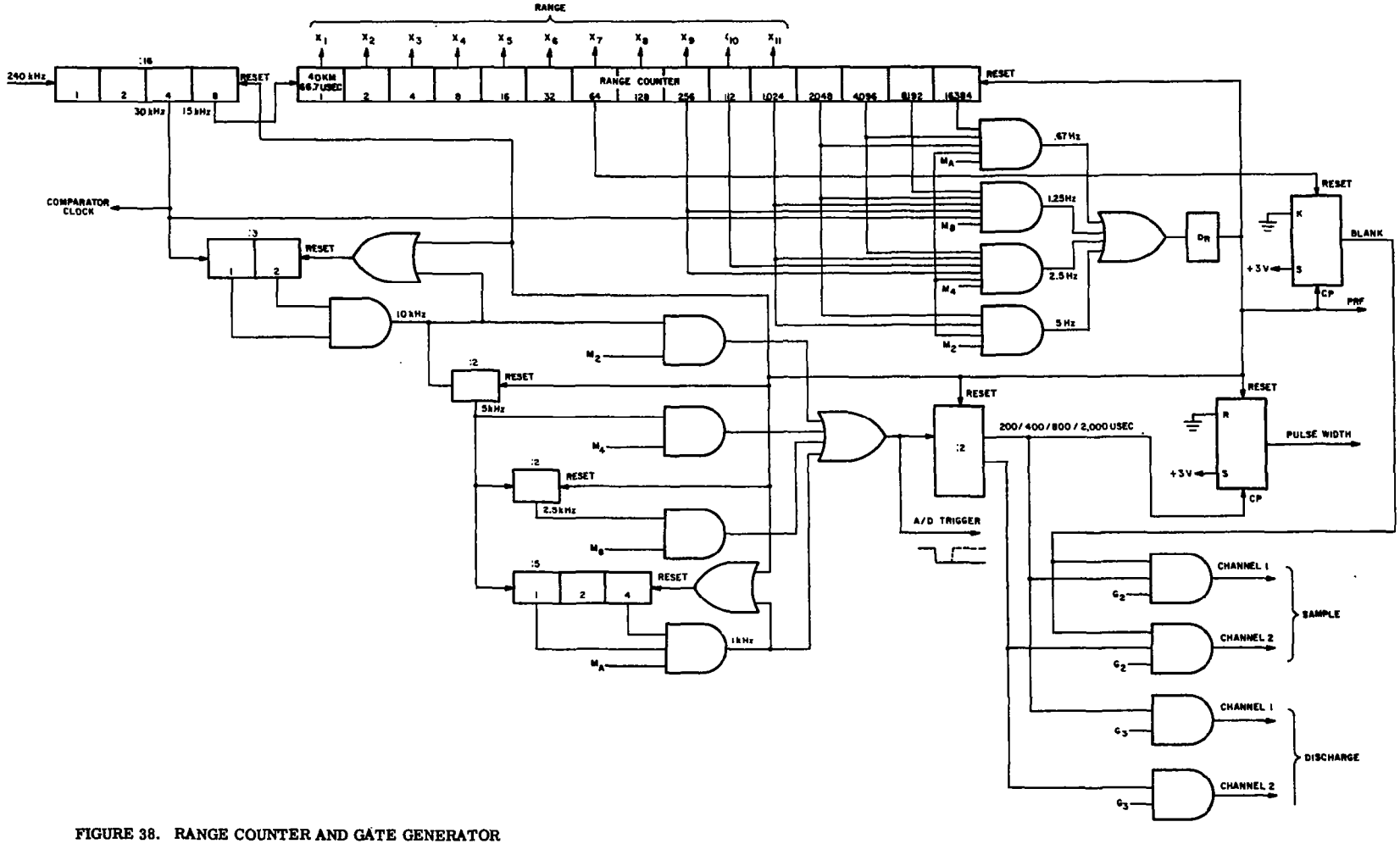

FIGURE 38. RANGE COUNTER AND GATE GENERATOR

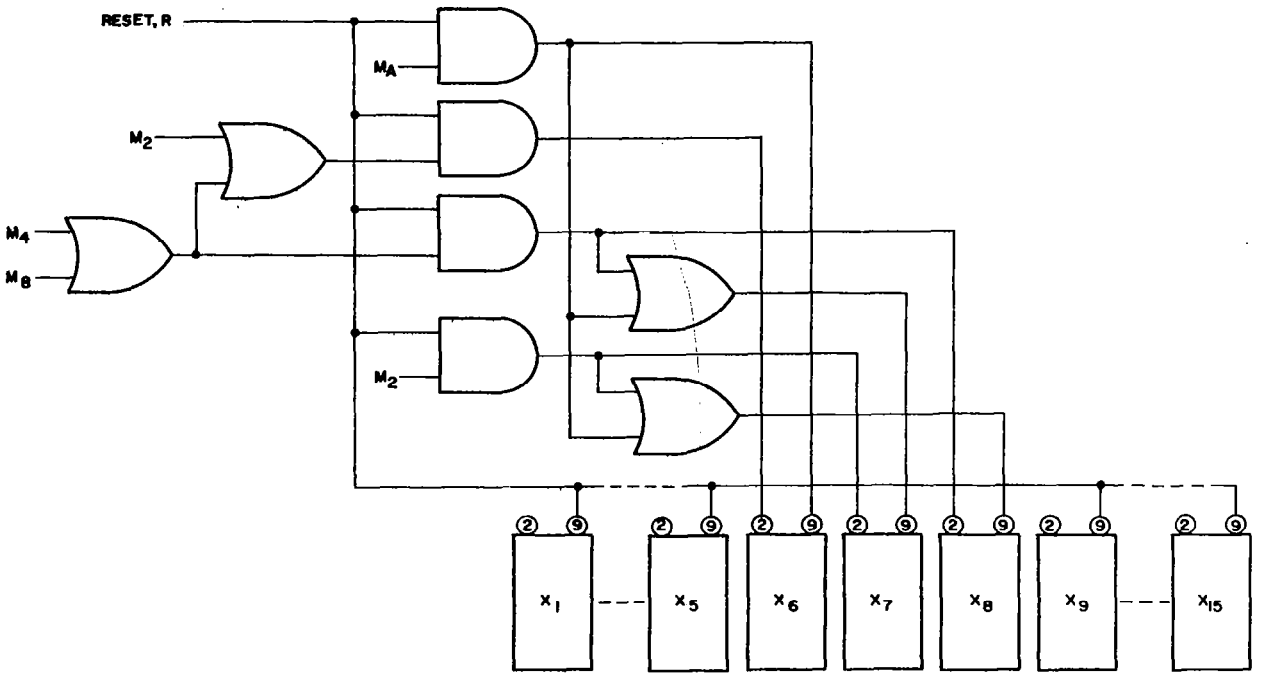

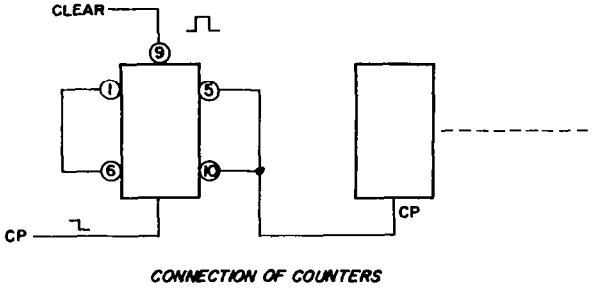

FIGURE 39. RANGE COUNTER AND GATE GENERATOR, RESETTING OF RANGE COUNTER AND CONNECTION OF COUNTERS

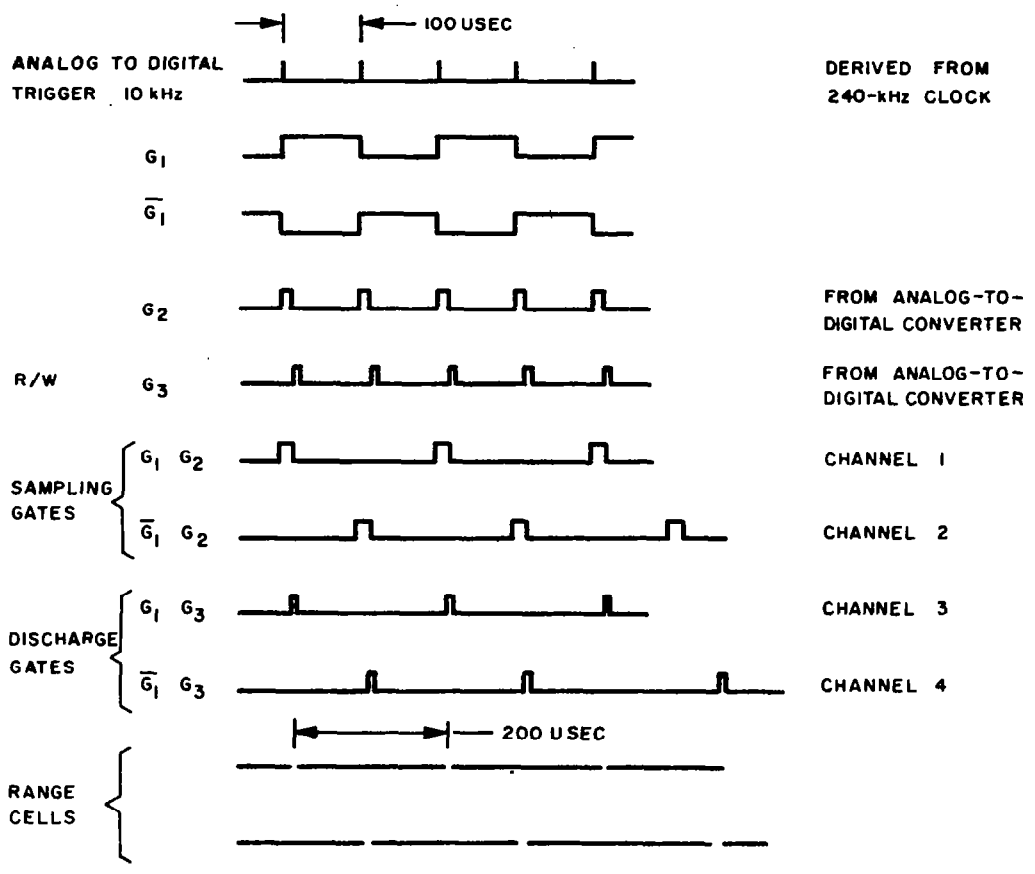

FIGURE 40. RANGE COUNTER AND GATE GENERATOR, TIMING DIAGRAM FOR 200 μSEC MODE

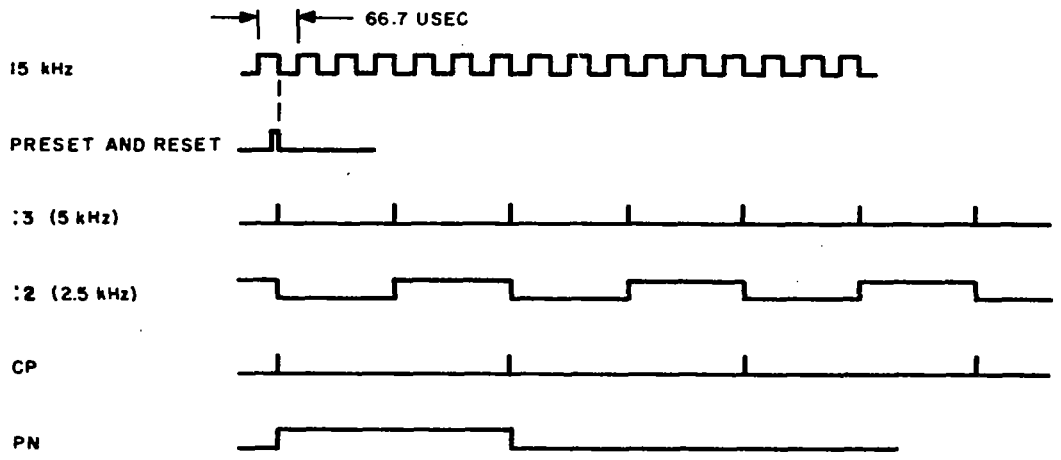

FIGURE 41. RANGE COUNTER AND GATE GENERATOR (TIMING DIAGRAM)

The Range Selector (Figure 44) divides the operating range into ten range sectors which are used by the Integration Selector to determine the number of integrations to be made. It also selects the intermediate range for the 400-μsec mode and the long range ($\geq$12, 000 km) at which reacquisition of the target must be made after each sounding cycle.

The Integration Selector (Figure 45) accepts the range sector and frequency information and determines how many integrations must be performed and also what the threshold setting should be. The numbers vary from one (or no integration) through 4, 8, 16, etc. up to the maximum number of 160. No attempt is made to integrate more than 160 pulses because in most cases the duration of integration would exceed the time that the target would remain within the range cell.

The Mode Selector (Figure 46) controls the operating modes and generates a mode code for telemetry purposes. Whenever a "No Detection" or "Reacquire" pulse is received, the selector initiates the

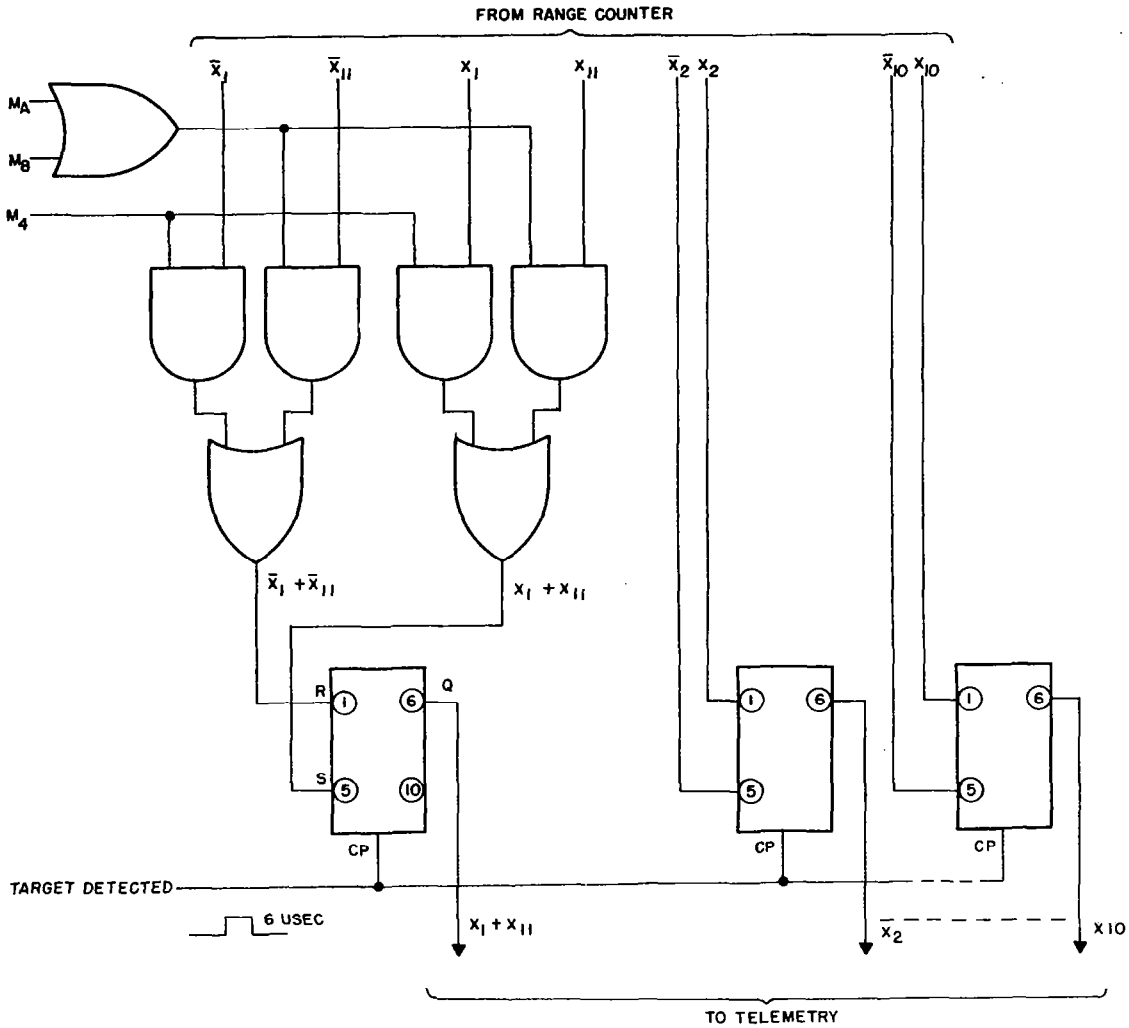

FIGURE 42. RANGE SHIFT REGISTERS

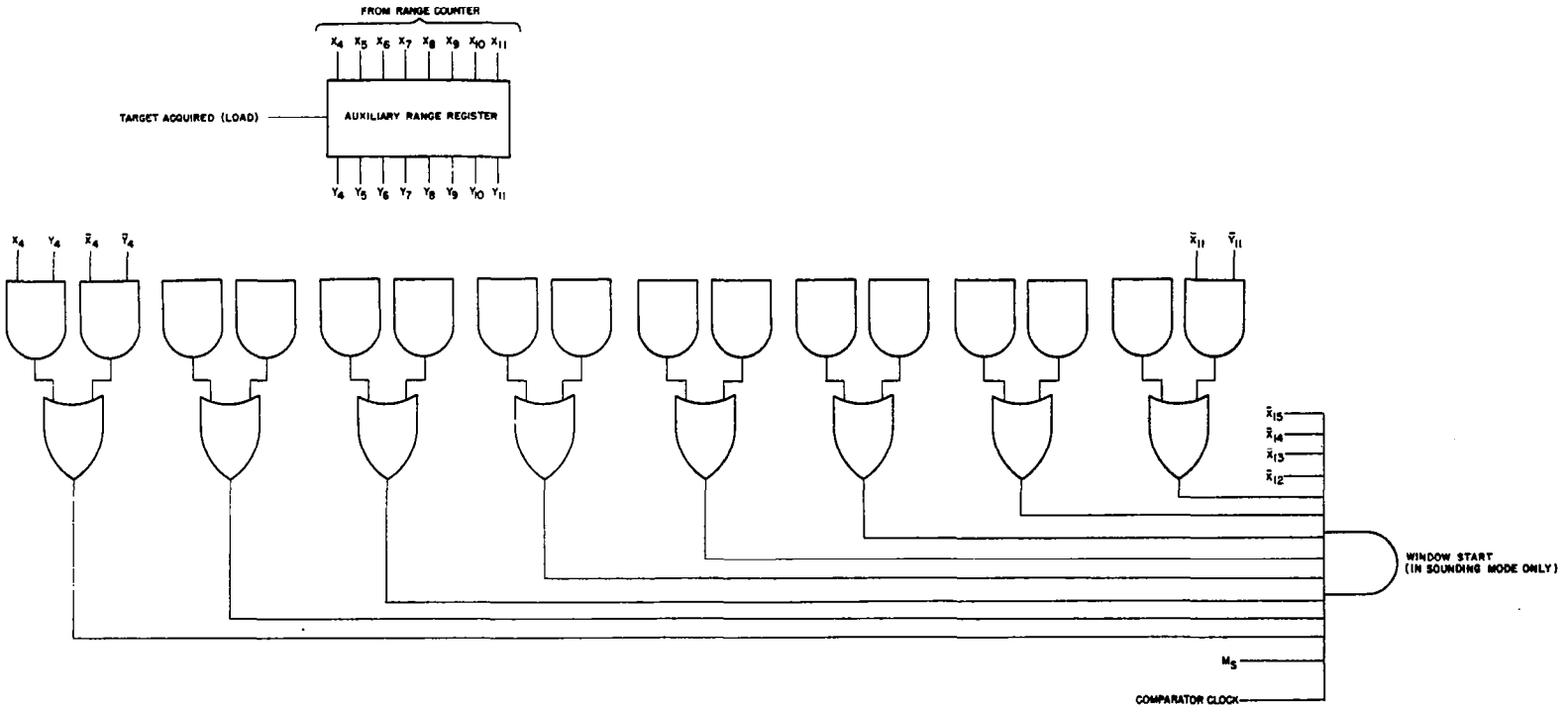

FIGURE 43. RANGE COMPARATOR

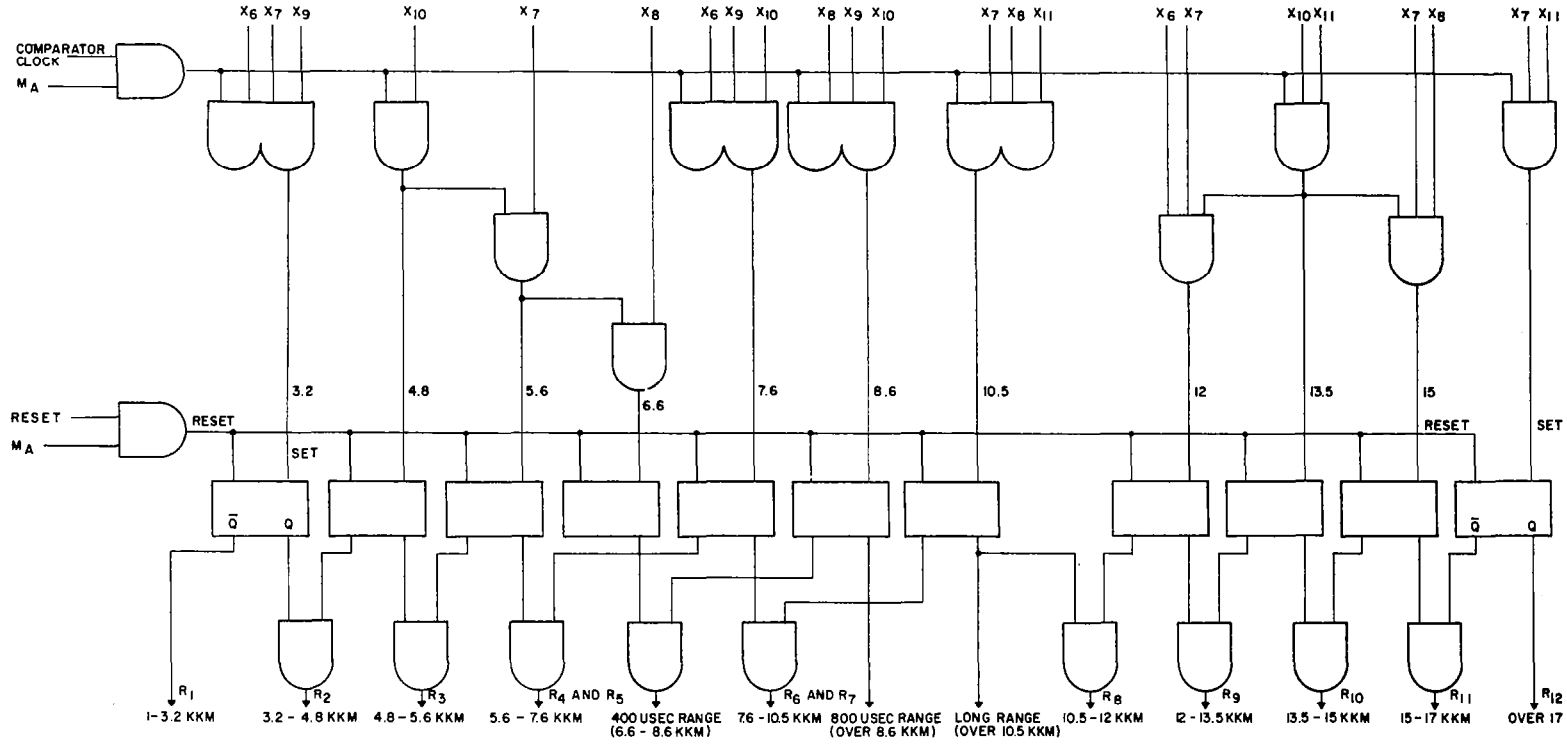

FIGURE 44. RANGE SELECTOR

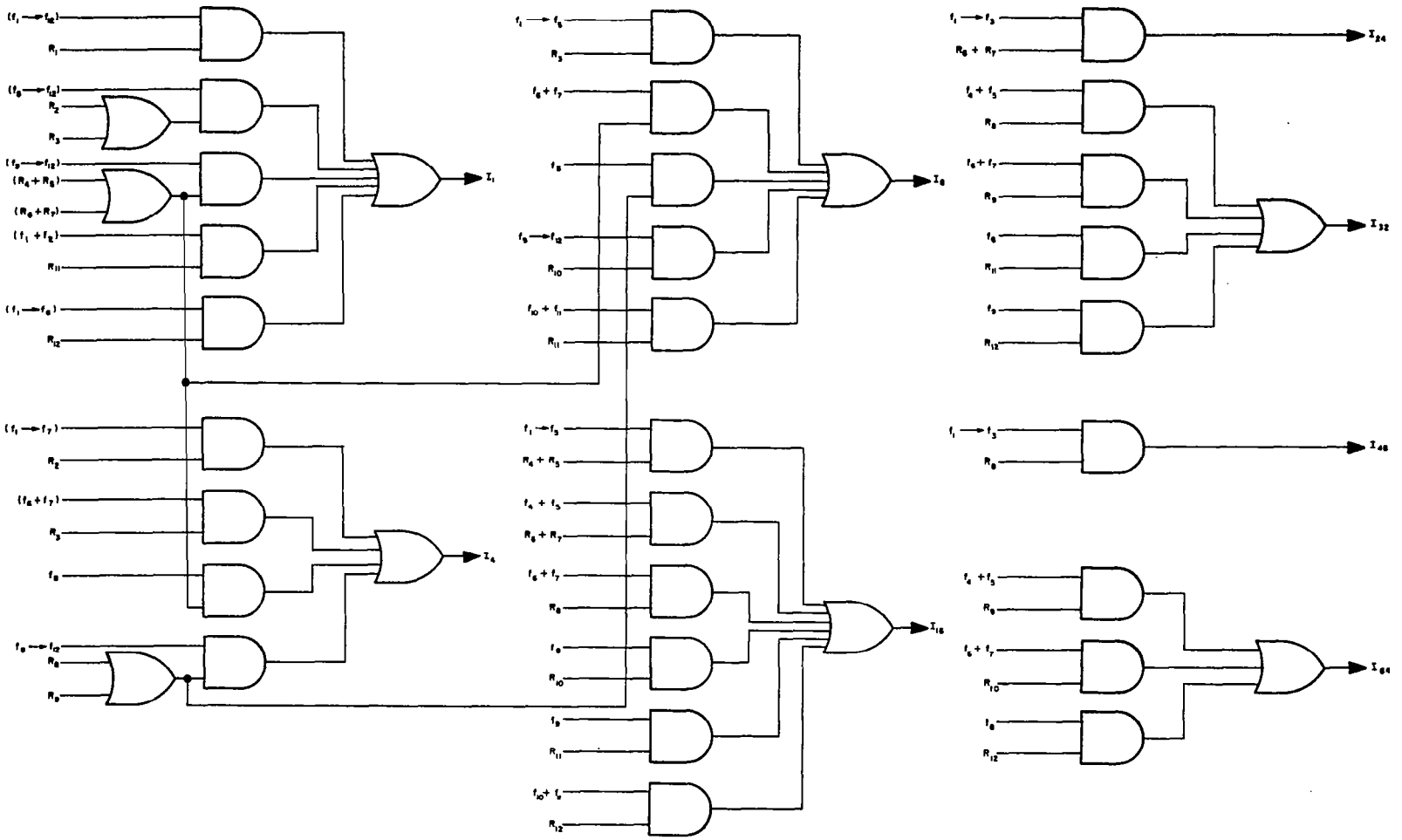

FIGURE 45. INTEGRATION SELECTOR
(SHEET 1 OF 2)

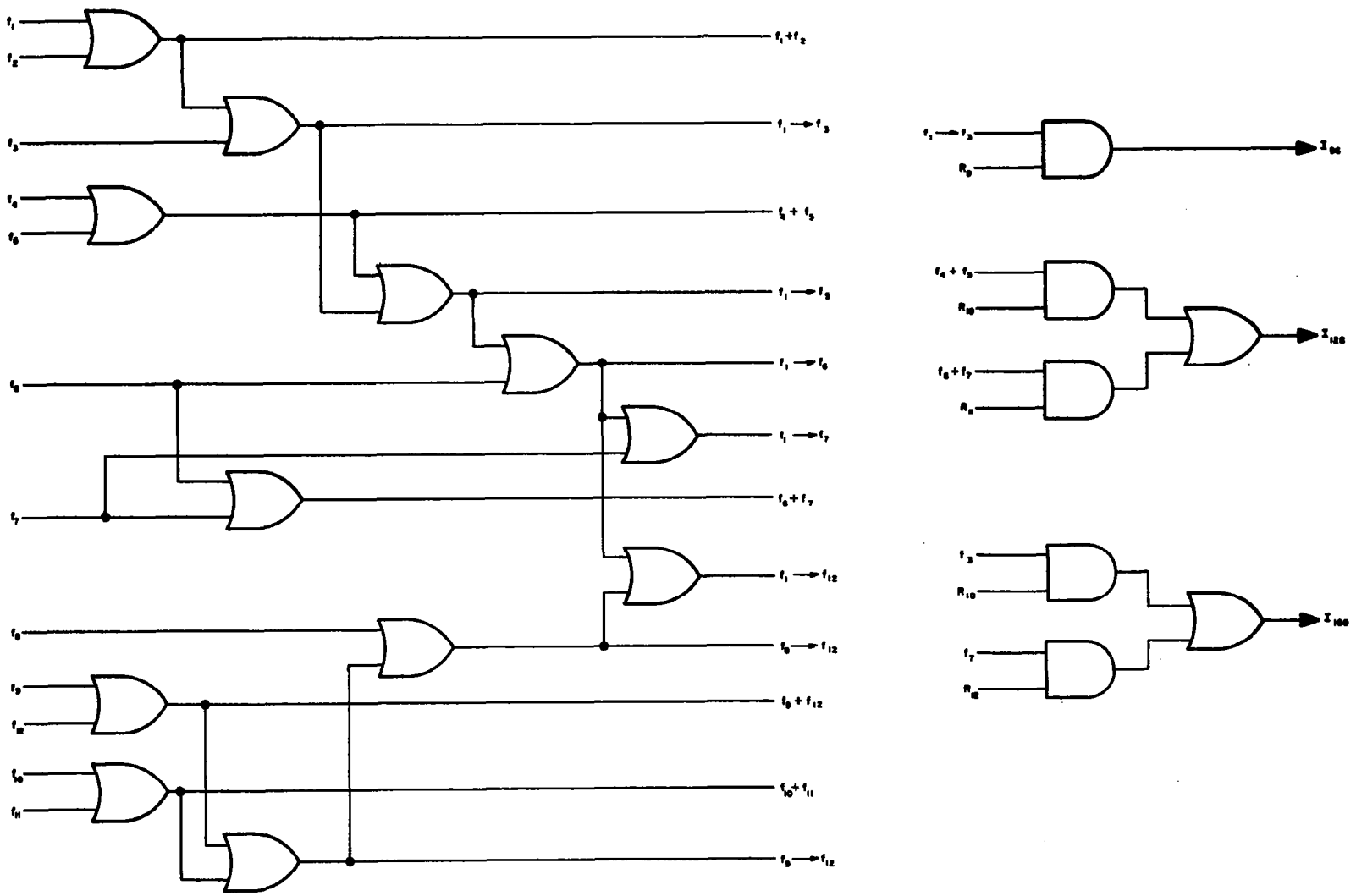

FIGURE 45. INTEGRATION SELECTOR (SHEET 2 OF 2)

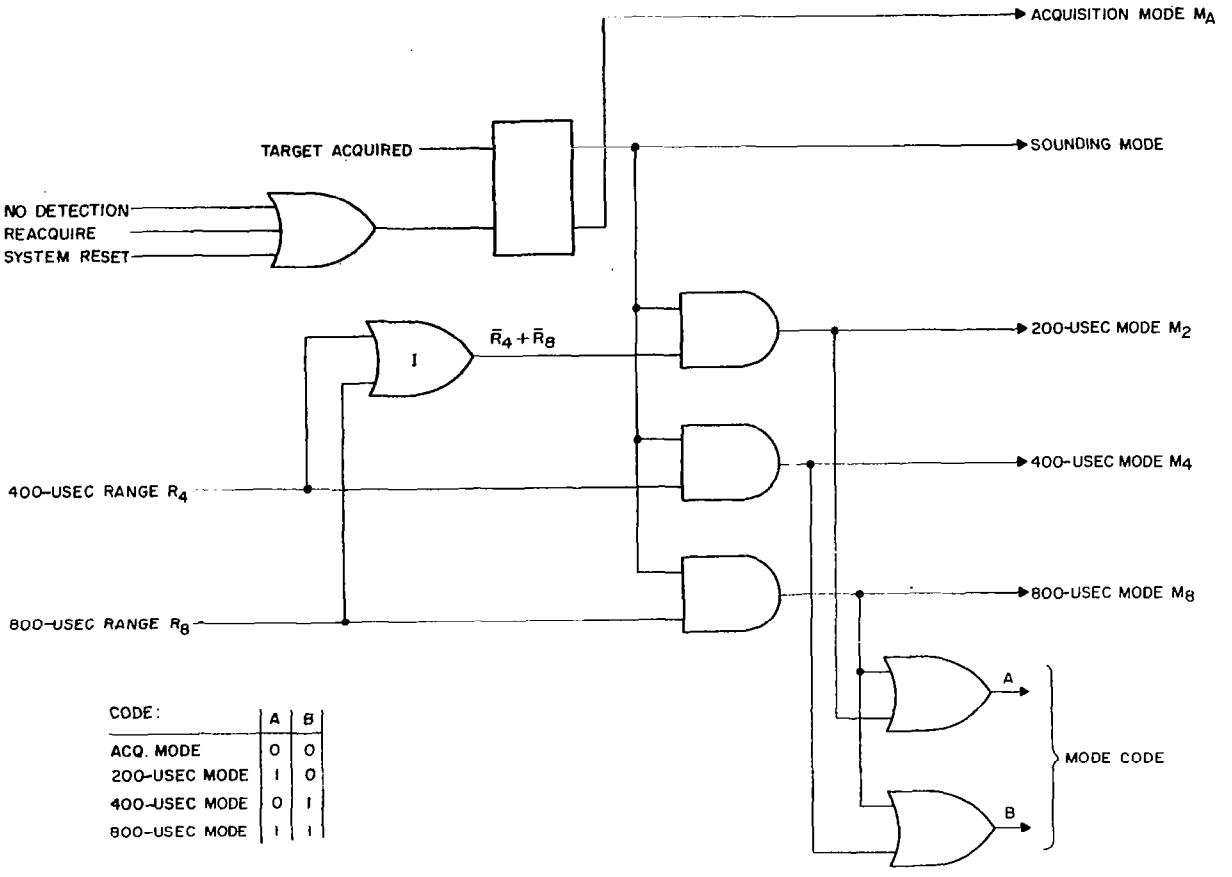

CODE:	A	B
ACQ. MODE	0	0
200-USEC MODE	1	0
400-USEC MODE	0	1
800-USEC MODE	1	1

FIGURE 46. MODE SELECTOR

acquisition mode. Upon target acquisition it selects one of the sounding modes depending on the distance to the target.

The Integration Counter and Frequency Encoder (Figure 47) is a bookkeeping circuit for the signal processor. It keeps the record of (1) the number of pulses already integrated, (2) the frequencies used in the sounding cycle, and (3) the number of sounding cycles between reacquisitions. Upon completion of the required number of integrations, the integration counter enables the Threshold and clears the Memory in preparation for the next cycle. The frequency counter selects the frequencies in a preset sequence which does not change. It provides a digital code to the Frequency Synthesizer directing the latter to generate the frequency specified in the code. (Note that this method of controlling frequency can be extended to any number of frequencies and to programming frequency selection.) At ranges below 12,000 km the cycle counter permits four sounding cycles to be performed before instructing the system to reacquire the target.

The Cell Counter (Figure 48) supplies the Detection Analyzer with the cell count information. It also generates 80 read-write triggers, one for each range cell word and each PRF period. In the acquisition mode the range cells are counted throughout the entire range of 20,000 km because that information is required by the Detection Analyzer for the purposes of sensing the detection coincidence. In the sounding mode, the cell count data is not used by the Analyzer and the cell counter has to supply only the read-write triggers. The window gate generated by the counter is used by the Switch to enable the range cell words from the Adder and to disable the direct path from the A/D converter.

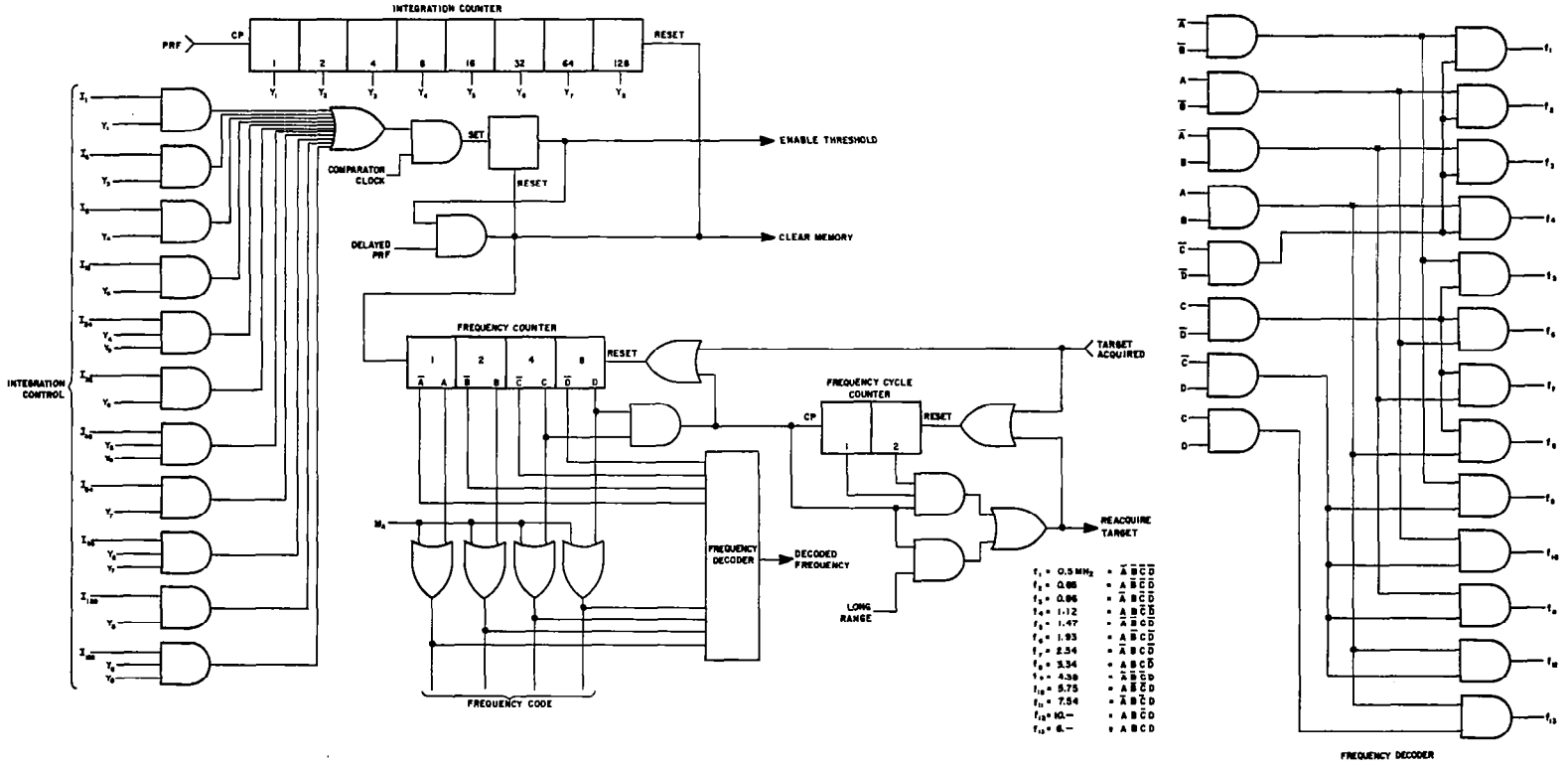

FIGURE 47. INTEGRATION COUNTER AND FREQUENCY ENCODER

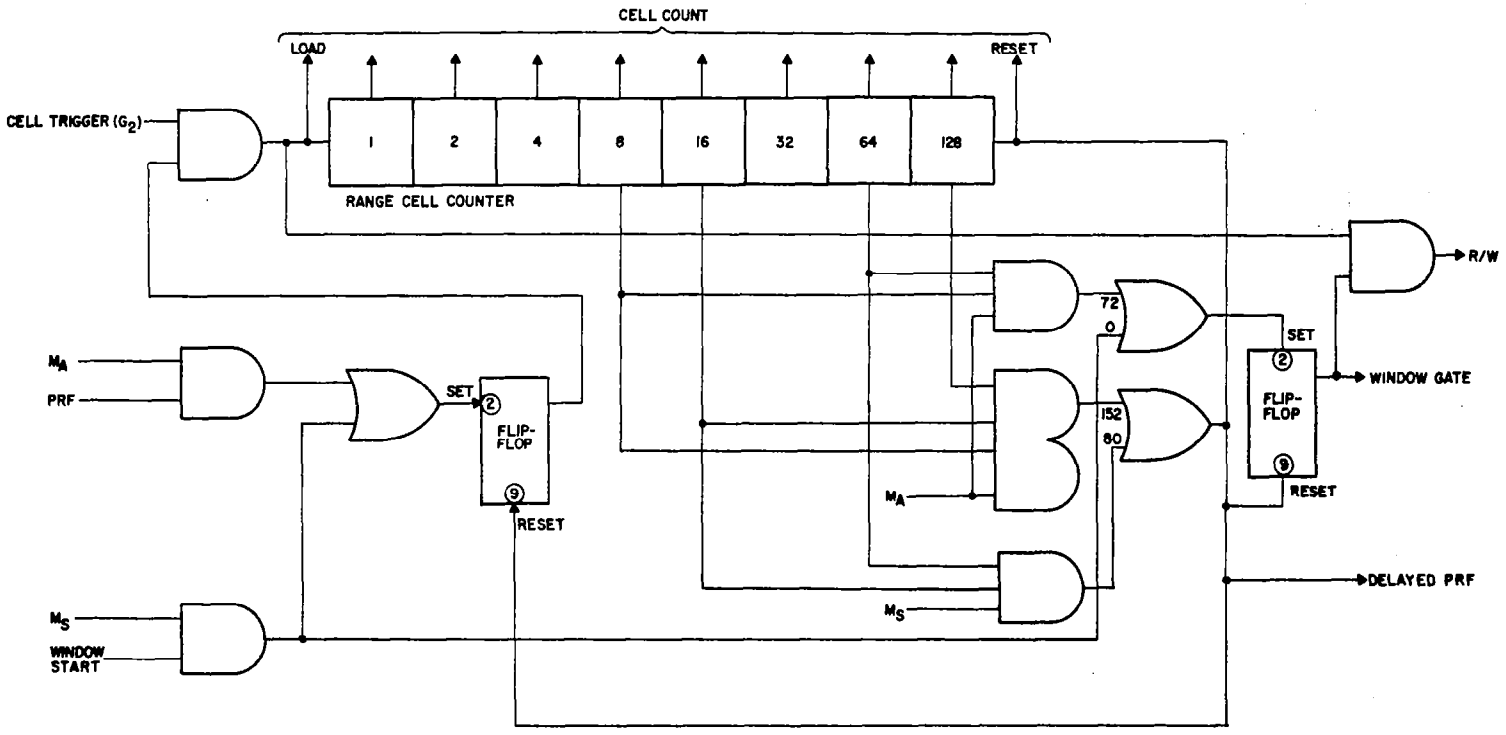

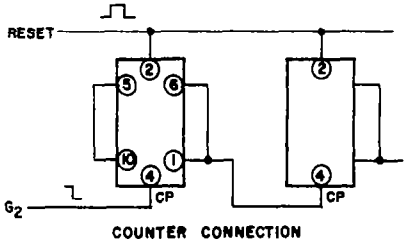

FIGURE 48. CELL COUNTER

3.4 SYSTEM PERFORMANCE AND LIMITATIONS

One of the characteristics that can be used in evaluation of system performance is the amount of good data gathered during the mission. The number of sounding cycles that the signal processor is capable of completing under the favorable conditions (a sounding cycle consists of 12 soundings-one at each frequency) depends on the "miss" distance as can be seen in Table VIII. (Note that the totals given in the table represent one-half the trajectory and, therefore, one-half the total.) There may be as many as 1860 complete soundings in the mission when the "miss" distance is 1000 km or as few as 54 with the "miss" distance of 15,000 km. Note that some of these cycles may not contain all frequencies. The absence of the low frequency readings which require more integrations may be caused by the target moving out of the range cell before the completion of the integration cycle, as explained below. Fortunately, there will not be many of these incomplete soundings and the amount of missing data will be insignificant.

Theoretically, the number of post-detection integrations can be as large as 1000 or more. However, in the Mariner mission, integration of the large number of pulses is complicated by two factors: (1) the relatively low PRF which makes integration a lengthy process, and (2) the change of the distance between the reflecting region and the spacecraft due to relative motion. The maximum expected rate of change of radial distance is about 2.2 km per second. Thus, while the integration process continues, the target may move out of the range cell. This could happen at low frequencies and at large distances when the number of required integrations is large. These limitations were plotted as a function of "miss" distance for different frequencies and are shown in Figure 49. In order to read this figure, one should first select the "miss" distance on the vertical axis. Then, by drawing a horizontal line corresponding to the selected "miss" distance, it is a simple matter to read off the frequencies and corresponding distances on the abscissa above which the integration process cannot be performed, without compensating for the relative motion. It can be

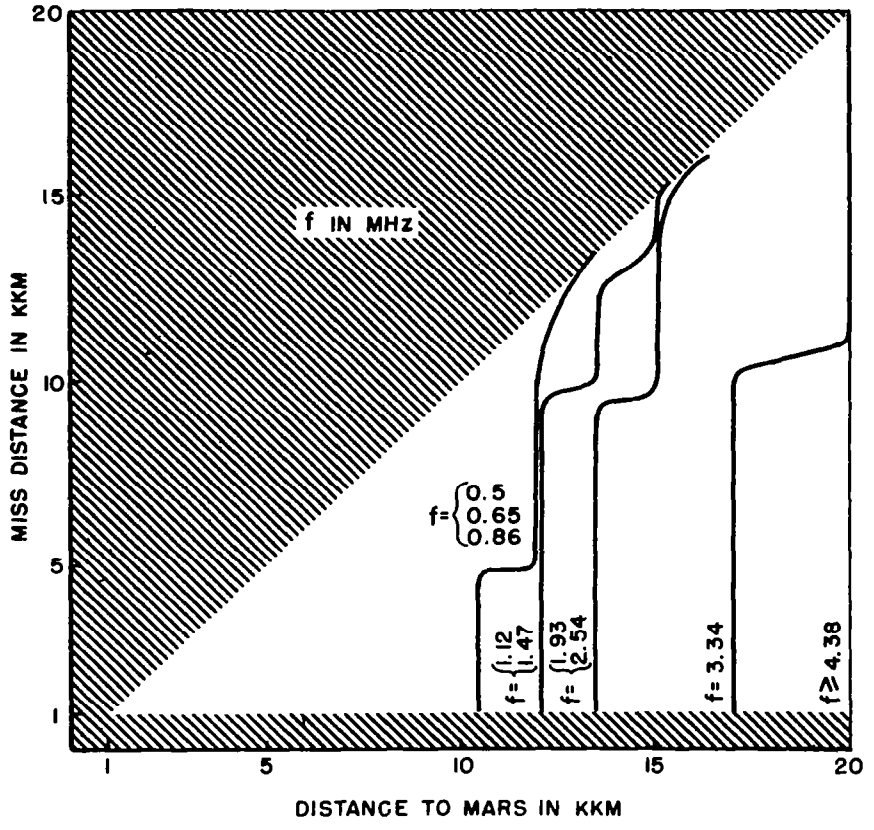

$\frac{S}{N}$ = 12.5 db, P_D = 90%, $P_{FA} = 10^{-6}$

PW = 200/400/800 USEC

P_{AVG} = 1/4 W

FIGURE 49. RANGE LIMITATION DUE TO TARGET MOTION

TABLE VIII. NUMBER OF SOUNDING CYCLES

Range Interval (in kkm)	Freq Cycle Duration (sec)	MISS DISTANCE									
		1000 km		2000 km		5000 km		10,000 km		15,000 km	
		T	N	T	N	T	N	T	N	T	N
1.0 - 3.2	2.4	1700	708	1300	540						
3.2 - 4.8	5.8	700	120	800	138						
4.8 - 5.6	10.6	400	37	400	37	1200	113				
5.6 - 6.6	20.4	500	24	500	24	1000	48				
6.6 - 7.6	40.8	400	9	400	9	800	18				
7.6 - 8.6	51.2	500	9	500	9	700	13				
8.6 - 10.5	102.4	1000	9	1000	9	1200	10				
10.5 - 12.0	211.0	800	3	800	3	800	3	1200	5		
12.0 - 13.5	404.0	800	2	800	2	800	2	2600	6		
13.5 - 15.0	475.0	800	2	800	2	800	2	1900	4		
15.0 - 17.0	475.0	1000	2	1000	2	1000	2	1500	3	6000	12
17.0 - 20.0	254.0	1400	5	1400	5	1400	5	1500	5	4000	15
1/2 Total			930		780		216		23		27

T = time in the range intervals (sec)

N = No. of sounding cycles (sounding cycle consists of 12 frequencies) in range interval.

seen that no limitations in range occur when making soundings at frequencies at or above 4.38 MHz for the range of distances to 20,000 km.

3.5 SIMPLIFICATIONS AND SUGGESTIONS

There are several areas where the Signal Processor may be simplified by reducing the amount of hardware or improving its operation. These improvements depend on the compromises made between resolution and sounding rate requirements. If the transmitter average power were increased from 1/4 watt to 1/2 watt, the range limitations described in the preceding section would be somewhat alleviated. Moreover, the system could be simplified by eliminating the 400-μsec mode. The 200-μsec mode would then extend its range to 7600 km and beyond that range the 800-μsec mode could be used. However, increasing the transmitter average power to 1/2 watt will increase the total power taken by the entire system by roughly 1.25 watts.

The design of the Integration Selector can be simplified by reassigning the numbers in Table VII. Smaller steps can be eliminated by promoting them to the next higher number. A resultant small increase in the duration of the sounding cycle would then occur.

A different scheme for detection and decision making should be investigated. Very preliminary investigation indicates that it may improve the quality of detection and evaluation as well as the system range accuracy. This scheme utilizes coincidence detection in fine range sounding. At the present time, the Detection Analyzer makes the decision on the basis of only one integration cycle and selects the range cell with the strongest signal. The proposed Coincidence Detection scheme could perform two integration cycles, instead of one, accomplishing only one-half the number of integrations and using a lower threshold. (Thus, the overall duration of the integration cycle would remain the same.) Each range cell of one integration cycle will be checked for coincidence of detection (if any) with the corresponding cell of the preceding cycle. Under these conditions it is expected that the likelihood of false multiple coincidences is rather remote. Implementation of the scheme requires additional memory capacity and re-

design of several circuits. It may be possible to utilize the existing memory unit by assigning an additional bit to each range cell word to indicate the presence or absence of detection.

The present design of the integrator assumes that the total number of bits required by all range cell words exactly equals the number of bits available in the memory unit. Therefore, as the last bit of the last range cell word is being loaded into the memory, the first bit of the first word simultaneously advances to the first position, ready to be read out on the next PRF. A more sophisticated design can be used to eliminate the restriction that the number of available and required bits be the same. The advantage of such a scheme would be a more flexible use of standard memory units. This can be done by an addition of an address code that would precede the first range cell word. Each time all the range cell words have been stored in the memory, the remaining storage bits would be filled in with blanks until the address code is recognized at the output, signifying the approach of the first range cell word. This feature was not implemented because no difficulty is anticipated in obtaining the memory unit with the exact number of bits required (once the system design has been completed). Whenever possible, the design philosophy has been not to overdesign the system unnecessarily, thereby keeping the weight, volume, and power consumption to the minimum.

3.6 ADDITIONAL WORK AND INTERFACE CONSIDERATIONS

There remains some design work to be completed before the breadboard phase can be started. The extent of additional design depends a great deal on interface considerations yet to be worked out. The present design uses AND/OR logic which must be converted to NAND/NOR if the proposed integrated circuits are to be used. Design of the limiter can be finished once the IF signal level has been established. Frequency and mode codes were tentatively selected but may have to be changed. The sequence at which the frequencies are to be used must be agreed upon. The parity check circuit will depend on the output word format. Detailed wiring drawings must also be prepared. While all

of these are only minor considerations details must be worked out and the design completed.

3.7 PARTS AND POWER SUPPLIES

The design of the Mariner experiment was based on the use of the parts listed below. Some of these parts are standard, or almost standard, off-the-shelf items. Others must be purchased to specifications that must be generated. Preliminary inquiries were made to ensure that the requirements imposed by this experiment are within the state of the art. The delivery of certain parts, for example, crystal filters, can be as long as 14 weeks. Therefore, purchase orders must be placed early so that the delivery of critical items does not interfere with the unit and system testing and, consequently, the on-time delivery of the equipment.

Integrated logic	TI series, 51RCTL
Integrated amplifier	Fairchild, uA702
Analog switch	Fairchild, SH3001
240-kc clock	Bulova or Bendix to AIL spec
Memory	Interstate Electronics, thin magnetic film to AIL spec
Crystal filter	McCoy Electronics to AIL spec

On the basis of the proposed parts, the following power supplies will be required:

+ 3 v DC for TI Integrated logic
+ 6 v DC for Amplifier and Memory
- 3 v DC for Amplifier
+12 v DC for Memory and Analog Switch
-12 v DC for Memory
-20 v DC for Analog Switch

Where parts are purchased to AIL specifications, preference should be given to the previously listed power supply requirements.

It is expected that the following design criteria will not be exceeded:

Power consumption:	3.0 watts
Weight:	2-1/2 pounds
Volume:	120 $in.^3$

SECTION IV
TRANSMITTER AND MATCHING NETWORK

This section is divided into two parts. The first part is a description of the transmitter breadboarding effort and the second part includes results of the study of the matching network and switching elements. The requirements of both efforts were mainly based upon the Mars-Mariner application. However, the results are useful for many other missions as well.

1. TRANSMITTER

1.1 GENERAL

The power versus frequency requirements at the input to the antenna matching network are shown in Figure 19. A breadboard sounder transmitter was constructed with these requirements as a design objective. Standard commercial hardware was used wherever possible for this feasibility study because it was readily available.

The transmitter input signal was derived from a signal generator. The techniques for frequency synthesis are well-established and low level frequency generation, therefore, was not included in this study.

The original intent was to develop a broad-band transmitter; however, the goal was hampered by high frequency limitations which are due to the internal construction of commercially available power transistors used for the driver and output stage. Therefore, the effort was directed toward obtaining the required performance at lower frequencies until suitable transistor modifications could be obtained.

Since the transmitter drives the two monopoles of a dipole antenna, it is planned to power each monopole from separate power stages. The development here was for the stages to drive one of the monopoles, so that the power requirement for this unit is half that shown

in Figure 19. The other pole is driven by a duplicate unit, 180 degrees out of RF phase. Duplication is only necessary above some power level. Below that level a common amplifier may be used.

1.2 CONFIGURATION

A schematic of the transmitter is shown in Figure 50; the transmitter consists of a pulser section and an RF section.

The pulser section applies power to the RF section for a prescribed pulse duration. The pulser is a series of emitter followers in cascade to provide a high power, low impedance output when driven from low power logic. The RF section contains two amplifiers, driver, and a push-pull output stage. Coupling between the amplifiers, driver, and output is achieved with broad-band transformers. In a final sounder configuration an additional stage would be required prior to the driver and used as a power splitter for the stages driving the second monopole.

1.3 TECHNICAL ASPECTS

The amplifiers consist of a 2N1506 and an FT34A. Broad-band performance was obtained in these stages by resistive degeneration in the emitter circuit of the 2N1506 with bypassing at the higher frequencies. Since the frequency response of the FT34A is less than the 2N1506, additional local feedback was employed with high frequency compensation in the feedback loop.

The power transistors used in the breadboard transmitter were existing commercial devices in standard case configurations. The driver and push-pull output stages utilize an NPN triple-diffused silicon transistor of the 2N1899 family. It is a single-ended power package with a steady-state power dissipation of 125 watts at 25^{o}C. The wafer is located on the mounting stud and connection to the emitter and base pins is accomplished internally through 3/4-inch leads. An additional 1/4-inch of pin exists between the internal lead connection and the exterior of the case. The long connection, primarily in the emitter lead, causes degeneration in wide-band applications. This series lead inductance can only be resonated out over a narrow frequency range. The reactance is comparable to the low impedance levels involved.

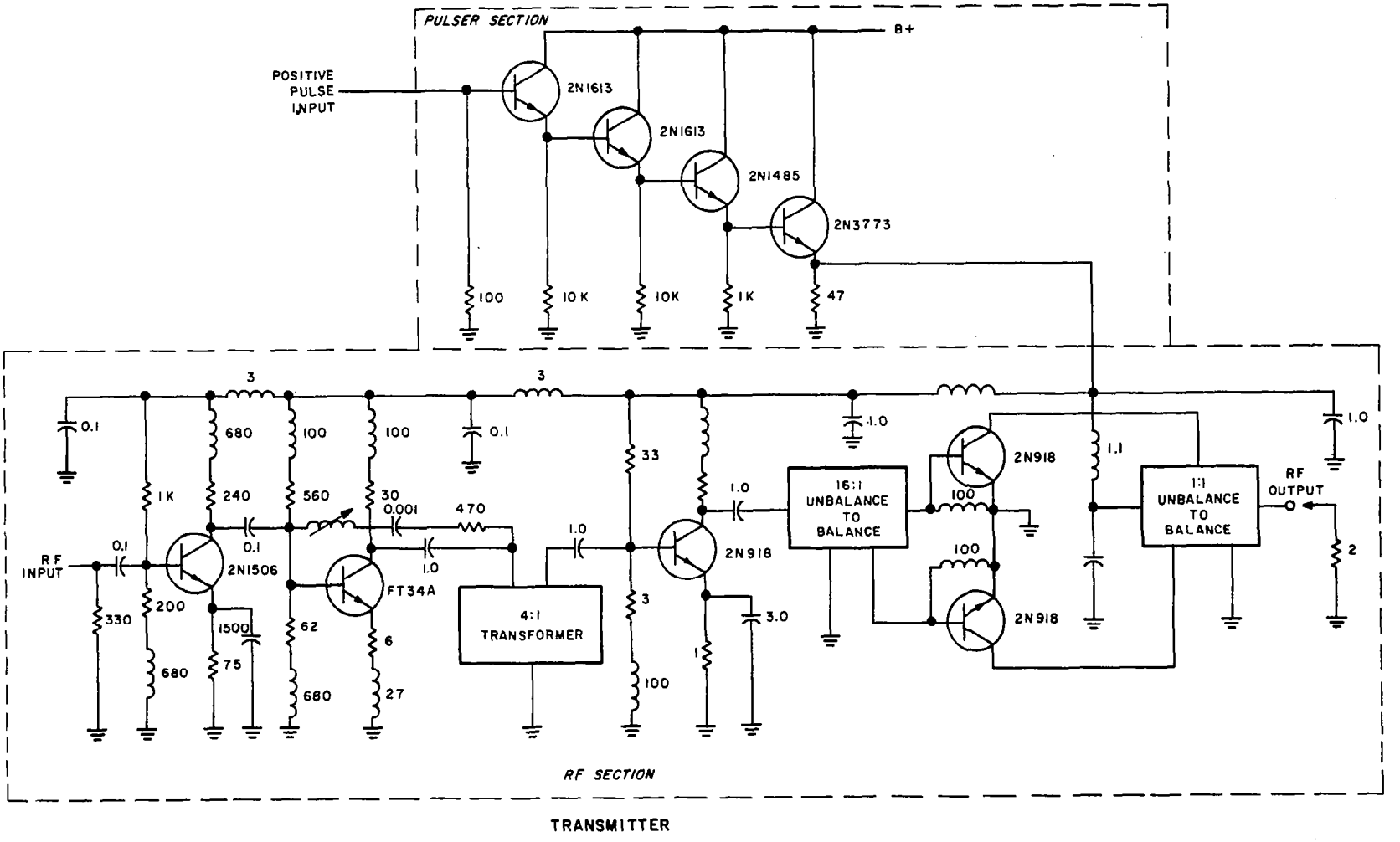

TRANSMITTER

FIGURE 50. TRANSMITTER

For final equipment the wafer could be incorporated into a smaller double-ended package with less lead inductance. The smaller case size is possible since the average power dissipation would be less than 0.2 watt and the thermal time constant of the wafer makes the maximum dissipation level a function of the peak power at the junction during the pulse. Improved performance with greater gain at the high frequencies and less degeneration across the band would result from this modification.

A considerable amount of time was devoted to broad-band transformer design. Various techniques have been described in the literature. In previous work, to obtain the greatest broad band operation at low power levels, ferrite cores have been employed. The ferrite provides high permeability at low frequencies, and a smaller number of turns can be used which, subsequently, provide better high frequency response. This process causes deterioration of the low frequency response. However, a suitable compromise was possible which provided an acceptable performance with low resistive loads.

1.4 PERFORMANCE

The performance of the transmitter is shown in Figures 51 and 52. Both figures show graphs of power output versus frequency for 100 μsec and 2 ms pulses, respectively. For comparison, the required output versus frequency is shown on the graph. It can be seen that the performance comes close to meeting the objective except above 8.5 MHz. The primary reason the design objective was not completely satisfied at the higher frequencies was due to the excessive internal lead length of the power transistors and, hence, the degenerative emitter inductance at the higher frequencies. In fact, it is believed that with better transistors, the performance at high frequencies can exceed the objectives. A power supply of +45 volts was used. A power converter would obtain this voltage level from the primary supply on any specific mission. A resistive output load of 2 ohms was used throughout the band. Monopole lengths and matching requirements would establish the impedance level which the transmitter would drive for a given mission.

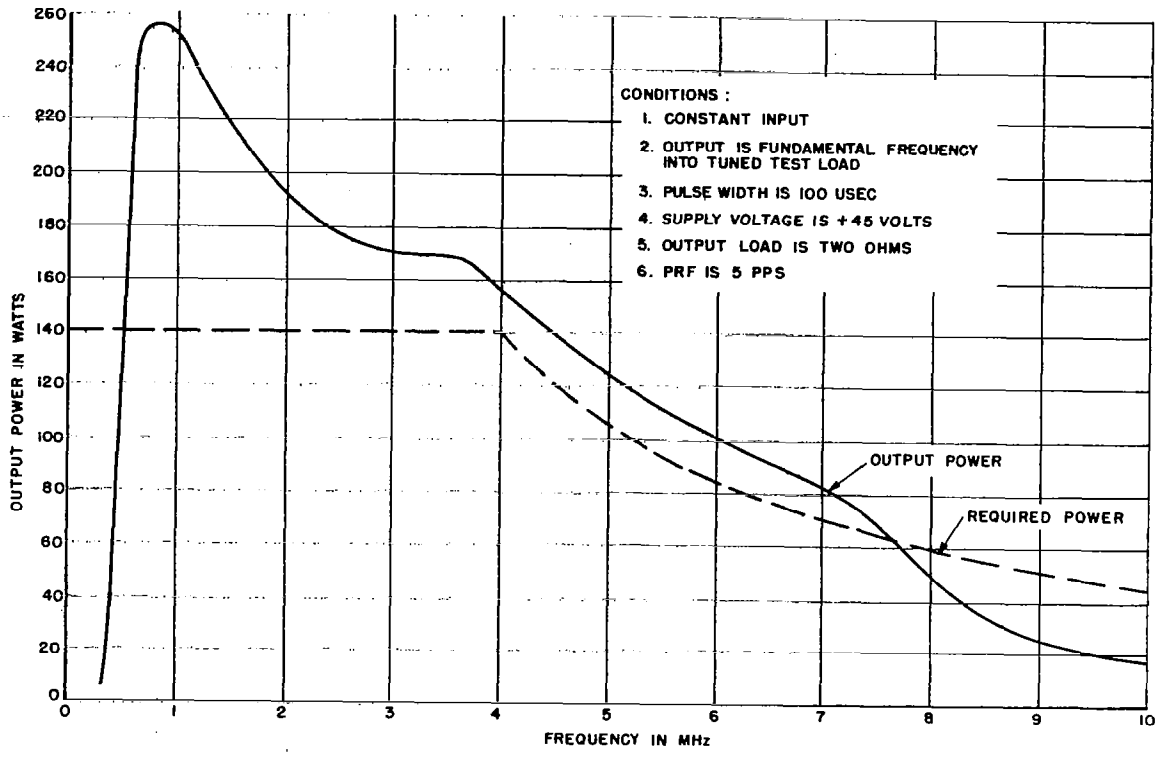

FIGURE 51. TRANSMITTER OUTPUT POWER VS FREQUENCY--100 μSEC PULSE

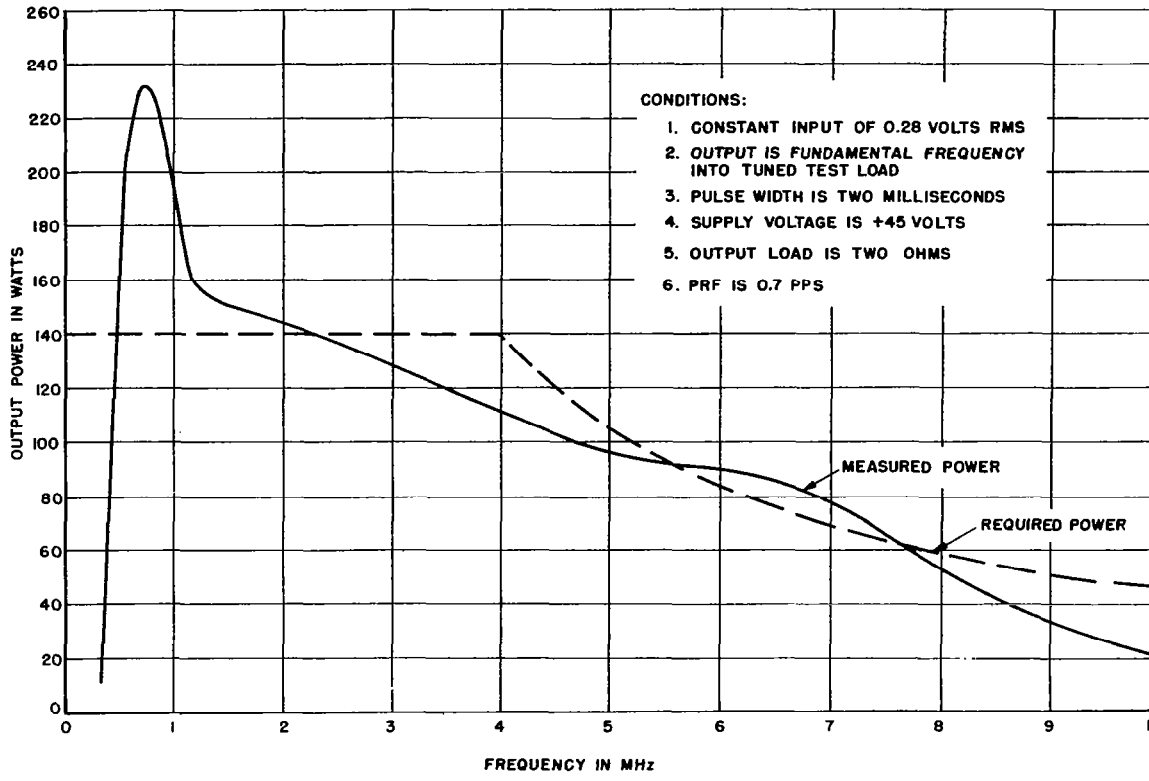

FIGURE 52. TRANSMITTER OUTPUT POWER VS FREQUENCY--2 MSEC PULSE

The load level previously mentioned is a realistic value where maximum power requirements exist. Matching to other load levels can be achieved by transformer ratio modifications.

The transmitter was operated during the design phase with a 100-μsec pulse width at a 5-pps repetition rate to provide an adequate dissipation margin. In the final breadboard configuration, testing was also performed for tentative mission parameters specified in Table IX. The 2000-μsec pulse width, which would normally be employed in an acquisition mode, only at a single frequency in the band above 6 MHz, was used at a 0.7-pps repetition rate to obtain the power output versus frequency curve shown in Figure 52. This was considered a worst-case condition. The power level was measured at the middle of the 2-msec pulse since the RF pulse exhibited some droop at these wider widths. A video pulse droop of 24 percent occurred at the output of the pulser during this test at the higher power levels, thus causing the droop in the RF pulse. The droop was not significant for narrower pulse widths. It is believed that this droop for the 2-msec pulse was caused by junction heating in the pulser output stage which, in turn, raised the saturation resistance and caused additional voltage drop as the pulse progressed. Figure 53 is a typical sketch of the droop of the RF pulse. An output transistor of greater capability will be required for the pulser section in a final design.

TABLE IX
PULSE WIDTHS AND PRF'S

PW (μsec)	PRF (pps)
200	5
400	2.5
800	1.25
2000	0.675

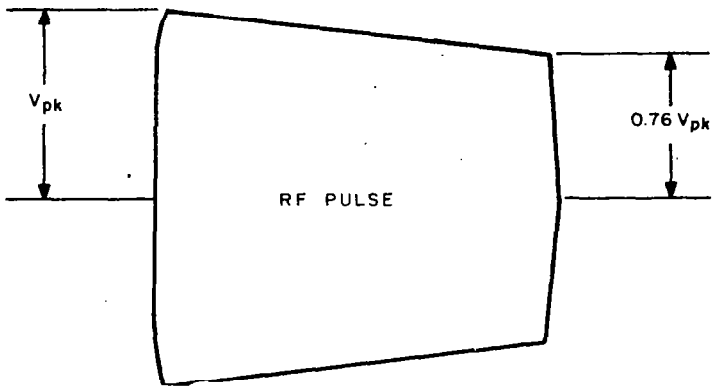

FIGURE 53. 2 msec PULSE DROOP

Figures 51 and 52 also exhibit peaks in the power output around 1 MHz. This is probably due to the inexact adjustment of time constants in the circuitry, particularly in the transformers. Further effort in this area would eliminate these sharp peaks. It is expected that the results would tend to flatten the entire curve out to 4 MHz at a level well above the required power, and that the ensuing fall-off would start from this level for still higher frequencies. The resulting curve should exceed the required power by a suitable margin out to 10 MHz.

The power curves of Figures 51 and 52 were obtained using spot tuning at each of the measurement frequencies. This ensured accurate measurement of the fundamental component, and it would be the operating condition for missions utilizing resonant matching networks. If broad-band antenna matching was used with the present transmitter breadboard, higher harmonics would be present in the output. Measurements over the band indicate that the third harmonic voltage level is about 15 percent at the lower frequencies and falls off below 10 percent at higher frequencies. The unbalance, as represented by the second harmonic voltage, is about 5 percent and this distortion can be eliminated to a great extent by more precise balancing of the output stage. The

present push-pull output stage is operated Class C. Operation to linear Class B is feasible and would reduce the third harmonic content further. The 15 percent third harmonic voltage constitutes a third harmonic signal that is about 4.5 percent, on a power basis, of the fundamental signal. This distortion should be acceptable under most circumstances if provisions are made in the receiver to avoid blocking due to third harmonic local ionospheric resonances and receiver image responses.

1.5 EFFICIENCY

The current drain of the transmitter was measured during the pulse interval by inserting a one-ohm resistor in the B+ supply line and measuring the resultant voltage drop on an oscilloscope. The average efficiency of the push-pull output stage was determined to be 43 percent. The efficiency of the entire transmitter breadboard was 25 percent. The large reduction in overall efficiency is due to the losses incurred in the power pulser section which switches supply power to the RF section. The efficiency in both of the above areas can be improved in a final configuration by the choice of better components.

2. MATCHING NETWORK

Maximum power transfer between transmitter and antenna is obtained when they are conjugately matched. A network is desired (Figure 54) which introduces minimum loss and optimizes the power delivered to the antenna. Ideally, the network should be lossless. However, any matching network design must necessarily consider the use of real circuit elements with finite Q's. With this in mind, let us review three schemes available to accomplish the match:

1. A filter network which tunes the antenna reactance at prescribed discrete frequencies,
2. Broad-band networks which match, or equalize, the transmitter and antenna continuously over a band of frequencies,
3. Simple series reactive element which resonates with the reactive component of antenna impedance.

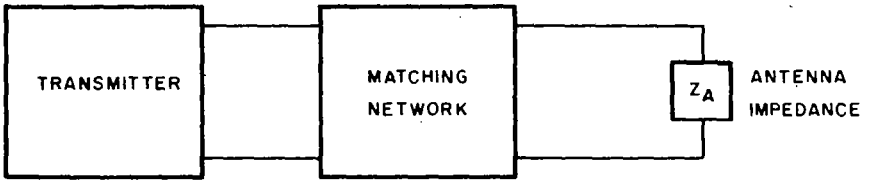

FIGURE 54. MATCHING NETWORK PROBLEM

The filter matching network could consist of inductors and capacitors arranged in Foster or Cauer canonical forms, such that the antenna reactance, consisting of the antenna impedance plus any base impedance introduced by the antenna's supporting structure, would be tuned out by a conjugate reactance. Figure 55 shows how a filter with poles at zero and infinite frequencies would tune out the antenna reactance at five frequencies. At each frequency, defined by the intersection of the filter's reactance characteristic and the conjugate antenna reactance, the filter and antenna form a resonant circuit. In addition to this resonance, the filter has its own resonant frequencies as shown in Figure 55. Any small deviation in frequency causes the filter reactance to vary drastically in the vicinity of a pole. Tuning near a filter pole, therefore, as shown by the first intersection, may prove to be difficult due to the large change in reactance for a small deviation in frequency. The presence of many circuit elements (especially inductors), when designed for many frequencies produce higher losses which further detracts from this method. At best, this method can be used to resonate a small number of frequencies, with switching between filters to cover the entire ber of frequencies, with switching between filters to cover the entire range of frequencies. Some small additional loss is suffered at the expense of switching complexity.

A broad-band matching network is most desirable, since a relatively constant power transfer over a band of frequencies would be obtained. Frequency drift would be of little significance, since,

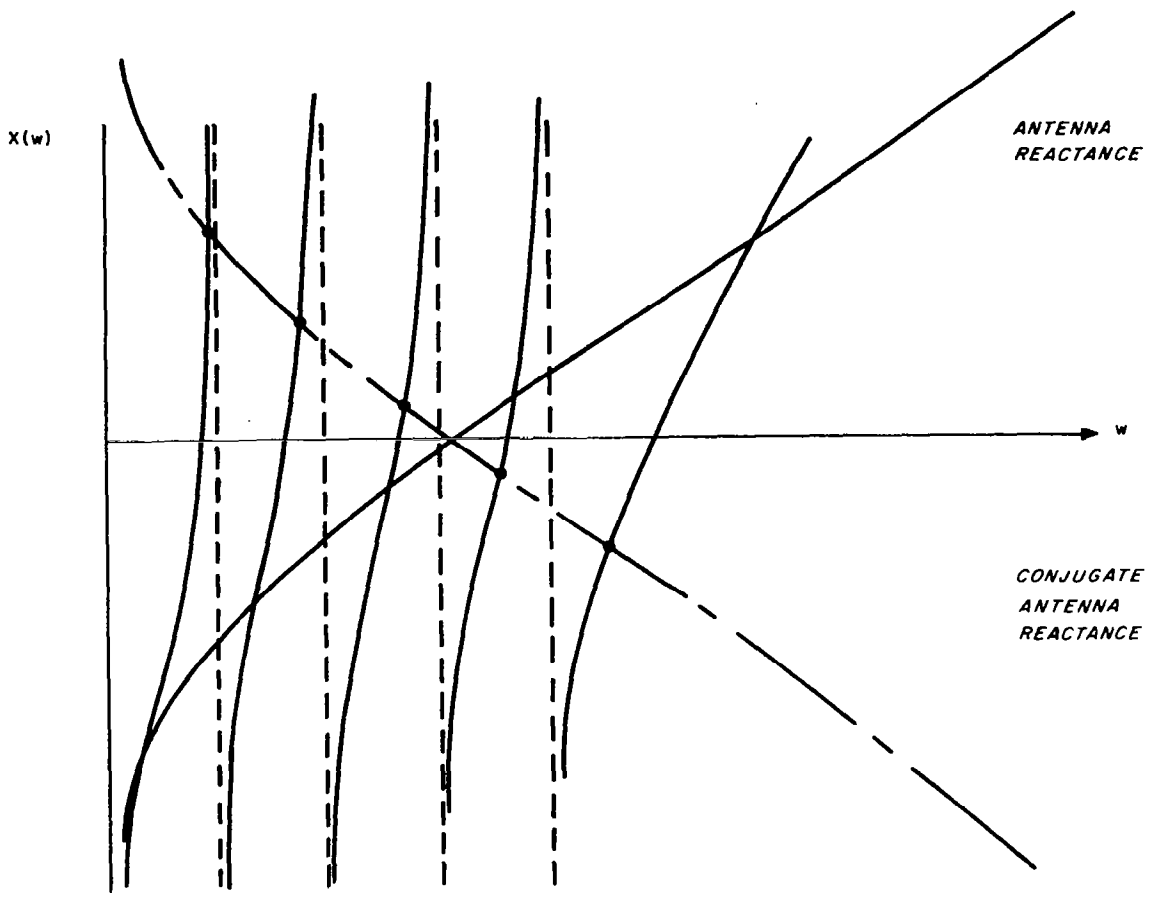

FIGURE 55. CONJUGATE MATCHING WITH LC FILTER

presumably, the antenna and transmitter are matched over the band. Theoretically, this problem has been solved by Bode[12], Fano[13], and Youla[14] in general terms. The problem is to synthesize a network which produces a given transfer gain function over an established band of frequencies. The bandwidth is determined once the desired transfer gain is established. Alternately, the transfer gain is determined if the bandwidth is prescribed.

The method is applicable to load impedances consisting of constant resistance, inductance, and capacitance. Approximations must be made in order to apply it to an antenna impedance which may be represented by frequency dependent circuit elements. The method also does not necessarily produce a minimum loss network and further suffers from the use of ideal transformers in the synthesis procedure, which must then be approximated by real transformers possessing inductance and losses.

The third technique is to simply resonate the antenna reactance with a series-reactive element. It is actually the simplest form of the resonant filter network. It offers the advantage of producing minimum loss by merely employing a minimum number of elements with highest possible Q's. Unfortunately, there are as many antenna impedances to resonate as there are frequencies. Consequently, this method presents a problem, namely, that of switching many resonant elements in and out of the transmitter-antenna circuit. It serves best where there are a limited number of frequencies and it is of utmost importance to minimize losses. The early planetary sounders fall in this class because of the possibility of large sounding ranges.

Over most of the frequency range of interest, inductance is required to resonate a capacitive antenna. The impedance of a 30-foot monopole, shown in Figures 56 and 57, is typical of dipole impedances. Up to 8 MHz, the 60-foot dipole displays a capacitive reactance after which the antenna becomes inductive to approximately 12.3 MHz. The impedance curves in the figures include 21 pf of assumed base capacitance to account for the capacitance introduced by the support structure of the

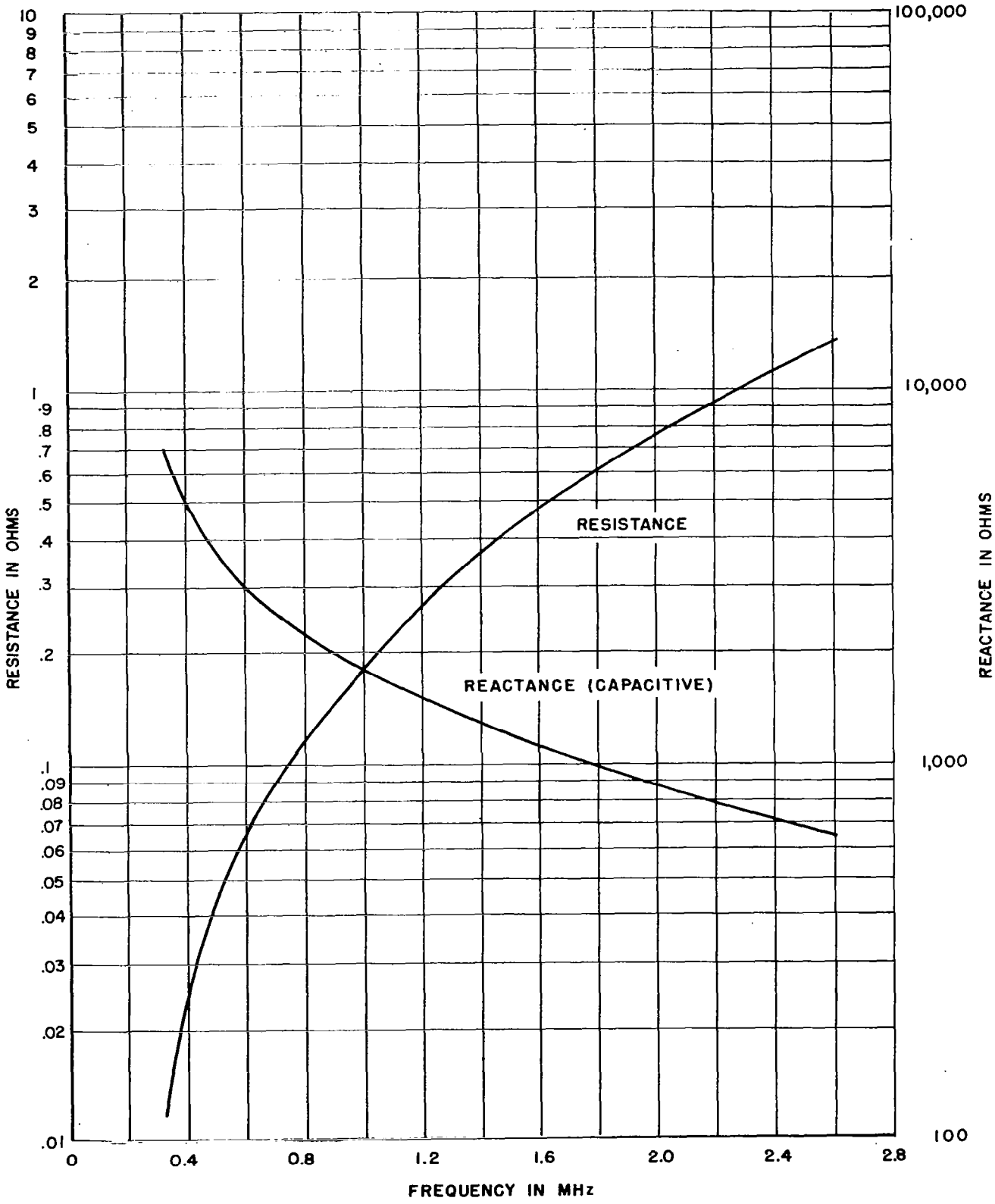

FIGURE 56. LOW-FREQUENCY MONOPOLE ANTENNA IMPEDANCE (30-FOOT POLE)

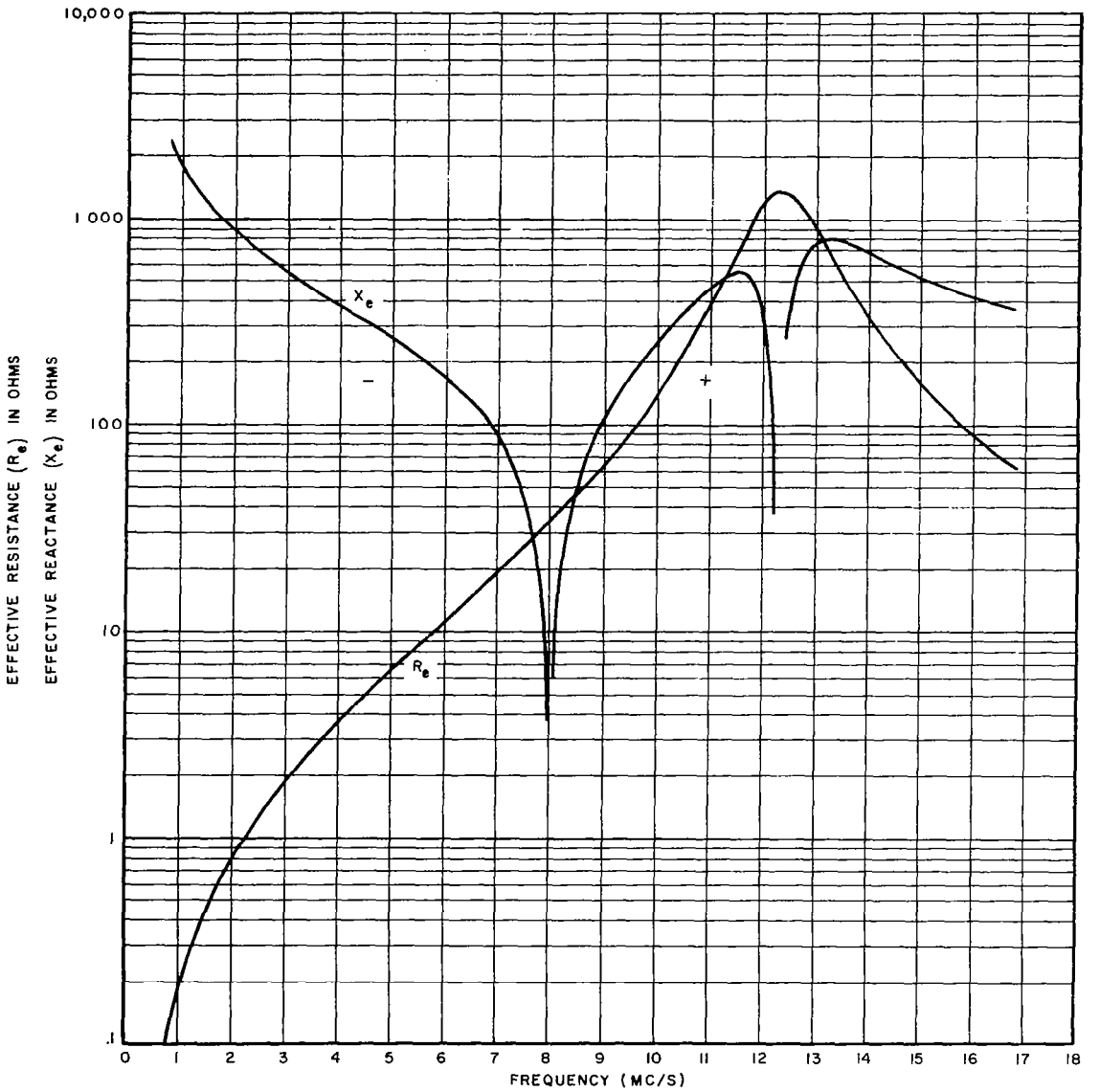

FIGURE 57. MONOPOLE ANTENNA IMPEDANCE (30-FOOT POLE)

antenna poles. Although measurements of the actual base capacitance must be made on a final antenna-vehicle configuration, 21 pf is a representative nominal value for the purpose of discussion.

The switching problem is demonstrated by a two-frequency resonant matching network shown in Figure 58. Switches S_1 and S_2 operate such that L_1 or L_2 is in series with the antenna, each resonating the antenna at a different frequency. Under this condition the voltage appearing across the remaining open switch is the full voltage drop across the inserted inductor. Since a series resonant condition exists, the voltage across the coil is the voltage across the transmitter terminals multiplied by the circuit Q. If the circuit Q were 50 and the applied voltage 50 volts, then the voltage appearing across the open switch would be 2500 volts. Therefore, a circuit must be designed which not only matches the antenna and minimizes losses, but also limits the voltages appearing across any open switches to a value which is within their rating. Figure 59 is an equivalent circuit of the matched antenna.

To illustrate the method and design of a configuration, a sample network has been worked out for possible planetary use, as shown in Figure 60. This network will tune a single antenna pole of

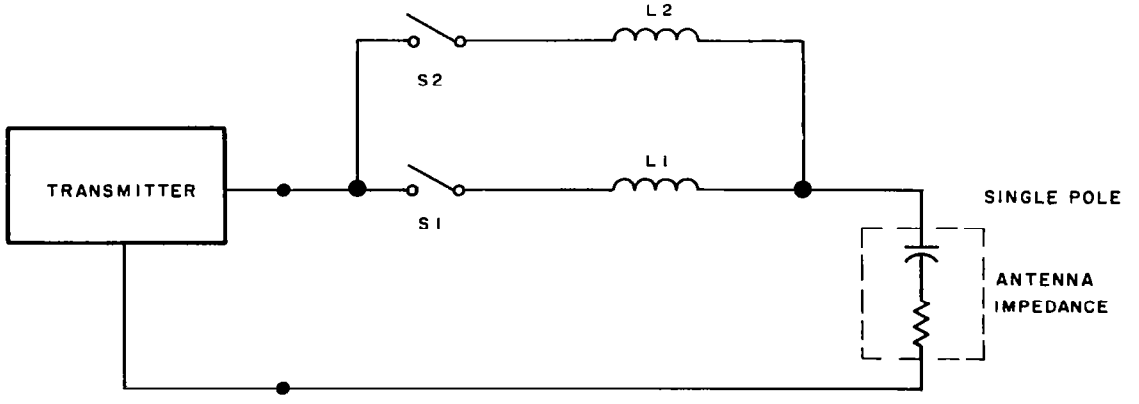

FIGURE 58. TWO-FREQUENCY MATCHING NETWORK

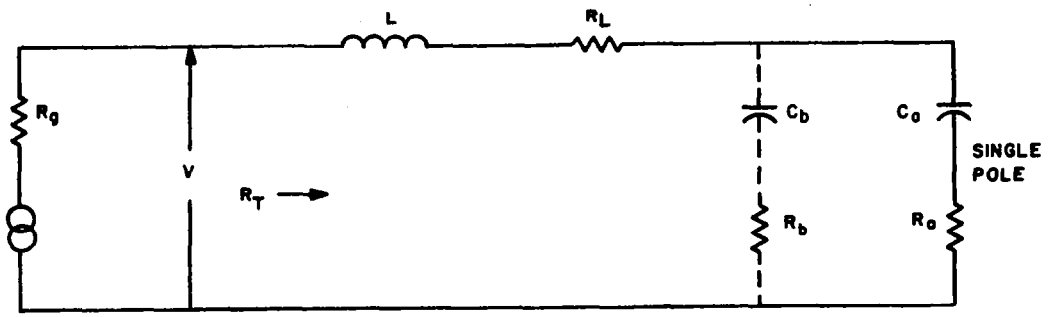

FIGURE 59. MATCHED ANTENNA EQUIVALENT CIRCUIT

30-foot length at nine frequencies within the range of 0.5 to 5 MHz. Selection of any other frequencies would, of course, necessitate different network parameters and possibly another configuration. Future missions which would be capable of incrementing the sounding frequency in small steps would require broad-band matching. However, for a limited number of frequencies with limited transmitter power, a network such as the one illustrated here is applicable. The details of the design are described below.

2.1 ILLUSTRATIVE MATCHING NETWORK

From 0.5 to 8 MHz the 60-foot dipole antenna is capacitive and conjugate matching is accomplished by resonating the antenna capacitance, C_a, with an inductor and by making the transmitter resistance equal to the remaining circuit resistance (Figure 59). Bisecting the antenna (for each pole), the peak voltage, V, appearing at the transmitter terminals is determined by the 140 watts of available power to a single antenna pole. The peak voltage is given by

$$V = \sqrt{280 R_T} \tag{7}$$

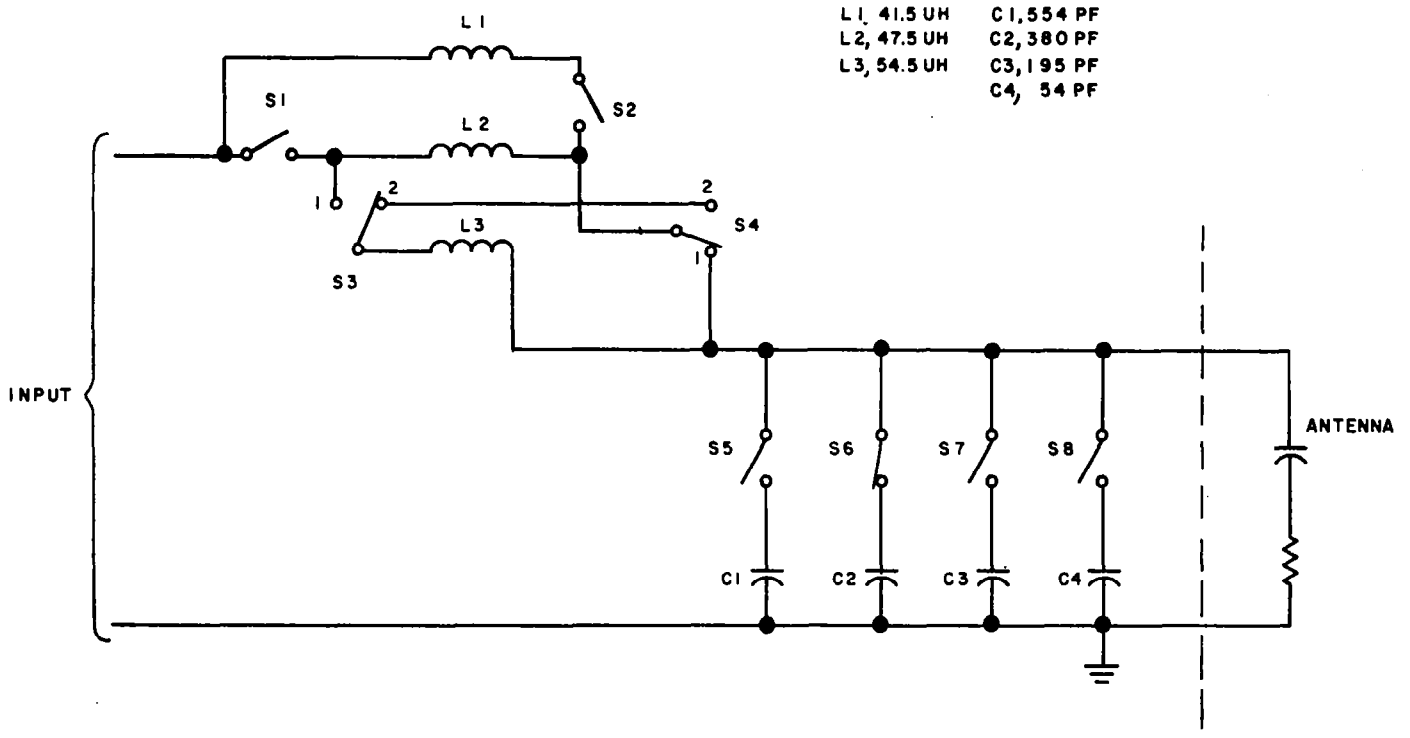

FIGURE 60. ILLUSTRATIVE MATCHING NETWORK FOR NINE FREQUENCIES

The voltage appearing across the inductor, or any open circuited switch (as in Figure 58) with one terminal tied between the matching coil and antenna, is given by

$$V_s = \sqrt{280 R_T}\ Q_C \qquad (8)$$

At low frequencies the radiation resistance is small and the load resistance is mainly that of the matching inductor. Therefore, with $R_g = R_L \approx R_T$ the circuit Q is approximately one-half the coil Q. To minimize losses the coil Q is made large, consistent with the space available. Coils with Q's of 100 to 200 are typical. Thus, from equation 7 the voltage across the coil and switches will be very large. A voltage of 4000 volts is about the present upper limit of small switches, such as a mechanical vacuum relay. Diode switching with small units would limit the voltages to much lower values since available diodes are not capable of withstanding this high a voltage under open circuit conditions. (Future fixed frequency sounders may be able to use semiconductor devices with advancements in their development.)

The only device able to handle both the open circuit voltage and closed circuit current appears to be a mechanical vacuum relay. These relays are further described in paragraph 2.2, below. The design procedure involves setting the switching voltage V_s to the desired value and finding the value of R_T, assuming Q_C. The condition is most critical for low frequencies when $R_L \approx R_T$ and Q_C can be taken as half the coil Q. Assuming a reasonable value for Q_L, the coil Q, a maximum inductance may be found which will maintain V_s no greater than the desired value. Since it is usually found at the lowest frequency that the inductance is insufficient to tune the antenna capacitance, additional base capacitance must be connected across the antenna as in Figure 59. C_b is the additional capacitance and R_b is its resistance. Typical capacitor Q's are much larger than the matching coil Q, and the losses in the capacitance shunting the antenna will be small compared to that of the matching coil. The method is also entirely equivalent to estab-

lishing a desired impedance level and can be interpreted in this fashion. The result is a circuit with a fairly constant impedance as frequency changes, which provides a good load for the transmitter over the band of frequencies. In this regard, it may be concluded that the lower the open circuit switching voltage, the higher is the closed circuit current to be carried by the switch.

Table X summarizes the results of calculations based on the technique mentioned with assumptions for V_s = 4000 volts and a 30-foot pole. These calculations are for a single antenna pole driven by half the total available power. Another network, identical in configuration and operation, is required for the other antenna pole. The frequencies that were chosen are the same as those for the Mariner Application, Section II, paragraph 3.2. The table shows the insertion loss to be expected as a function of frequency. The values are typical for a 60-foot dipole.

Since R_T is the load on the transmitter when the circuit is tuned, it should be noted that it varies slightly between 0.5 and 1.47 MHz. For higher frequencies the level varies from 7 to 8 ohms. Although there is more variation than at the lower frequencies, its variation is small enough to provide a good transmitter load. The difference in the two impedance levels exists because no further capacitance can be placed across the antenna and the antenna contributes significantly to R_T at the higher frequencies. As a tuned circuit with a $Q_c \approx Q_L/2$, the configuration also filters the harmonics of the transmitter output, clearing up the signal. The transmitter has to be matched for both impedance levels over the frequency band.

The suggested configuration in Figure 60 provides tuning at the nine frequencies utilizing seven circuit elements and eight switches. S_3 and S_4 are SPDT and the remaining switches are SPST. The switching sequence for the relays is given by Table XI for the various combinations of required circuit elements. Also listed are the number of relays which must be switched to go from one frequency to the next higher frequency.

To cover the additional frequencies in the logarithmic progression above 4.38 MHz in the Mariner scheme, additional switching is required. With two such assemblies, one for each pole, the reliability, weight, and power aspects may become of critical importance. Therefore, it may be preferable to pair or triple the frequencies utilizing the more complex two-port reactive networks, sacrificing some radiated power as a result of some additional losses. Because of the greater losses in wide-band networks and the uncertainty of the distance of nearest approach in early planetary missions, the constraints on experiment weight and power dictate the use of the simplest system: fixed frequencies and two-port matching. In this regard, further optimization studies are necessary.

TABLE X

RESULTS OF MATCHING NETWORK CALCULATIONS

f (MHz)	L (μh)	Q_L	C_b (pf)	R_T	Insertion Power Loss (db)
0.5	122	150	748	2.774	27.8
0.65	94	150	554	2.780	24.1
0.86	71	150	397	2.79	20.6
1.12	54.5	150	373	2.82	17.3
1.47	41.5	150	195	2.89	13.6
1.93	47.5	100	54	6.48	11.8
2.54	42.0	100	0	8.25	8.2
3.34	22.8	100	0	7.33	5.0
4.38	11.8	100	0	8.02	2.4

f = frequency

L = inductance required to produce a maximum voltage of 4 kv across the tuning inductor

Q_L = assumed Q of the coil

C_b = additional base capacitance needed to produce resonance of the antenna with the coil

R_T = equivalent series resistance seen looking into the circuit consisting of the matching coil, base capacitance, and antenna

TABLE XI

SWITCHING SEQUENCE FOR ILLUSTRATIVE MATCHING NETWORK

f (MHz)	Combination	S_1	S_2	S_3	S_4	S_5	S_6	S_7	S_8	Number Switched
0.5	$L_1 + L_2 + L_3$ $C_1 + C_3$	O	C	1	2	C	O	C	O	
0.65	$L_1 + L_3$ C_1	O	C	2	2	C	O	O	O	2
0.86	$L_3 + \frac{L_1 L_2}{L_1 + L_2}$ C_2	C	C	2	2	O	C	O	O	3
1.12	L_3 C_2	C	O	1	2	O	C	O	O	2
1.47	L_1 C_3	O	C	2	1	O	O	C	O	5
1.93	L_2 C_4	C	O	2	1	O	O	O	C	3
2.54	L_1	O	C	2	1	O	O	O	O	3
3.34	$\frac{L_1 L_2}{L_1 + L_2}$	C	C	2	1	O	O	O	O	1
4.38	$\frac{L_1 L_2 L_3}{L_1 + L_2 + L_3}$	C	C	1	1	O	O	O	O	1

O - Open

C - Closed contacts

1 - Position 1 as indicated

2 - Position 2 as indicated

2.2 SWITCHES AND RELAYS

Electronic and electromechanical devices were considered to perform the necessary antenna matching network switching functions. Some of the semiconductor devices considered were silicon diodes, PIN diodes, varactor diodes, and SCR's. All of the diode devices had a very high bias voltage requirement as well as a very low breakdown voltage for this application (approximately 1000 volts). To use the lower voltage level, too high a closed circuit current is required for reasonable size devices. Varactor diodes also add unwanted capacitance to the circuit and SCR's are not suitable for RF frequencies.

Suitable magnetic latching vacuum relays are not available from most sources. A latching relay manufactured by Torr Laboratories appeared to possess the necessary electrical and mechanical specifications. The switch construction is definitely not qualified for space use and its electrical characteristics are poor. An unusually high insertion loss of 1.94 db was measured as well as relatively poor crosstalk isolation of 23.9 db for an SPDT unit. This relay would have to be improved extensively both mechanically and electrically to be suitable.

The Jennings Radio Manufacturing Corp. fabricates a small vacuum relay that meets the electrical requirements and can be readily modified. Some improvement of the electrical characteristics is necessary and there appears to be no difficulty in meeting a set of preliminary electromechanical specifications which were devised for this purpose. These requirements are listed in Table XII.

TABLE XII

PRELIMINARY VACUUM RELAY (LATCHING) SPECIFICATIONS

ELECTRICAL SPECIFICATIONS

Test RF voltage (0.25 to 15 MHz)	6 kv between terminals 500 volts between coil and frame
Operating RF voltage (0.25 to 15 MHz)	2 to 4 kv
Pulsed RF current (closed circuit) duration 100 μsec to 10 msec	20 amps peak at 0.01 duty cycle
Contact resistance	0.010 ohm maximum
Capacitance between contacts	1.6 pf maximum
Capacitance contacts to ground	2.0 pf maximum
Interrupting ratings	Not applicable since relay will be switched under no power conditions

PHYSICAL SPECIFICATIONS (nonoperating)

Contact arrangement	SPDT
Shock Vibration	According to shock and vibration specification in NASA document S-615-P10, pp 23, 24
Life (mechanical)	2 million operations
Weight	3/4 to 1 ounce maximum
Operate time (open and closed)	10 msec maximum

SECTION V
PROPAGATION ANALYSES

In this section, the effects of a dipole magnetic field on the propagation delay of the ionosphere and absorption at the critical frequency are described. The definitions and terminology used in these discussions are as follows:

The magneto-ionic parameters are defined by X, Y, and θ where

$X = e^2N/4\pi^2f^2\epsilon_o m = f_n^2/f^2$, normalized plasma frequency parameter,

$Y = eB_o/2\pi fm = f_H/f$ = normalized gyro-frequency parameter,

θ = angle between magnetic field and wave normal,

e = electronic charge,

m = electron mass,

ϵ_o = permittivity of free space,

B_o = magnetic field in gauss,

N = electron density,

f = sounding frequency.

The group refractive index is related to the phase refractive index (μ) by

$$\mu' = \frac{\partial}{\partial f}(f\mu) = \frac{1}{D\mu}\left\{1 - X - \mu^2 \pm \frac{\frac{Y^2}{2}\cos^2\theta\,(1 - X^2)\,(1 - \mu^2)}{\left[Y^2\cos^2\theta\,(1 - X)^2 + \frac{Y^4}{4}\sin^4\theta\right]^{1/2}} + D\right\} \tag{9}$$

$$\mu^2 = 1 - \frac{X(1 - X)}{D} \tag{10}$$

$$D = 1 - X - \frac{Y^2}{2} \sin^2 \theta \pm \left[\frac{Y^4}{4} \sin^4 \theta + Y^2 (1 - X)^2 \cos^2 \theta \right]^{1/2} \tag{11}$$

$\pm$ signs correspond (by definition) to ordinary waves (0) for the upper sign and extraordinary (x) waves for the lower sign.

where

X_m = maximum value of X at density maximum N_m,

$Z = \nu/2\pi f$,

ν = electron collision frequency,

C = cosine of the angle between the vertical and propagation direction,

z = altitude,

z_m = altitude of maximum electron density,

$k = \omega/c$,

$c = 3 \times 10^8$ m/s speed of light in free space.

1. INCREMENTAL DELAY OF IONOSPHERE WITH DIPOLE MAGNETIC FIELD

In a previous report (NASA CR-493) calculations and analyses of both ordinary and extraordinary wave propagation in ionospheres in the presence of a constant magnetic field were presented. These results are applicable when the magnetic field variation between the sounder and reflection region is small. Incremental delays or differential virtual depths were computed for ray paths originating infinitely far from a planet since, in many applications, the sounder would be in a very tenuous ionosphere. The incremental delay was defined as the additional delay, over that of free space, contributed by the presence of a gyrotropic medium.

$$\Delta h'(f) = \int_{\infty}^{z_r} (\mu' - 1)\, dz, \tag{12}$$

where z_r is the reflection altitude.

For a finite sounder altitude, the incremental depth is obtained by subtracting the incremental delay due to the medium above the sounder from the total incremental delay defined by equation 12. This method lends itself to situations where the sounder is close enough to the reflection region and small magnetic field variations become insignificant. However, for very great distances between sounder and reflection level, the variation in magnetic field has a significant effect upon wave delay times. Results are given here which demonstrate the effect of a dipole magnetic field upon the incremental delay of an extraordinary mode propagating in a simple ionosphere for the case $Y < 1$. For all planetary missions (except possibly Jupiter) the sounder location and sounding frequency will probably be such that the normalized magnetic field parameter is less than unity. The model ionosphere assumed has only a single scale height, H, to which $\Delta h'(f)$ is normalized.

For an X-wave where $Y < 1$, the reflection level is defined by $X = 1 - Y_r$, where Y_r is the value of Y at the reflection point. Equation 12 may then be rewritten as

$$\Delta h'(f) = \int_{0}^{1-Y_r} (\mu' - 1)\frac{dz}{dX}\, dX \tag{13}$$

The lower limit is $X = 0$, since it is assumed that at great distances from a planet the electron density is insignificant for the sounding frequency. Assuming a singly exponential ionosphere

$$X = X_0 \epsilon^{-\frac{z - z_0}{H}} = \frac{e^2 N}{4\pi^2 \epsilon_0 m f^2} \epsilon^{-\frac{z - z_0}{H}} \tag{14}$$

where

N_o = electron density at an arbitrary altitude z_o,

H = electron density scale height.

Differentiating equation 14 and substituting into equation 13, we obtain

$$-\frac{\Delta h'(f)}{H} = \int_o^{1-Y_r} (\mu' - 1) \frac{dX}{X} \tag{15}$$

The relationship between X and Y is found by assuming a dipole variation for the magnetic field with the reflection level, z_r, as a reference,

$$Y = Y_r \left(\frac{R_o + z_r}{R_o + z} \right)^3, \tag{16}$$

where R_o is the planetary radius and z the altitude of interest. This may be rewritten in a more convenient form if the reflection altitude is considered small compared to the planetary radius. With this assumption

$$Y = \frac{Y_r}{\left(1 + \frac{z - z_r}{R_o} \right)^3} \tag{17}$$

Setting $z_o = z_r$ in equation 14, the relationship between X and Y is

$$Y = \frac{Y_r}{\left(1 - \frac{H}{R_o} \ell n \frac{X}{X_r} \right)^3} \tag{18}$$

The group refractive index, μ', is given by equation 9 in terms of X, Y, and θ.

The integration of equation 15 was performed with Y_r and H/R_o as variable parameters. Varying these two parameters has the effect of varying the size of the ionosphere relative to the planet size and of moving the electron density profile with respect to the magnetic field profile. In order to make the results useful for finite sounder altitudes, the integration interval was divided into segments, each segment computed separately. Finally, all segments were added together to give the total incremental delay. Calculations for a finite altitude are made by adding up the appropriate number of segments. This will become clear from the following discussion.

Dividing the integral of equation 15 into m segments, we may write the summation

$$-\frac{\Delta h'(f)}{H} = \sum_{n=1}^{m} \int_{\frac{n-1}{m}(1-Y_r)}^{\frac{n}{m}(1-Y_r)} (\mu' - 1) \frac{dX}{X} \tag{19}$$

The integrand in this form has a singularity at the turning point since μ' has a singularity at $X = 1 - Y_r$. It also appears to have a singularity at $X = 0$ (infinite z). However, the integrand is well behaved at $X = 0$ since we require $\mu' \equiv 1$, the free space value, at infinity. In order to keep the integral in this form, the last segment will be treated separately and the region of the singularity isolated. By a suitable transformation the contribution at the singularity may be evaluated. Separating the summation of equation 19 we obtain

$$-\frac{\Delta h'(f)}{H} = \sum_{n=1}^{m=1} \int_{\frac{n-1}{m}(1-Y_r)}^{\frac{n}{m}(1-Y_r)} (\mu' - 1) \frac{dX}{X} + \int_{\frac{m-1}{m}(1-Y_r)}^{1-Y_r-\eta} (\mu' - 1) \frac{dX}{X} + \overbrace{\int_{1-Y_r-\eta}^{1-Y_r} (\mu' - 1) \frac{dX}{X}}^{\Delta I} \tag{20}$$

where $\eta \ll 1$.

The interval of the last term containing the singularity may be made as narrow as desired by making η as small as required.

Using the transformation

$$\sin \phi \equiv \frac{f_x}{f} \tag{21}$$

where

$$f_x = \frac{1}{2}\left[\left(f_H^2 + 4f_N^2\right)^{1/2} + f_H\right] \tag{22}$$

ΔI of equation 20 may be rewritten as

$$\Delta I = \int_{\frac{\pi}{2}-\alpha}^{\frac{\pi}{2}} (\mu' - 1) \frac{2 \sin \phi + Y}{\sin^2 \phi + Y \sin \phi} \cos \phi \, d\phi \tag{23}$$

where α corresponds to η for the variable ϕ.

The singularity produced at the reflection point is removed by this transformation since it may be shown that $\mu' \cos \phi$ remains finite at $\phi = \pi/2$ (see Appendix I, NASA CR-493). A relationship between α and η is found by noting that, using equation 21 and equation 22 any value of X is given by

$$X = \sin^2 \phi - Y \sin \phi \tag{24}$$

Therefore, at the lower limit

$$1 - Y_r - \eta = \sin^2\left(\frac{\pi}{2} - \alpha\right) - Y \sin\left(\frac{\pi}{2} - \alpha\right) = \cos^2 \alpha - Y \cos \alpha \tag{25}$$

where Y is $Y_r + \eta$. Since $\eta \ll 1$, $Y \approx Y_r$, α is small and we may approximate

$$1 - Y_r - \eta \approx 1 - \alpha^2 - Y_r \left(1 - \frac{\alpha^2}{2}\right) \tag{26}$$

or

$$\alpha \approx \left(\frac{\eta}{1 - \frac{Y_r}{2}}\right)^{1/2} \tag{27}$$

The integral ΔI may now be readily evaluated by using an asymptotic form for μ' in the vicinity of the reflection level.

Utilizing the above integration scheme, normalized incremental delays are calculated by incrementing X in any number of desired steps.

Figure 61 presents the results of adding 20 integration intervals for parametric combinations of Y and H/R_o. Only curves for longitudinal and transverse propagation are given, since there is very little difference between the results for these two cases. The calculations for other values of θ lie between these extremes. The pair of curves labeled $H/R_o = 0$ correspond to the previous results for a constant magnetic field, whereas the curves labled $H/R_o = 0.05$, 0.2, and 0.5 are for variable magnetic fields. It is seen from these curves that the incremental delay is significantly affected by a variable magnetic field intensity.

2. ABSORPTION NEAR CRITICAL FREQUENCY

For frequencies very near the penetration frequency, occurring at the maximum electron density, absorption may become a significant factor in determining the amplitude of the reflected signal. Budden[15] gives the electric field reflection coefficient of a parabolic layer of thickness 2a. This relationship is

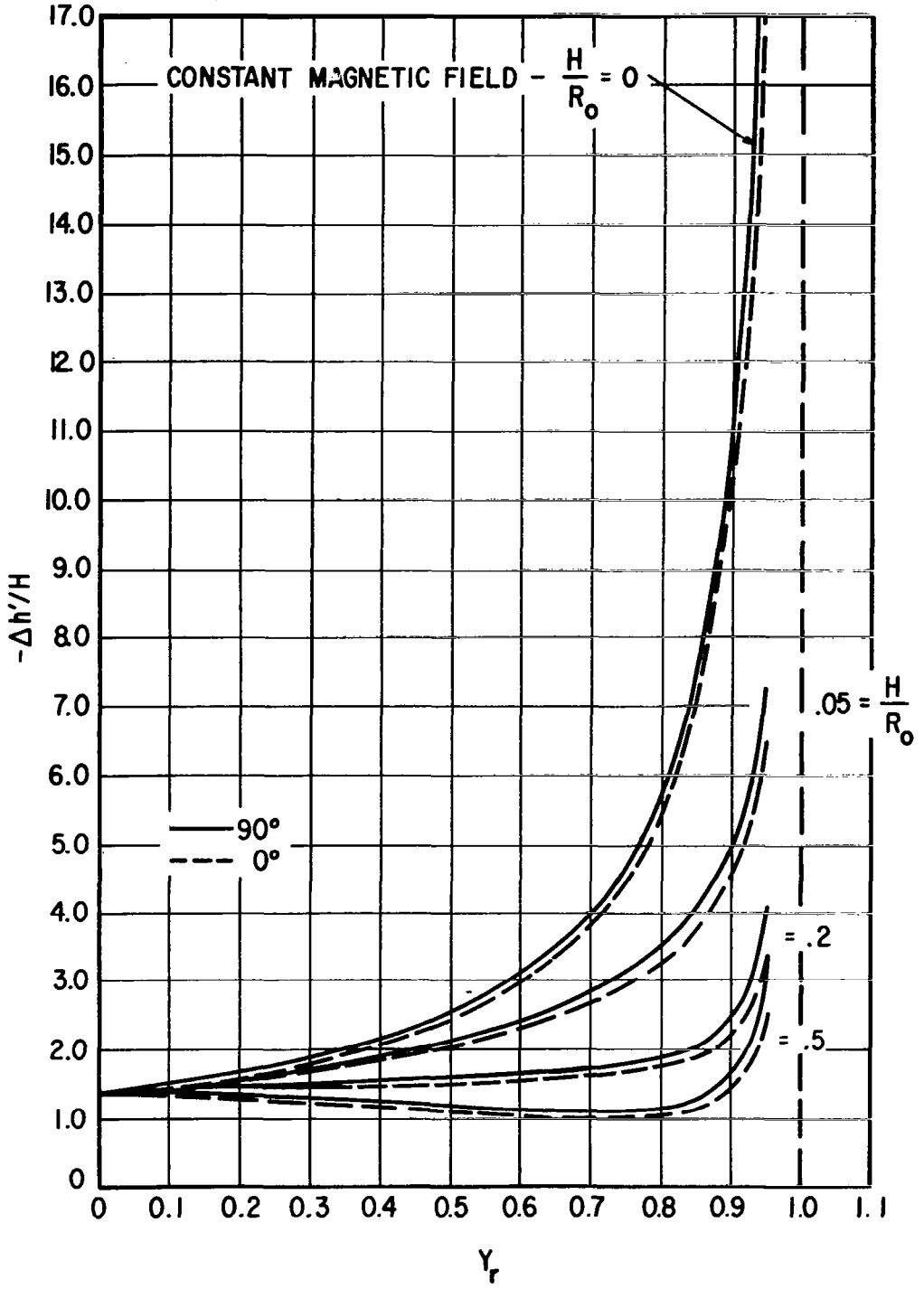

FIGURE 61. INCREMENTAL DELAY OF X-WAVE IN SINGLE LAYER

$$R = -(-n-1)!\ \epsilon^{in\pi}\ \epsilon^{-\frac{1}{2}}\ \xi_{-a}^{2}\ \xi_{-a}^{2n+1}\ \frac{1}{\sqrt{2\pi}} \tag{28}$$

$$\xi = \left\{\frac{-4k^2 X_m}{(1 - iZ)a^2}\right\}^{1/4} (z - z_m), \xi_{-a} = \xi(z - z_m = -a) \tag{29}$$

$$n + \frac{1}{2} = \left\{\frac{-4k^2 X_m}{(1 - iZ)a^2}\right\}^{-1/2} k^2 \left(C^2 - \frac{X_m}{1 - iZ}\right) \tag{30}$$

The parabolic profile which yields this solution is given by

$$X = X_m \left\{1 - \left(\frac{z - z_m}{a}\right)^2\right\} \text{ for } |z - z_m| \leq a$$

To determine the variation of $|R|^2$ with frequency, typical results can be obtained by computing $|R|^2$ for rather reasonable values of the parameters. Assuming a penetration frequency of 2.85 MHz corresponding to a maximum electron density of 10^5 electron/cc and a collision frequency of 2000 Hz, the value Z is approximately 10^{-4}. The values of $|R|^2$ obtained from equation 28 for a parabolic layer 50 km thick (a = 25 km) and the above parameters are presented in Figure 62 versus X_m. The value $X_m = 1$ corresponds to equality between the radiated frequency and the penetration frequency; $X_m < 1$ corresponds to the radiated frequency being greater than the penetration frequency. For this case the reflection coefficient is negligibly small and the wave penetrates unattenuated, for all practical purposes, through the peak density. For $X_m > 1$, the radiated frequency is less than the penetration frequency. In this case reflection is partial and a wave can partly penetrate. At such frequencies the composite signal at the sounder would consist of the partially reflected

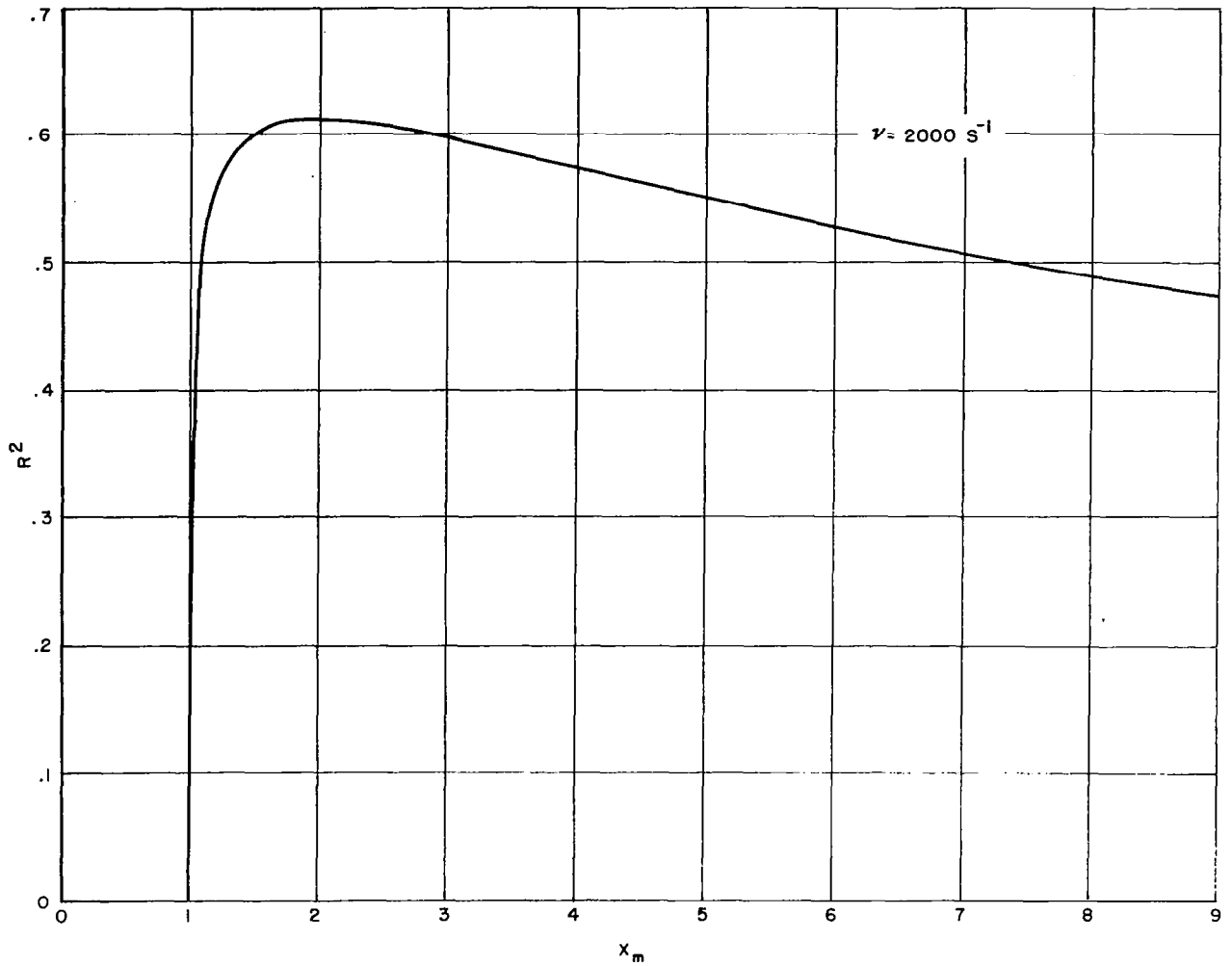

FIGURE 62. REFLECTION COEFFICIENT FOR PARABOLIC LAYER

wave plus a secondary wave which penetrates through the region in both directions after reflection from the planetary surface. This second wave will be attenuated compared with the primary reflected wave.

The figure also exhibits a peak value of 0.61 near $X_m = 2$, corresponding to a frequency that is roughly 70 percent of the penetration frequency. For this large a deviation from the penetration frequency, the reflection coefficient should be nearly unity. In fact, the curve in Figure 62 decreases further for larger values of X_m, corresponding to even greater deviations from the penetration frequency; however, it has been demonstrated by Gross[16] that equation 28 is valid only near $X_m = 1$ and that the reflection coefficient does indeed approach unity. Gross' formulation is a more general solution utilizing Whittaker functions which includes magnetic field effects and which reduces to the solution presented here in the region of maximum electron density. Equation 28 can be used for accurate results very near the penetration frequency (for example, to $X_m = 1.05$ in Figure 62). The results of the analysis demonstrate that except for an extremely narrow band about the penetration frequency partial reflection can be ignored, and the primary effect of the peak density is the propagation delay.

SECTION VI
CONCLUSIONS AND RECOMMENDATIONS

The investigation of planetary ionosounding has resulted in the material contained in this report. The techniques recommended to advance the state of the art consist of digitizing, frequency synthesis, pulse compression, and coherent and noncoherent integration. Digitizing offers the advantages of precision and resolution over existing analog forms, avoiding unnecessary and annoying errors in data reduction and interpretation. Digitizing also offers advantages in packaging equipment for lightweight, more efficient utilization of power. Other advantages are lower demands on data rate and capacity of the spacecraft telemetry and data storage facilities, which are so important in view of the severe constraints of planetary missions. Frequency synthesis provides a full frequency band, yet permits selection of frequencies for specific purposes and maintains a constant frequency and coherence during the transmitted pulse, in contrast with a swept frequency system. Pulse compression and integration offer the advantages of long range sounding with fine resolution capability, while permitting practical transmitter design for spacecraft use within the state of the art. All echoes can be readily received, identified, and analyzed and precise measurements made of their distances. Although these techniques are new to ionospheric sounders, they are well developed in the radar technology.

The applications of these techniques are practical, as demonstrated by the detailed examinations described here. The most difficult and complex subsystems were studied ensuring their feasibility. Although there are still areas worthy of further investigation, the study has been carried to the point where demonstration of these capabilities should logically follow. A complete breadboard system packaged for flight should be the next step, as well as a demonstration of the advantages of the techniques by bottomside sounding and comparison with

conventional equipment. For the latter purpose, the required system differs from a planetary sounder in that the system must be scaled for the smaller ranges. The breadboarded planetary system should be directed toward a Voyager mission. A possible secondary purpose of this breadboard would be for utilization in sounding the Earth from a synchronous altitude. These efforts should also include the further study of tradeoffs for optimization with respect to the applicable mission and of systems and subsystem design and equipment specifications. Once a breadboard system is evolved, the technique may be further evaluated by rocket tests.

The theoretical analysis was carried further by treating the propagation characteristics of the medium in a magnetic field that varies with altitude. The variation was simplified by assuming the field has a dipole structure.

Many aspects of the theoretical studies remain to be investigated. It is recommended that the effort be continued to include more comprehensive models which would include electron and ion temperatures, charge transfer and gravitational constants. It is also highly recommended that an error analysis be performed for the purposes of improved data reduction and interpretation. Errors could be purposely introduced into virtual depth data derived from an ionospheric model. Such errors would represent measurement errors as well as those arising from physical assumptions. Comparison of a true profile with that derived from the inaccurate virtual depth data will exhibit the errors in the computed profile due to the inserted virtual depth errors. The information gathered can also be related to system accuracies and requirements and their variation with frequency.

In order to guide the design of planetary ionospheric instrumentation it would also be desirable to include theoretical treatments of the planetary atmospheres and ionospheres, updating previous efforts by the inclusion of such additional measurement data as may become available. This effort would attempt to predict the ionospheres of the terrestrial planets and Jupiter, so as to establish more realistic models and to guide in the selection of appropriate sounder frequency bands, for the design of the sounder and analysis of data.

SECTION VII
NEW TECHNOLOGY

This section is included in accordance with NASA Specification TID-S-100. The technology involved in this study consists of techniques that are well-known in the radar discipline. The only novel aspect, to date, is their application to ionospheric sounding. However, ionospheric sounding is in many aspects a radar-type application. In the course of this work many discoveries were made in the analysis of difficult matters not treated elsewhere and circuit designs are involved which do not appear to have been developed elsewhere in the form peculiar to ionospheric sounding. Yet these involve well-known principles and do not constitute new technologies or inventions. As such, no new basic developments have evolved and the data that has resulted from this study is not applicable.

APPENDIX I
PULSE CODE INVESTIGATION

The codes investigated are those where a radar pulse is divided into sections of 0 and 180 degrees carrier phase. A range resolution of T/n is desired where T is the radar pulse length and n the number of code sections. The receiving (decoding) network performs a correlation between the received pulse and a replica of the pulse. If the code is a "perfect" one the decoder will have a peak output of nE when the received pulse is in alignment with the decoding network, and a peak output of $\pm$E when the received pulse is x code elements out of alignment. A number of perfect codes, called Barker[17] codes, have been found that are of length 1, 2, 3, 4, 5, 7, 11, and 13. Longer Barker codes have not been found and recent work[18] indicates that they must be longer than 144 if they exist. Denoting C_k as the output of the decoder when the code is out of alignment, an exhaustive search[19] has found codes where C_k = 2 when n = 17 and n = 20 and 28. For C_k = 3 a 31-pulse code has been found. Also of interest is a shift register generatable code with C_k = 4 of 31 elements. This code can be generated by 5 shift register flip-flops where $X_n = X_{n-2} + X_{n-4} + X_{n-5}$ where + stands for addition, modulo 2. The importance of a low value of C_k relates to the limited dynamic range of the processor under which conditions the range sidelobes will not result in additional detections.

The two 31-pulse codes (which satisfy a requirement for a pulse compression ratio of better than 30/1 for this project) also have the interesting feature that the Barker n = 7 code is imbedded in them. Thus, the same decoding network can be readily switched to decode a Barker 7 coded pulse in the long range operation mode. A modification to the first 31-pulse code was found containing 28 elements, where the Barker 7 code is the first 7 elements. For this code C_k = 4. Switching between the two modes of operation with this code set is simple and the

worst peak-to-side-lobe ratio is fixed at 7/1 (17 db) in both modes. However, this first 31, or modified 28, pulse set is more difficult to encode than the shift register generatable code. The shift register generatable code has the Barker 7 as elements 14-20 and no similar modification to the first 7 elements has yet been found with it. A listing of the codes mentioned follows:

BARKER CODES

3. ++-
4. ++-+
5. +++-+
7. +++--+-
11. +++---+--+-
13. +++++--++-+-+ (Found after Barker's article)

GOOD CODES

31. (C_k = 3) +----++-+--++++++-+--+++-+++-
28. (C_k = 4) ---++-+--++++++-+-+--+++-+++ (first 7 Barker)
31. (C_k = 4) -+-+---+++-++++-+-+--++----+-++ (Shift Register)

APPENDIX II
COHERENT PROCESSING (DIGITAL PULSE COMPRESSION)

The analytical investigation was concerned with a binary phase coded sequence of 31 elements. The transmitted pulse of duration T was subdivided into 31 contiguous subpulses each having the relative phase of zero or pi. Upon reception, the echo sequence would ideally be converted to a 31-element binary sequence. The receiver spectral response is assumed matched to an IF pulse of duration T/31. The doppler shift was assumed to be limited to a 90-degree phase advance, or retard of the last subpulse relative to the first. The mismatch of the doppler shifted subpulses to the receiver is therefore negligible; that is, only about 3 degrees of phase rotation across the subpulse.

1. EFFECT OF DOPPLER SHIFT ON COMPRESSED PULSE

Computation of the ambiguity functions of the two proposed 31-bit Barker type codes was done along normalized doppler planes spaced by $fT = 0.05$ from $fT = 0$ to $fT = 0.5$ where f is the doppler shift and T is the pulse duration. The shift register code was observed to hold up better with regard to side-lobe performance over the doppler range. Three of the cuts computed for this code are given in Figure 63. These results are for a continuous (analog) phase detector with a perfect phase reference assumed.

2. QUANTIZED PHASE DETECTOR

Whereas the phase detector assumed for the preceding computations had the characteristics $v = \cos\theta$, the quantized phase detector has the characteristic

$$v = 1 \quad \text{for} \quad \pi(2k - 0.5) < \theta \leq (2k + 0.5)\pi$$

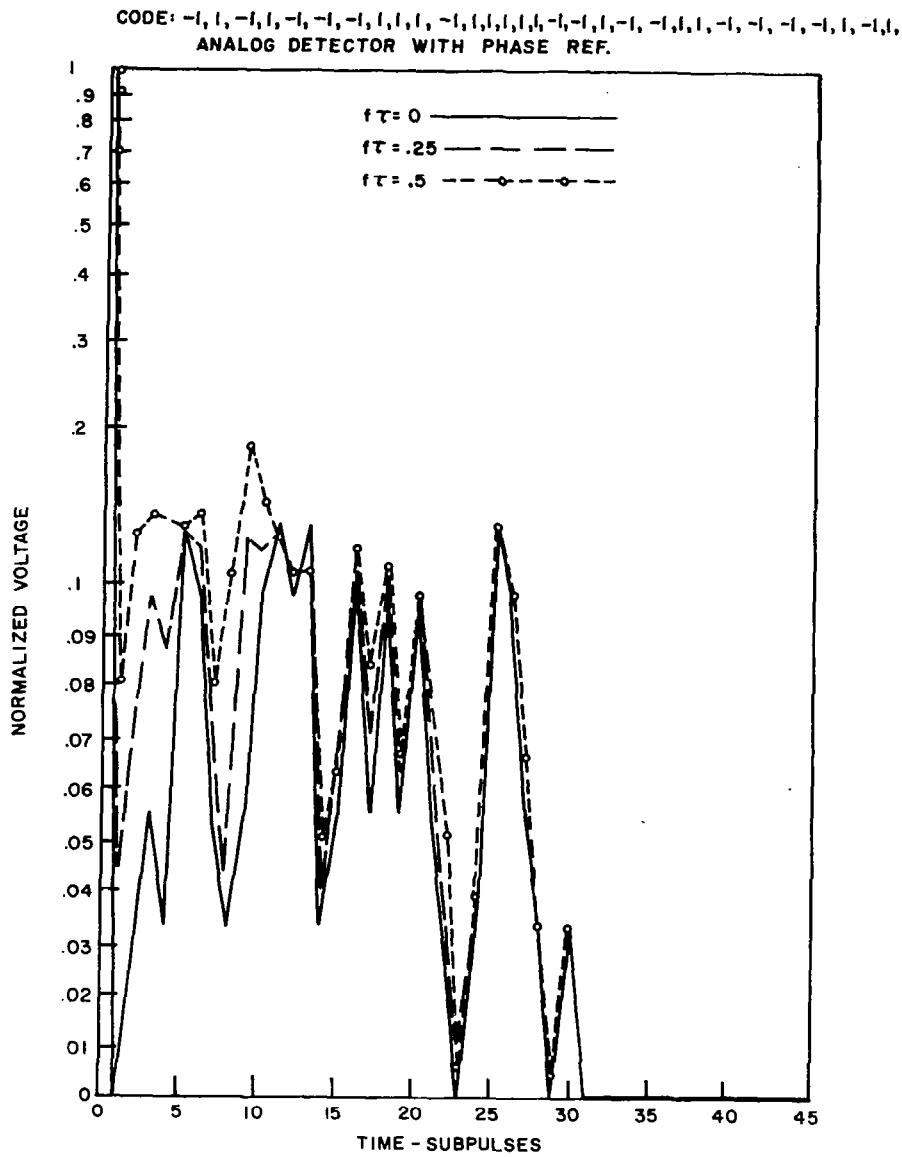

FIGURE 63. DOPPLER EFFECT ON 31-BIT CODE

$$= -1 \quad \text{for} \quad \pi(2k + 0.5) < \theta \leq (2k + 1.5)\pi$$

where $k = 0, \pm 1, \pm 2, \ldots$

Because the range is unknown, no phase reference is actually available, and recourse is made to using two quadrature phase detectors. Their responses are characterized by the sketches in Figure 64. It can be seen that for θ in the first quadrant, both phase detectors correctly decode the phase sequence; for θ in the second and fourth quadrants, one phase detector is correct and the other produces the complement sequence; in the third quadrant both detectors provide complemented sequences. The effect of complementing the entire sequence is to multiply the output time waveform by minus one. This, in itself, will cause no difficulty.

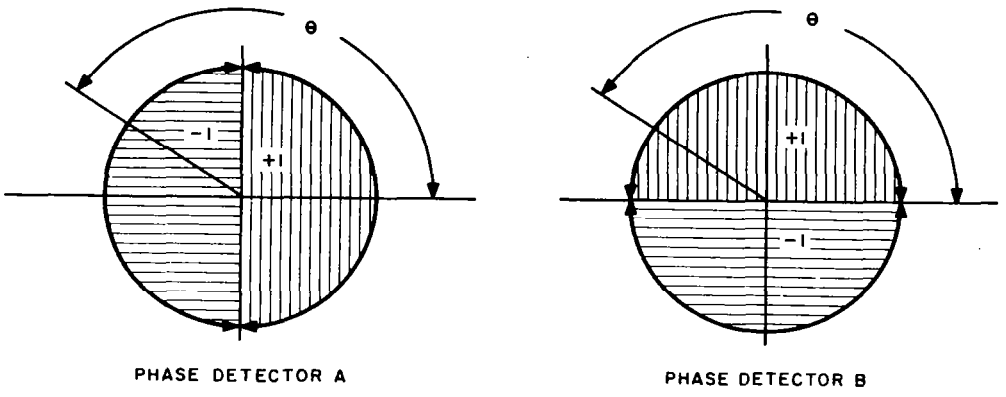

FIGURE 64. ONE-BIT QUADRATURE PHASE DETECTOR RESPONSES

The changing round trip path length of the echo results in a progressive phase shift along the sequence. To the degree that the doppler shift is constant, the phase shift is linear with position along the sequence. As indicated in Figure 65, for phase detector B, the

effect of this spread, θ_s, in conjunction with the random phase θ_r, is to complement portions of the code sequence.

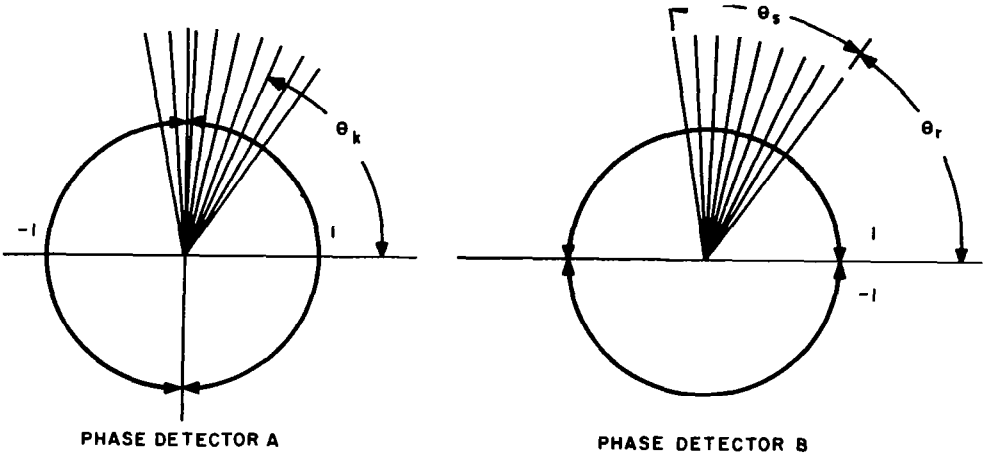

FIGURE 65. CONSEQUENCE OF DOPPLER SPREAD

If, as is the case in this application, the doppler spread is limited to less than 90 degrees, then only one "split" can occur in the decoded sequence. That is, only one reversal from direct to complemented (or complemented to direct) can occur. Further, and more important, at least one of the two quadrature phase detectors must produce an "unsplit" sequence.

The 1-bit quantized phase detector ambiguity functions for the two proposed 31-element codes were computed for each of the 31 possible split locations. The results were produced in graphical form directly by the computer and selected results are included in Figure 66. The heading line gives the 31-element code, and the number of elements complemented is on the right-hand side. The ambiguity function, plotted with voltage along the abscissa (-31 to +31) and range along the ordinate (1 to 31), normally peaks at 31, 31. As the number of contiguous elements complemented increases, the main lobe level drops and side lobes appear. These side lobes are about 6 db down from the normal main lobe and are about 4 to 10 elements out in range.

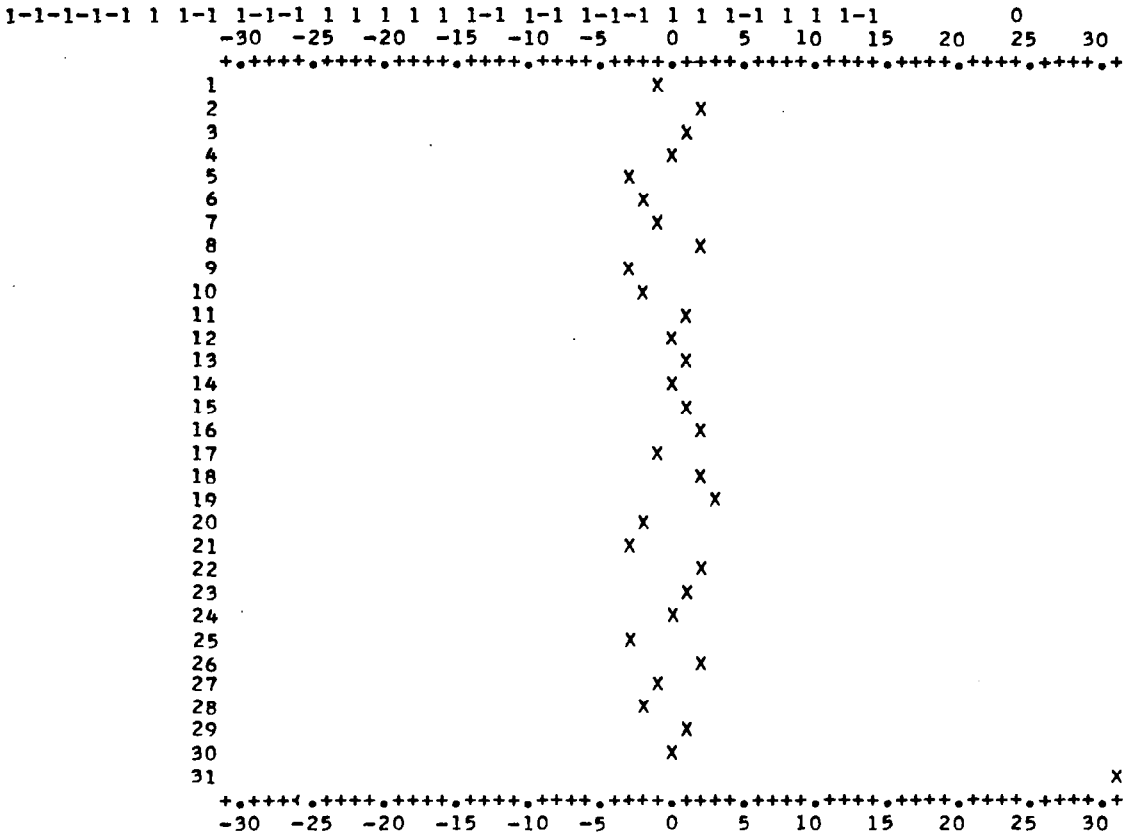

FIGURE 66. AMBIGUITY FUNCTIONS
(SHEET 1 OF 8)

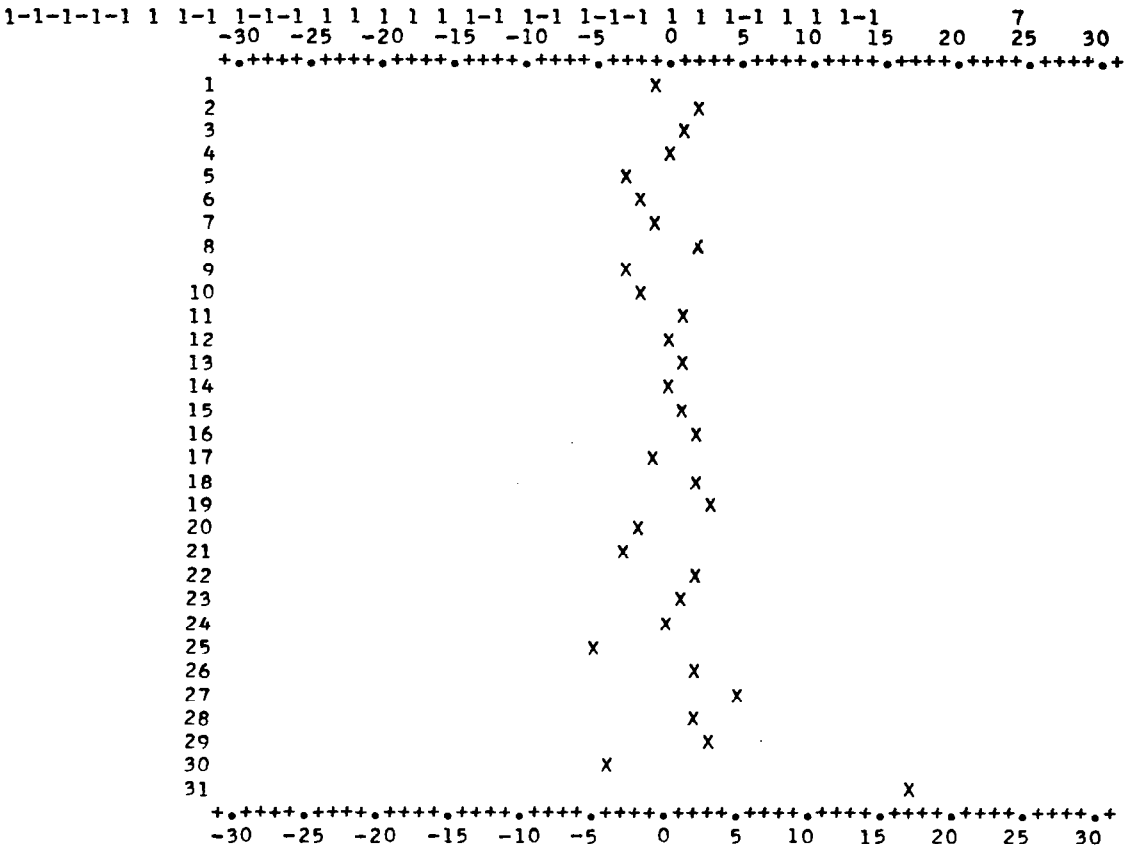

FIGURE 66
(SHEET 2 OF 8)

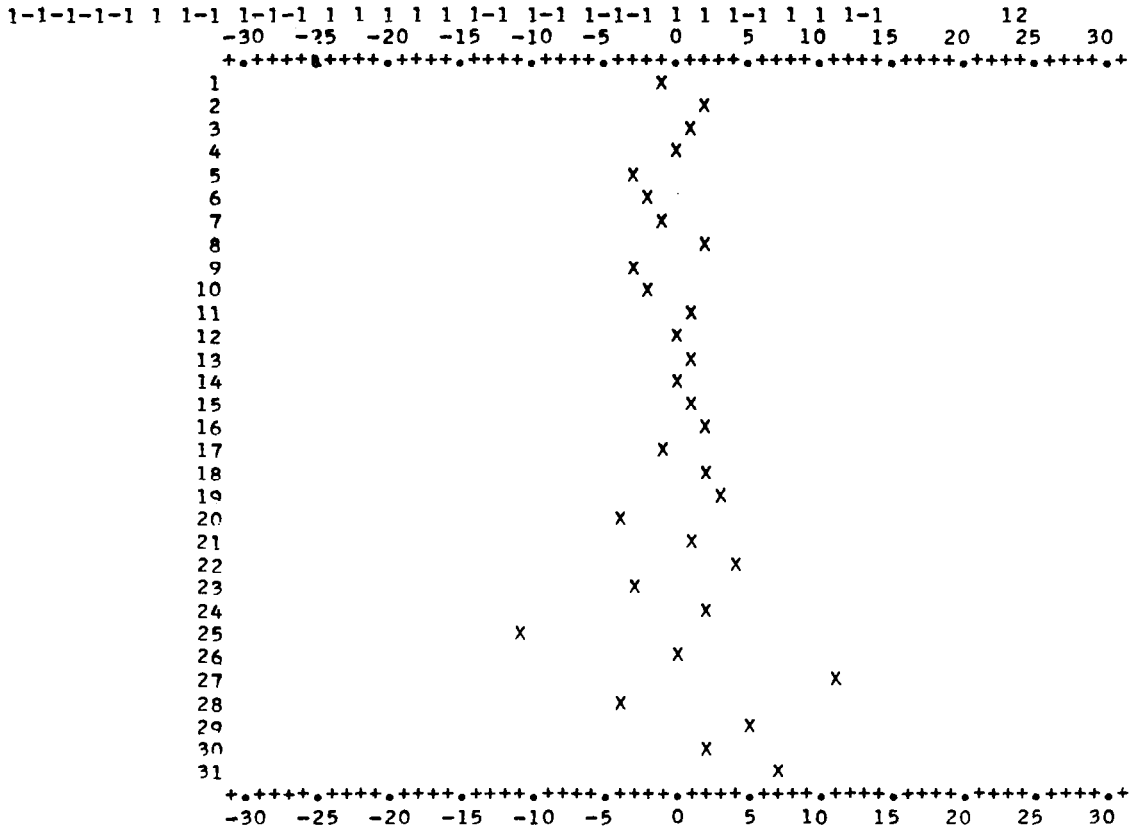

FIGURE 66
(SHEET 3 OF 8)

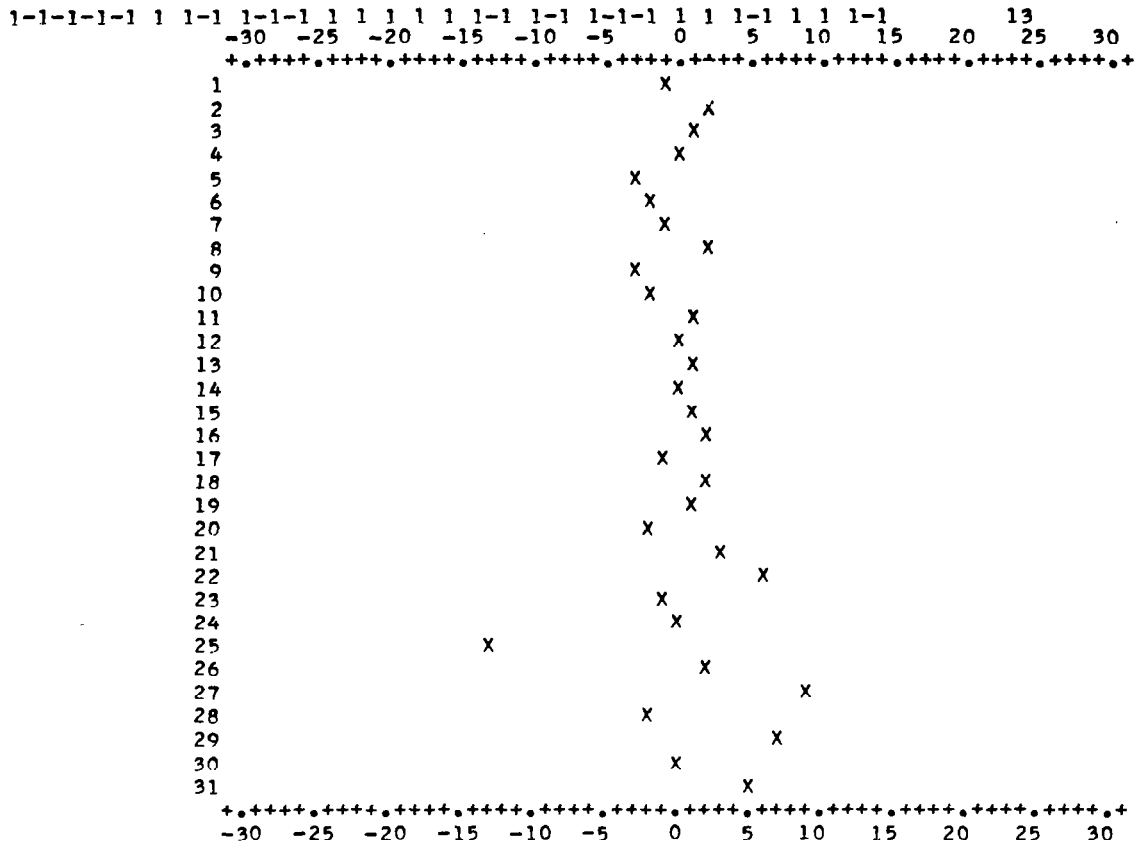

FIGURE 66
(SHEET 4 OF 8)

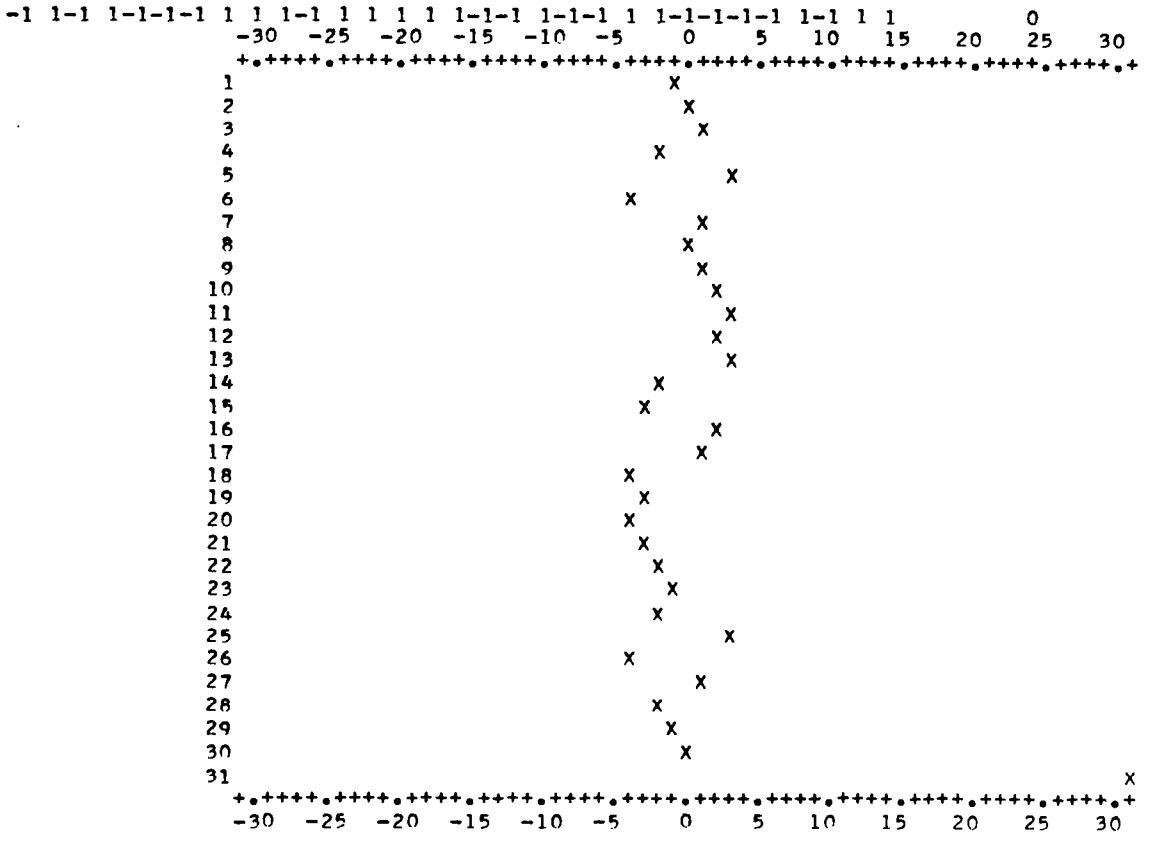

FIGURE 66
(SHEET 5 OF 8)

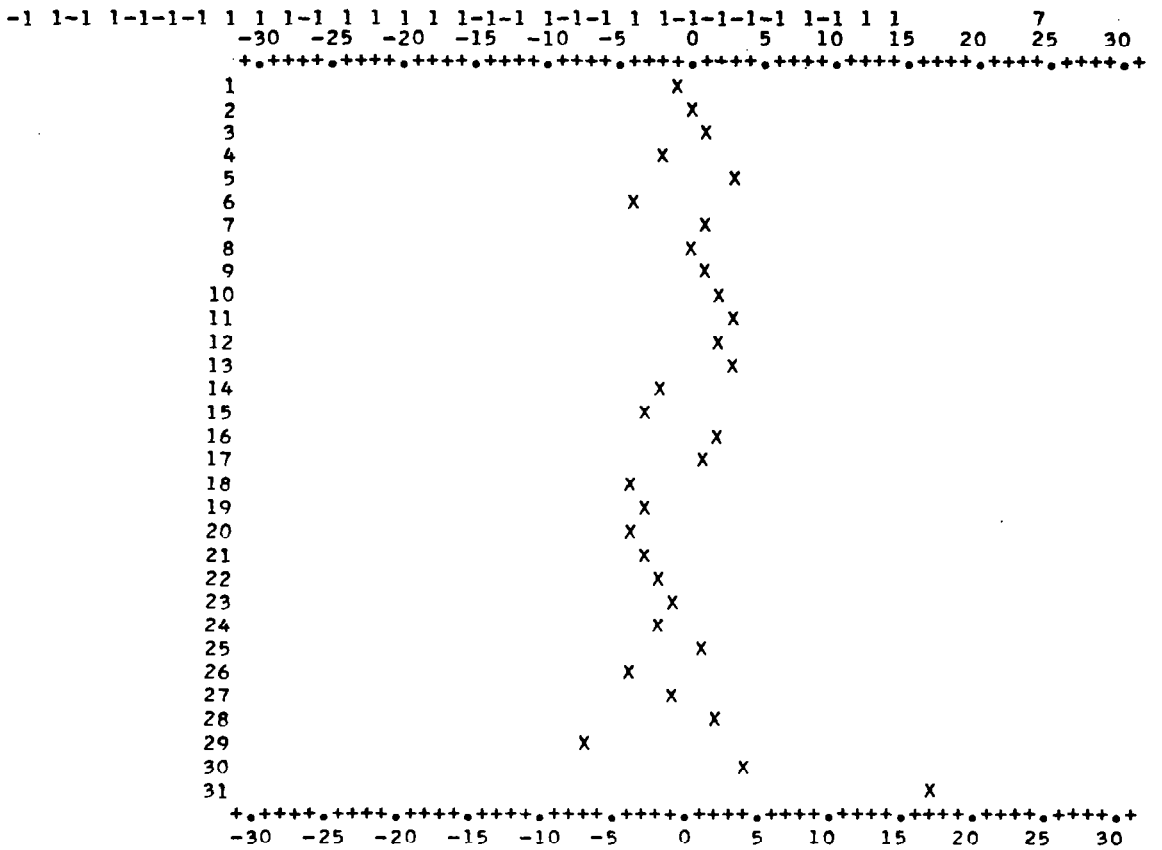

FIGURE 66
(SHEET 6 OF 8)

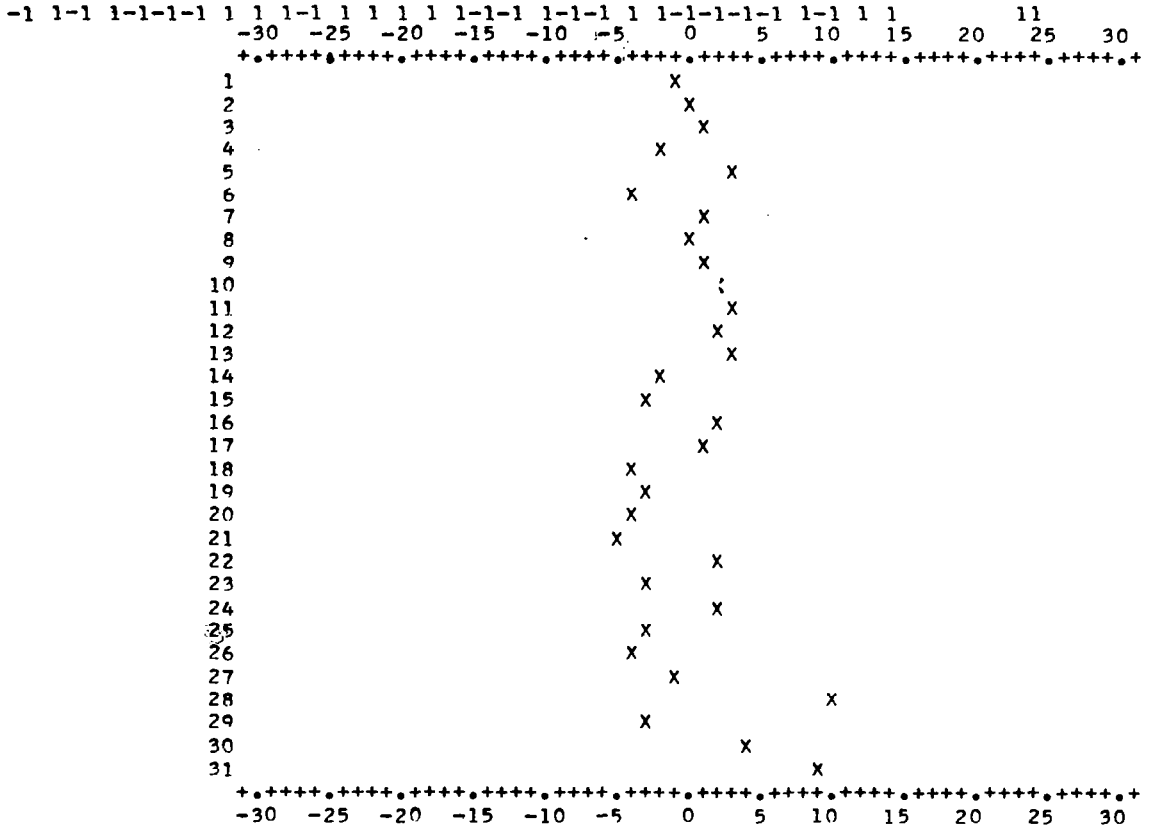

FIGURE 66
(SHEET 7 OF 8)

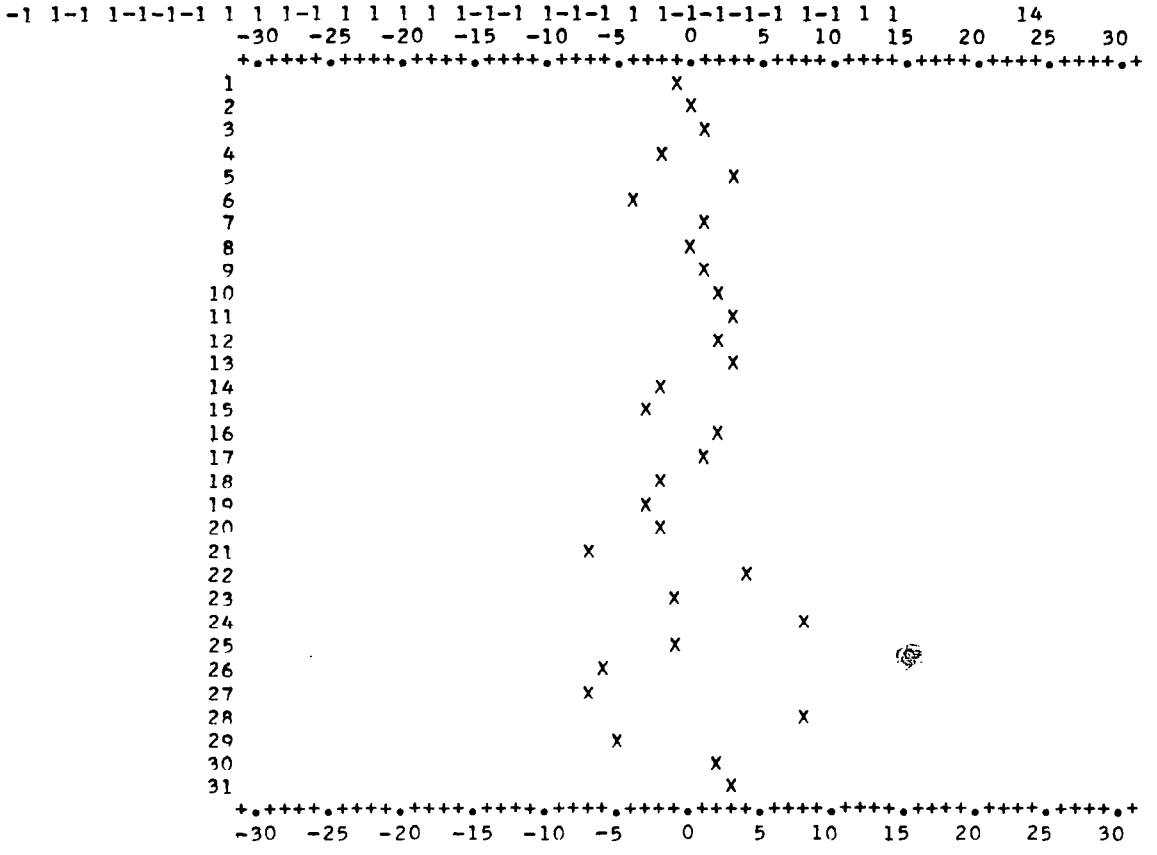

FIGURE 66
(SHEET 8 OF 8)

It was observed that the shift register code is somewhat better in that the frequency of spurious side lobes is lower although they are slightly more intense when they do occur. The plots presented in Figure 66 were selected to show the worst side-lobe responses. These occurred with a different number of elements complemented in each of the two codes investigated.

3. NOISE EFFECT

As indicated in Figure 65, each element of the phase sequence has a phase θ_k, due to the random (θ_r) and doppler (θ_s) effects, of

$$\theta_k = \theta_r + \theta_s(k - 1)/(n - 1) \ , \ k = 1,2,3,\ldots,n.$$

n = number of code elements = 31

In the presence of additive gaussian noise from a narrow-band process each element of the phase sequence has a probability density function[20] for its phase of

$$P_k(\theta) = 0 \ , \ |\theta| > \pi$$

$$= \left(\exp - w^2\right)/2\pi + \left[w \cos\left(\theta - \theta_k\right)\right] \left\{1 + \operatorname{erf}\left[w \cos\left(\theta - \theta_k\right)\right]\right.$$

$$\left. \dot{x} \ \exp - w^2 \sin^2\left(\theta - \theta_k\right) / \ 2\sqrt{2\pi} \right\}, \ |\theta| \leq \pi$$

where $\theta = \theta_k - \theta_r$, and w is the rms signal to rms noise ratio. In this formulation θ_k represents the phase angle of the k^{th} element in an n element sequence which was originally a sequence of zeroes and pi's. The θ_r term represents a random phase shift common to all the elements of the sequence and accounts for the unknown initial round trip path length. The θ_s term accounts for the rate of change of round trip

path length under the assumption that it is constant; that is, the doppler shift is a constant. The argument of the probability density function $P_k(\ )$ is properly $(\theta - \theta_r)$.

For w of the order of 6 db or better, the distribution is very nearly gaussian with $\bar{\theta} \approx \theta_k$ provided $|\ \theta_k\ | \lesssim 2\pi/3$. As indicated in Figure 67 the area under the probability density function between the limits of correct phase detector response is the probability of correct rendition of a code element. This probability is different in general for the two quadrature phase detectors.

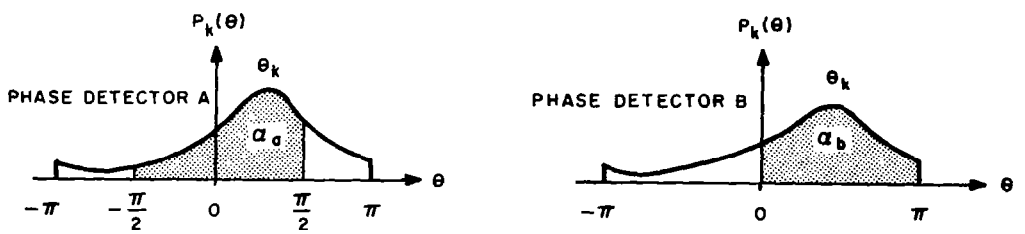

FIGURE 67. PROBABILITY DENSITY FUNCTION AND TRANSITION PROBABILITIES

In the time cells before and after those of the 31-element sequence, only noise is assumed to be present. Thus, the probability densities for the phases in these cells is uniform. The entire detected sequence of 1's and -1's, in the time interval allocated to echoes, comprises a given number of elements with +1 and -1, equiprobable in the noise only region, and probabilities for +1 and -1 in the signal region, as determined from the integrals of $p_k(\theta)$ appropriate to each of the quadrature phase detectors.

4. JOINT PROBABILITY DENSITY FUNCTIONS

The question of how to combine the outputs of the two quadrature phase detectors was approached by investigation of the joint probability density for the compressed outputs of the two detectors.

Intuitively, the optimum combining law for the two voltages should result in a maximally peaked unimodal distribution with the greatest displacement between the mean for noise alone and the mean for signal plus noise. Thus, the combining law, $c = f(a,b)$ where c is the output and a and b are the two voltages to be combined should conform to the topography of the joint distribution.

Monte Carlo generation of the joint histogram for the two phase detector outputs was done for signal-to-noise ratios of -6 db per element and 12 db per element at doppler-spread angles of 0 and 90 degrees. The joint histogram for the case of noise alone was calculated theoretically. The magnitudes of the compressed outputs can assume only 16 values in the case of a 31-element sequence of plus ones and minus ones: $v_i = 2i - 1$, $i = 1, 2 \ldots 16$. Figure 68 shows these results.

In the figures, the joint histogram is presented as a 16 × 16 array in which $n_{i,J}$ is the number of times the joint occurrence of v_i and v_j took place in the Monte Carlo trials. The values of i and j are unity at the upper left corner of the array. Their ordering is not important. At the right and bottom of the array the marginal, individual phase detector, histograms, and sum polygons are printed. Below these are the histograms and sum polygons for the outputs that would result with the "greatest-of" and linear processing techniques. These are found from

$$n_J = \sum_{i=1}^{J} n_{i,J} + \sum_{i=1}^{J-1} n_{J,i}, \quad J = 1, 2, 3, \ldots 16.$$

-1 1-1 1-1-1-1 1 1 1-1 1 1 1 1 1-1-1 1-1-1 1 1-1-1-1-1 1-1 1 1

SAMPLE SIZE = 500
DOPPLER SPREAD ANGLE = 0.0000DEGREES/ ELEMENT S/N RATIO,DB = 12.0

HISTOGRAM

0	0	0	0	0	0	0	0	0	0	0	0	0	0	0	2	2	2
0	0	0	0	0	0	0	0	0	0	0	0	0	0	0	5	5	7
0	0	0	0	0	0	0	0	0	0	0	0	0	0	0	4	4	11
0	0	0	0	0	0	0	0	0	0	0	0	0	0	0	3	3	14
0	0	0	0	0	0	0	0	0	0	0	0	0	0	0	3	3	17
0	0	0	0	0	0	0	0	0	0	0	0	0	0	0	2	2	19
0	0	0	0	0	0	0	0	0	0	0	0	0	0	0	5	5	24
0	0	0	0	0	0	0	0	0	0	0	0	0	0	0	8	8	32
0	0	0	0	0	0	0	0	0	0	0	0	0	0	0	8	8	40
0	0	0	0	0	0	0	0	0	0	0	0	0	0	0	6	6	46
0	0	0	0	0	0	0	0	0	0	0	0	0	0	0	10	10	56
0	0	0	0	0	0	0	0	0	0	0	0	0	0	0	8	8	64
0	0	0	0	0	0	0	0	0	0	0	0	0	0	0	11	11	75
0	0	0	0	0	0	0	0	0	0	0	0	0	0	0	12	12	87
0	0	0	0	0	0	0	0	0	0	0	0	0	0	0	23	23	110
3	6	3	5	1	3	5	2	9	6	10	8	10	13	32	274	390	500
3	6	3	5	1	3	5	2	9	6	10	8	10	13	32	384	500	
3	9	12	17	18	21	26	28	37	43	53	61	71	84	116	500		

HISTOGRAM FOR GREATEST OF

0	0	0	0	0	0	0	0	0	0	0	0	0	0	0	500		
0	0	0	0	0	0	0	0	0	0	0	0	0	0	0	500		

HISTOGRAM FOR LINEAR

0	0	0	0	0	0	0	0	0	0	0	0	0	0	0	5		
11	7	8	4	5	10	10	17	12	20	16	21	25	55	274			
0	0	0	0	0	0	0	0	0	0	0	0	0	0	0	5		
16	23	31	35	40	50	60	77	89	109	125	146	171	226	500			

FIGURE 68. HISTOGRAM (SHEET 1 OF 5)

-1 1-1 1-1-1-1 1 1 1-1 1 1 1 1 1-1-1 1-1-1 1 1-1-1-1-1 1-1 1 1

SAMPLE SIZE = 500
DOPPLER SPREAD ANGLE = 90.0000DEGREES/ ELEMENT S/N RATIO,DB = 12.0

HISTOGRAM

0	0	0	0	0	0	0	0	0	0	0	0	0	0	0	20	20	20
0	0	0	0	0	0	0	0	0	0	0	0	0	0	0	18	18	38
0	0	0	0	0	0	0	0	0	0	0	0	0	0	0	16	16	54
0	0	0	0	0	0	0	0	0	0	0	0	0	0	0	22	22	76
0	0	0	0	0	0	0	0	0	0	0	0	0	0	1	14	15	91
0	0	0	0	0	0	0	0	0	0	0	0	0	0	0	18	18	109
0	0	0	0	0	0	0	0	0	0	0	0	0	0	0	17	17	126
0	0	0	0	0	0	0	0	0	0	0	0	0	0	2	15	17	143
0	0	0	0	0	0	0	0	0	0	0	0	0	0	0	9	9	152
0	0	0	0	0	0	0	0	0	0	0	0	0	1	2	16	19	171
0	0	0	0	0	0	0	0	0	0	0	0	0	2	3	11	16	187
0	0	0	0	0	0	0	0	0	0	0	0	0	1	7	10	18	205
0	0	0	0	0	0	0	0	0	0	0	0	0	4	4	13	21	226
0	0	0	0	0	0	0	0	0	0	2	0	3	3	6	7	21	247
0	0	0	0	0	0	0	0	2	2	3	10	11	7	5	3	43	290
15	19	19	18	18	18	16	14	20	13	13	13	6	4	2	2	210	500
15	19	19	18	18	18	16	14	22	15	18	23	20	22	32	211	500	
15	34	53	71	89	107	123	137	159	174	192	215	235	257	289	500		

HISTOGRAM FOR GREATEST OF

0	0	0	0	0	0	0	0	0	0	0	0	0	16	65	419		
0	0	0	0	0	0	0	0	0	0	0	0	0	16	81	500		

HISTOGRAM FOR LINEAR

0	0	0	0	0	0	0	0	0	0	0	0	0	0	0	35		
37	35	41	32	36	35	32	37	36	48	41	32	16	5	2			
0	0	0	0	0	0	0	0	0	0	0	0	0	0	0	35		
72	107	148	180	216	251	283	320	356	404	445	477	493	498	500			

FIGURE 68
(SHEET 2 OF 5)

-1 1-1 1-1-1-1 1 1 1-1 1 1 1 1 1-1-1 1-1-1 1 1-1-1-1-1 1-1 1 1

SAMPLE SIZE = 3000
DOPPLER SPREAD ANGLE = 90.0000DEGREES/ ELEMENT S/N RATIO,DB = -6.0

HISTOGRAM

1	9	12	19	32	43	37	34	46	23	11	9	0	0	0	0	276	276
8	11	12	14	32	35	37	38	36	36	13	7	5	1	0	0	285	561
16	17	22	21	29	40	37	41	30	18	14	5	2	1	0	0	293	854
23	22	27	28	47	35	34	46	29	16	16	4	0	0	0	0	327	1181
29	37	27	35	50	38	45	33	41	20	11	7	1	0	0	0	374	1555
28	26	48	46	47	39	33	24	24	17	7	2	3	0	0	0	344	1899
29	42	35	43	35	31	35	18	16	18	7	2	1	0	0	0	312	2211
36	46	45	45	31	27	19	13	17	9	3	3	1	0	0	0	295	2506
41	24	31	33	23	19	16	10	11	1	0	0	0	0	0	0	209	2715
24	23	19	22	13	11	15	5	1	3	3	1	0	0	0	0	140	2855
11	11	17	16	11	9	3	2	1	3	0	0	0	0	0	0	84	2939
6	8	8	5	7	4	0	1	0	0	0	0	0	0	0	0	39	2978
2	6	6	1	2	0	1	0	0	0	1	0	0	0	0	0	19	2997
0	1	1	0	1	0	0	0	0	0	0	0	0	0	0	0	3	3000
0	0	0	0	0	0	0	0	0	0	0	0	0	0	0	0	0	3000
0	0	0	0	0	0	0	0	0	0	0	0	0	0	0	0	0	3000
254	283	310	328	360	331	312	265	252	164	86	40	13	2	0	0	3000	
254	537	847	1175	1535	1866	2178	2443	2695	2859	2945	2985	2998	3000	3000	3000		

HISTOGRAM FOR GREATEST OF

1	28	79	154	318	425	473	496	447	294	169	79	32	5	0	0
1	29	108	262	580	1005	1478	1974	2421	2715	2884	2963	2995	3000	3000	3000

HISTOGRAM FOR LINEAR

1	17	39	71	119	188	211	319	374	355	352	266	236	169	114	93
44	13	10	7	1	0	1	0	0	0	0	0	0	0	0	
1	18	57	128	247	435	646	965	1339	1694	2046	2312	2548	2717	2831	2924
2968	2981	2991	2998	2999	2999	3000	3000	3000	3000	3000	3000	3000	3000	3000	

FIGURE 68
(SHEET 3 OF 5)

-1 1-1 1-1-1-1 1 1 1-1 1 1 1 1 1-1-1 1-1-1 1 1-1-1-1-1 1-1 1 1

SAMPLE SIZE = 3000

DOPPLER SPREAD ANGLE = 0.0000DEGREES/ ELEMENT S/N RATIO,DB = -6.0

HISTOGRAM

3	3	4	8	11	25	29	40	30	28	27	15	4	1	0	1	229	229
4	7	2	12	19	22	27	45	43	29	25	12	8	5	1	0	261	490
6	8	13	15	19	34	37	37	46	28	20	11	5	2	0	0	281	771
6	8	17	18	20	36	33	35	32	24	28	6	2	1	0	0	266	1037
13	18	26	20	32	33	45	43	24	21	17	8	3	2	0	0	305	1342
25	30	29	23	29	37	26	28	31	20	14	7	5	1	0	0	305	1647
24	31	18	41	36	41	39	29	15	24	10	7	4	1	0	0	320	1967
34	30	49	33	32	37	36	22	23	18	3	3	1	1	1	0	323	2290
44	40	33	46	36	28	19	16	14	5	6	1	1	0	0	0	289	2579
29	32	18	22	24	17	16	13	9	4	2	1	0	0	0	0	187	2766
23	12	23	16	16	7	7	8	5	4	1	0	0	0	0	0	122	2888
16	9	18	10	8	6	5	2	1	1	0	0	0	0	0	0	76	2964
5	3	4	4	4	2	3	1	0	0	0	0	0	0	0	0	26	2990
2	3	2	1	0	0	0	0	0	0	0	0	0	0	0	0	8	2998
0	0	0	1	0	0	0	0	0	0	0	0	0	0	0	0	1	2999
0	0	0	0	0	1	0	0	0	0	0	0	0	0	0	0	1	3000
234	234	256	270	286	326	322	319	273	206	153	71	33	14	2	1	3000	
234	468	724	994	1280	1606	1928	2247	2520	2726	2879	2950	2983	2997	2999	3000		

HISTOGRAM FOR GREATEST OF

3	14	33	84	178	323	427	530	520	381	274	147	59	22	3	2
3	17	50	134	312	635	1062	1592	2112	2493	2767	2914	2973	2995	2998	3000

HISTOGRAM FOR LINEAR

3	7	17	24	57	119	168	235	295	362	376	334	283	256	159	128
84	47	28	11	6	1	0	0	0	0	0	0	0	0	0	
3	10	27	51	108	227	395	630	925	1287	1663	1997	2280	2536	2695	2823
2907	2954	2982	2993	2999	3000	3000	3000	3000	3000	3000	3000	3000	3000	3000	

FIGURE 68
(SHEET 4 OF 5)

```
-1 1-1 1-1-1-1 1 1 1-1 1 1 1 1 1-1-1 1-1-1 1 1-1-1-1-1 1-1 1 1

        SAMPLE SIZE  =99938
DOPPLER SPREAD ANGLE =    0.0000DEGREES/ ELEMENT S/N RATIO,DB =-9999.9999
```

HISTOGRAM

7834	6912	5376	3678	2207	1156	525	205	68	19	4	0	0	0	0	0	27984	27984
6912	6099	4743	3245	1947	1020	463	181	60	16	3	0	0	0	0	0	24689	52673
5376	4743	3689	2524	1514	793	360	141	47	13	3	0	0	0	0	0	19203	71876
3678	3245	2524	1727	1036	542	246	96	32	9	2	0	0	0	0	0	13137	85013
2207	1947	1514	1036	621	325	148	57	19	5	1	0	0	0	0	0	7880	92893
1156	1020	793	542	325	170	77	30	10	2	0	0	0	0	0	0	4125	97018
525	463	360	246	148	77	35	13	4	1	0	0	0	0	0	0	1872	98890
205	181	141	96	57	30	13	5	1	0	0	0	0	0	0	0	729	99619
68	60	47	32	19	10	4	1	0	0	0	0	0	0	0	0	241	99860
19	16	13	9	5	2	1	0	0	0	0	0	0	0	0	0	65	99925
4	3	3	2	1	0	0	0	0	0	0	0	0	0	0	0	13	99938
0	0	0	0	0	0	0	0	0	0	0	0	0	0	0	0	0	99938
0	0	0	0	0	0	0	0	0	0	0	0	0	0	0	0	0	99938
0	0	0	0	0	0	0	0	0	0	0	0	0	0	0	0	0	99938
0	0	0	0	0	0	0	0	0	0	0	0	0	0	0	0	0	99938
0	0	0	0	0	0	0	0	0	0	0	0	0	0	0	0	0	99938

```
279842468919203131377880 4125 1872  729  241   65   13    0    0    0    0    0 99938

279845267371876850139289397018988909961999860999259993899938999389999389993899938
```

HISTOGRAM FOR GREATEST OF

```
 783419923239272062114029 7842 3673 1451  482  130   26    0    0    0    0    0

 783427757516847230586334941769784999300997829991299938999389999389993899938
```

HISTOGRAM FOR LINEAR

```
 7834138241685116842145931125 7845 4994 2923 1582  792  364  157   60   19    4
    0    0    0    0    0    0    0    0    0    0    0    0    0    0    0

 7834216583850955351699448119889043940379696098542993349969899855999159993499938
99938999389999389993899938999389993899938999389993899938999389993899938999389938
```

FIGURE 68
(SHEET 5 OF 5)

in the "greatest-of" processor, and from

$$n_J = \sum_{i=1}^{J} n_{i, J+1-i} \quad , \quad J = 1, 2, 3, \ldots 16$$

$$n_J = \sum_{i=J-16}^{16} n_{i, J-i} \quad , \quad J = 17, 18, 19, \ldots 32$$

in the linear processor.

It is seen that for the 1-bit phase detectors, the joint distribution at very high signal-to-noise ratios form a pair of intersecting ridges at maximum output levels (Figure 68). This follows from the fact that either one or the other of the two phase detectors will decode the 31-element sequence perfectly when doppler (up to a 90-degree spread) and the random phase are the only sources of error. The optimum combining law at high S/N is therefore

$$C = \frac{1}{2}(|a+b| + |a-b|) \qquad (A-1)$$

that is, c is the max (a, b). The joint distributions at lower S/N ratios do not reveal any obvious topographical characteristics.

The five joint distributions were processed according to the "greatest-of" criterion (equation A-1) and also according to the "linear" or average criterion

$$C_L = \frac{1}{2}(a+b) \qquad (A-2)$$

The results are shown in Figures 69 and 70. Interpolating as though the distributions were continuous indicates that, for a false alarm probability of 0.01, the detection probabilities are the same for both processes

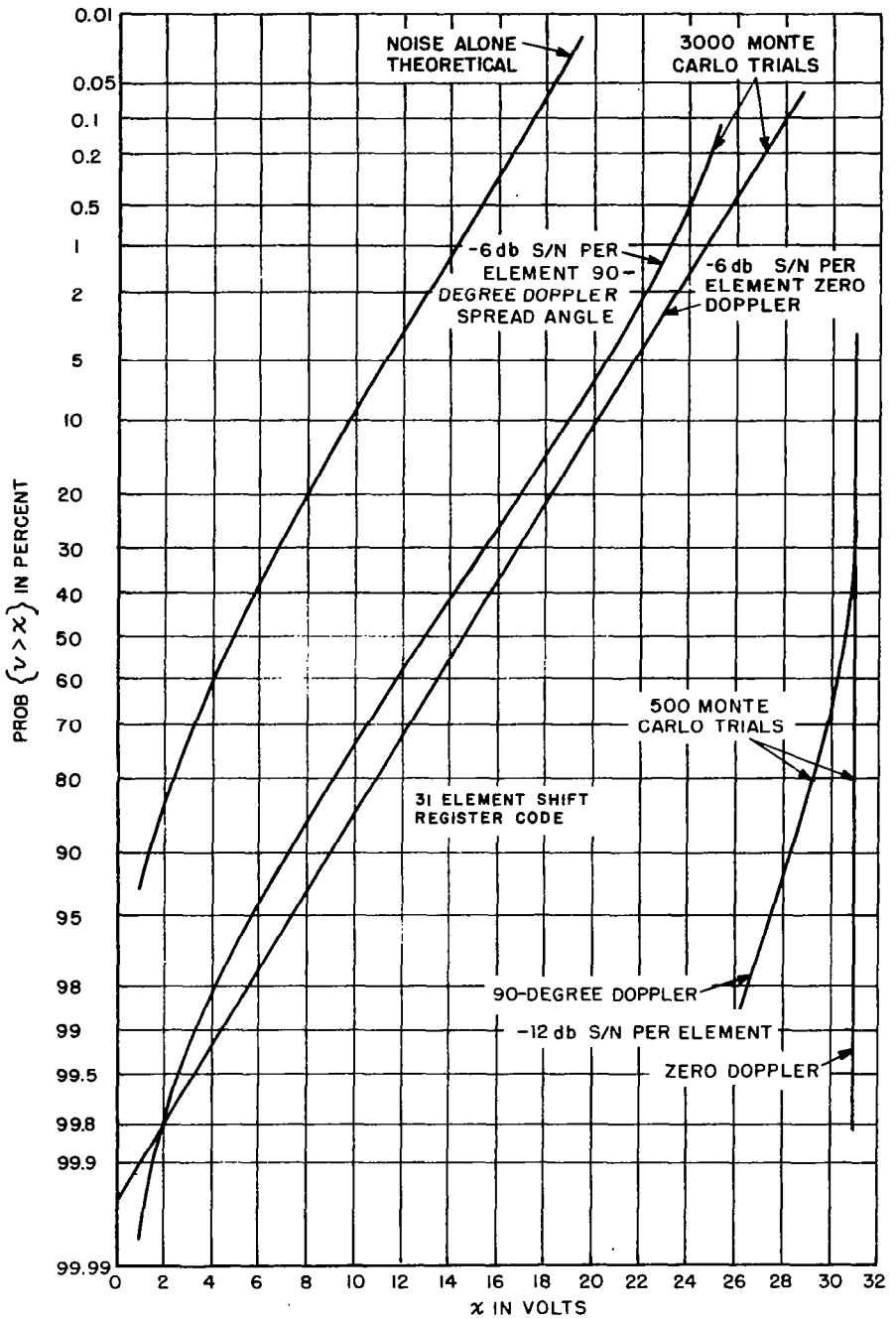

FIGURE 69. "GREATEST OF" DISTRIBUTIONS

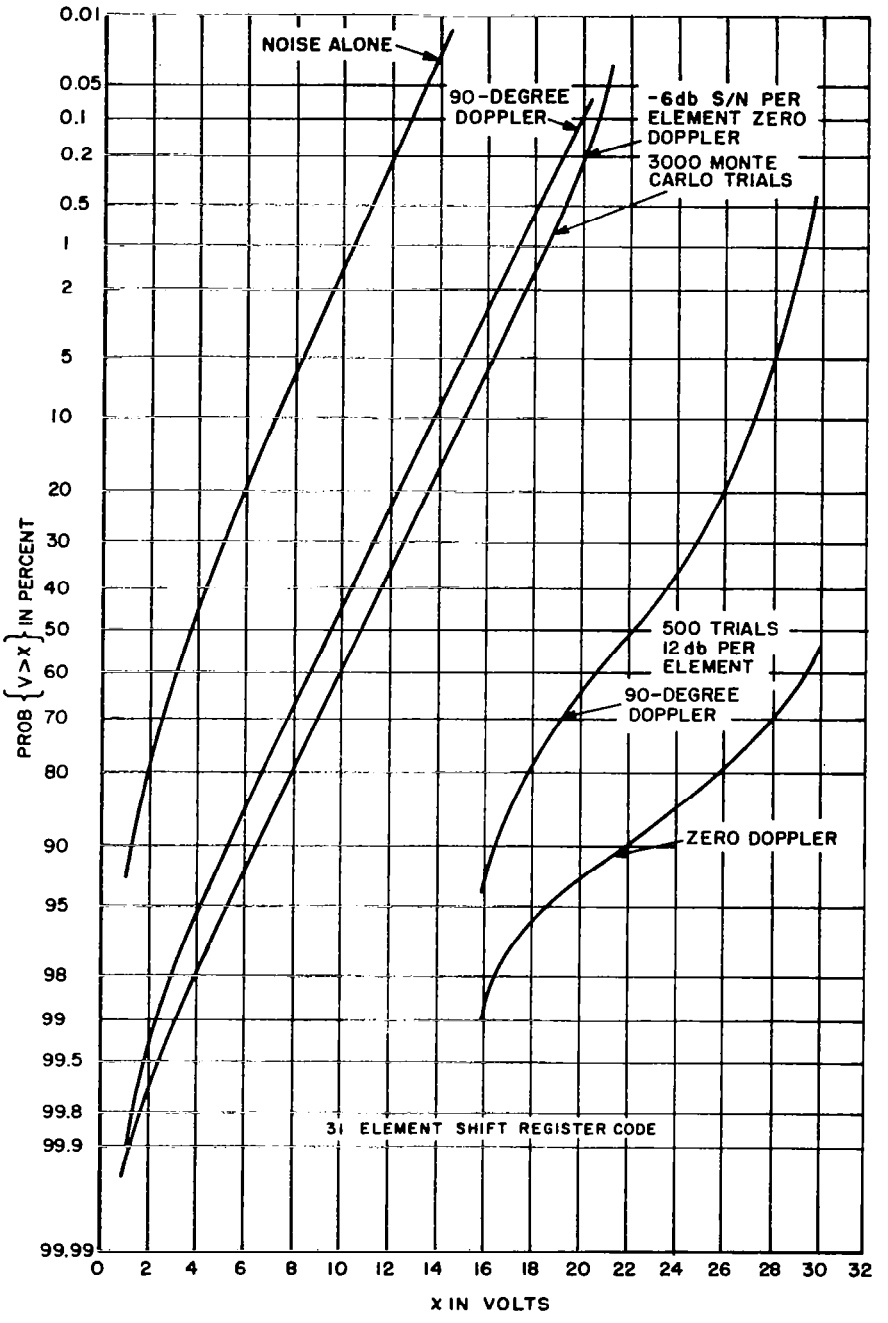

FIGURE 70. "LINEAR" DISTRIBUTIONS

at -6 db S/N per element, namely, 40 and 53 percent at maximum and zero doppler, respectively. The ideal equivalent to 31 elements with -6 db S/N each is a S/N ratio of 8.91 db. A single pulse system provides the same false alarm and detection probabilities with 5.6 and 6.6 db S/N, respectively. This means that at zero doppler the system has a loss of about 3.31 db relative to a simple, single-pulse system. An additional 1 db loss is sustained at maximum doppler.

APPENDIX III
INCOHERENT PROCESSING

The analysis was divided into three phases. In the first phase, wide-band limiting followed by matched IF filtering (sometimes known as Dicke-Fix) was investigated by Monte Carlo simulation on a 1620 Model II digital computer. These results were applied in the second phase to the computation of S/N ratio losses with postdetection integration after the Dicke-Fix process. Lastly, the losses associated with and the the requirements on quantizing the video before integration were examined.

1. DICKE-FIX ANALYSIS

In this analysis the wide-band spectral characteristic was assumed to be shaped such that the succeeding matched IF filter acted to sum independent samples. The number of independent samples summed is set equal to the bandwidth ratio (BWR). In the Monte Carlo simulation pseudo-random number, n_{x_k} and n_{y_k}, Gaussian, independent, with zero mean and unit variance were generated K times each to form a single sample of the envelope r, after matched filtering

$$r = \sqrt{x^2 + y^2}$$

where

$$x = \sum_{k=1}^{K} \frac{x_k}{r_k}$$

$$y = \sum_{k=1}^{K} \frac{y_k}{r_k}$$

$$x_k = S + n_{x_k}, \quad y_k = n_{y_k}$$

$$r_k = \sqrt{x_k^2 + y_k^2}$$

and

$$S = \sqrt{2 \cdot 10^{0.05\,(S/N\ db)}}$$

K = bandwidth ratio (BWR)

S/N db = ratio of rms signal to rms noise, db.

This was carried out for BWR's of 10, 20, and 40 at 7 wideband S/N ratios ranging from -21 db to -3 db in 3 db steps. The size of the Monte Carlo simulation was 4000, 2000, and 1000 trials for the 40, 20, and 10 BWR's, respectively, except at 0 db where 800, 400, and 200 trials were run.

The output of the simulation was a 100 class sum, the sample mean and sample variance. Figures 71 and 72 show the mean and variance results; Figure 73 shows the 100 class sum at 4 db matched S/N ratio. Figure 74 shows the relation between false alarm (α) and miss (β) probabilities at 4 db S/N using the theoretical cumulatives in Figure 75 for the noise distribution. Also, in Figure 74 is the α versus β relation for a single bit linear system. Examination indicates that the BWR is not very important at this stage. At 0.1 false alarm probability the single bit linear system provides 0.63 detection probability at 4 db S/N. The Dicke-Fix system results in 0.5 detection probability which is obtained by a linear single bit system at 2.6 db S/N. In this sense the Dicke-Fix system has a 1.4 db loss at this operating point.

2. POSTDETECTION INTEGRATION AFTER DICKE-FIX

It was assumed for the signal plus noise case that the distribution of the sum of a large number (64 or more) of independent samples was Gaussian with the mean value

$$m = Km_e$$

and variance

$$\sigma^2 = K\sigma_e^2$$

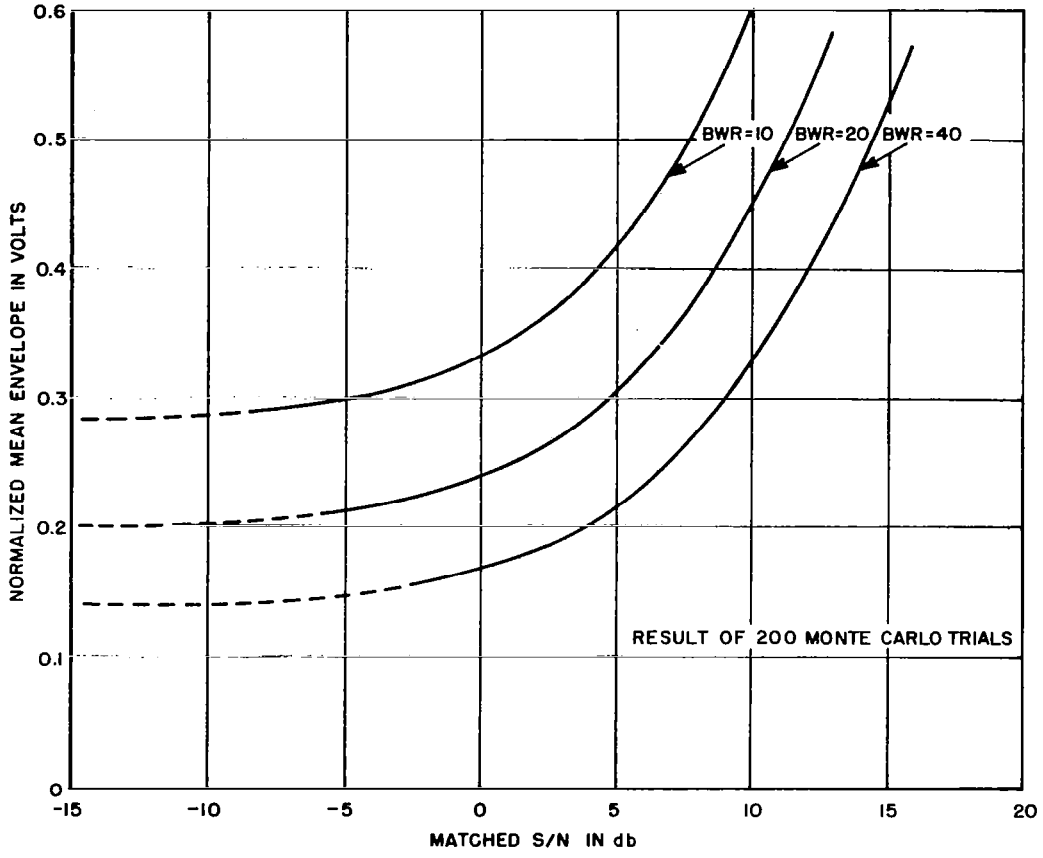

FIGURE 71. MEAN VALUE OF DICKE-FIX ENVELOPE

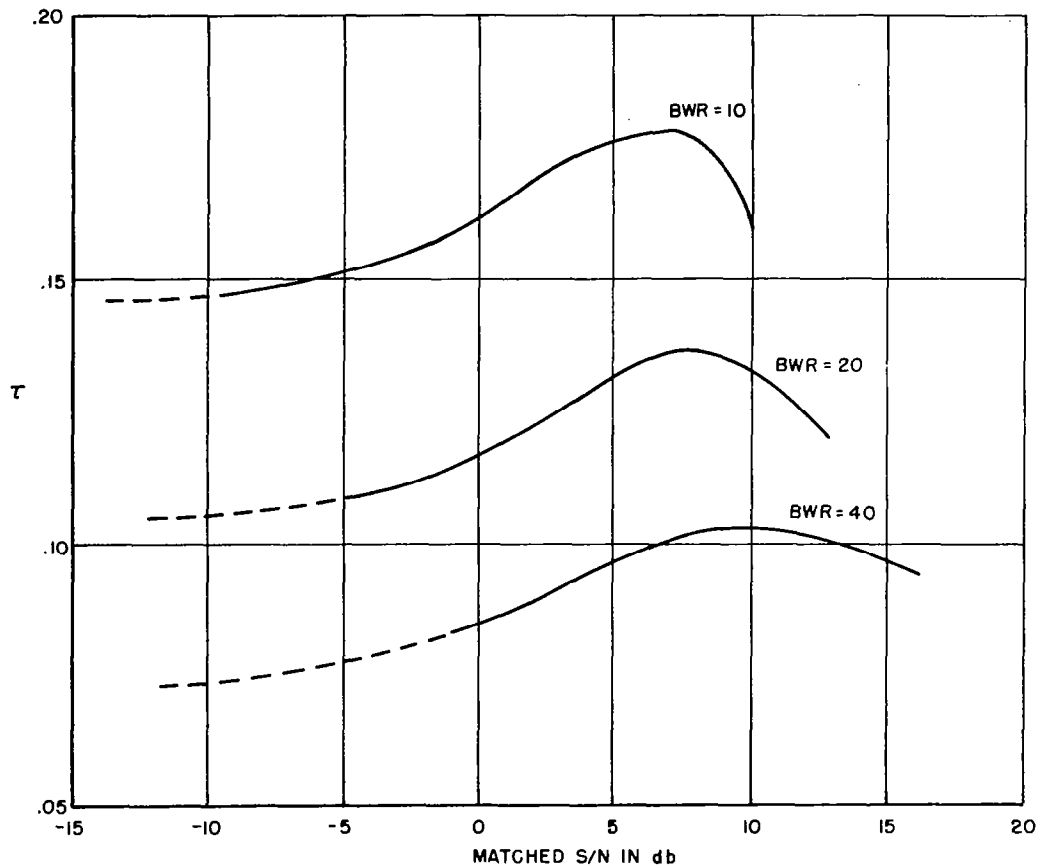

FIGURE 72. RMS VALUE OF DICKE-FIX ENVELOPE

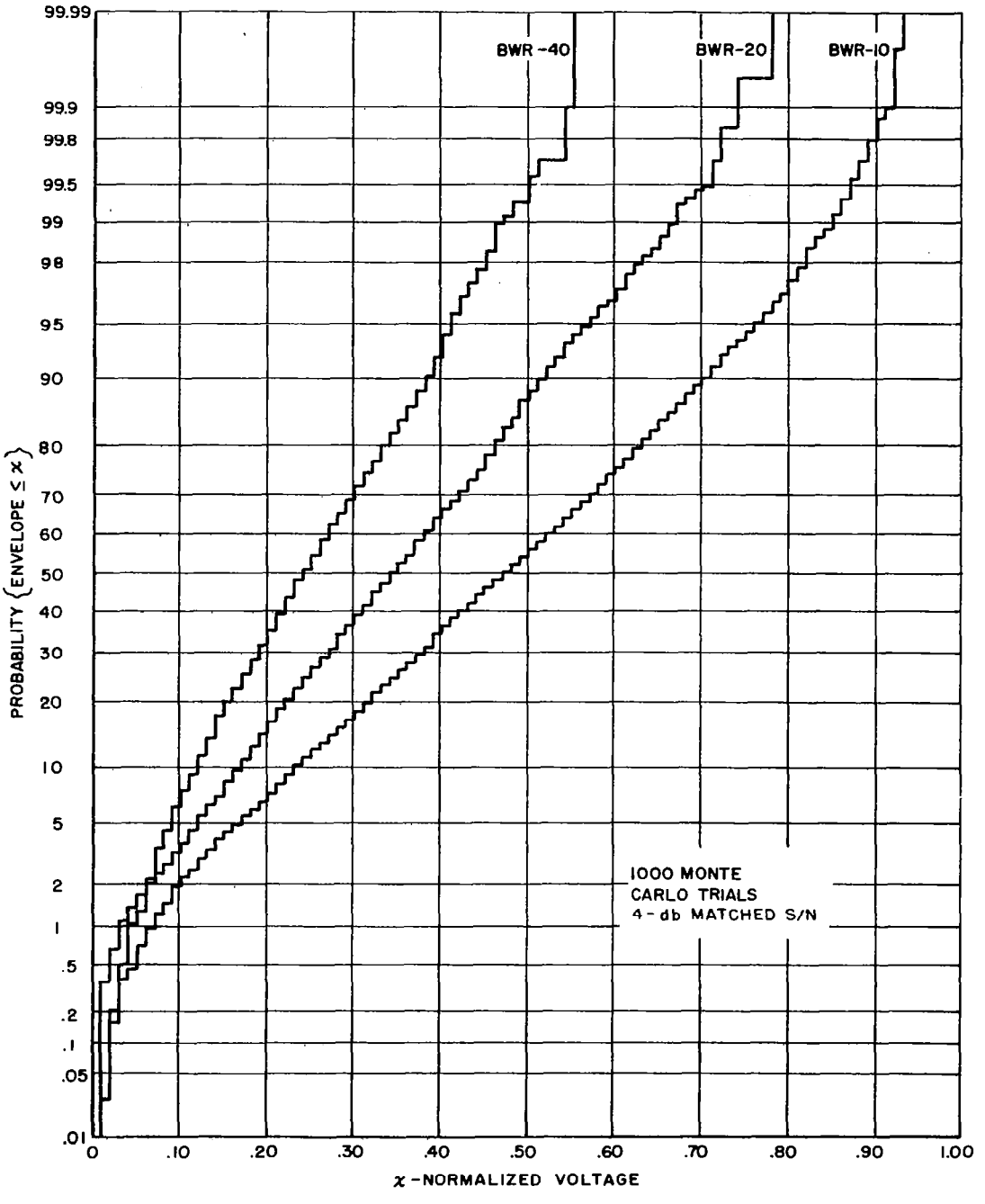

FIGURE 73. DICKE-FIX ENVELOPE CUMULATIVE RESULT

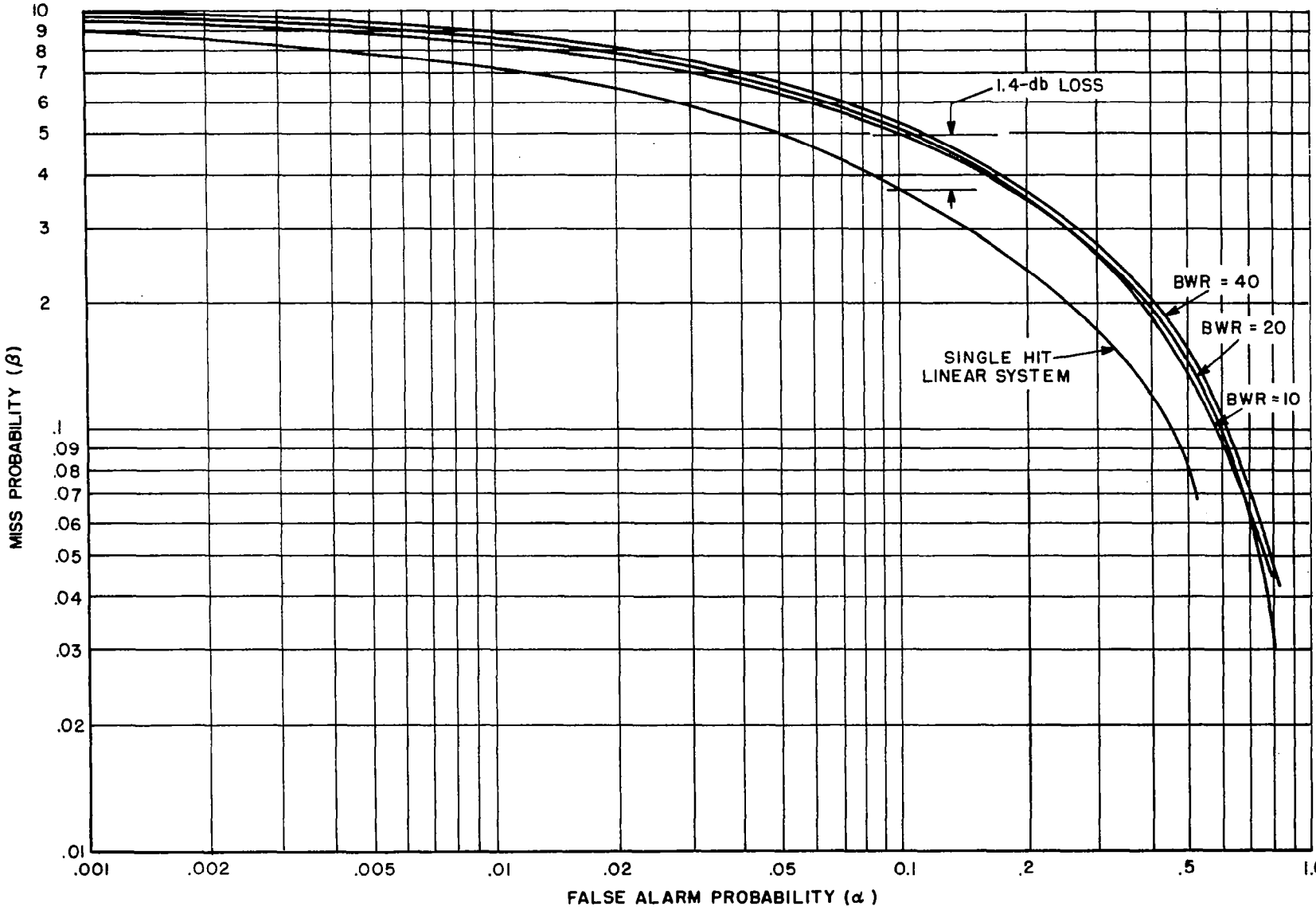

FIGURE 74. DICKE-FIX DETECTION PERFORMANCE

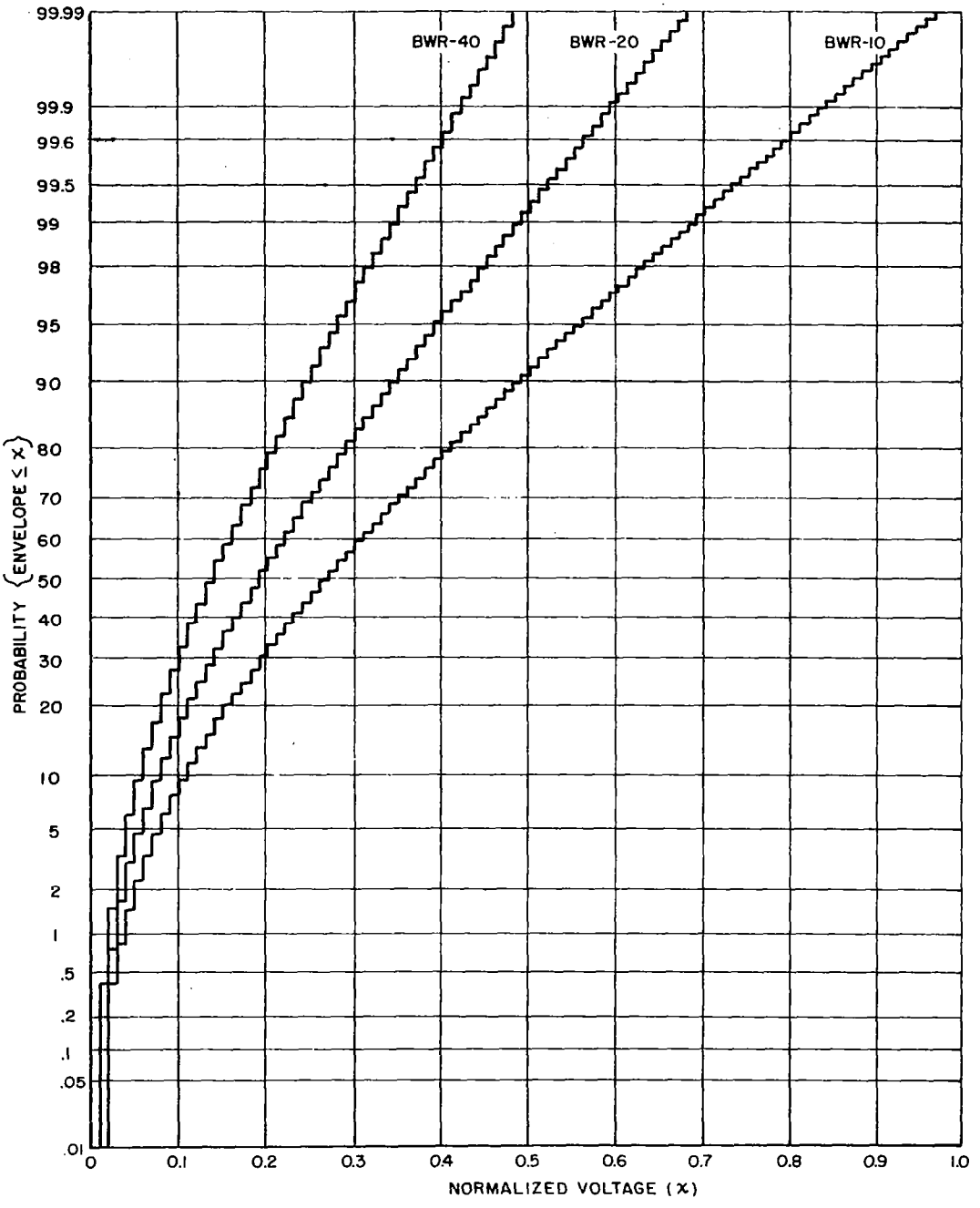

FIGURE 75. DICKE-FIX ENVELOPE NOISE

where K is the number of samples summed; m_e and σ_e are the mean and rms values of the Dicke-Fix envelope as found by the Monte Carlo technique described in paragraph 1. Both m_e and σ_e are dependent on the BWR and S/N ratio.

Under the Gaussian assumption for the signal and noise hypothesis, the detection probability is calculated from

$$P_d = 0.5 + 0.5 \text{ erf } \frac{m - Y_b}{\sigma\sqrt{2}}$$

where

$$\text{erfu} = \frac{2}{\sqrt{\pi}} \int_o^u e^{-x^2} dx$$

and Y_b is the detection threshold.

For the calculation of the threshold, the tails of the distribution are significant and are inaccurately given by the central limit theorem. The linear detector threshold was then computed using Marcum's[21] work. Let

$$t = \frac{Y_b - K\sqrt{\frac{\pi}{2}}}{\sqrt{2K(2 - \frac{\pi}{2})}}$$

then

$$Kp_o \simeq 0.5\ (1 - \text{erft}) + \frac{0.07445}{\sqrt{K}}\ s(t) \cdot (4t^2 - 1) - \frac{0.0216}{K} t\ s(t)\ (4t^2 - 3)$$

$$- \frac{0.0222}{K}\ t\ s(t) \left[(4t^2)^2 - 10\,(4t^2) + 15 \right]$$

where p_o = false alarm probability and $s(t) = 2/\sqrt{\pi}\ \epsilon^{-t^2}$

By this relation Y_b was found for each p_o, K, and BWR of interest. Selected results are plotted in Figures 76, 77, and 78 which show the detection probability versus matched S/N ratio for $p_o = 10^{-6}$ and for BWR's of 10, 20, and 40, respectively.

The computation of the overall losses is facilitated by the entries in Table XIII which show the S/N requirements of a normal post-detection system and those of one with the Dicke-Fix. The losses attributable to the Dicke-Fix process range from 0.5 to 1.4 db.

3. QUANTIZING LOSSES

To estimate the quantizing loss, the detection probability for a given false alarm probability was estimated for both the 3-bit quantized and the analog video after Dicke-Fix. The difference in detection probability was converted to a loss which was approximated by using previously published single-bit detection-probability versus S/N curves at the appropriate false alarm probability. The detection probabilities for the quantized and analog video were estimated under the approximation of Gaussian distributions with means and variances equal to those of the actual distributions.

In the noise alone case the analog video is very nearly Rayleigh,

$$P_o(v) = 2nv\, \epsilon^{-nv^2}$$

where n is the Dicke-Fix bandwidth ratio. Quantizing with 3 bits with thresholds uniformly placed out to unity yields for the quantized video

$$P_{io} = \int_{T_{i-1}}^{T_i} P_o(v)\, dv \qquad i = 1, 2, \ldots I$$

$$I = 2^B$$

$$T_o = 0$$

$$T_i = i/I$$

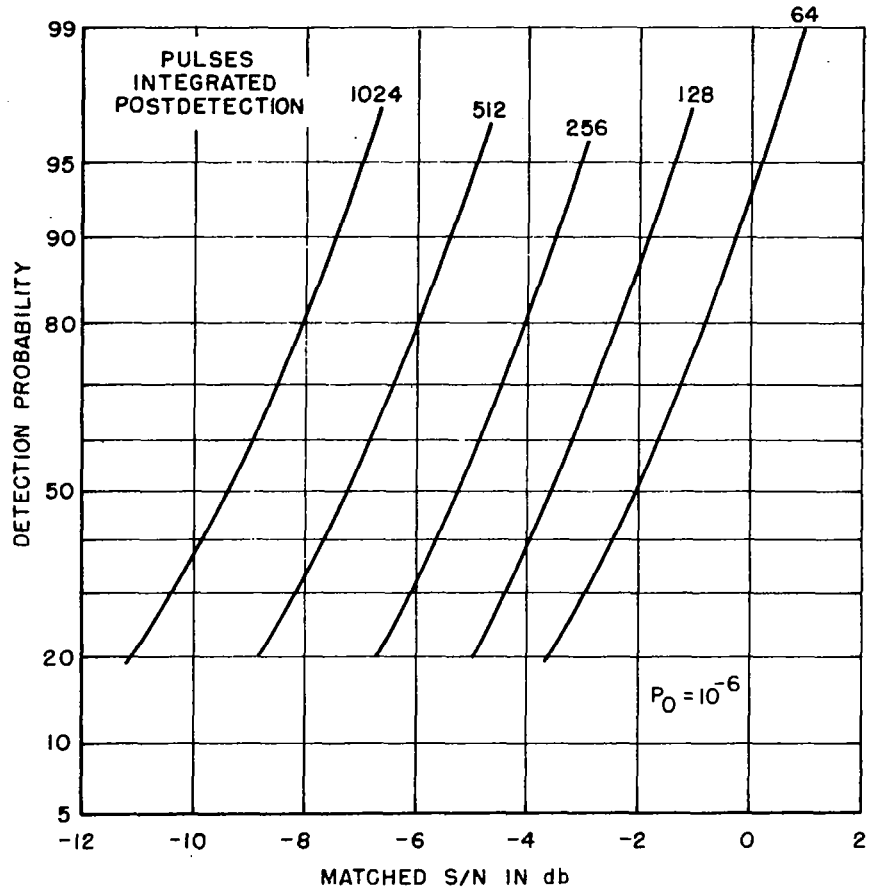

FIGURE 76. DICKE-FIX DETECTION PERFORMANCE BWR = 10

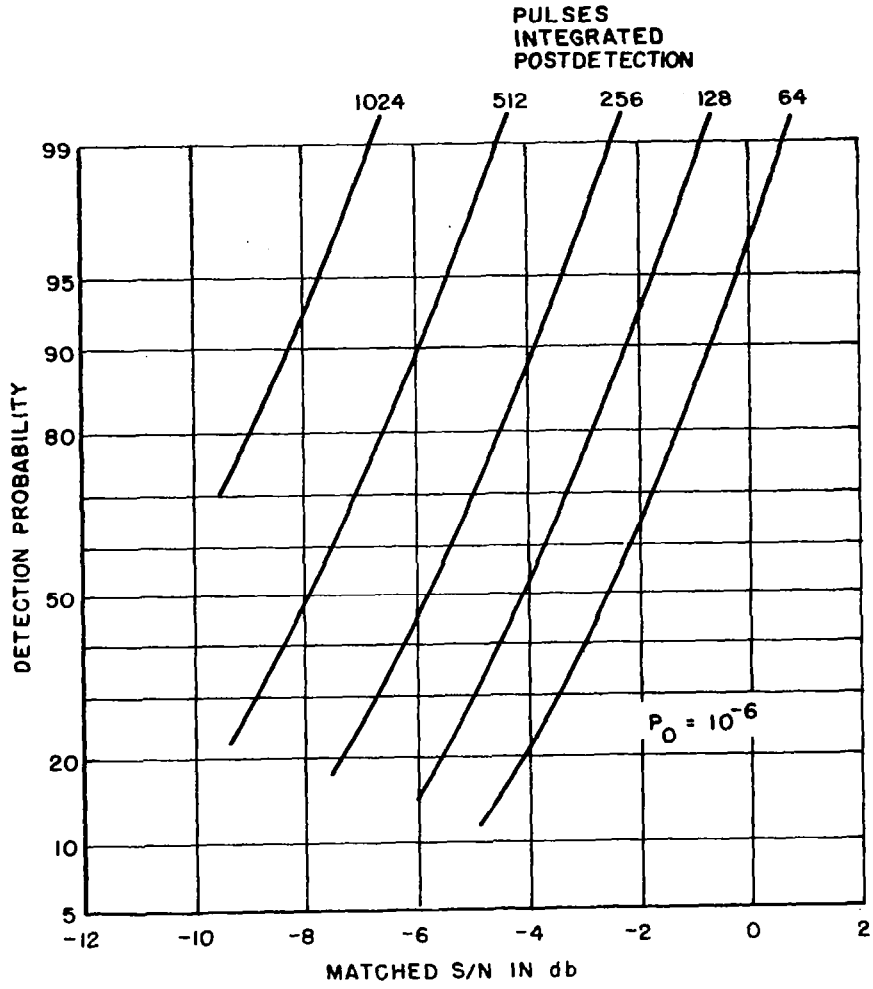

FIGURE 77. DICKE-FIX DETECTION PERFORMANCE BWR = 20

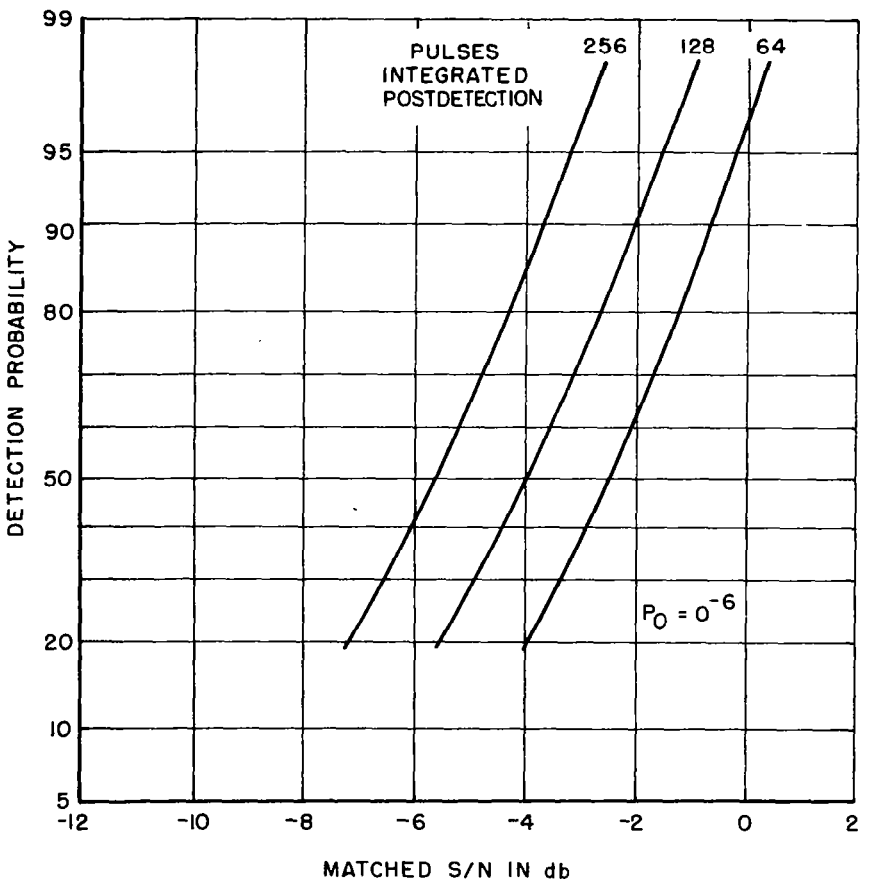

FIGURE 78. DICKE-FIX DETECTION PERFORMANCE BWR = 40

TABLE XIII

CALCULATIONS OF DICKE-FIX LOSSES

FOR: $P_d = 0.9$, $f_{ap} = 10^{-6}$

K=No. of Pulses Integrated	Normal Integration (loss-db)	Single Hit S/N Required (db)	Normal Postdetection (total)	Integration Gain (ideal-db)	Normal Postdetection (db/hit)
64	3.65	13.2	16.85	18	-1.15
128	4.70	13.2	17.90	21	-3.10
256	5.90	13.2	19.10	24	-4.90
512	7.10	13.2	20.30	27	-6.70
1024	8.50	13.2	21.7	30	-8.30

	Postdetection db/hit with Dicke-Fix			Dicke-Fix Loss/db		
	BWR = 10	BWR = 20	BWR = 40	BWR = 10	BWR = 20	BWR = 40
64	-0.30	-0.60	-0.60	0.85	0.55	0.55
128	-1.80	-2.	-2.00	1.30	0.90	1.10
256	-3.50	-3.80	-3.80	1.40	1.00	1.10
512	-5.50	-6.10	-	1.20	0.60	-
1024	-7.50	-7.80	-	0.80	0.50	-

where P_i is the probability of the i^{th} level $L_i = T_i + T_{i-1}/2$. Thus,

$$P_i = \epsilon^{-n\left(\frac{i-1}{I}\right)^2} - \epsilon^{-n\left(\frac{i}{I}\right)^2}$$

and mean and variance of the quantized video are

$$m_{oq} = \sum_{i=1}^{I} P_{io} L_i$$

$$\sigma_{oq}^2 = \sum_{i=1}^{I} P_{io} L_i^2 - m_{oq}^2$$

For the signal plus noise cases, the histograms, classified to 100 bins (about 6-2/3 bits) resulting from the Monte Carlo simulation of the Dicke-Fix Video, were used to compute the mean and variance

$$m_{1q} = \sum_{i=1}^{I} L_i P_{i1}$$

$$\sigma_{1q}^2 = \sum_{i=1}^{I} L_i^2 P_{i1} - m_{iq}^2$$

where

$$P_{i1} = \left(\sum_{k=K_i}^{K_{i+1}} n_k \Big/ \sum_{k=1}^{100} n_k \right)$$

in which P_{i1} is the probability of being at the i^{th} level, n_k is the number of outcomes in the k^{th} class, $k = 1, 2 \cdots 100$, of the Dicke-Fix Monte Carlo simulation and $K_i = 100\ T_i$.

No attempt was made to optimize the uniformly spaced analog-to-digital conversion threshold levels with respect to the Dicke-Fix bandwidth ratio. Under the assumption of a Gaussian distribution for the video but with mean and variance equal to those of the actual distribution, the detection threshold, A, is found from

$$P_o = 0.5 - 0.5 \text{ erf } A$$

where P_o is the false alarm probability and

$$\text{erf } X = \frac{2}{\sqrt{\pi}} \int_0^X \epsilon^{-v^2} \, dv$$

The detection probabilities for the analog and quantized cases were then found from

$$P_i = 0.5 + 0.5 \text{ erf} \left(\frac{m_1 - m_o}{\sigma_1 \sqrt{2}} - \frac{\sigma_o A}{\sigma_1} \right)$$

$$P_{iq} = 0.5 + 0.5 \text{ erf} \left(\frac{m_{iq} - m_{oq}}{\sigma_{1q} \sqrt{2}} - \frac{\sigma_{oq} A}{\sigma_{1q}} \right)$$

Only the case BWR = 10, S/N = 4 db (matched) was considered. The results for 2, 3, and 4 bits are shown below:

False Alarm Probability	Detection Probability				Loss-db		
	Analog	2 Bits	3 Bits	4 Bits	2 Bits	3 Bits	4 Bits
10^{-6}	0.0026	0.0016	0.0017	0.0018	0.7	0.6	0.5
10^{-3}	0.0760	0.0570	0.0632	0.0655	0.6	0.5	0.4
10^{-2}	0.2098	0.1727	0.1875	0.1930	0.5	0.4	0.3

It is concluded that the quantizing loss using 3 bits is trivial in this application.

REFERENCES

1. "Investigation of New Ionosounder Techniques," NASA Contractor Report NASA CR-493, June 1966.

2. Skolnik, M. I., "Introduction to Radar Systems," McGraw-Hill Book Co., 1962.

3. Fjelbo, G., Fjelbo, W. C., and Von R. Eshleman, "Models for the Atmosphere of Mars Based on the Mariner IV Occultation Experiment," Stanford Radio Science Report SU-SEL-66-007, Stanford Electronics Laboratory, Stanford University, January 1966.

4. Chamberlain, J. W., and McElRoy, M. B., "Martian Atmosphere: The Mariner Occultation Experiment," Science 152, 21, 1966.

5. Smith, N., and Beutler, A., "A Model Martian Atmosphere and Ionosphere," Report No. 66-3, University of Michigan, Radio Astronomy Observatory, March 1966.

6. Gross, S. H., McGovern, W. E., and Rasool, S. I., "Mars: Upper Atmosphere," Science 151, 1216, 1966.

7. Alexander, J. K., and Stone, R. G., Goddard Space Flight Center, NASA, Report X-615-65-185, 1965.

8. Walsh, D., Haddock, F. T., and Schulte, H. F., COSPAR, 6th Plenary Meeting, Warsaw, 1963.

9. Huguenin, G. R., Lilley, A. E., McDonough, W. H., and Papagiannis, M. D., Harvard College Observatory Report HSRP-107, 1963.

10. Ellis, G. R. A., Nature 204, 171, 1964.

11. Hartz, T. R., Ann. d'Astrophys., 27, 823, 1964.

12. Bode, H., "Network Analysis and Feedback Amplifier Design," D. Van Nostrand Co., Inc., New York, 1947.

13. Fano, R. M., "Theoretical Limitations on the Broadband Matching of Arbitrary Impedances," J. Franklin Inst, Vol 249, p 57-83, January 1960; and p 139-155, February 1960.

14. Youla, D. C., "A New Theory of Broad-Band Matching," IEEE Trans on Circuit Theory, p 30-50, March 1964.

15. Budden, K. G., "Radio Waves in the Ionosphere," Cambridge University Press, 1961.

16. Gross, S. H., "Propagation in Non-Uniform Ionospheric Media," paper presented at Spring URSI meeting, Washington, D. C., April 1966.

17. Jackson, W., "Communication Theory," Academic Press, New York, 1953.

18. Turyn, R., Sylvania Electronic Systems Final Report, "Optimum Codes Study," on Air Force Contract AF 19(604)-5473, January 1960.

19. DeLong, D. F., Lincoln Lab., MIT, Report, "Experimental Autocorrelation of Binary Codes," October 1960 (AD152974).

20. Davenport, W. B., and Root, W. L., "Introduction to Random Signals and Noise," McGraw-Hill Book Co., Inc., New York, 1958.

21. Marcum, J. I., and Swerling, P., "Studies of Target Detection by Pulsed Radar," Special Monograph Issue, IRE Transactions on Information Theory," Vol IT-6, No. 2, April 1960.